Semi-Quantitative Assessment Framework for Corrosion Damaged Slab-on-Girder Bridge Columns Using Simplified Nonlinear Finite Element Analysis

Amina M. Mohammed

Thesis submitted to the
Faculty of Graduate and Postdoctoral Studies
in partial fulfillment of the requirements
for the degree of Doctor of Philosophy degree in Civil Engineering

Department of Civil Engineering
Faculty of Engineering
University of Ottawa

Abstract

Most of existing North American bridge infrastructure is reported to be deficient. Present infrastructure management mainly relies on qualitative evaluation, where bridge safety and serviceability are judged through routine visual inspection. With the successive increase in the number of severely deficient bridges and the limited available resources, it is crucial to develop a performance-based quantitative assessment evaluation approach that enables an accurate estimation of aging bridges ultimate and seismic capacities and ensures their serviceability. Reinforcement corrosion is the main cause of most of North American concrete infrastructure deterioration. Experimental investigations prove that reinforcement corrosion results in reduction of the steel reinforcement cross sectional area, localized (or global in very extreme cases) loss of bond action, concrete spalling, loss of core concrete confinement, and structural collapse. Field observations show that damage due to reinforcement corrosion in reinforced concrete (RC) bridge columns is localized in highly affected zones by splash of deicing water.

In this thesis, an innovative performance-based semi-quantitative assessment framework is developed using newly developed simplified nonlinear static and dynamic finite element analysis approaches. The framework integrates the bridge's available design and after-construction information with enhanced inspection and additional material testing as sources for accurate input data. In order to evaluate the structural performance and the capacity of the corrosion-damaged bridge columns, four nonlinear static and dynamic analysis approaches have been developed: (i) simplified nonlinear sectional analysis (NLSA) approach that presents the basis of the

analysis approaches to estimate the ultimate and seismic capacities, and serviceability of bridge columns; (ii) simplified nonlinear finite element analysis (NLFEA) approach, which enables estimating the ultimate structural capacity of corrosion-damaged RC columns; (iii) simplified hybrid linear/nonlinear dynamic finite element analysis (SHDFEA) approach to evaluate the serviceability of the bridge; and, (iv) simplified non-linear seismic analysis (SNLSA) approach to evaluate the seismic capacity of the bridge columns. The four analysis approaches are verified by comprehensive comparisons with available test experimental and analytical results. The proposed semi-quantitative assessment framework suggests three thresholds for each performance measure of the evaluation limit states to be decided by the bridge management system team. Case studies are presented to show the integrity and the consistency of using the proposed assessment framework. The proposed assessment framework together with the analysis approaches provide bridge owners, practicing engineers, and management teams with simplified and accurate evaluation tools, which lead to reduce the maintenance/rehabilitation cost and provide better safety, and reduce the variation in the data collected using only traditional inspection methods.

Acknowledgements

This thesis would not have been possible without the encouragement, help, guidance, and support of the kind people around me, to only some of whom it is possible to give particular mention here.

This thesis would not have been possible without the help, support, and patience of my supervisor, Dr. Husham Almansour, not to mention his advice, unsurpassed knowledge and the tremendous amount of time dedicated that enabled learning different aspects of all research challenges, specifically in areas of bridge engineering and evaluation of bridges which need extensive experience in structural engineering. Indeed, I am glad to be his student. Also, my thanks are going to my supervisor Dr. Beatriz Martin-Pérez for her efforts in this research work.

My deepest gratitude and appreciations are going to my wonderful family, in particular to my father and mother for their great support and patience at all times. They always believed in my potential and positively influenced my life in spite of the physical distance. My thanks are also due to my brothers, sisters and friends for their encouragement and kindness throughout the course of my academic progress.

My sincere thanks are directed to the National Research Council Canada and University of Ottawa for the technical and academic supports.

I would like lastly to express my deep appreciation to the Libyan Ministry of Higher Education and Scientific Research for the financial support through the Libyan National PhD Scholarship Program that enables the completion of this research work.

Table of Contents

List of Figures

List of Figures in Appendixes

List of Tables

List of Tables in Appendixes

List of Symbols

$\mathbf{A_{p,i(t)}}$ = Cross-sectional area of a pit after time t of corrosion.
$\mathbf{A_{sti}}$ = The corresponding reinforcement area.
$\mathbf{A_s}$ = Cross-sectional area reinforcing bars.
BAZ = The length of the bond affected zone of the rebar.
BSD = The constant bond stress after stress re-distribution takes place.
$\mathbf{B_{ci}}$ = width of strip(i).
$\mathbf{b_i}$ = The vehicle axle position from its center of gravity.
$\mathbf{c_i}$ = The spring damping of an axle of the moving system.
[C] = The structural damping matrix.
$\mathbf{corr_i}$ = Successive corrections
$\mathbf{Corr\text{-}_i}$ = The displacement correction.
$\mathbf{D_o}$ = Initial reinforcing bar diameter
$\ddot{d}$ = The nodal acceleration vector
$\dot{d}$ = The nodal velocity vector
d = The nodal displacement vector.
$\mathbf{E_{sti}}$ = The reinforcement modulus.
EA = Axial rigidity of the cross section.
EI = Flexural rigidity of the cross section.
$\mathbf{E_{ci}}$ = Concrete modulus.
$\mathbf{E_s}$ = Steel modulus.
F = Faraday's constant.
{F} = Overall vector load of the bridge structure.
fi = The magnitude of a concentrated force.
$\mathbf{F_i^{diff}}$ = The instantaneous difference in the force vector
f_c = Compressive stress
f_{cc} = The compressive stress in confined concrete.
f'_{co} = Strength of unconfined concrete.
$\mathbf{F_e}$ = Applied forces of free nodes.
$\mathbf{F_o}$ = Applied forces of roller and hinge nodes.
$\mathbf{f_{sh}}$ = Hardening stress.
$\mathbf{f_u}$ = Ultimate stress.
F_x = Internal axial force.
$\mathbf{f_u(t)}$ = Ultimate tensile strength at time t of corrosion.
$\mathbf{f_y}$ = Yield stress.
$\mathbf{f_y(t)}$ = Yield strength at time t of corrosion.
H = = the section depth.
$\mathbf{i_{corr}}$ = Corrosion current density.
[K] = The structural stiffness matrix.
[*k*] = Overall stiffness matrix of the bridge structure.

$\mathbf{K_{ee}}$	= Stiffness of free nodes.
$\mathbf{K_{eo}= K_{oe}}$	= Interaction stiffness.
$\mathbf{K_{i=1}}$	= The structural stiffness based on linear finite element analysis.
$\mathbf{k_i}$	= The spring stiffness of an axle of the moving system.
$\mathbf{K_i^{corr}}$	= The stiffness correction
$\mathbf{K_{oo}}$	= Stiffness of roller and hinge nodes.
M	= Metal molar mass.
[M]	= The structural mass matrix.
$\mathbf{m_1}$	= The spring mass of an axle of the moving system.
$\mathbf{M_{in}}$	= Internal bending moment.
N	= The number of reinforcement layers.
n	= A group of *n* reinforcing bars.
$\boldsymbol{NRS}$	= The number of strips in the section.
[N]	= The shape function.
P(t)	= Depth of the corrosive penetration attack.
R	= The ratio between the maximum penetration of a pit(t) ,and average penetration corresponding to uniform corrosion.
T	= Time elapsed since corrosion started.
$\mathbf{t_{ci}}$	= thickness of strip(i).
$\mathbf{U_{i=1}}$	= The global structural deformation.
$\mathbf{U_i^{corr\text{-}i}}$	= The modification of the deformation vector.
$\mathbf{V_{i=1}}$	= Vertical displacement.
$\mathbf{V_i^{corr\text{-}i}}$	= The modification of the maximum displacment.
w(x,t)	= The transverse displacement of the structure.
x(t)	= Thickness reduction of reinforcing steel bar.
y	= The vertical displacement of the spring mass.
ẏ	= The velocity of the spring mass.
ÿ	= The acceleration of the spring mass.
$\mathbf{Y_C}$	= depth of inelastic centroid position from bottom fiber of the section.
$\mathbf{Y_G}$	= location of the geometric centroid.
$\boldsymbol{y_i}$	The distance from the centroid of strip i to the section inelastic centriod.
$\boldsymbol{y_j}$	= The distance from the centriod of reinforcement layer j to the section inelastic centroid.
$\mathbf{Y_N}$	= location of the inelastic centroid.
$\mathbf{Y_o}$	= The current position of the neutral axis.
Z	= Valence of the ion formed as a result of iron oxidation.
$\boldsymbol{\varepsilon_y}$	= Yield strain.
$\boldsymbol{\varepsilon_{sh}}$	= Hardening strain.
$\boldsymbol{\varepsilon_u}$	= Ultimate strain.
$\boldsymbol{\varepsilon_o}$	= the axial strain at the inelastic centroid.

$\boldsymbol{\varepsilon_{o1}}$ = Strain at peak unconfined strength.

$\boldsymbol{\varepsilon_{o85}}$ = 85% of the peak unconfined strength.

$\boldsymbol{\varepsilon_{ci}}$ = concrete strain.

$\boldsymbol{\rho_s}$ = Density of iron.

$\boldsymbol{\lambda_u(t)}$ = Ultimate strain at time t of corrosion.

$\boldsymbol{\alpha_y, \alpha_u, \alpha_1}$ = Regression coefficients.

$\boldsymbol{\Delta_e}$ = Deformations of free nodes.

$\boldsymbol{\Delta_o}$ = Deformation of roller and hinge nodes.

$\boldsymbol{\theta_{beam}}$ = Beam rotation.

$\boldsymbol{\theta_{column}}$ = Column rotation.

Chapter 1

Introduction

1.1 General

It is reported that significant number of North American bridges are deficient. Present infrastructure management mainly relies on qualitative evaluation, where bridge safety and serviceability are judged through routine visual inspection. As the number of severely deficient bridges is increased while the available resources are limited, it becomes important to develop a performance-based quantitative assessment evaluation approach that enables an accurate estimation of aging bridges ultimate and seismic capacities and ensures their serviceability. Reinforcement corrosion is the main cause of most of North American concrete infrastructure deterioration. Experimental investigations prove that reinforcement corrosion results in reduction of the steel reinforcement cross sectional area, localized (or global in very extreme cases) loss of steel-to-concrete bond, concrete spalling, loss of core concrete confinement, and structural collapse. Field observations show that damage due to reinforcement corrosion in reinforced concrete (RC) bridge columns are localized in highly affected zones by splash of deicing water.

Such a quantitative evaluation approach requires the development of structural analysis models that are capable to simulate the damaged and non-damaged zones. The present simplified linear or nonlinear static or dynamic analysis approaches are mainly developed for “new” structures and requires significant modifications to ensure their accuracy, numerical efficiency and stability, and their simplicity and ability to be integrated in the evaluation approach.

The initiation, rate and progress of the corrosion process are highly dependent on several material and environmental conditions and parameters. The development of a time dependent quantitative approach to evaluate the structural performance and residual capacities is very challenging and time consuming. However, it is more important to correlate the structural capacities and the dynamic performance to specified states of damages that can be visually observed. If the material properties can be evaluated by tests or simplified empirical methods, then the evaluation approaches can have acceptable accuracy yet they require minimum numerical effort.

1.2 Justification for Need of a Semi-Quantitative Assessment Framework for Evaluation of Aged Bridge Columns

Most of North American bridge infrastructure that was built during the development boom from the 1950's to 1970's has different levels of deterioration, and their safety and serviceability are susceptible. Present infrastructure management systems mainly rely on qualitative evaluation approaches, where the bridge structural performance status is judged through routine visual inspection (usually every two years). If a "severe" deterioration case is captured, more refined inspection is conducted. The bridge management systems (BMS) in North America and many other countries around the world are based on identification of four general condition states under which the bridge elements are categorized. The four condition states are (i) Excellent, (ii) Good; (iii) Fair; and (iv) Poor (see MTO- OSIM, 2008 and AASHTO- MCEB, 1994). The accuracy of bridge rating and management decisions of bridge engineers relies on the accuracy of the bridge condition assessment (Rashidi, 2012), which is mainly based on different levels of visual inspection. Different bridge management systems recognise many types of visual

inspection such as the typical visual inspection (VI), in-depth VI, and enhanced in-depth VI (see FHWA-RD-01-020, MTO- OSIM, 2008 and AASHTO- MCEB, 1994). The comparison of bridge inspection standards among various international organisations indicates that each organisation has a different approach to bridge inspection in terms of the types of inspection, the frequency of the inspections, the definition of the various inspection types and the type of personnel that undertakes the inspections (Brown et al. 2010). The lack of a practically simple and cost-effective quantitative assessment approach that is capable to accurately determine the state of the performance in terms of safety and serviceability of critical bridge elements is now identified as a major research gap.

Reinforcement corrosion has been identified as the major cause of RC infrastructure deficiency (deterioration/damage). However, the initiation and progression of corrosion in reinforcing steel can have unlimited number of scenarios that are yet not fully understood or modeled. It is very challenging to develop practical time-dependent analytical models that are capable to accurately estimate the effects of different reinforcement corrosion scenarios on the structural behavior of damaged RC elements. Instead, detailed measurements of the damaged zones together with any required material testing can be performed during an enhanced inspection of aged bridge elements, which usually follows the routine visual inspection in most international BMS (see FHWA-RD-01-020, MTO- OSIM, 2008 and AASHTO MCEB, 1994).

This thesis proposes a semi-quantitative assessment framework (SQAF), wherein the results of the enhanced in-depth VI (or enhanced inspection, as referred later in this thesis) can be used as input data. The proposed SQAF addresses the three major

evaluation limit states of corrosion-damaged bridge elements that are consistent with existing bridge design codes: ultimate limit state (ULS), serviceability limit state (SLS), and earthquake limit state (ELS) (CHBDC 2006/ CAN/CSA-S6-06, or AASHTO-LRFD, 2007). All the three limit states are based on simplified non-linear static and dynamic finite element analysis approaches developed and verified throughout the thesis (see Chapters 2 through 5), where the combined effects of mechanical loads and measured corrosion damage on structural performance of beam-columns are quantitatively evaluated.

1.3 Thesis Objectives

The objectives of this thesis are to develop and verify simplified analysis tools to assess the ultimate capacity, serviceability, and seismic capacity of beam-columns. The three analysis approaches are used to develop a semi-quantitative assessment framework for aging slab-on-girder bridge columns that enables a more accurate, yet simplified assessment as part of a cost-effective bridge management system.

1.4 Thesis Scope

The scope of this thesis can be summarized by the following:

I. Develop a simplified nonlinear sectional analysis (NLSA) approach for aged RC beam-columns to simulate their nonlinear behaviour up to ultimate capacity.

II. Develop a nonlinear finite element analysis (NLFEA) approach to evaluate the reduction of the ultimate structural capacity of corrosion damaged RC columns subjected to different combinations of axial load and flexure

III. Develop linear and nonlinear dynamic finite element analysis approach to evaluate the changes of the vibration frequencies and amplitudes of the bridges

under moving truck (or traffic) when their columns are subjected to reinforcement corrosion and the resulting damages.

IV. Develop nonlinear time history analysis of corrosion damaged structural element to estimate the reduction of the structural capacity due to earthquake loads.

V. Develop a semi-quantitative assessment framework using the four analysis approaches developed in I through IV above. The assessment framework should integrate the bridge available design and after-construction information with the enhanced inspection and additional material testing as source for acceptably accurate input data.

1.5 Description of the Thesis

This thesis consists of seven chapters:

Chapter 1 introduces the general need for a semi quantitative assessment framework of evaluation of aged bridge columns, the thesis objectives, the thesis scope, the description of the thesis content, and the thesis format.

Chapter 2 proposes a simplified nonlinear sectional analysis (NLSA) approach for aged bridges. The proposed NLSA is capable to simulate the nonlinear behavior up to ultimate capacity of a critical section of an aged RC beam-column element subjected to reinforcement corrosion and mechanical loads. The input data is gathered from observations and measurements obtained from an enhanced inspection and any required material testing for corrosion-damaged steel. Chapter 2 has been submitted for publication in the Structure and Infrastructure Engineering Journal (Mohammed et al. 2014a).

Chapter 3 proposes a simplified nonlinear finite element analysis (NLFEA) approach for aged bridge beam-columns subjected to reinforcement corrosion combined with mechanical loads. As in the NLSA, the input data is also gathered from an enhanced inspection and any further material testing performed on corrosion-damaged steel. The nonlinear stiffness is based on the nonlinear sectional analysis presented in Chapter 2. Chapter 3 has been submitted for publication in the Structure and Infrastructure Engineering Journal (Mohammed et al. 2014b).

Chapter 4 proposes a simplified hybrid linear/nonlinear dynamic finite element analysis (SHDFEA) based on enhanced inspection, which is introduced as part of the proposed semi quantitative assessment approach of aged bridge columns. Its focus is on the evaluation of the dynamic characteristics and behaviour of slab-on-girder bridges under moving trucks when their columns are subjected to severe corrosion damage. Chapter 4 has been published in the Engineering Structures Journal (Mohammed et al. 2014c).

Chapter 5 proposes a simplified non-linear seismic analysis (SNLSA) approach as part of the semi-quantitative assessment framework (SQAF). The approach is based on the nonlinear sectional analysis (NLSA) proposed in Chapter 2, the DRAIN-RC nonlinear time history analysis program, and Takeda hysteretic analysis. Chapter 5 is intended to be submitted for publication in the ASCE Journal of Bridge Engineering (Mohammed et al. 2014d).

Chapter 6 develops a semi quantitative assessment framework (SQAF) of aged bridge columns based on enhanced inspection, any required material testing, and simplified static and dynamic nonlinear analysis approaches of the three major evaluation limit

states developed in Chapters 3, 4 and 5. Chapter 6 is intended to be submitted for publication in Engineering Failure Analysis (Mohammed et al. 2014e).

Chapter 7 presents the major conclusions from the different chapters of this thesis. It also presents suggested future work that would lead to an improvement of the proposed analysis approaches and move the proposed semi-quantitative assessment approach a step forward to a fully quantitative assessment framework.

The thesis also includes six appendices that cover additional materials related to the thesis chapters, four of which are published conference papers.

Comprehensive literature reviews are available in each chapter and in Appendix A.

1.6 Thesis Format

This thesis is prepared as a "paper format" thesis. Each chapter, except the first and the last chapters, is presented as a paper with its own bibliography and without the abstract. The tables and figures for each chapter are grouped at the end of each chapter before the bibliography. Additional figures, information, and conference papers are provided at the end of the thesis. Appendices C and F present additional supporting figures that are not provided in the main chapters. Appendices A, B, D and E are reproduction of four papers published in different conferences (as mentioned in each appendix) and reflect different analysis approaches and/or concepts that were initiated and developed throughout or parallel to the evolution of this thesis and led to its final approaches and framework.

1.6 References

American Association of State Highway and Transportation Officials, AASHTO LRFD Bridge Design Specifications SI Units (4th Edition); 2007.

American Association of State Highway and Transportation Officials, Manual for condition evaluation of bridges, Washington, DC, 1994.

Brown, G., Grave, S., Boorman, G., Bridge inspection standards - A review of international practice to benchmark bridge inspection standards for KiwiRail Network's bridges; Beca and KiwiRail; 2010.

Canadian Standards Association, Canadian Highway Bridge Design Code, S6-06, A;2006.

Federal Highway Administration, Reliability of visual inspection for highway bridges, volume I: final report,; FHWA-RD-01-020; June, 2001.

Ministry of Transportation, Ontario, Ontario Structure Inspection Manual (OSIM), Policy, planning & Standards division engineering standards branch bridge office; April, 2008.

Mohammed, A., Almansour, H., Martín-Pérez, B., Nonlinear flexural analysis of reinforced concrete beam-column subjected to ultimate gravity loads combined with reinforcement corrosion, Part I: Sectional Analysis. Structure and Infrastructure Engineering, submitted, ID NSIE-2014-0014; 2014a.

Mohammed, A., Almansour, H., Martín-Pérez, B., Nonlinear flexural analysis of reinforced concrete beam-column subjected to ultimate gravity loads combined with reinforcement corrosion, Part II: finite element analysis. Structure and Infrastructure Engineering, submitted, ID NSIE-20143-0015; 2014b.

Mohammed, A., Almansour, H., Martín-Pérez, B., Evaluation of dynamic of slab-on-girder-bridge under moving trucks with corrosion-damaged columns", Engineering Structures, (6), 159-172;2014c.

Mohammed, A., Almansour, H., Martín-Pérez, B., Seismic performance of aged reinforced concrete bridge columns subjected to reinforcement corrosion. Journal of Bridge Engineering (ASCE),to be submitted; 2014d.

Mohammed, A., Almansour, H., Martín-Pérez, B., A semi-quantitative assessment framework for aging reinforced concrete bridge columns. Engineering Failure Analysis; to be submitted; 2014e.

Rashidi, M., Gibson, P., A methodology for bridge condition evaluation. Journal of Civil Engineering and Architecture; 2012, 6 (9), 1149-1157.

Chapter 2

Nonlinear Flexural Analysis of Reinforced Concrete Beam-Column Subjected to Ultimate Gravity Loads Combined with Reinforcement Corrosion, Part I: Sectional Analysis

2.1 Introduction

Estimation of the ultimate capacity of reinforced concrete (RC) structural elements subjected to reinforcement corrosion is of great interest to infrastructure owners, practicing engineers and researchers. It presents a key element in the development of an efficient cost effective tool for the management of aging infrastructure based on a quantitative rather than the existing qualitative assessment approach. Such estimation requires the use of an efficient elasto-plastic nonlinear material model that is capable to simulate the behavior of RC elements subjected to combined axial and flexural stresses and different levels of damage due to reinforcement corrosion. The development of such model involves two stages: (i) the sectional level, which is the focus of the present chapter; and (ii) the structural level (which is the focus of chapter 3; Mohammed et al. 2014b).

In the past six decades, various analytical, semi-analytical and numerical approaches were introduced and progressively developed aiming at simulating the non-linear elasto-plastic structural behavior of RC structures. Most of these models were based on simplified models for the material nonlinearity of both the concrete and the reinforcing steel. All these models were developed for “new structures” assuming: (i) average mechanical properties for all materials; (ii) negligible or consistent geometrical cross-sectional variation over the length of structural elements; and (iii) typical loading and boundary conditions. The focus in the development of these models was on one or more of the following: (i) high numerical efficiency and stability; (ii)

high accuracy in terms of matching experimental results; and/or (iii) practicality, simplicity and adaptability of the model (see Mohammed et al. 2012; Appendix A).

The use of early computer generations raised critical technical challenges to the developers of iterative non-linear finite element models such as: (i) very limited access to memory storage; (ii) expensive editing, compilation and running time; and (iii) limitations in the numerical techniques that would increase the development/processing time. In order to overcome these limitations and to reduce the cost, by targeting "efficient" nonlinear models that are capable to simulate the nonlinear behavior of large RC structural systems, it was thought that semi-analytical models are appropriate. Lazaro and Richards (1973) Gunnin et al. (1977), and Carol and Murica (1989a &b) proposed the use of special elements types, which are compatible with the geometrical characteristics of RC frame structures. These special elements were semi-linear elements and their stiffness formulations were based on an assumed distribution of the section rigidities. The formulations of these nonstandard frame elements were based on simplifying assumptions and techniques such as neglecting axial deformations, inserting internal degrees of freedom, using finite difference schemes, simplified moment-curvature relationships, and stiffness variations along the elements and/or striped sectional analysis algorithms. Resheidat et al. (1995) developed an analytical model to calculate the flexural rigidity of RC columns subjected to short-term axial load and biaxial bending. In most of the mentioned models, material properties, steel ratio and the axial load were taken into account to establish simplified formulae for the flexural rigidity of the columns. The use of such ready-formulation packages were supposed to result in a considerable saving of modeling efforts and computational cost. However, most of these models are numerically sensitive and unstable as they require significant

efforts to establish or verify the convergence of the solutions, which are based on a case by case approach.

By 1970's, the use of numerical models became more popular. However, the computing cost and the memory limitations enforced the development of explicit formulations of the stiffness matrices in one- and two-dimensional nonlinear finite element (FE) procedures. The focus was on: (i) the ability of the model to match experimental results; and (ii) the numerical efficiency in terms of accuracy, minimizing the computing time, and minimizing the use of random access memory (RAM). Kreonke et al. (1973) and Pulmano et al. (1987) developed nonlinear analysis schemes of RC frames using one-dimensional FE. In their models, the computations were performed incrementally to take into account the sectional rigidity variations due to the inelastic material properties during successive load application steps. Then, from the element rigidities, the variations of beam-column element stiffness were characterized.

With the considerable advances in computers and the successive reduction in their operation cost, more efficient nonlinear sectional and finite element models have been developed in the last decade. Bentz (2000) proposed a non-linear sectional analysis for various types of RC elements. The model is based on (i) Euler-Bernoulli beam theory; (ii) assuming no transverse clamping stresses; and (iii) the biaxial behavior modeled using the Modified Compression Field Theory (MCFT). The author developed a computer program (Response-2000) to perform nonlinear sectional analysis of RC beams or columns subjected to arbitrary combinations of axial load and flexure. The program output shows good match with experimental results for beams. However, the approach did not address the effects of lateral reinforcement on the confinement of the core concrete of RC columns. Hence the variations of the structural behavior and the ultimate strength

of RC members subjected to axial load, or combined axial and lateral loads in relation to lateral steel reinforcement and the level of axial load are not covered.

On the other hand, reinforcement corrosion is the main cause of reduction in concrete structural capacity. Field observations and experimental investigations show that the main effects of reinforcement corrosion on RC sections are: (i) reduction of the steel rebar cross-sectional area and ductility, (ii) reduction of concrete section as a result of the concrete cover spalling, and (iii) loss of bond between the rebars and the surrounding concrete in the affected zones. It is important to investigate if these effects result in a significant reduction of the structural stiffness and ultimate capacity of RC elements. Several studies have introduced simplified or advanced models to predict the effect of corrosion on the concrete and the steel reinforcement at the material level. In order to understand the structural performance of RC flexural elements subjected to combined or coupled effects of service or ultimate loads and reinforcement corrosion, these studies involved either experimental or analytical approaches. Among many others, Yoon et al. (2000), Ballim et al. (2001), El Maaddawy et al. (2005), Yingang et al. (2007), Berto et al. (2008), Choe et al. (2008), and Yalciner et al. (2012) present pioneer research in this area (for more details, see Mohammed et al. (2012)).The objectives of many of such studies were to understand the deterioration mechanism, damage stages, and their effects on flexural and shear stiffness and material ductility, progressive changes of internal forces and stress distribution due to mass loss, and bond loss/slip, and spalling. To date, no analysis approach is available to accurately predict the instantaneous structural performance of RC sections suffering from active corrosion. Empirical, analytical and numerical models to predict the mechanical behavior and the time profile of the corrosion damage of RC elements in ideal lab conditions have been proposed as a direct application of the material-level models. However, no

studies are conducted on the nonlinear behavior of concrete structures subjected to corrosion-induced damage combined with axial and lateral loads.

The development of an efficient quantitative assessment framework (QAF) requires the integration of all the time-dependent processes in corrosion damaged zones of an aged concrete structure with the nonlinear sectional analysis or nonlinear finite element modeling analysis. It is very challenging and computationally expensive to develop and verify such time-dependent QAF. Such an assessment framework of aging structure should: (i) be able to match the real state of damage of the structural element; (ii) accurately estimate the corrosion initiation time, the rate of corrosion and the resulting state of damage; (iii) have the ability to match field observation at any time throughout the life of the structure. However, it is difficult to develop accurate corrosion deterioration patterns due to (i) lack of enough field data on the corrosion damage states and time frame; (ii) lack of accurate record on the maintenance cycles and their impact on the bridge deterioration process; and (iii) the complications in modeling different time-dependent environmental and materials parameters that affect the corrosion process itself. As a practical stage in the development of the QAF, the integration of visual inspection/observations and some additional material testing into a simplified non-linear sectional and FE analysis could lead to a semi-quantitative assessment framework SQAF that enables a practical and cost effective evaluation of corrosion damaged RC structural elements. If the SQAF is integrated with accurate time-dependent estimations of the corrosion deterioration/damages of the structural element, then an efficient QAF is feasible through further stages of developments of the SQAF.

The main objective of this chapter is to develop a comprehensive yet simplified sectional analysis approach that is capable to simulate the nonlinear behavior up to ultimate capacity of a

critical section of an aged RC beam-column element subjected to reinforcement corrosion. The procedure aims at the use of a conceptually simple and numerically efficient approach simulating the mechanical behavior at the section level together with visual inspection and minimum material testing. The sectional analysis presents a key stage in the development of a simplified nonlinear finite element analysis as part of a proposed semi-quantitative assessment framework (see Chapter 3; Mohammed et al. 2014b). The emphasis in this chapter is on (i) the accuracy in terms of matching available experimental results; and (ii) the numerical efficiency with minimum number of iterations and being less sensitive to the size of load increments in the nonlinear analysis.

2.2 Modeling the effects of reinforcement corrosion on the steel rebar and concrete

As mentioned earlier, the proposed analysis approach employs visual inspection and any required material testing as the major source of the data input data of the corrosion damage and material properties for the proposed analysis approaches for. Hence, it is not the purpose of proposed analysis approaches to study, identify or simulate how the corrosion grew up, what the real corrosion rate was, or whether the corrosion rate was uniform or highly fluctuated. The focus is only on quantifying the effects of the ongoing corrosion process on the material properties, the distribution of the damage or its size, and the integrity of the RC element in the damaged zone at the visual inspection/assessment time. In order to prepare the data for the analysis approaches, a uniform rate can be assumed, where the observed level of damage at the time of the inspection can be matched, and hence the instantaneous material properties can be estimated.

Once the reinforcement corrosion is initiated in an RC structural element, in most cases, it propagates and continues over long time with variable rates that are depending on the

surrounding environmental conditions, concentrations of aggressive agents, and the material properties of concrete and steel. Reinforcement corrosion can lead to different damage mechanisms that are developed in the steel and the surrounding concrete in the affected zones. If progressive local damages affect flexural or shear critical zones, the structural capacity of the RC element could significantly decrease. The structural behavior and capacity of corrosion damaged RC elements are affected by the changes in: (i) the geometrical/sectional properties of the corrosion-damaged zones; (ii) the materials properties of the steel and the concrete; and (iii) the steel-to-concrete bond surface and stress distribution in the affected zone and elsewhere along the rebars.

2.2.1 Reduction in reinforcement cross-sectional area and ductility

If the corrosion is uniform around the rebar perimeter as shown Figure 2.1-a (assuming the rebar is made from carbon steel), and if there is no separation of the concrete cover ("delamination" or "spalling"), then the changes in the cross sectional area and moment of inertia at the corrosion-affected zones would not result in significant stiffness reduction of the RC elements. Conversely, it is observed that pitting corrosion (or localized corrosion with high rate as shown in 2.1-b) can severely affect the structural behavior and capacity of an RC element. If pitting corrosion takes place in critical stirrups, it could result in the loss of confinement in the concrete core and extension of the non-supported length that would lead to a premature buckling of the main rebars (Rodríguez et al. 1996). It is also reported that the steel ductility and strength are reduced when affected by corrosion (see Rodríguez et al. (1996), Lay and Schiebl (2003), and Cairns et al. (2005)).

By applying Faraday's law and after time (t) from initiation of the corrosion process, the reduction in the reinforcing steel thickness due to corrosion, x(t), can be calculated as:

$$x(t) = \frac{M}{zF\rho_s}.i_{corr}.t = 0.0116.i_{corr}.t \quad (2.1)$$

where M is the metal molar mass (55.85 g/mol for iron), z is the valence of the ion formed as a result of iron oxidation (i.e., z = 2 for $Fe \rightarrow Fe^{2+} + 2e^-$), F is Faraday's constant (F = 96,485 C/mol), ρ_s is the density of iron (ρ_s = 7.85 g/cm^3), i_{corr} is the corrosion current density($\mu A/cm^2$), and t is the time elapsed since corrosion started in years. The depth of the corrosive penetration attack $p(t)$ is calculated from:

$$p(t) = R.x(t) = R.0.0116.i_{corr}.t \quad (2.2)$$

where R is the ratio between the maximum penetration of a pit, $p(t)$,and the average penetration corresponding to uniform corrosion (Val 2007). Parameter *R* is also known as the pitting ratio. Val (2007) has reported that the maximum penetration of pitting on the surface of a rebar is about 4-8 times the average penetration corresponding to uniform corrosion. Assuming that the pit can be idealized as a hemisphere, as illustrated in Figure 2.1-b, the reduced cross-sectional area A_s of a group of *n* reinforcing bars after *t* years of corrosion can be estimated as:

$$A_s(t) = n\frac{\pi D_o^{\,2}}{4} - \sum_{i=1}^{n} A_{p,i}(t) \geq 0.0 \quad (2.3)$$

where D_o is the initial reinforcing bar diameter and $A_{p,i}(t)$ is the cross-sectional area of a pit after time t, which is a function of $p(t)$ and calculated according to Val (2007).

Several empirical formulae have been proposed to estimate the loss of strength and ductility of reinforcement subjected to corrosion attack. Lay and Schiebl (2003) and Cairns et al. (2005) have established the following empirical equations to assess indirectly the residual ductility of reinforcement due to corrosion:

$$f_y(t) = (1.0 - \alpha_y.A_{corr}(t))f_y \quad (2.4)$$

$$f_u(t) = (1.0 - \alpha_u.A_{corr}(t))f_u \quad (2.5)$$

$$\lambda_u(t) = (1.0 - \alpha_1 . A_{corr})\lambda \quad (2.6)$$

where $f_y(t)$ is the yield strength at time t, $f_u(t)$ is the ultimate tensile strength at time t, $\lambda_u(t)$ is the ultimate strain at time t, f_y,f_u *and* λ are the yield and ultimate tensile strengths and strain of a non-corroded bar, respectively, $A_{corr}(t)$ is the cross section loss as a function of time t, and α_y, α_u , $\alpha_1$are regression coefficients (Lay and Schiebl 2003). The effect of reinforcement corrosion on the rebar cross-sectional area, moment of inertia and ductility are included in the nonlinear sectional model proposed in this study.

2.2.2 Loss of concrete cover

Among many parameters that affect cracking of the concrete cover, tensile strength and concrete cover thickness are the most important. For RC members subjected to axial compression, it is assumed that the cracking of the cover takes place when the maximum hoop stress is equal to the tensile strength of the concrete, while for RC members subjected to flexure, cracking of concrete is initiated when the tensile stresses at the extreme tensile fibers reaches the tensile strength of the concrete. Throughout their experimental investigation and modeling, many researchers observed the reduction in the overall stiffness and strength of RC structural elements subjected to reinforcement corrosion. Progression of the cracks around corroded rebars can result in delamination of the concrete cover from the core concrete and hence part of the concrete section may lose its continuity from the rest of the RC section (Rodríguez et al. 1996, Tapan and Aboutaha 2009, and Yoon et al. 2000). With the progress of reinforcement corrosion, a full separation of the concrete cover and spalling result in a smaller concrete cross section with less area and moment of inertia. Oyado et al. (2007) and Rodríguez et al. (1996) observed that depending on the corrosion zone and loading process, concrete cover spalls out from one side or

more. In the present study, the effect of this cover spalling on the stiffness and strength, and hence the structural performance is investigated by removing one or more concrete covers in the corrosion affected zone as shown in case study 2.5.4.

2.3 Modeling the effects of local bond loss of tensile steel reinforcement due to corrosion

2.3.1 Background and assumptions:

Many researchers have studied the effects of reinforcement corrosion on the deterioration of rebar-to-concrete bond. El Maaddawy et al. (2005) concluded that if the corrosion affected zone extends over a large part of the tensile steel rebars, it results an increase in deformations of an RC element subjected to bending and could lead to bond failure. In the case of seismic loads, the degradation of bond-slip as a consequence of reinforcement corrosion increases the global drift ratio of RC framed structures due to the increase of the lateral displacement (Yalciner et al. 2012). In their analytical investigations, the researchers found that the bond reduction due to corrosion has become a concern for aged RC structures located in seismic areas. Yalciner et al. (2012) adopted a simplified approach based on empirical equations to calculate the slip rotation, and then the additional displacement due to the slip is calculated as a function of corrosion rate for different time periods and member lengths.

Several studies have been conducted assuming that the corrosion damage propagates over the entire RC element length where the bond loss also extends cover the entire length of the tensile reinforcement (e.g. Ballim et al. 2001) and El Maaddawy et al. 2005)). Assuming such an extreme condition do not reflect the cases in bridge columns where in most cases only a localized corrosion over part of the column length is common. Consequently, field observations have not shown that significant or “total” bond loss in RC bridge columns has led to the development of structural collapse. With the typical two years inspection cycle in most of North American

infrastructure jurisdictions and management regulations, the development of a full bond loss over the entire length of an RC element is unlikely. It is also worthy to mention here that most of the RC bridge columns are overdesigned. Hence they are subjected to relatively low service load-to-capacity ratios, which are expected to reduce the effect of the localized bond loss on the column capacity.

All the mentioned studies among others were conducted either in the lab environment or using analytical approaches. However, there were no studies that investigated the frequency of occurrence of RC element collapse (or significant strength drop) due to local or global loss of bond. Also there are no studies that identify the differences in the structural behavior between RC beam-columns suffering from local bond-loss versus other RC beam-columns with “total” bond-loss.

2.3.2 Redistribution of the stresses due to local loss of bond

The reinforcement and the concrete in RC structural elements are considered as a composite system. Hence a fully effective composite action of the two components, the concrete and the reinforcing steel, is assumed. The bond stresses that are developed on the tensile reinforcement due to application of external load combinations should not exceed the bond strength. If a flexural RC member is affected by local bond failure due to corrosion, then redistribution of the bond stresses should take place along the tensile reinforcement. The bond stresses in the non-affected zones of the RC flexural member are increased. If the bond stresses outside the “bond failure zone” do not exceed the bond strength, then no progressive bond failure will take place. Figure 2.2 shows the bond stress redistribution on the bottom bars that are subjected to tensile stress.

2.3.3 Proposed model for local loss of bond of tensile steel reinforcement (pure bending)

If a beam-column element that has local bond failure is subjected to lateral loads or pure moment (no axial load), the sections of the bond failure zone are not subjected to flexural rotations. In this case, the steel and the concrete are not in composite action and hence the resistant couple (compressive and tensile forces) on each of these sections is not formed. The equilibrium of forces acting on each section of the bond failure zone is not directly satisfied. In this study, it is assumed that a self-supported arch is developed to join the internal tensile and compressive forces into a couple. Figure 2.2 shows the tensile reinforcement passing through a corrosion bond-failure zone and two side zones with active bond. The arch is formed from the compressive force in the compressive region of the concrete in the bond failure zone to two inclined forces at each of the side zones or active-bond zones. The arch is self supported through the tensile force in the tensile reinforcement.

At any cross sections of the RC element under flexure and when the bond is active, internal compressive and tensile forces balance each other on the section and they form a resisting couple. According to Euler-Bernoulli beam theory, this couple (or resistance moment) develops a linear strain distribution from maximum compressive strain to maximum tensile strain that results in rotating the cross-section around its neutral axis. In the other cross-sections where bond has failed, only the compressive force is acting directly on the section, while due to the bond loss the tensile force is not acting directly on the section. Hence the tensile and compressive forces are not forming a resisting couple on the section. However, the two forces satisfy the equilibrium only through the self-supported arch action and they are not able to rotate the section. The extension of the tensile steel and the contraction of the concrete in the compression region of the bond failure zone result in the deflection of these sections. The flow of forces in the bond failure zone can follow a truss rather than a beam mechanism.

It is assumed in this study that the extensions and contractions of the steel and concrete, respectively, develop a fictitious linear distribution of strains over each of the cross sections of the bond failure zone. Hence, these sections have fictitious rotations similar to the sections where bond is active. In order to simplify the calculations, the strain distribution and the location of the neutral axis in this case are found by the same iterative process as in applying beam theory; however, the calculations of the internal forces are based on the tensile force in the non-bonded tensile steel and the compressive force developed by the arch action. Once the fictitious strain distribution is identified, it is assumed that the same procedure to calculate all the structural parameters using the proposed nonlinear sectional analysis is applicable.

2.3.4 External axial load in beam column as part of the proposed model for local loss of bond

When a beam-column is subjected to an axial compression in addition to flexure (for example slab-on-girder bridge column), then the tensile stress in the tensile steel of the bond loss zone is significantly reduced. The force flow mechanism (or the proposed self-supported arch) could not be developed if the applied external compressive stress is very high. Hence the effects of losing bond in the corrosion affected zone could marginally affect the behavior of the beam column. From the modeling point of view, if the stress distribution of the combined axial and bending moment results in tensile stresses in the reinforcement, then the proposed model for local loss of bond is applicable; otherwise, the proposed nonlinear sectional analysis is assumed to be directly applicable without the development of the arch action.

2.4 Stress-strain relationships of concrete and steel

2.4.1 Constitutive stress-strain relationships of unconfined and confined concrete in compression

Modeling the stress-strain relationship of concrete in compression has been widely investigated. One of the well accepted models was developed by Hognestad (1951), which consists of a

second-order stress-strain relationship (parabola) up to the ultimate stress followed by a linear stress drop with relatively large increase of the strain up to collapse. Kabaila (1964) and Basu (1967) proposed fourth-degree polynomials with more precise consideration of the post ultimate stage. Although such models have been widely used by many researchers (for example, Rasheed and Dinno (1994)), they are not capable to simulate the change in concrete properties under different states of confinement.

Saatcioglu and Razvi (1992) proposed stress-strain relationships for unconfined and confined concrete considering various levels of confinement based on reinforcement details. The researchers verified the applicability of their approach to almost all popular cross-sectional shapes and reinforcement details. For accurate estimation of the ultimate strength of RC elements subjected to axial and flexure loads, the cross-section is divided into two parts: (i) unconfined concrete cover; and (ii) confined core concrete. When the axial pressure is relatively high and the beam-column has adequate lateral reinforcement properly detailed, Saatcioglu and Razvi's approach shows that the concrete strength and ductility are enhanced significantly due to the well-developed lateral confinement pressure. They assumed that the confinement pressure vanishes when the applied axial load is less than 10% of the member axial capacity. The method also conservatively underestimates the capacity of RC members with variable ties/stirrups spacing. Saatcioglu and Razvi (1992) stress-strain relationship for unconfined concrete is reduced to Hognestad's stress-strain relationship with an ascending part described by a second degree parabola, and a descending part linearly changing to a strain corresponding to 20% of the peak (see Figure 2.3). The slope of the descending part is defined by specifying the strain at 85% of strength. This stress-strain relationship is used for unconfined concrete (e.g., for the concrete cover or for the entire RC section when the axial load is less than 10% of the column axial

capacity). The following expressions are used to describe the stress-strain relationship for unconfined concrete:

$$f_c = f'_{co}\left[2\frac{\varepsilon_c}{\varepsilon_{o1}} - \left(\frac{\varepsilon_c}{\varepsilon_{o1}}\right)^2\right] \text{ for } 0 \le \varepsilon_c \le \varepsilon_{o1} \quad (2.10)$$

$$f_c = f'_{co} - (\varepsilon_c - \varepsilon_{o1})\left(\frac{0.15f'_{co}}{\varepsilon_{o85}-\varepsilon_{o1}}\right) \text{ for } \varepsilon_{o1} \le \varepsilon_c \le \varepsilon_{cu} \quad (2.11)$$

where f'_{co} is the in-place strength of unconfined concrete; ε_{o1} and ε_{o85} are the strain at peak and 85% of the peak unconfined strength respectively; and ε_c and ε_{cu} are strain and ultimate strain in concrete compression respectively.

Figure 2.3 shows the stress-strain relationships of unconfined and confined concrete with key stresses and strains definitions. It also shows the possible enhancement of the strength and ductility of the confined concrete compared to that of the unconfined concrete. In this study, it is found that this model is the most suitable model for its capability to include the characteristics changes of the concrete mechanical properties with the change in the reinforcement details. This is essential to capture the changes in the concrete strength and deformation capacity when the lateral reinforcement is damaged due to corrosion. The following expression (Saatcioglu and Razvi (1992)) is used for the parabolic ascending part, where coefficient k is found based on the materials and geometric properties of the RC column (Saatcioglu and Razvi 1992).

$$f_{cc} = f'_{cc}\left[2\frac{\varepsilon_c}{\varepsilon_1} - \left(\frac{\varepsilon_c}{\varepsilon_1}\right)^2\right]^{1/(1+2k)} \text{ for } \varepsilon_c \le \varepsilon_{o1} \quad (2.12)$$

where f_{cc} refers to the compressive stress in confined concrete.

2.4.2 Stress-strain relationship of concrete in tension

In this study, the stress-strain relationship of the concrete subjected to tension proposed by Gilbert and Warner (1978) is used to estimate the concrete contribution to the resistance of the tensile strain region of the RC sections subjected to flexure. As shown in Figure 2.1.4, the concrete in tension is assumed to behave linearly up to the cracking strain, where the modulus in tension is assumed equal to the initial tangent modulus of the concrete in compression, followed by a linear descending curve that represents strain softening.

2.4.3 Constitutive model for steel

Reinforcing steel is assumed to have the same stress-strain relationship in both tension and compression provided that no local buckling of the rebars is expected. For an accurate representation of the steel in nonlinear numerical modeling of RC elements, the actual stress-strain data collected from tensile tests can be used. However, this would result in a complicated non-generalized modeling approach. On the other hand, three simplified representations of the stress-strain relationship of the steel, namely bilinear, tri-linear, and multi-linear stress-strain relationships, are widely used. In all these representations, the elasto-plastic behavior is simplified with or without including the strain hardening stage. In most cases, using such simplified relationships has provn to give reasonable accuracy when compared to experimental results.

A tri-linear relationship is considered adequate for the simulation of the steel stress-strain relationship whereas the strain hardening effect is simulated by assuming the slope of the second and third lines on an energy basis. This study uses a modified tri-linear relationship using bi-linear relationship up to the start of the strain hardening stage and a parabola afterwards up to

ultimate. The modified tri-linear expressions of the stress-strain relationship of black steel adopted from Yalcin and Saatcioglu (2000) used here and illustrated in Figure 2.5 follow:

$$f_s = E_s \varepsilon_s \quad \text{for } 0 \leq \varepsilon_s \leq \varepsilon_y \tag{2.13}$$

$$f_s = f_y + \left(\varepsilon_s - \varepsilon_y \right) \left(\frac{f_{sh} - f_y}{\varepsilon_{sh} - \varepsilon_y} \right) \quad \text{for } \varepsilon_y \leq \varepsilon_s \leq \varepsilon_{sh} \tag{2.14}$$

$$f_s = f_y + \left(f_u - f_y \right) \left[2 \frac{\varepsilon_s - \varepsilon_{sh}}{\varepsilon_u - \varepsilon_{sh}} - \left(\frac{\varepsilon_s - \varepsilon_{sh}}{\varepsilon_u - \varepsilon_{sh}} \right)^2 \right] \quad \text{for } \varepsilon_{sh} \leq \varepsilon_s \leq \varepsilon_u \tag{2.15}$$

where f_y, f_{sh} and f_u are yield, strain hardening and ultimate stresses respectively; ε_y, ε_{sh}, ε_u are the corresponding strains; f_s, E_s and ε_s are stress, modulus of elasticity and strain in reinforcing steel respectively It is important to mention here that the given stress-strain relationships are for non-corroded steel. For corroded steel, the yield and ultimate stresses and strains are updated according to Eqs.2.4 through 2.6.

2.5 Proposed procedure for nonlinear sectional analysis

The details of the proposed nonlinear sectional analysis procedure of aging RC beam-columns that has local corrosion damage and subjected to axial and/or flexural loads is presented in this section. The objectives of the development of this procedure are to ensure its capability to model the behavior of aging beam-columns at the section level and to being numerically stability. The procedure is based on: (i) assuming linear strain distribution; (ii) adopting popular nonlinear material stress-strain models (as presented earlier); (iii) using visual inspection to locate and measure the corrosion damaged zones dimensions and state of damage; (iv) identifying the level of corrosion damage of the steel reinforcement and hence quantifying the current density (i_{corr}), assuming that the corrosion rate was constant up to the level of damage identified; (v) quantifying the stiffness deterioration based on the changes in the geometrical and material

properties of the section; and (vi) satisfying the equilibrium of internal and external forces throughout the nonlinear analysis process.

2.5.1 General assumptions and strain distributions

The proposed procedure is an incremental iterative nonlinear technique using numerical integration of the sectional stresses and satisfying force equilibrium in every load increment step. It takes into account the changes in the geometrical and materials properties due to the localized corrosion damage. The shear deformations over the cross section are assumed very small and negligible. Henceforward, Bernoulli-Navier hypothesis of plane sections before deformations remain plane after deformations is assumed valid, which results in linear strain distributions over the cross section. If the bond between the steel and concrete is active, then the strains in the concrete and reinforcing steel normal to the cross sections are linearly proportional to the distance from the instantaneous neutral axis throughout all the steps of the nonlinear analysis. In case no corrosion takes place in the reinforcement, the local bond slip is included by assuming a homogenized softening behavior (Rasheed and Dinno 1994). While in the case in which reinforcement is affected by corrosion and the bond has locally failed, the proposed local bond failure and resulting stress redistribution mechanism presented earlier are incorporated.

Assuming the linear strain distribution over the cross section, Figure 2.6 shows the external forces (axial force and moment) acting on a cross-section of an RC member and all the possible resulting strain distributions. For the general loading of a beam-column, three major strain distributions are shown: (i) pure flexure strain distribution due to lateral loading (Figure 2.6-c); (ii) constant compressive strain distribution due to concentric axial loading (Figure 2.6-d); and (iii) combined flexure & axial strain distribution due to combined axial and lateral loading or eccentric axial loading (Figures 2.6-e through 2.6-g). Depending on the ratio of the axial to

flexural strains, there are three possibilities of strain distributions; case iii-1: variable compressive strain over the section with compressive strain at both extreme fibers (see Figure 2.6-e); case iii-2: variable compressive strain over the section with compressive strain at one extreme fiber and zero strain at the other extreme fiber (see Figure 2.6-f); case iii-3: strain varies from maximum compressive at one extreme fiber to maximum tensile at the other extreme fiber over the section (see Figure 2.6-g).

2.5.2 Concepts, member rigidities and sectional forces using numerical integration

It has been found that explicit forms based on mathematical integrations to calculate the forces and the stiffness could result in a numerically sensitive model. The use of semi-analytical and numerical integration of the stresses over the cross section is proposed by many studies (Carol and Murcia 1989, Zeris and Mahin 1988). In these studies, the section is usually divided into a finite number of strips over which the stress is assumed constant. However, none of these studies use direct numerical integration for the calculation of the sectional forces and the stiffness. Carol and Murcia (1989) proposed a semi-analytical approach in their nonlinear model of reinforced concrete. Zeris and Mahin (1988) proposed a model using the flexibility method, where the forces are calculated using numerical integration. In their formulation of the flexibility matrices, a mix of tangent and secant concrete moduli is used, and the formulation is based on the application of a constant axial force and then the gradual increase of the lateral (flexural) forces. In both papers above, the validation and verification of the procedures are not mentioned.

In the present study, the forces and stiffness are calculated using numerical integration. The concepts of the procedure presented here are based on the sectional analysis approach developed by Rasheed & Dinno (1994). However; Rasheed & Dinno's approach does not take into account

the variation of mechanical properties of the core concrete for different lateral reinforcement spacing.

In the proposed nonlinear sectional analysis (NLSA) procedure, the forces on the cross section are calculated using numerical integration. The cross section is divided into finite number of strips of width equal to the width of the cross-section and thickness equal to t_{ci} (see Figure 2.7-a). Figure 2.7-b, shows the instantaneous strain distribution over the cross section as a result of combined axial and flexural forces acting on the cross section at any loading step after concrete cracking. Figure 2.7-c shows the stress distribution related to the strain distribution in Figure 2.7-b. The stresses of the concrete in compression (above the inelastic centroid) vary from zero to a maximum stress at the extreme compression fiber. However, the stresses of the concrete in tension (below the inelastic centroid) increase up to the concrete tensile strength and then drop to zero at ten times of the concrete fracture tensile strain (see Figure 2.4). The concrete that has no tensile resistance is ignored (see Figures 2.7-a through 2.7-c). The stresses on the reinforcement are related to the strains at the center of the rebar as shown in Figure 2.7-b. The forces acting on the section, which are the summation of each of the forces on the strips, are shown in Figure 2.7-d.

The overall axial rigidity (EA) is the summation of the area of each of the individual strips times the corresponding modulus of elasticity related to the level of stress acting on that strip, i.e.,

$$EA = \sum_{i=1}^{NRS} E_{ci}\, B_{ci} t_{ci} + \sum_{j=1}^{N} (E_{stj} - E_{cj}) A_{stj} \qquad (2.16)$$

where NRS is the number of strips in the section; N is the number of reinforcement layers; $E_{ci}, B_{ci}\ and\ t_{ci}$ are concrete modulus, width, and thickness of strip (i); E_{sti} is the reinforcement

modulus; E_{cj} is the concrete modulus at reinforcement level; and A_{sti} is the corresponding reinforcement area.

The overall flexural rigidity (EI) is the summation of the individual concrete strips and reinforcement layers flexural rigidities about the inelastic centriod(Y_N)

$$EI = \sum_{i=1}^{NRS} E_{ci} \cdot B_{ci} \cdot t_{ci} \cdot y_i^2 + \sum_{j=1}^{N} (E_{stj} - E_{cj}) A_{stj} \cdot y_j^2 \quad (2.17)$$

Where y_i is the distance from the centroid of strip i to the section inelastic centroid; y_j is the distance from the centroid of reinforcement layer j to the section inelastic centroid.

The internal axial force (F_x) is calculated as

$$F_x = \sum_{i=1}^{NRS} E_{ci} \cdot \varepsilon_{ci} \cdot B_{ci} \cdot t_{ci} + \sum_{j=1}^{N} (E_{stj} - E_{cj}) \varepsilon_{stj} \cdot A_{stj} \quad (2.18)$$

where ε_{ci} is the concrete strain of strip; ε_{sti} is the strain of reinforcement layer.

The internal bending moment (M_{in}) is calculated as

$$M_{in} = \sum_{i=1}^{NRS} E_{ci} \cdot \varepsilon_{ci} \cdot B_{ci} \cdot t_{ci} \cdot y_i + \sum_{j=1}^{N} (E_{stj} - E_{cj}) \varepsilon_{stj} \cdot A_{stj} \cdot y_j \quad (2.19)$$

2.5.3 Proposed numerical procedure

The numerical nonlinear sectional analysis (NLSA) proposed in this study is developed for two cases (i) as an independent model for the direct evaluation of the ultimate capacity of an RC beam-column subjected to reinforcement corrosion by assessing the critical section(s); and (ii) to be integrated in a non-linear finite element analysis (NFEA) of an RC beam-column subjected to reinforcement corrosion. Figure 2.8 shows the flowchart of the proposed NLSA, where the input data at the top of the flowchart and the end (or return) are different for the two cases. As

mentioned earlier and in order to cover all the possible ratios of axial compressive to flexural stresses, the proposed NLSA considers all the possible strain distribution cases shown in Figure 2.6.

The procedure starts by calculating the stress-strain parameters. According to the applied axial force and moment, the preliminary strain distribution over the section is defined to identify whether the compressive stresses are dominant and only compressive stresses are distributed over the section. On the other hand, if the flexural stresses are dominant, then the procedure develops variation of stresses from tension to compression over the section. For simplicity, the subscript “top” and “bot” refer to the extreme top fiber and extreme bottom fiber of the section, respectively.

Once the strain distribution is defined, then the instantaneous stresses in the concrete and the steel together with the axial rigidity (EA) and the flexural rigidity (EI) for all concrete strips and steel reinforcement layers are calculated. The axial force (P) is then transferred to the most recently evaluated location of the inelastic centroid, Y_N,(see Figures 2.7-b and 2.8), and the effective moment(M_o)about this centroid is calculated according to:

$$M_o = M + P * (Y_G - Y_C) \tag{2.20}$$

The curvature of the section (φ) and the axial strain at the inelastic centroid (ε_o) are calculated from the applied load and moment and the most recent values of axial and flexural rigidities. Hence it is possible to quantify the strain distribution over the section at this stage:

$$\varphi = \frac{M_o}{EI}, \quad \varepsilon_o = \frac{P}{EA} \tag{2.21}$$

The current position of the neutral axis (Y_o)is calculated from its distance from the most recent inelastic centroid:

$$Y_o = \frac{\varepsilon_o}{\varphi} \tag{2.22}$$

$$Y_N = Y_o - Y_C \tag{2.23}$$

The compressive and tensile zones of the section and hence the strips and steel strains within them are defined based on the extreme (top and bottom) fiber strains;

$$\varepsilon_{top} = \varphi \cdot (H + Y_N), \quad \varepsilon_{bot} = \varphi \cdot Y_N \tag{2.24}$$

The internal axial force and bending moment together with the section rigidities are then calculated for the present strain distribution using Eqs. 2.16 through 2.19. The equilibrium is then checked satisfying a predefined acceptable tolerance through an iterative process to find the right location of the inelastic centroid and hence the location of the neutral axis. In the following case studies for example, the tolerance is such that the difference between the absolute values of the sum of the compressive and tensile forces should be less than 0.001 kN or 1.0 N. Failure is defined in the proposed NLSA as either by the concrete crushing (when the strain of the extreme compressive fiber reaches the maximum strain) or the failure of the steel in tension (see Figure 2.8).

2.5.4 Numerical stability of the proposed procedure

The procedure proposed by Rasheed & Dinno (1994) is efficient only when limited computing abilities (low memory and computing speed) are available to the user, which was the case when the procedure was originally developed. However, this procedure is numerically sensitive when adjusting the load steps and tuning the convergence parameters as suggested by Rasheed &

Dinno taking a very long time. The use of this procedure may require a time consuming case by case convergence study, and in the case of highway bridge columns with high axial stresses compared to flexural stresses (due to the low eccentricity in most cases), it is very difficult to satisfy the convergence of the model even if small load increments are used.

As shown earlier, the proposed NLSA uses numerical integration to calculate the internal forces on compressive and tension stiffening zones. The procedure involves iterative cycles to find the most accurate location of the inelastic centroid and hence the instantaneous neutral axis location. The approach promises to be numerically efficient with steady convergence in all the studied cases. With the very high processing speed of recent computers, the high computation efforts in terms of number of arithmetic tasks required to perform the proposed NLSA does not result in a long performance time. However, the high computational stability and simplicity enable the effective integration of the procedure into the nonlinear finite element analysis.

2.6 Case studies

The proposed sectional model is verified and evaluated through the comparison with available analytical and experimental results and by a demonstration through an evaluation of the structural behavior of a beam-column subjected to axial load, moment and reinforcement corrosion. Four case studies have been conducted and are presented in the following subsections. Case studies 2.6.1 through 2.6.3 verify the ability of the proposed NLSA approach to simulate the nonlinear structural behavior at the section level with high accuracy and with reasonable conservativeness. Case study 2.6.4 demonstrates the capability of the proposed approach to quantify the nonlinear changes of the column structural parameters, such as structural capacities, rigidities, ductility, etc, at the section level.

2.6.1 Verifications of the proposed NLSA on a non-corroded RC beam (no confinement)

The NLSA procedure developed in this study is verified against the example presented by Rasheed and Dinno (1994), in which they compared their model results to the test results reported by Espion and Halleux (1988). Rasheed and Dinno (1994) proposed an incremental iterative algorithm where nonlinear sectional response was traced using explicit expressions for the nonlinear sectional forces and stiffness. Espion and Halleux (1988) test was carried out on a rectangular RC beam of 3 span and 150 mm wide by 280 mm deep section. The beam was tested under two different loading conditions: (i) under lateral load only using four points load set up (or simply supported beam under two point loads at one and two thirds of the span); and (ii) under axial load of 200 kN fully applied prior to the application of the lateral loads, which were increased up to failure using the same four-point load set up as in (i). The beam was reinforced for shear only in the two support zones (the left and right thirds of the beam), while the mid span zone (between the two loads) has no shear reinforcement (Figure 2.9).

For the loading case (i), the resulting moment-curvature of the proposed NLSA for the mid-span section throughout the applied loading is compared with the related results of Rasheed and Dinno (1994) as well as results from Response 2000 (Bentz 2000). Figure 2.10 shows that the proposed model conservatively gives a very slight underestimation for the moment and a very slight overestimation of the curvature when compared to other model. The flexural and axial rigidities are functions of the material and section properties and in the non-linear analysis, their instantaneous values depend on verifying equilibrium at the section level. When both rigidities are related to the variation of the moment at successive loading steps, they reflect the damage and deterioration of the section from the non-cracked stage to the failure stage. The deterioration in the flexural and axial rigidities with the increase of the applied moment predicted by the proposed NLSA compared to those rigidities predicted by Rasheed and Dinno (1994)’s model is

shown in Figure 2.11 for the case of no axial load. The figure shows a good match between the two analytical approaches, where the proposed approach gives a slightly conservative estimation of the rigidities. The conservative estimation of the strength, deformations, and rigidities in the new model could be explained by the conservative estimation of the modulus of elasticity of the concrete in the nonlinear numerical process using the secant modulus method.

For the loading case (ii), the NLSA result for moment-curvature relationships are compared with the original test data reported by Espion and Halleux (1960) and adopted by Rasheed and Dinno (1994). Espion and Halleux (1960) mentioned that there was a delay in the initiation of the curvature up to a large bending moment had been applied. This was not indicated in Rasheed and Dinno study (1994). The moment-curvature relationships in both papers are presented as if they are started from the point of zero moment and zero curvature. However, the axial force (and the resulting compressive stress) is delaying the development of the tensile stress as the applied moment is increasing during the loading process. The curvature does not start to have a value until the tensile strain is developed in one of the beam-column faces. In the proposed NLSA results, it has been found that the curvature in the moment-curvature relationship starts to have a value only after the applied bending moment reached a specified level (for instance, 20 kN.m) in the load incremental process as shown in Figure 2.12. The rest of the moment-curvature relationship for the mid-span section according to the proposed NLSA compares well with the related test results of Espion and Halleux (1960). Again, the proposed model gives more conservative results for the same reason mentioned earlier.

The deterioration in the flexural and axial rigidities with the increase of the applied moment for loading case (ii) predicted by the proposed NLSA compared to those rigidities predicted by Rasheed and Dinno (1994)’s model is shown in Figure 2.13 when an axial load of 200 kN is pre-

applied. In high moment, the figure shows a good match between the two approaches where the proposed approach gives again a slightly more conservative estimation of the rigidities.

2.6.2 Verifications of the proposed NLSA on a non-corroded RC column (with confinement)

The objective of this case study is to verify the capability of the proposed NLSA model to simulate the effect of confinement on the core concrete in an RC column subjected to pure axial compression. Previous non-linear sectional analysis approaches have been mainly developed for the case of pure flexural behavior or flexural-dominant behavior where low axial compression is combined. However, in many cases, columns are subjected to either an eccentric compressive force or a compressive force with slight eccentricity, and hence the column is considered as an "axial-load dominant" column.

As mentioned earlier, the proposed procedure involves the stress-strain relationship for confined and non-confined concrete suggested by Saatcioglu and Razvi (1992). In their study, they provided results of their tests performed on different RC columns where the column studied herein is selected for comparison. The column has a 250 mm x 250 mm square cross section, and 1500mm height with a clear concrete cover of 10 mm. The concrete compressive strength (using standard cylinder test) $(f_c^{'})$ is 60 MPa. The longitudinal reinforcement is 8 No 15 rebars (16mm in diameter) with steel yield strength of 450 MPa and equally spaced all around the column's four sides. The volumetric ratio (ρ_s) of the lateral reinforcement is 1.4% and the spacing of transverse reinforcement is 85mm. The column is tested under monotonically increased axial compressive force and the results are plotted in terms of compressive stress σ versus compressive strain ε (i.e. averaged measured strain) at the column mid height. Figure 2.14 shows a good agreement between the test and the proposed NLSA results when the confinement of the core concrete is taken into account. The figure also shows that when the concrete confinement is

ignored, the proposed NLSA gives a very poor match to the experimental results, and the estimated strength and deformations are significantly lower than the test results.

2.6.3 Beam subjected to flexure and reinforcement corrosion

Among the available previous studies, very limited details are provided about the corrosion process and the detailed mechanical properties of the materials. In the present study, one of specimens tested by Ballim et al. (2001) (Beam 1/2; or series 1, beam 2) has been selected for comparison. The objective of Ballim et al. (2001)'s study was to assess the effects of reinforcement corrosion on the structural performance of the beam when loaded up to its ultimate capacity. From Ballim et al. (2001)'s selected beam has 1,550 mm overall length with cross section dimensions of 160 mm by 100 mm. The concrete compressive strength (using standard cylinder test) (f_c') is 40 MPa. A single 16 mm, deformed high tensile steel bar (Y16) with 0.2 % offset proof stress of 574 MPa was used as the tensile reinforcement and two 8 mm smooth mild steel rebar were used for the compressive and shear reinforcement. The shear stirrups were only distributed in the two support zones with 60 mm spacing, and the clear concrete cover was 32 mm.

The beam was tested using a four-point load setup over the 1,050 mm overall span, length leaving two out of support overhang spans of 250 mm in length. The central span (between the simple supports) was divided into three equal parts of 350mm each. The two loads were applied using springs supported by a rigid frame. The beam was tested under 23 % and 34 % of its design ultimate load capacity and subjected to an accelerated corrosion process at main tensile reinforcement, where the current density (i_{corr}) was 0.4 mA/cm^2 applied for 30 days. The corrosion was accelerated by impressing a DC current on the main tension steel while the loads

were applied. The central deflection was monitored over 30 days. Figure 2.15 shows that the proposed NLSA gives a large underestimation for both, the load and the displacement. According to Ballim et al. (2001), this specimen developed early yielding and concrete crushing. The proposed NLSA results show large underestimation compared to the test results. It has been reported that corrosion-induced damage in accelerated corrosion studies depend on the level of current density applied. Hence, the large underestimation of NLSA in this case study can be explained by the underestimation of steel strength and ductility using the adopted empirical equations (Eqs. 2.4-2.6). This mentioned empirical equations are based on lower current density rate than the current density used by Ballim et al. (2001).

2.6.4 Beam-Column subjected to axial load, moment and reinforcement corrosion

The objective of the following case study is to present the capabilities of the proposed model in simulating the nonlinear behavior of beam-columns subjected to reinforcement corrosion combined with axial load and moment. A 3m height column fixed at both ends shown in Figure 2.16 is designed for this purpose. The column has 8 rebars of 20 mm diameter as longitudinal reinforcement and 10 mm diameter ties (lateral reinforcement) distributed at 50 mm center to center. The cross section (see Figure 2.6) is 350 mm by 350 mm, and the cover is 25 mm (or 20 mm clear cover). The concrete compressive strengths (f_c') is 30 MPa while the longitudinal bars have a yield strength (f_y) of 400 MPa, ultimate strength (f_u) of 460 MPa and a strength upon which strain hardening starts (f_{sh}) of 420 MPa. The column is loaded up to failure by increasing the eccentric axial load with constant eccentricity (15% of the column depth in the traffic direction).

It is assumed that a preliminary assessment using visual inspection would provide details about corrosion-induced damage and the critical section in the corrosion-affected zone. Assuming that

the load eccentricity is only in one direction, the possible damage states of a critical section of the beam-column as shown in Figure 2.17 are: (a) no damage, which is considered to be the control case; (b) concrete covers spalling off two sides parallel to the eccentricity plane; (c) concrete covers spalling the tension side opposite to the axial compressive load eccentricity direction (ACLED); (d) concrete cover spalling off two sides perpendicular to the ACLED;(e) concrete cover spalling off all sides; (f) loss of stirrup and local drop of the confinement. The corrosion affected zone in this case study is assumed to be over a half meter from the lower support where the critical design moment and design shear sections are located.

Figure 2.18 shows the moment-curvature of the column at a critical corrosion section close to the column base as shown in Figure 2.17 for the different cases mentioned earlier (case(a) through case (f) above) in addition to the one extreme case of complete loss of confinement. The figure shows the drop in the strength and ductility in terms of the ratio of the ultimate displacement to the yield displacement. In this case study, the bond loss due to the corrosion is considered in the NLSA when the flexural stresses are developed throughout the loading stages and the tensile stresses are developed in the tension side of the sections at the bond failure zone. The high axial load reduces the effect of bond loss in this case study. As the proposed NLSA approach has been verified in the previous case studies, given acceptable results, it is believed that the proposed approach gives reasonably conservative estimations of the structural performance of the discussed column. However, verification with experimental data is needed to investigate the accuracy of the proposed model in different beam-column loading cases and boundary conditions. Figures 2.19 and 2.20 show the change in the flexural and axial rigidities of the critical cross section due to different cases of deterioration when the column is loaded up to failure. These figures show the drop of the rigidities with the growth of the applied moment

(which results from the eccentricity of the load in this case). Figure 2.21 shows the changes in the interaction diagram of the column when subjected to different damage cases.

2.7 **Conclusions**

A simplified yet comprehensive nonlinear sectional analysis approach (NLSA) of aged RC structures based on numerical integration, visual inspection, and minimum material testing and simplified empirical estimation of the deterioration due to reinforcement corrosion has been presented in this chapter. It can be used to perform sectional analysis of aged beam, column, and beam-column elements subjected to service or ultimate loads combined with reinforcement corrosion. The procedure is also developed to be part of a numerically efficient nonlinear finite element analysis (NLFEA) proposed in the next chapter (see Mohammed et al. 2014b). The nonlinear element stiffness in the proposed NLFEA is based on the nonlinear rigidities at the section level derived in this chapter.

The proposed NLSA is capable to simulate the mechanical behavior of RC beam-columns at the section level for all loading situations including pure flexure, pure axial load, or any combination of axial and flexural stresses. The model is capable to integrate the visual inspection as a main source of its input together with any required geometrical measurements and material testing to identify the level of damage and the materials properties due to the reinforcement corrosion at the assessment time. Empirical equations developed by other researchers and material testing results are used to evaluate the materials properties at the visually observed corrosion damage zones. It also integrates an empirical approach that estimates the confined concrete behavior and the level of confinement based on reinforcement details. The possible bond loss, loss of lateral ties/stirrups and loss of confinement are taken into account in estimating the effects of corrosion on the structural behavior of the RC beam-column.

The numerical integration of stresses over the section, which is divided into arbitrary number of strips, improves model convergence and enables accelerated verification of equilibrium. The number of strips in the numerical integration can be calibrated together with the load steps for maximum accuracy and numerical efficiency. In all the case studies, the proposed NLSA shows high numerical stability and consistent convergence for all geometrical and material properties and loading cases.

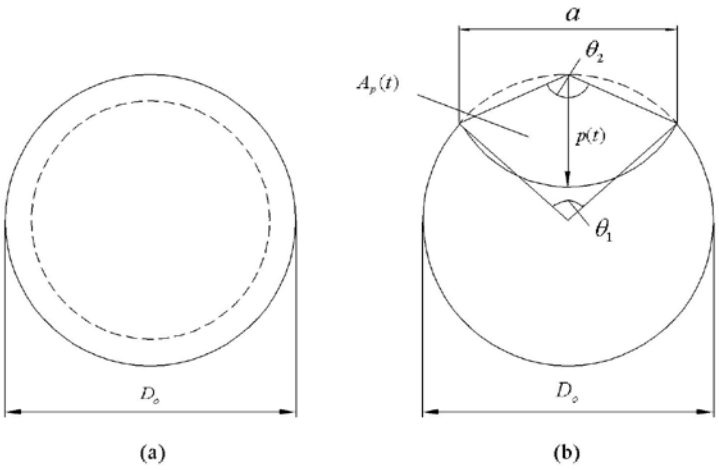

Figure 2.1: Corrosion model; (a) uniform corrosion; (b) pit configuration (after Val, 2007)

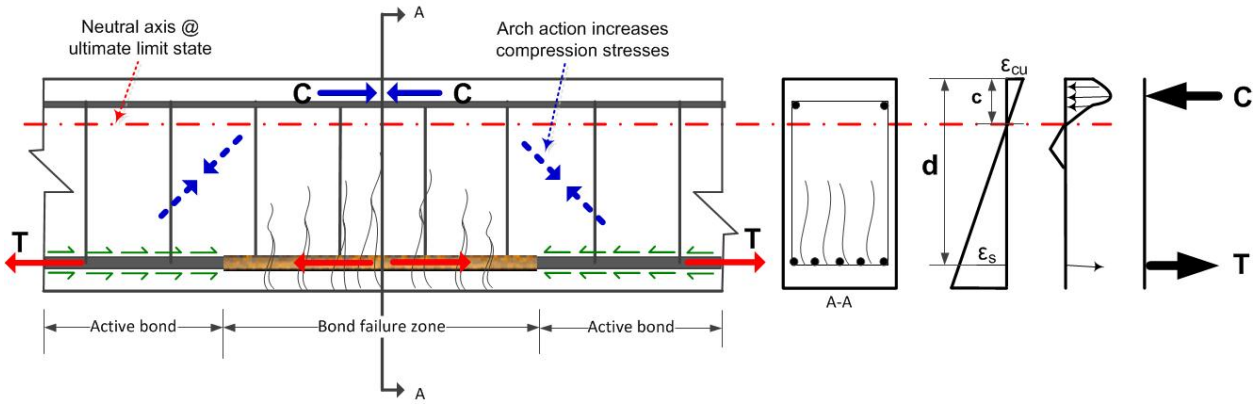

Figure 2.2: Local bond failure due to corrosion and force redistribution on a section subjected to flexure (failure at ultimate limit state).

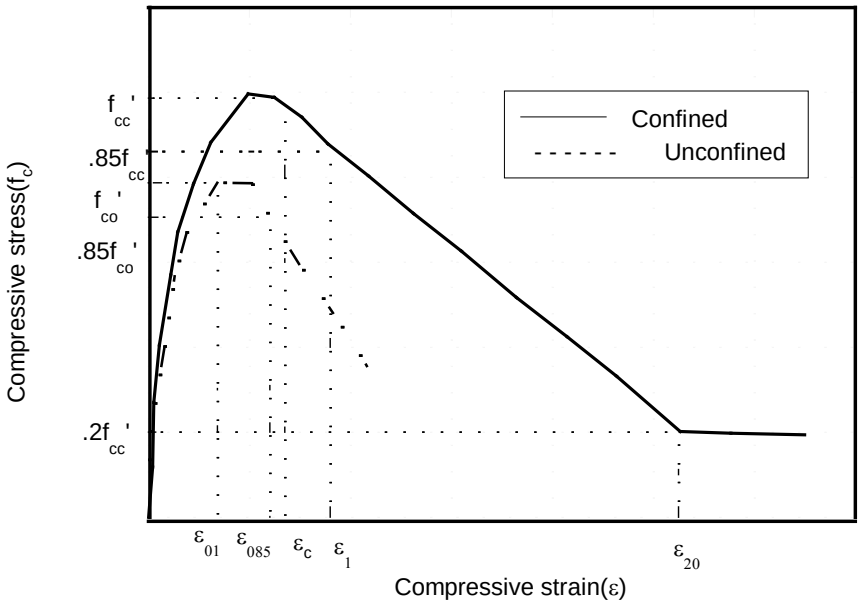

Figure 2.3: Stress-strain relationship for unconfined and confined concrete (after Saatcioglu and Razvi 1992).

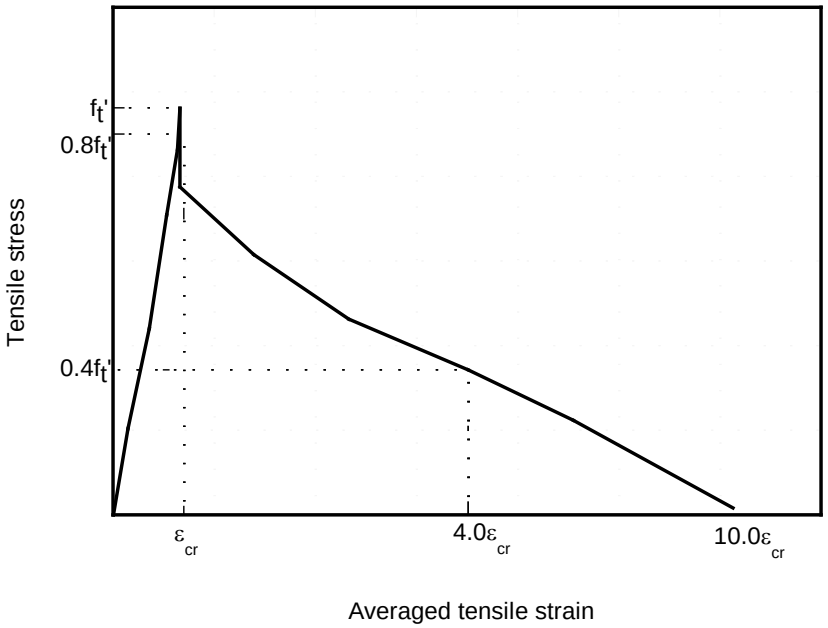

Figure 2.4: Tensile stress-average tensile strain relation (after Gilbert and Warner 1978).

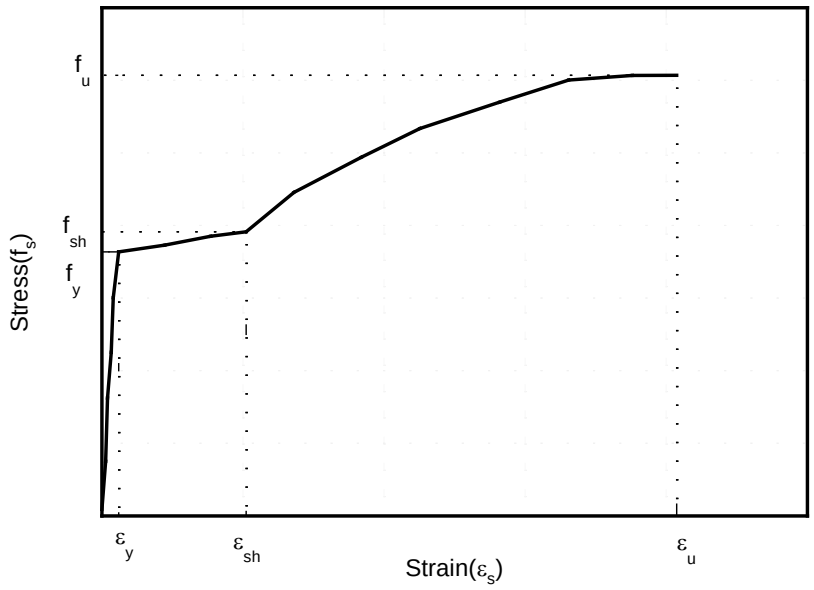

Figure 2.5: Stress-strain relationship for reinforcing steel (after Yalcin and Saatcioglu 2000).

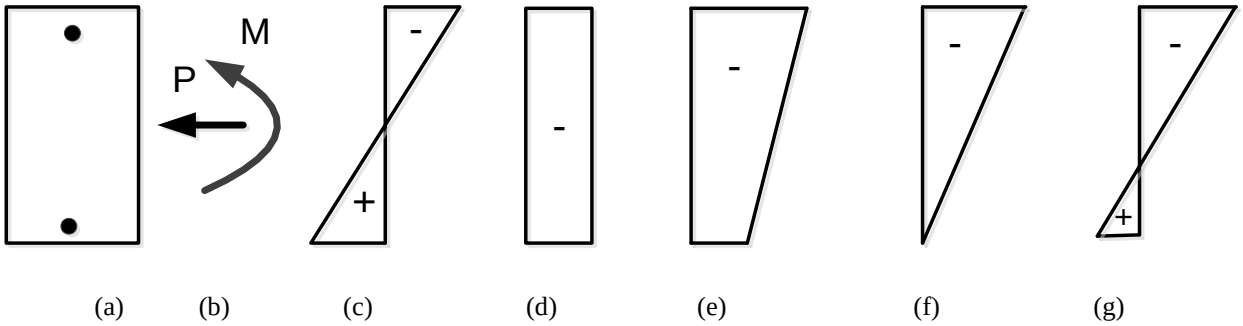

Figure 2.6: External forces on the section and possible strain distributions: (a) cross section;(b) forces on the section;(c) strain distribution due to flexure: case(i);(d)strain distribution due to axial load & flexure: case(ii);(e)strain distribution due to axial load &flexure: case(iii-1); (f)strain distribution due to axial load &flexure: case(iii-2); (g)strain distribution due to axial load &flexure: case(iii-3).

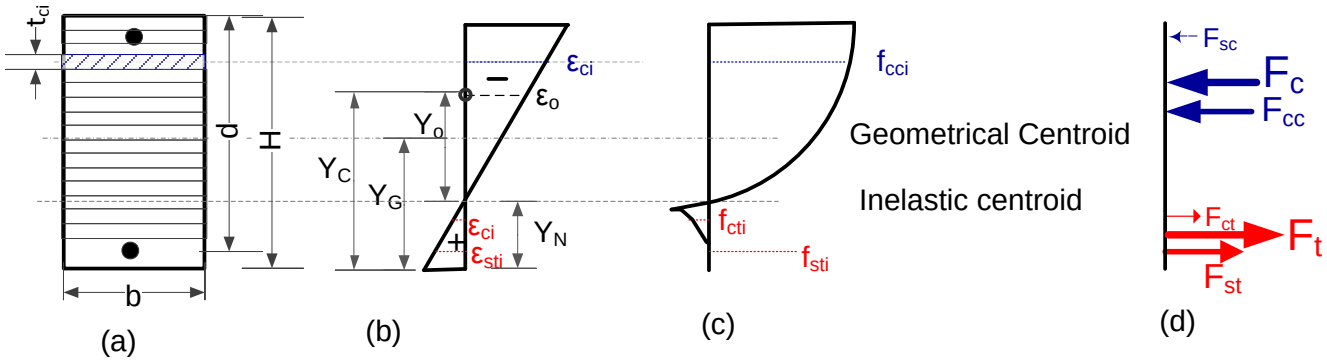

Figure 2.7: Numerical integration of nonlinear stresses over the cross section: (a) cross section divided into strips; (b) strain distribution due to axial load & flexure: ε_{ci} concrete strain, ε_{sti} steel strain; (c) stress distribution in concrete & steel: f_{cci} concrete stress at compressive level, f_{cti} concrete stress at tensile level, and f_{sti} steel stress; (d) internal forces in concrete & steel: F_c summation of internal forces of concrete($F_{cc)}$ and steel (F_{sc})in compressive level, F_t summation of internal forces of concrete ($F_{ct)}$ and steel (F_{st})in tension level .

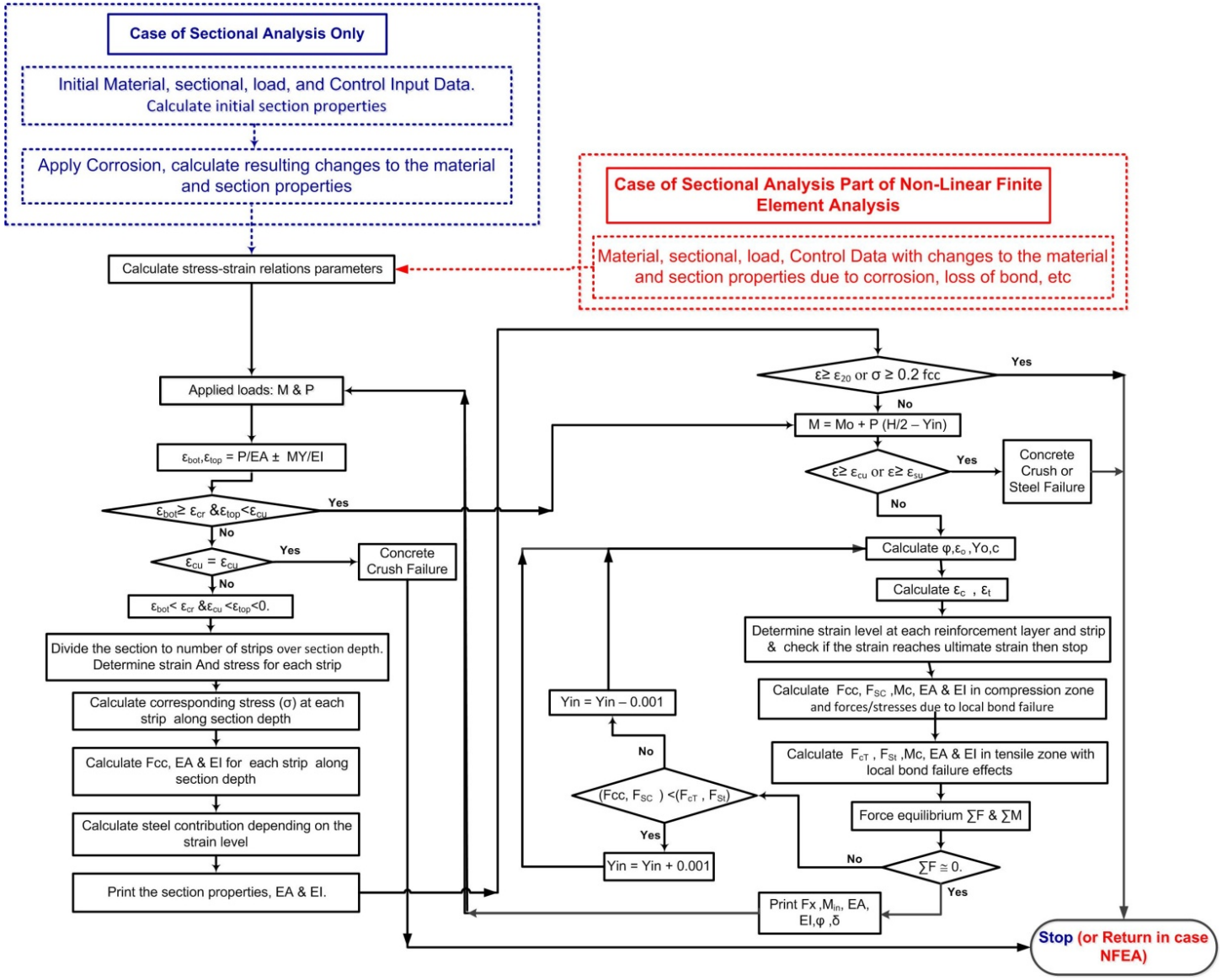

Figure 2.8: Proposed nonlinear numerical sectional analysis procedure of an RC section subjected to axial load and flexure.

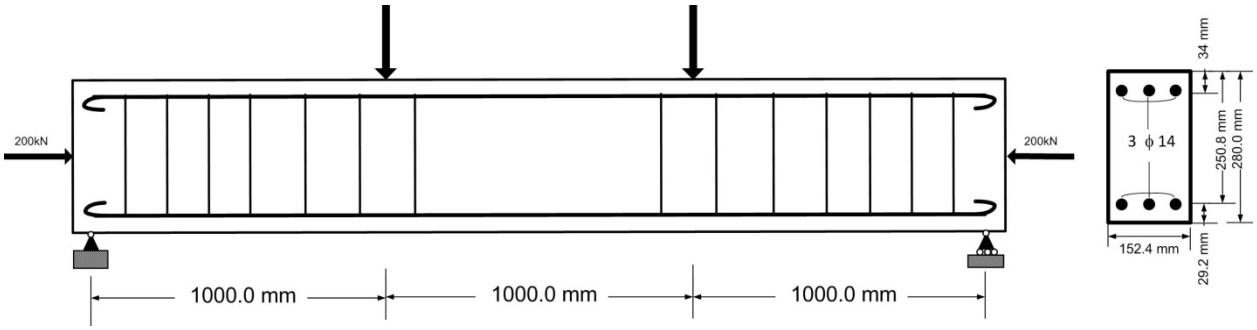

Figure 2.9: Beam under four points loading and axial load (Rashid & Dinno, 1994).

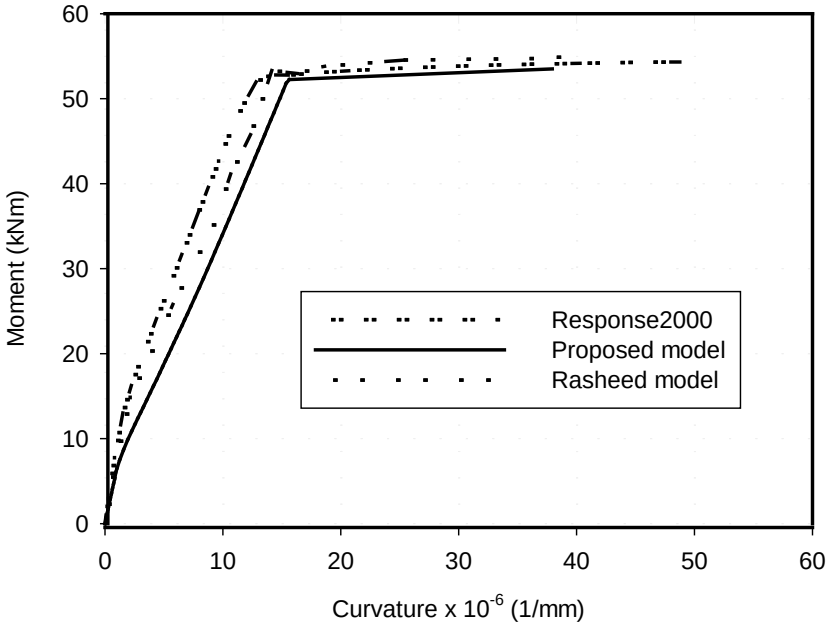

Figure 2.10: Comparison of proposed NLSA with Rasheed and Dinno (1994) and Response2000 models for load case (i) with no axial load.

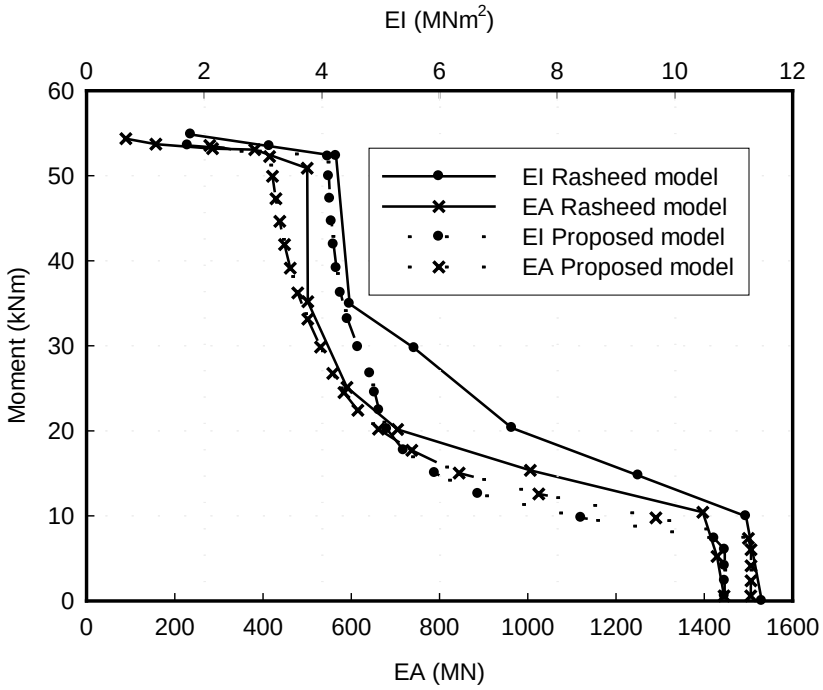

Figure 2.11: Comparison of the proposed NLSA with Rasheed and Dinno (1994) results for axial and flexural rigidities of the mid-span section, load case (i) with no axial load.

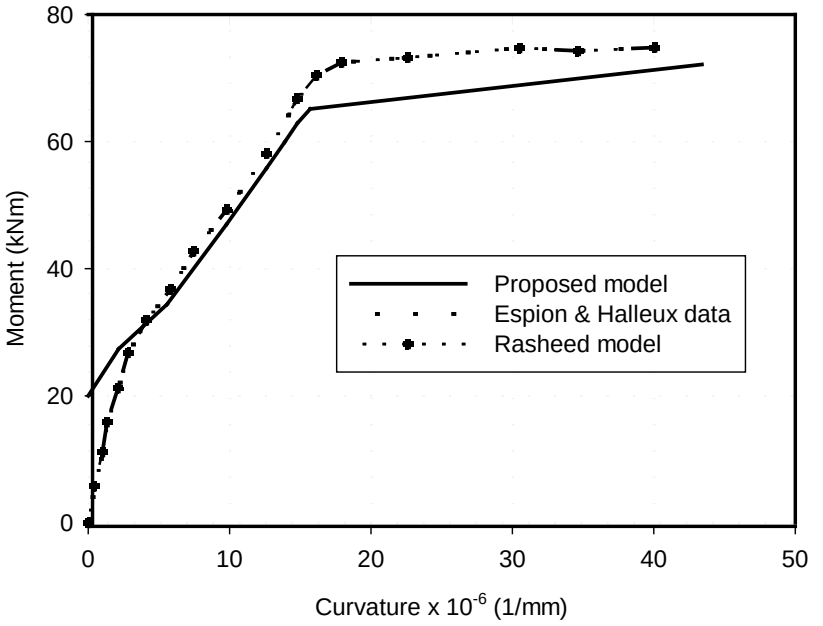

Figure 2.12: Comparison of proposed NLSA results with Espion and Halleux (1988) test results and Rasheed and Dinno (1994) results for load case (ii) with axial load.

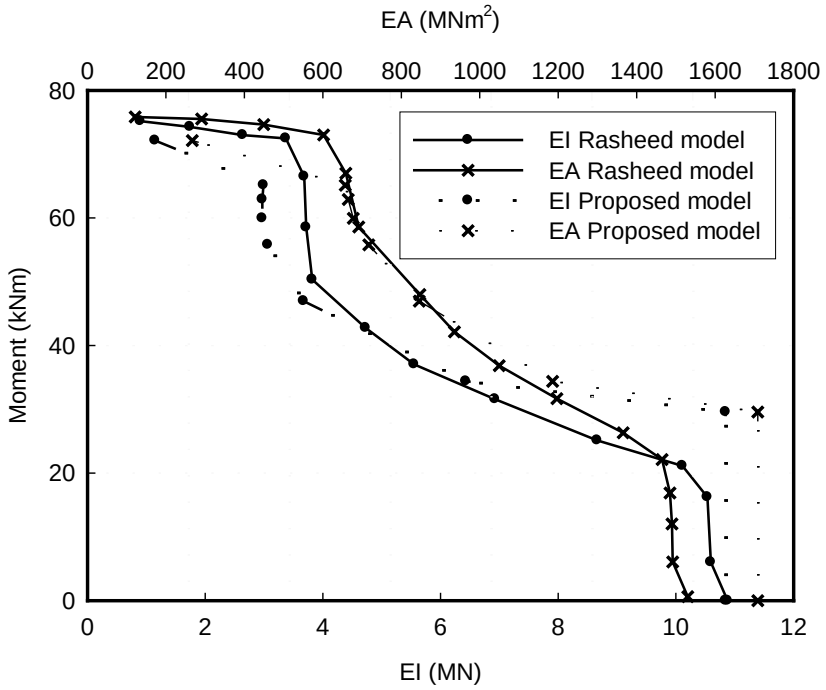

Figure 2.13: Comparison of proposed NLSA results with Rasheed and Dinno (1994) results for axial and flexural rigidities of mid-span section and for load case (ii) with axial load.

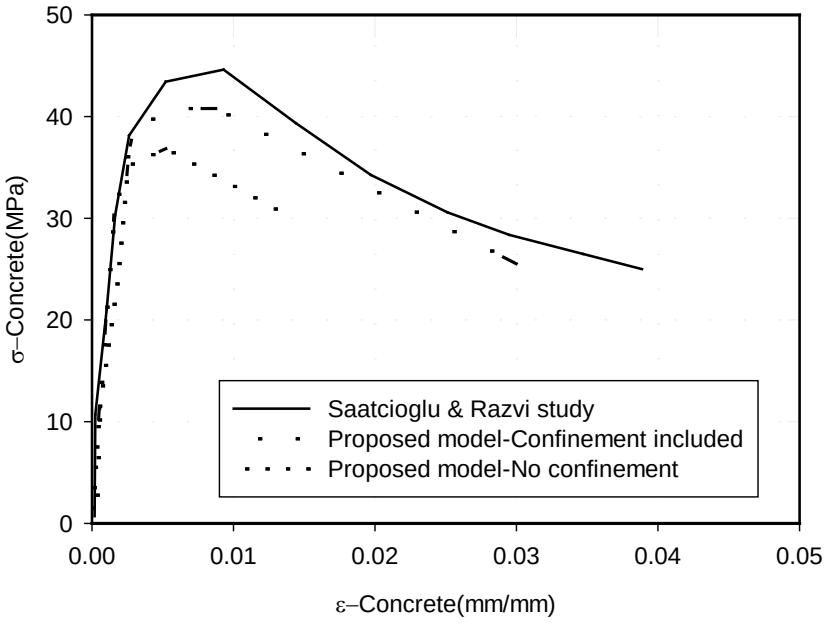

Figure 2.14: Comparison of proposed NLSA results with Saatcioglu & Razvi (1992) test results.

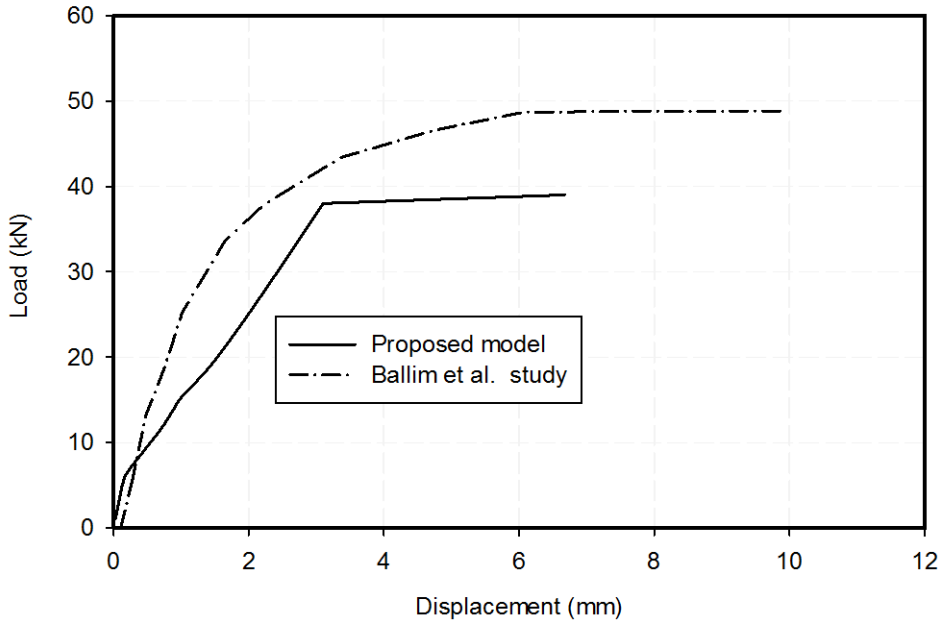

Figure 2.15: Comparison of proposed numerical integration and Ballim et al.(2001)'s test results.

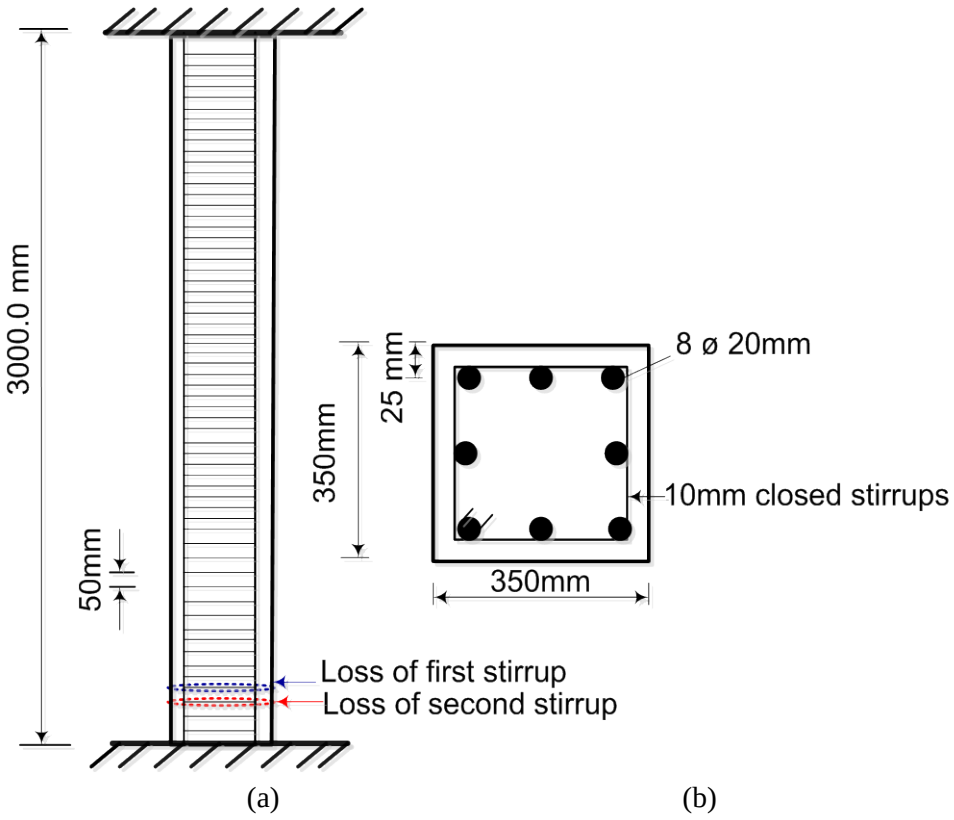

Figure 2.16: RC column under axial load and moment and subjected to reinforcement corrosion (case study 2.6.4): (a) column details; (b) cross-sectional details.

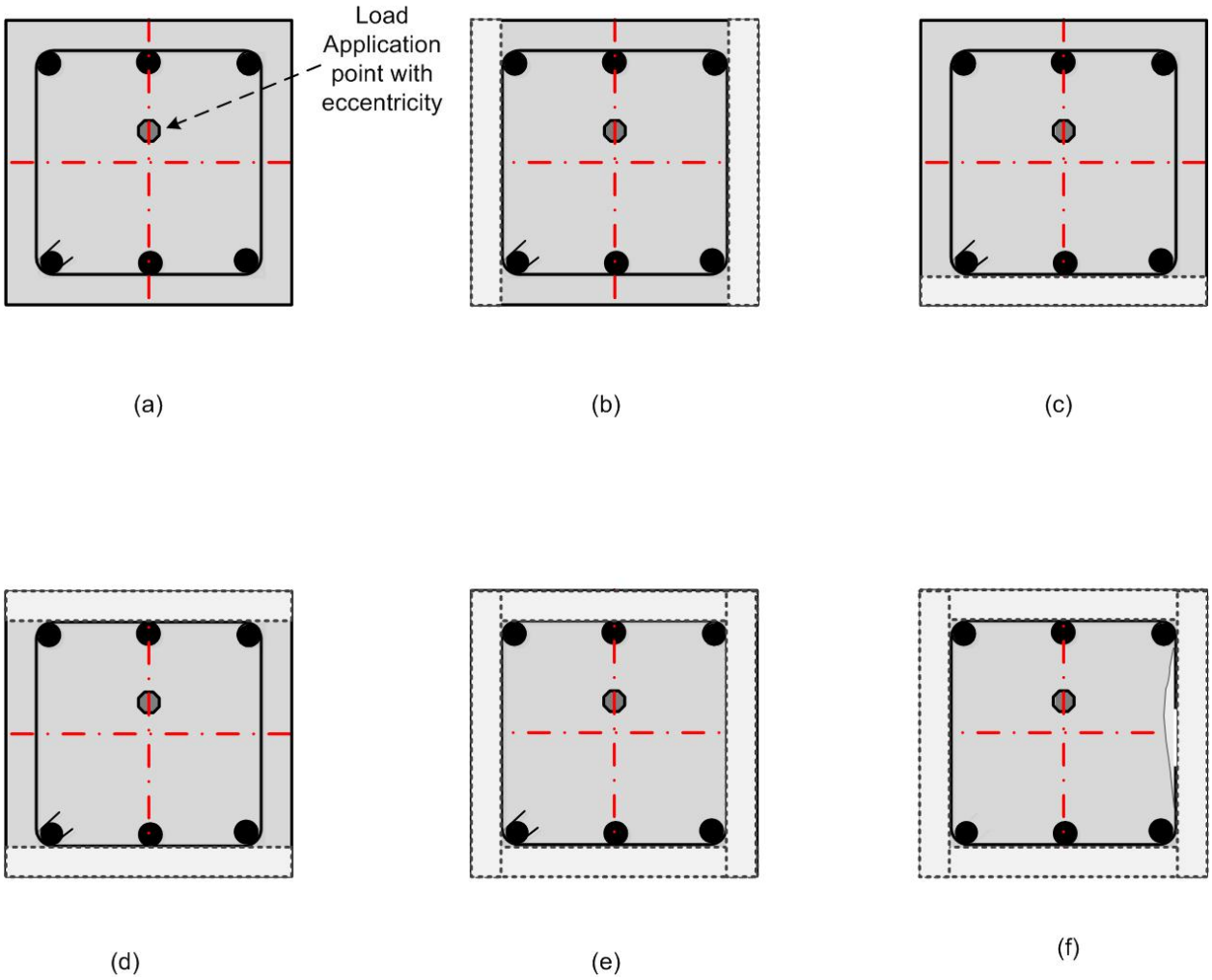

Figure 2.17: Possible damage in an RC column section due to corrosion (case study 2.6.4).

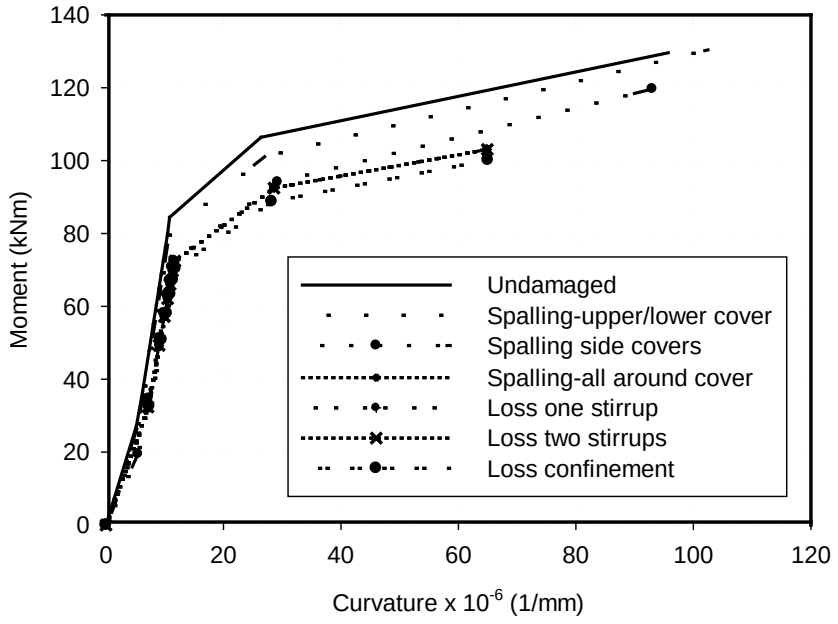

Figure 2.18: Moment curvature of an RC column section (case study 2.6.4) for different corrosion states.

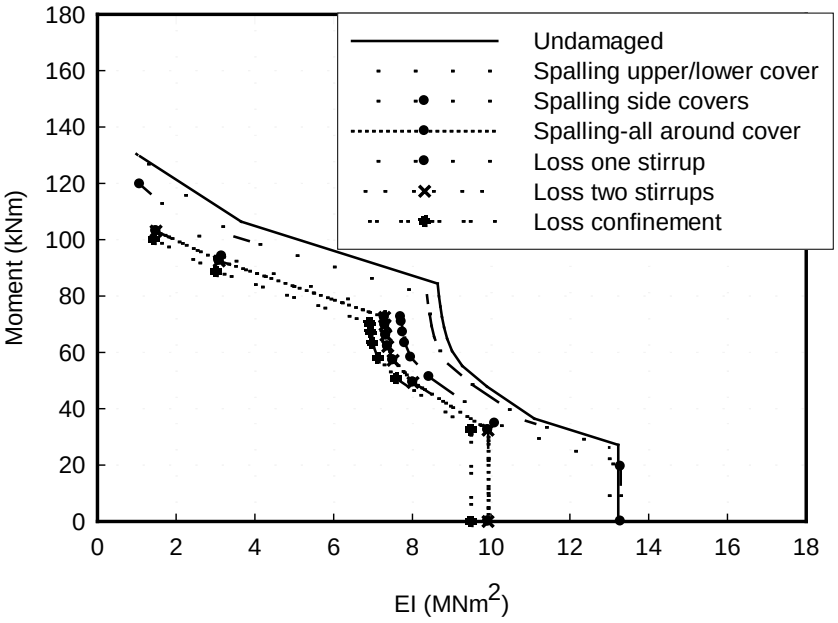

Figure 2.19: Comparison of flexural rigidity of an RC column section (case study 2.6.4) for different corrosion states.

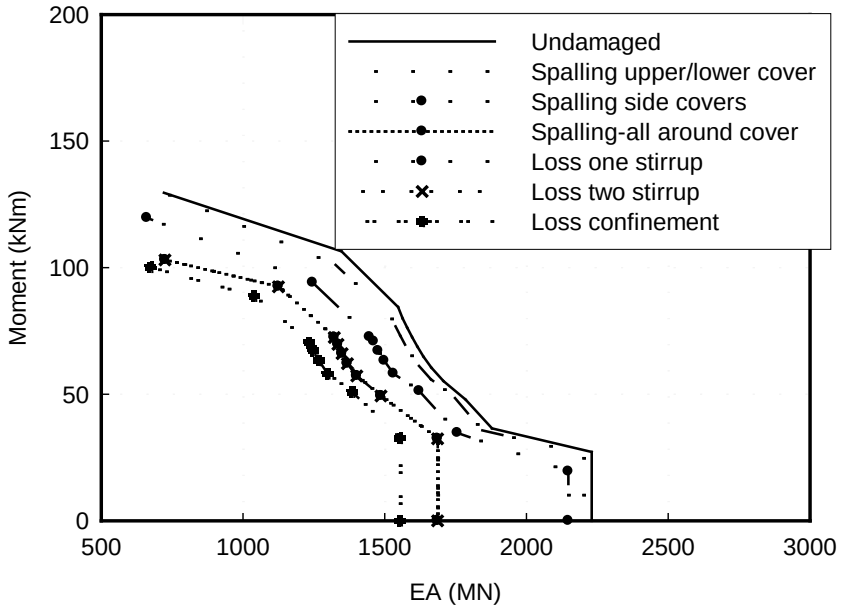

Figure 2.20: Comparison of axial rigidity of an RC column section (case study 2.6.4) for different corrosion states.

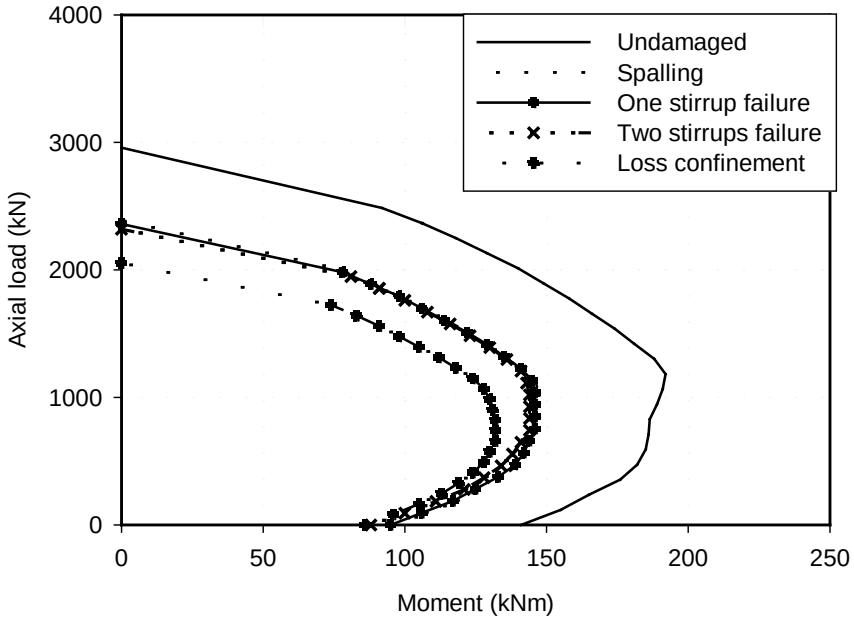

Figure 2.21: Interaction diagram of RC column (case study 2.6.4) for different corrosion states.

2.8 References

Ballim, Y., Reid, J., and Kemp, A., Deflection of RC beams under simultaneous load and steel corrosion. Magazine of Concrete Research;2001,53(3),171-181.

Basu. K., Computation of failure loads of composite column. Inst. Civ. Engrs, London;1967, 36: 557-578.

Bentz, E., Sectional analysis of reinforced concrete. PhD. Thesis, Dept. of Civil Engineering, University of Toronto, Toronto, Canada (2000), 318pp.

Berto, L., Vitaliani, R., Saetta, A., and Simion, P., Seismic assessment of existing structures affected by degradation phenomena. Structural Safety;2008, 31 (4),284-297.

Cairns, J., Plizzari, G., Du,Y., Law, D., Franzoni, C., Mechanical properties of corrosion reinforcement. ACI Materials Journal; 2005, 02(4): 256-264.

Carol, I., and Murcia, J.,Nonlinear time-dependent analysis of planar frames using an exact formulation –I. Theory. Computer and structures; 1989a, 33: 79-87.

Carol, I., and Murcia, J.,Nonlinear time-dependent analysis of planar frames using an exact formulation –II. Structures and examples. Computer and structures;1989b, 33: 89-102.

Choe, D.-F., Gardoni, P., Rosowsky, D., and Haukaas, T., Probabilistic capacity models and seismic fragility estimates for RC columns subject to corrosion. Reliability Engineering and System Safety; 2008, 93(3),383-393.

El Maaddawy, T., Soudki, K., and Topper, T., Analytical model to predict nonlinear flexural behavour of corroded reinforced concrete beams. ACI Structural Journal; 2005, 102(56),550-559.

Espion B., and Halleux P. Moment curvature relationship of reinforced concrete sections under combined bending and normal force. Material and Structural.1988;21:341-351.

Gilbert, R. and Warner R., Tension stiffening in reinforced concrete slabs. J. Strcut. Div. ASCE;1978 .104(ST12),1885-1900.

Gunnin, B.,Rad,F., and Furlong, R.,A general nonlinear analysis of concrete structures and comparison with frame test. Computer and structures; 1977, 7:257-265.

Kabalia, A., Disc. of equation of the stress-strain curve of concrete. P. Desayi and S. Krishnana, J. Am. Concr. Inst.;1964, 61,1227-1229.

Kroenke, W., Gutzwiller, M., Lee, R., Finite element for reinforced concrete frame study. Journal of the Structural Division; 1973, ST (7), 1371-1390.

Lay, S. and Schiebl, P. Life cycle management of concrete infrastructures for improved sustainability. European Community Fifth Framework Program: GROWTH; 2003.

Lazaro, A., and Richards, R., Full-range analysis of concrete frames. Journal of the Structural Division;1973, ST (8), 1761-1783.

Mohammed, A., Almansour, H., Martín-Pérez, B., State-of-the-Art in nonlinear modeling of concrete frame structures under the combined effect of ultimate loading and reinforcement corrosion. CSCE 3rd International Structural Specialty Conference, Edmonton, Alberta, Canada; 2012,June 6 to 9.

Mohammed, A., Almansour, H., Martín-Pérez, B., Nonlinear flexural analysis of reinforced concrete beam-column subjected to ultimate gravity loads combined with reinforcement corrosion, Part II: finite element analysis. Structure and Infrastructure Engineering, submitted, ID NSIE-2014-0015; 2014b.

Oyado, M., Saito, Y., Yasojima, A., and Kanakubo, T. Structural performance of corroded RC column under seismic Load. First International Workshop on Performance, Protection & Strengthening of Structures under Extreme Loading, Whistler, Canada;2007.

Pulmano, V., Bakoss, S., and Shin, Y. A simplified non-linear analysis of concrete frames. Magaz. Conc. Res.;1987, 39: 29-34.

Rasheed, H., and Dinno, K., 1994. An efficient nonlinear analysis of RS sections. Computer and structures;1994,53(3)613-623.

Resheidat, M., Ghanma, M., Sutton, C., Chen, W., 1995. Flexural rigidity of biaxially loded reinforced concrete rectangular column sections. Computer and structures;1995, 55(4)601-614.

Rodríguez, J., Ortega, L. M. and Casal, J.,1996. Load bearing capacity of concrete columns with corroded reinforcement. Corrosion of Reinforcement in Concrete Construction, Royal Society of Chemistry;1996,220-230.

Saatcioglu, M., and Razvi, S., 1992. Strength and ductility of confined concrete. Journal of Structural Engineering; 1992, 118(6): 1590-1607.

Tapan, M., and Aboutaha, R., 2009. Load carrying capacity of deteriorated reinforced concrete columns. Computer and Concrete Construction;2009, 6(6):473-492

Yalcin C, Saatcioglu M. Inelastic of reinforced concrete columns. Computer and Structures 2000; 77(5):539-55.

Yalciner H., Sensoys., and Eren O., 2012. Time-dependent seismic performance assessment of a single-degree-of-freedom frame subject to corrosion. Engineering Failure Analysis;2012,(19):109-122.

Yingang, D., Leslie, A., and Chan, A.,2007. Impact of reinforcement corrosion on ductile behavior of reinforced concrete beams. ACI Structural Journal;2007,104(28),285-293.

Yoon,S., Wng,K., Weiss,W., and Shah,S.,2000. Interaction between loading, corrosion, and serviceability of reinforced concrete. ACI Materials Journal;2000,97(6),637-644.

Val, D.V. Deterioration of strength of RC beam due to corrosion and its influence on beam reliability. Journal of Structural Engineering; 2007, 133(9): 1297-1306.

Zeris, Ch. A. and Mahin, S. A., 1988. Analysis of Reinforced Concrete Beam-Columns under Uniaxial Excitation. Journal of Structural Engineering;1988,114(4): 804-820

Chapter 3

Nonlinear Flexural Analysis of Reinforced Concrete Beam-Columns Subjected to Ultimate Gravity Loads Combined with Reinforcement Corrosion, Part II: Finite Element Analysis

3.1 Introduction

It is reported that a large percentage of North American infrastructure, specifically bridges, are deficient (Lounis et al. 2010), while limited public resources are available for their maintenance/rehabilitation. The qualitative assessment approaches adopted by different states in the US or different provinces in Canada are based on periodic visual inspections (usually every two years). With variable inspectors' experience, it is difficult to have a consistent evaluation of critical bridge elements residual ultimate and seismic capacities as well as allowable service loads. The increasing gap between the deterioration demand and available infrastructure management resources raise the need to develop a practical yet efficient quantitative assessment framework (QAF). Based on evaluating the risk of failure, such assessment framework enables cost-effective decisions on service load reduction or bridge (bridge elements) rehabilitation, strengthening, or replacement. The development of QAF requires the development of accurate analytical/numerical models that are capable to estimate both the time-dependent deterioration of ultimate and seismic capacities of different critical bridge elements and the bridge allowable service loads.

Reinforcement corrosion has been identified as the major cause of RC infrastructure deficiency (deterioration/damage). However, the initiation and progression of corrosion in reinforcing steel can have unlimited number of scenarios that are yet not fully understood or modeled. Hence, it is very challenging to develop practical time-dependent analytical models that are capable to accurately estimate the effects of different reinforcement corrosion scenarios on the structural

behaviour of damaged RC elements. Instead, visual inspection can be used to measure the damage zones and the degree of local damage at the time of the assessment. Therefore, practical simplified models can be developed to evaluate the changes in the geometrical and material properties of the steel and the related damage of the RC element/structure. Hence, an intermediate step towards the development of a semi-quantitative assessment framework (SQAF) is possible based on the present knowledge and the present visual inspection approach (more details are presented in Chapter 6; Mohammed et al. 2014e). Such SQAF should address the three major evaluation limit states of corrosion-damaged bridge elements that are consistent with existing bridge design codes: ultimate limit state (ULS), serviceability limit state (SLS), and earthquake limit state (ELS) (see CHBDC 2006, or AASHTO-LRFD 2007). All the three limit states can be based on a simplified, yet accurate non-linear finite element analysis approach (NLFEA), where the combined effect of mechanical loads and reinforcement corrosion on structural performance is evaluated.

The advances in the experimental investigation enable better understanding of the damage and failure mechanisms of reinforced concrete (RC) structures under extreme external loads (see Appendix A: Mohammed et al. (2012), and Chapter 2: Mohammed et al. (2014a)). It is widely believed that the development of NLFEA approaches to simulate the structural behavior of RC elements and structural systems enables a practical and cost-effective estimation of their structural capacity. The damage and failure mechanisms under combined external loads and reinforcement corrosion become of most importance for aged infrastructure.

The objective of this chapter is to introduce a simplified nonlinear finite element analysis (NLFEA) based on enhanced in-depth visual inspection (or enhanced inspection), material testing and the nonlinear sectional analysis presented in Chapter 2. The enhanced in-depth visual

inspection provides the input data about the location and size of the damaged zone and the level of damage while material testing enables the evaluation of the instantaneous material properties at the time of the assessment. The focus of this study is on the structural behavior of aged slab-on-girder bridge columns (or beam-columns) because: (i) slab-on-girder bridges are the most common types of bridges in North America; (ii) the columns are the most critical elements for the stability and robustness of the slab-on-girder bridges; and (iii) beam-column elements are the most general frame elements that simulates the behavior of beams, columns, or beam-columns, and hence they can be adopted in modeling buildings as well (e.g., parking garages).

This NLFEA requires the use of an efficient elasto-plastic nonlinear model that takes into account different levels of geometrical, material, and bond damage due to reinforcement corrosion at the section level, which was already presented in Chapter 2 (Mohammed et al. 2014a). In order to establish the instantaneous element stiffness and hence the global stiffness of the structure at each load step, the instantaneous axial and flexural rigidities at the sectional level are to be effectively transferred to the element level in the NLFEA. Furthermore, the NLFEA has to safely match the available experimental and/or field test results for the case of external loading without corrosion and for the case of combined load and reinforcement corrosion. However, it has to be simple, numerically stable, and able to be integrated into the proposed SQAF procedure.

3.2 Proposed nonlinear finite element analysis (NLFEA) as a part of semi-quantitative assessment framework (SQAF)

The NLFEA plays the most important role in the SQAF. It presents part of the evaluation at the ultimate limit state (or evaluation-ULS, versus the typical design ULS) and hence the residual strength capacity, the evaluation at serviceability limit state (or evaluation-SLS) and hence the

allowable traffic load, and the evaluation at the earthquake limit state (or evaluation-ELS). Figure 3.1 shows the proposed SQAF, which has six major parts: (I) data input; (II) qualification of reinforcement corrosion and its effects; (III) evaluation of columns performance under combined corrosion and ultimate loads (evaluation-ULS); (IV) evaluation of columns performance under combined corrosion and traffic loads (evaluation-SLS); (V) evaluation of columns performance under corrosion and seismic loads (evaluation-ELS) (only in high risk seismic zones); and (VI) semi-quantitative assessment and reporting. The NLFEA presented in this chapter is a major part of each of the three limit states in (III), (IV) and (V) above. The evaluation of the column structural performance under combined reinforcement corrosion and traffic loads, and the evaluation of the column structural performance under combined reinforcement corrosion and seismic loads are presented in the next two chapters 4 and 5; Mohammed et al. (2014c&d).

The first part of the proposed SQAF, includes three data-input tasks: (I-a) the structural material and geometrical data including boundary conditions; (I-b) the loading data; and (I-c) the enhanced in-depth visual inspection (or enhanced inspection) and any required material test. In the first task, the data is collected from the original design information/sketches (if available), and the field tests on the materials (if possible). The difference between the original design loads and the present loads on the bridge column under consideration are to be determined. The enhanced in-depth visual inspection can provide very important measurements and details that can identify the affected zone, state of corrosion and the resulting local damage. The deteriorations of the structural parameters are then re-evaluated quantitatively through the NLFEA as shown in the following sections.

The proposed SQAF identifies four major damage cases due to the reinforcement corrosion as shown in Figure 3.2, which are: (a) cracking of concrete due to the corrosion; (b) spalling of concrete cover (number 5 in Figure 3.2); (c) failure of one or more stirrups (number 6 in Figure 3.2); and (d) a more advanced state of corrosion progress, which may lead to structural failure of the column through complete loss of confinement or rebar buckling (number 7 in Figure 3.2). The details of each of these major possible deterioration states are shown in Figure 3.2.

The ULS is interactively integrated with step (II) above, where at each major case of quantifying the effects of reinforcement corrosion; the flowchart shows an end-link to the NLFEA (see Figure 3.2). For instance, the NLFEA is the base of four tasks of the evaluation-ULS, which are:(III-a) establishing the load-displacement relationship;(III-b) establishing the moment-curvature relationship;(III -c) evaluation of the deterioration of the load capacity compared to the state where there is no damage; and, (III -d) evaluation of the deterioration of the structural ductility. These four tasks of evaluation-ULS end with the preparation of the required data for the SQAF. The detailed presentation of the proposed SQAF is presented in Chapter 6 (Mohammed et al. 2014e).

3.3 Modeling the effects of reinforcement corrosion at the element level

In the Chapter 2 (Mohammed et al. 2013a), it is pointed out that reinforcement corrosion could lead to different damage mechanisms in the steel and the surrounding concrete in the affected zones. The resulting damage results in significant change of the concrete and steel strength and ductility, deterioration of the composite action and integrity at the section level, and hence a reduction in the axial and flexural stiffnesses. It is also shown that if local damage affects a critical flexural or shear zone, the structural capacity of the RC element based on sectional analysis can significantly decrease. In this chapter, the investigation on the effects of

reinforcement corrosion on the structural behavior is extended to the element/structural level. The objective here is to comprehensively integrate these effects into the NLFEA.

In order to present the integration of the combined effects of reinforcement corrosion and external loads and possible damages into the proposed nonlinear finite element approach, Figure 3.3 shows a beam-column element subjected to axial force and bending moment. Figure 3.3(a) shows a possible general loading, boundary condition, and reinforcement of a beam-column element. In most practical cases, bridge columns are subjected to eccentric axial loads, and flexural cracks usually form at the maximum moment zone. If the external moment is constant over the column height and the axial load is dominant (the moment is too small to generate tensile stress on any section along the beam-column), then no flexural cracks would develop. However, the high axial load could result in cracks due to lateral expansion (Poisson's ratio effect). The service load range in columns is between 25-50 % of their ultimate capacity, where bridge columns are conservatively designed for the lower bound service-to-ultimate loads ratios. If the external moment is high enough to generate tensile stress in one of the column side faces, then flexural cracks develop laterally parallel to each other and distributed over the column height. When reinforcement corrosion is initiated over the main reinforcement as shown in Figure 3.3(b), then corrosion cracks could develop parallel to the rebar crossing flexural cracks. Hence, an accelerated cover spalling would take place if both cracks are developed at the same time. If corrosion progress, more longitudinal cracks will be developed and the local corrosion damage of the surrounding concrete could lead to local loss of bond followed by spalling of the concrete cover as shown in Figure 3.3(c). In addition, uniform loss of the reinforcement cross-sectional area over the corrosion-damaged zone also takes place. The properties of the steel are also changed with the progress of corrosion. A possible local severe reduction of the cross-

sectional area of some rebars due to pitting corrosion could also be observed, but it is not be discussed in this study as it can be studied on case by case basis. These changes could result in a large decrease of the axial and flexural sectional rigidities (as shown in Chapter 2; Mohammed et al. 2014a). Further progress of the corrosion process could result in some stirrups failure (rebar fracture) as shown in Figure 3.3(d) and this would increase the local spacing between the lateral reinforcement ties. This would result a reduction of the confinement of the core concrete and a local strength critical zone that could be lower than the typical strength critical zones. In relation to the finite element discretization, three types of elements are distinguished in beam-columns with local corrosion damage: (i) no-corrosion damaged zone; (ii) partly corrosion damaged or corrosion-transition zone; (iii) fully-corrosion damaged zone (see Figure 3.3(e)).

3.3.1 Reduction in reinforcement cross-sectional area and ductility, and loss of concrete cover

The changes in geometrical properties of the corrosion-damaged zones and in the materials properties of the steel and the concrete at the section level are shown in Chapter 2(Mohammed et al. 2014a). Each element at the finite element analysis at the structural level has its geometrical and material properties as the average properties of its characteristic sections (see Section 3.4.2) that are evaluated at the sectional level. The instantaneous element stiffness estimated at each load step is based on the average of the axial rigidities and the average of the flexural rigidities of all characteristic sections of that element. Hence, the damage and the change in the material properties at the section level are transferred to the element level through the average changes in the instantaneous element stiffness.

3.3.2 Loss of bond in the corrosion affected zone

The background and the deterioration mechanisms of rebars to-concrete bond are discussed in Chapter 2 (Mohammed et al. 2014a). It is shown that if the bond stresses outside the "bond failure zone" do not exceed the bond strength, then arch mechanisms are developed provided ends of rebars are adequately anchored. If no progressive bond failure takes place, then the possibility of high deformations due to loss of bond action is reduced. A proposed approach to estimate the effects of the local bond loss due to corrosion on the redistribution of the stresses/forces acting on the cross sections is presented in Chapter 2 (Mohammed et al. 2014a).

It has been shown in Chapter 2 (Mohammed et al. 2014a) that in the characteristic sections of the bond failure zone of flexural members, the equilibrium of sectional forces is not directly satisfied (at the section level). A self-supported arch is developed over three zones: the corrosion damaged zone and two adjacent zones that are not affected by corrosion, equilibrium being satisfied along the three (see Figure 3.4 (a)). The tensile reinforcement passing through the three zones and the distributions of the tensile and bond stresses are shown in Figure 3.4(a), where the excessive extension of the corroded part develops balancing mechanisms of additional and migrated stresses through the development of the arch action. In all sections where bond is active, compressive and tensile forces act as a couple to rotate the cross-sections around the neutral axis (Euler-Bernoulli beam theory). In the other cross-sections where bond has failed, the internal forces acting on the sections satisfy equilibrium only in the RC structural element across the three mentioned zones (i.e., the "bond failure zone" and the two neighboring "active bond zones"). Since the tension and compression forces acting on the section are not balancing each other across the section itself in the "bond-failure" zone, then two additional inclined compressive forces develop in the two side zones forming an arch which is self-supported by the

tensile force in the steel. As corrosion begins and propagates, the loss of bond is also extended along the reinforcement. While bond loss propagates along the longitudinal reinforcement, the bond stresses increase at the two ends of the bond failure zone, forming a high stress transition zone where the stress redistribution takes place. Figures 3.4(b-i) through 3.4(b-iii) show the migration of the high bond stress wave when corrosion-induced bond loss is expands longitudinally; where (i) BAZ is the length of the bond affected zone of the rebar; and (ii) BSD is the constant bond stress after stress re-distribution takes place. With a very high level loading case where the load exceeds the service load but is still less than the ultimate load, further propagation and migration of the bond loss zone beyond that developed due to corrosion would likely take place. The additional bond stress due to the high increase of external loads would increase the peak stress of the "bond stress waves" at the transition region between the bond failure zone and the adjacent active bond zones beyond the bond strength; hence resulting in progressive bond loss.

With a significant sectional loss of tension reinforcement, and if the tensile stresses in the affected steel are relatively high (beyond yield but still under the ultimate stresses), high local axial deformations in the tensile reinforcement are expected. This would result in large widening of flexural cracks, accelerating the local damage and spalling of the concrete. Furthermore, the formation of a compression arch (as shown earlier) would increase the compressive stresses in the compressive stress region of the "bond-failure" zone. On the other hand, when the structural member is subjected to axial compression in addition to bending moment (in beam-columns), then the tensile stresses in the tensile steel could be significantly reduced. Hence, the stress redistribution mechanisms could not be developed and the effects of losing the bond in the corrosion affected zone could marginally affect the lateral deformation. In the present study, the

focus is on beam-columns of slab on girder bridges that are subjected to axial load and moment as a result of the load eccentricity. Typically these columns are designed conservatively for low service load over capacity ratios. For the proposed NLFEA the equilibrium is satisfied in the sectional and element levels taking into account the redistribution of the stresses due to the formation of the arching action. Checking whether the bond stress level exceeds the bond strength in none corroded zones (active bond zone as shown in Figure 3.4(a)).

3.3.3 Loss of stirrups and concrete confinement, and longitudinal rebar buckling

At advanced corrosion stages, fracture of critical stirrups in the corrosion-damaged zones is widely observed, which could result in premature buckling of the main rebars (Rodríguez et al. 1996). In flexural members, severe localized corrosion or pitting corrosion could develop in zones that are located away from moment or shear critical sections. The reduction in structural capacity due to stirrups corrosion could be specifically serious in RC columns, as they provide confinement to the core concrete in addition to their major contribution to shear resistance. This significant effect of losing stirrups due to corrosion on the axial and bending moment carrying capacities of deteriorated RC columns has been observed by Rodríguez et al. (1996) and Oyado et al. (2007).

3.4 NLFEA of RC beam-column subjected to external loads and reinforcement corrosion

The nonlinear finite element analysis approach is presented in this section. It includes the background assumptions, the nonlinear approach steps, and the “displacement field tuning convergence” (DFTC) technique, which are discussed in the following sections.

3.4.1 Assumptions

The proposed NLFEA is based on the following assumptions: (i) concrete and steel are isotropic materials; (ii) the “local” stiffness matrix (with its 6 x 6 entries related to 3 degrees-of- freedoms

for each of the two nodes in the finite element) is established from the average of the axial and the flexural rigidities calculated over all characteristic sections of that element; (iii) the flexural rigidity of each section is calculated from the base sectional analysis (as developed in the first part of this chapter; Mohammed et al.(2014a)); (iv) all deformations (displacements, rotations, etc.) are continuous functions over the discretized continuum (structural element or structural system) throughout all load steps; (v) Euler-Bernoulli beam theory is applicable in all the combined external loads and corrosion level; however, the effect of stress redistribution due to bond loss is added; and (vi) equilibrium is satisfied at the section and structural levels.

3.4.2 Discretization

A typical general finite element discretization approach is followed in the proposed NLFEA. The structural element is divided into a number of finite elements of constant or variable length. Depending on the length of the structural member, the number and length of the elements for each member, and the size of the corrosion damage, each element has a number of characteristic sections. The locations of these sections are identified according to the variation of the sectional properties and the required accuracy. In Figure 3.4 (a) element (j) joins node (i) and node (i+1), and it includes as an example three characteristic sections (k), (k+1), and (k+2). Two approaches can be followed to select the number of elements and number of sections per element: (i) if the required processing time and the size of the structure are large, then the smallest possible number of elements with a reasonable number of sections per element has to be selected; or (ii) if the variation of stresses are very high or the change in properties due to corrosion progress is significant, then selecting a large number of elements with a minimum number of sections is the best approach. Refined analysis is also possible when the preliminary trials raise the need to capture the steep variation of the displacements or stresses in a specified zone of the structural

element. Whatever the discretization approach is followed, fine tuning the convergence parameters on a case by case basis is a key for efficient modeling, as shown in the following sections.

3.4.3 Nonlinear finite element procedure

In order to enable an efficient simplified nonlinear structural analysis with high accuracy, it is imperative to ensure: (i) the numerical efficiency in terms of minimum use of random access memory (RAM) and minimum processing time; (ii) systematic and fast approaching to highly-controlled convergence with minimum sensitivity; and (iii) minimum trials in idealizing, discretization, and convergence to achieve acceptable model performance and accurate results. The base line for a finite element model efficiency and accuracy is the model simplicity, matching available experimental results, and numerical efficiency in terms of computing time memory use and adaptability. Throughout the development of nonlinear finite element analysis of reinforced concrete frame structures (see Mohammed et al. 2014a) and Mohammed et al. 2012), the nonlinear (material, geometrical or both) element stiffness was derived using analytical approaches with closed-form integration, semi-analytical approaches, or numerical integration. High-numerical sensitivity and time-consuming convergence have been experienced when closed-form nonlinear formulation was used. At the early development of non-linear finite element programs, on the other hand, the use of numerical integration for each section at each load step required large memory and impractically long preparation and running time.

As shown in Chapter 2 (Mohammed et al. 2014a), a numerically efficient nonlinear sectional analysis (NLSA) has been developed and verified, which is part of the proposed NLFEA introduced here. The model involves the use of an innovative convergence approach ("displacement field tuning convergence or DFTC"), where the trial and errors process to verify

equilibrium at the element level is controlled by correcting the displacement vector based on the correction of the maximum displacement normal to the axis of the structural element. The correction is based on proportioning the change in the displacement in successive load increment steps and correction trials. The corrections of other deformations are assumed linearly proportional to the correction of the maximum deformation. This approach was originally developed by Almansour (1988) for non-linear analysis of plates and shells and simplified here for the application to RC frame structures. Figure 3.5 shows the trial deformation fields and successive corrections (corr $_{i}$, corr $_{i+1}$, corr $_{i+2}$, ..., corr $_{i+n}$) where the deformation field is corrected successively until equilibrium is satisfied allowing very small tolerance in the tuning process. For simplicity and conceptual purpose only, the figure shows that the corrected displacement curve is successively moving in one direction only, which is not always the case in the trial and error process. Figure 3.6 shows the NLFEA procedure assuming constant increments of the load throughout. The procedure is as follows:

1. For first applied load increment, $P_{i=1} = \Delta P$:
    i. Find the structural stiffness, $K_{i=1}$ based on linear finite element analysis
    ii. Solve $P_{i=1} = K_{i=1}U_{i=1}$ for the global structural deformation vector, $U_{i=1}$.
    iii. Identify maximum vertical displacement over the deformation field (deformation vector) $V_{i=1}$
    iv. Find the element forces and hence the sectional forces involving bond loss effects at the element level
    v. Perform nonlinear sectional analysis based on the results of step 1to define the rigidities at the section level, and hence the stiffness for next step
    vi. Check if the section is failed (see Mohammed, et al. 2014a).

2. For subsequent load increment, $P_{i+1} = P_i + \Delta P$

   i. Construct the nonlinear stiffness matrix based on the sectional properties of each element in the previous load step, K_i,

   ii. Solve $P_{i+1} = K_{i\,x}\, U_{i+1}$ for the global structural deformation vector, U_{i+1}.

   iii. Identify V_{i+1} and calculate the correction, Corr-$_i$, which is found as (maximum V_{i+1} - maximum V_{i1})/ maximum V_i, where maximum V_i should be compared to the tuning variable, α, which is introduced to control "tune" the convergence.

   iv. The modification of the deformation vector is assumed linearly proportional to the maximum displacement normal to the structural member axis, $U_i^{\text{corr-i}} = U_i * (1+$ Corr-$_i$). That is corresponding to maximum displacement, $V_i^{\text{corr-i}}$

   v. Check the tolerance for the displacement

   vi. If the tolerance is not satisfied, intiate a second cycle of correction based on the instantaneous difference in the force vector, or, $F_i^{\text{diff}} = P_{i+1} - K_i^{\text{corr}}\, U_{i+1}^{\text{corr}}$

   vii. Solve , $F_i^{\text{diff}} = K_i^{\text{corr}}{}_x\, U_{i+1\_\text{diff}}^{\text{corr}}$ for $U_{i+1\_\text{diff}}^{\text{corr}}$

   viii. Find the element using the present element deformation vector, $U_{i+1}^{\text{corr-i}}$

   ix. Find sectional forces and properties using the present element properties

   x. Perform nonlinear sectional analysis to find the stiffness for the next step

   xi. Check for section failure (concrete crushing in the compressive zone or tensile failure of the steel in the tensile zone. For more details, see Chapter 2 (Mohammed, et al. 2013a).

   xii. Re-assemble the instantaneous corrected stiffness matrix and solve the finite element matrix equilibrium equation for displacement, and then find the maximum displacement at this correction sub-step.

xiii. Check the tolerance until satisfied; otherwise establish a new correction cycle

xiv. If the tolerance is satisfied, save the results and increase the load

It is important to mention that the above proposed procedure recognizes the direction of the reference displacement component (normal or parallel to the structural element axis) for the use in DFTC based on the dominant load. If the external moments due to eccentricity or bending moment due to lateral loading are controlling the structural behaviour (where the flexural stresses are significantly higher than the axial stresses, such as in beams), then the tuning is based on the maximum deformation normal to the structural member. If the external axial load generates sectional stresses that are control the behavior (column action), then the tuning is based on the maximum deformation in the direction of the structural member.

3.4.4 Convergence studies

In nonlinear finite element analysis, the procedure basically involves load increments; of course, the material and geometrical properties of the elements and their characteristic sections are variable with the progress of the load increments. The equilibrium should be satisfied in every element, section and in the overall structure. As mentioned earlier, the numerical stability of the approach and its sensitivity to the load increment, number of elements, number of sections per element, and number of cycles in the iterative approach are key parameters in the evaluation of the numerical efficiency of the proposed NLFEA. It is essential to verify the adoptability of the proposed procedure in the assessment approach or any other application without complicated requirements for accuracy and the convergence, which are on case by case basis in many previously proposed models in the literature (see Appendix A; Mohammed et al. 2012).

In this chapter, among many others, two convergence studies are comprehensively performed to examine the relation between the tuning parameter of DFTC,α, and the load increment for

different number of elements and number of sections per element. Table 3.1 shows an example of the sensitivity of the convergence for different values of α and ΔP for case study I (see following section and Figures 3.7-a through 3.7-d for more details). The selected values for α came from few preliminary trials. The table illustrates that fast convergence is evident in most of the trials although high values for the load increment are also investigated. Figure 3.7-b shows that the maximum lateral displacement becomes very stable in a relatively low number of elements for all examined load increments. Figure 3.7-c shows the maximum lateral displacement versus the number of elements for the case of both an undamaged and a corrosion-damaged beam. In the second convergence study, Case study II, a uniformly distributed load is applied on a simply-supported beam (see the following sections and Figures 4.8-a through 8-c) and the results of the NLFEA are compared to the test results. This study also shows fast convergence in all investigated cases. Figure 3.8-b shows a similar relation between the maximum lateral displacement and the number of elements for the cases of undamaged and corrosion-damaged beams. It is observed that for the case of damaged beams the convergence becomes slow or unsatisfied when the number of elements is high. Figure 3.8-c shows that for the case of an undamaged beam, the use of large number of elements with one characteristic section per element gives similar results to the case of using small number of elements with many sections per element. The results show that it is possible to optimize α, the load step, the number of elements, and number of sections per element for numerical efficiency with fast convergence.

3.5 Case studies

Five case studies are presented in the following section, four of which are to verify the performance and accuracy of the proposed NLFEA versus experimental results, and the fifth is to

show the capability of the model to analyze a beam-column under different loading cases. Two of the four verification case studies correspond to structural elements subjected to only external "mechanical" loads and no reinforcement corrosion. The other two verification case studies correspond to structural elements subjected to combined external loads and reinforcement corrosion. For all case studies, the results are shown for the optimum tuning parameter of DFTC, α, and number of elements

3.5.1 Verification of the proposed model for the case of non-damaged structure (no corrosion)

In the first case study (case study I), a simply-supported beam subjected to four-point loading is loaded up to failure as shown in Figure 3.7-a, (see Rasheed and Dinno 1994a). The beam is modeled to verify the accuracy and numerical stability of the proposed NLFEA. The beam is 3.0m long and has a cross section of 152.4 mm by 280.0 mm with 29.2 mm and 34 mm as bottom and top concrete covers, respectively. The beam is doubly-reinforced at the top and bottom faces by 3 carbon steel rebars of 14 mm diameter on each side, as shown in the cross section of Figure 3.7-a. The compressive strength of the concrete is (f'_c = 41MPa), and the stress strain of the steel is as modeled in the Chapter 2 (see Mohammed et al. 2014a). The beam is modeled for verification purposes, by comparing the finite element results to the original experimental results in terms of the moment versus mid-span curvature for the case when the beam is undamaged. On the other hand, reinforcement corrosion is assumed to occur along the middle third of the beam span at the tension zone. Figure 3.7-a shows the location and the expected damage due to corrosion.

As mention earlier, a comprehensive parametric study to optimize the convergence is conducted and shown in Figures 3.7-b and 3.7-c together with Table 3.1. Figure 3.7-d shows that the moment versus mid-span curvature relationship of the proposed NLFEA for the case of no

corrosion (undamaged) is conservatively close to the experimental results of Espion and Halleux (1988). The figure also shows the drop in moment strength and the change in the curvature capacity as a result of the tensile reinforcement corrosion. The corrosion in this case study affects the beam through stiffness reduction and stress redistribution from: (i) the reduction of the cross-sectional area of steel reinforcement is based on a steel mass loss of 30%;; (ii) loss of bond between the steel and the concrete in the tension reinforcement of the corrosion-affected zone section; (iii) reduction of steel ductility; and (iv) concrete spalling as shown in Figure 3.7-a. As there is no axial force, the failure of stirrups would only affect the shear capacity of the affected area, and it has no effect on the concrete confinement. It is observed from Figure 3.7-d that the structural ductility of the beam measured on the basis of curvature (ductility index equal to ultimate curvature divided by yield curvature) is slightly increased. However, the beam ultimate moment strength is reduced and the yield curvature is increased which reflects more softening of the beam.

In case study II, a simply-supported beam subjected to uniform distributed load up to failure as shown in Figure 3.8-a (see Rasheed and Dinno 1994b), is modeled using the proposed NLFEA. The beam is 2.235 m long and has a cross section of 152.4 mm by 304.8 mm with 51.3 mm cover. The beam is reinforced in the lower face (tension zone) by 3-carbon steel rebars of 20 mm diameter. The compressive strength of the concrete is (f'_c = 34MPa) and the stress-strain behaviour of the steel is as modeled in Chapter 2 (see Mohammed et al. 2014a). This beam is also modeled for verification purpose, by comparing the finite element results to both the original experimental results in terms of the load versus mid-span deflection and to Rasheed and Dinno's closed-form finite element analysis (FEA) (see Rasheed and Dinno 1994b). A second analysis of the beam assumes reinforcement corrosion to affect the middle-third of the beam span

at the tension zone. Figure 3.8-a shows the location and the expected damage due to corrosion assuming a steel mass loss of 40%.

Figure 3.8-c shows that the load versus mid-span displacement relationship of the proposed NLFEA and that of Rashid and Dinno closed-form FEA are very close to the test results (De Cossio and Siess (1960)). The figure also shows that using a small number of elements with more than one characteristic section per element gives similar results to the load-mid span displacement when a relatively large number of elements with one characteristic section per element is used. In this case study, the reinforcement corrosion affects the beam in a similar manner as the previous case, where reduction of the steel reinforcement section and ductility and concrete spalling would occur in an extreme corrosion state (Figure 3.8-d). Similar to the previous case study, the failure of stirrups would only affect the shear capacity of the affected area, and it has no effect on the concrete confinement.

In both case studies, the proposed model gives very good results that match with acceptable accuracy the experimental test results in case of non-damaged beams. The approach is numerically stable and insensitive over a wide range of number of elements and size of load increments. The tuning parameter, α, of the displacement field tuning convergence (DFTC) can be calibrated with only few trials in both case studies, and the convergence of the model becomes systematic in almost all the studied cases.

3.5.2 Verification of the proposed model for the case of combined external loads and reinforcement corrosion

In case studies III and IV, comparisons of the proposed NLFEA results with the results of analytical and experimental studies are presented. In case study III, NLFEA is compared to a nonlinear two-dimensional FEM proposed by Coronelli & Gambarova (2004) and to the

background test performed by Rodriguez et al. (1996). In Coronelli & Gambarova's model, the concrete was modeled using a four-node plane-stress element with thickness equal to the section width, while the steel bars were represented by two-node truss elements; a bond-link element exhibiting a relative slip between the two materials coupled the concrete elements to the corresponding bar elements. The model takes into account the effects of corrosion on the behaviour of steel and concrete through: (i) the reduction of the steel rebars cross-sectional area; (ii) changes of the constitutive stress-strain relationships of steel and concrete in the corrosion affected zone; (iii) changes of the material interface properties; and (iv) loss of the concrete area due to spalling.

Coronelli & Gambarova (2004) compared their model results with Rodriguez et al. (1996) experimental results of a test conducted on a simply-supported beam subjected to four-point loading and reinforcement corrosion. Rodriguez et al. (1996) tested several beams with different properties; however, only one of those beams (11.6, as named in Rodriguez et al. study) is selected for present case study. The beam dimensions are 2,300 x 200 x 150 mm, the concrete compressive strengths is $f_c^{'} = 34$ MPa, the stirrups are φ6 (US) distributed at 170 mm c/c (center to center), and the longitudinal bars yield strength is $f_y = 575$ MPa . Figure 2.2.9-i shows the design, the reinforcement and the finite element model as proposed by Coronelli & Gambarova (2004). Load versus mid-span deflection relationships of the proposed NLFEA compared to both Coronelli & Gambarova (2004) modeling results and the original Rodriguez et al. (1996) test results are shown in Figure 3.9-ii. A close agreement is observed between the proposed model and the two studies results where the proposed model shows slightly conservative results.

In case study IV the results of the proposed NLFEA are compared to Yingang et al. (2007) test results. Nineteen reinforced concrete beams were loaded under two-point loading up to failure;

they were subjected to a process of electrochemically accelerated corrosion. The beam specimens have dimensions of 150 x 200 x 2100 mm and a span of 1,800 mm. The beams are reinforced with tension reinforcement ratio of 0.87, 1.6, 3.2 and 6.2 % in four groups (very under-reinforced, under-reinforced, balanced, and over reinforced). The beams are reinforced with 8 mm ties at 150 mm spacing, either with 0.56 or 0.87 % transverse reinforcement ratios, and. The nominal concrete cover to the longitudinal bars was 20 mm. In the present research, an over reinforced specimen (T322) was selected for the comparison in case study IV. The longitudinal bars diameter is 31.61 mm with yield strength (f_y) of 498 MPa and ultimate strength (f_u) of 604 MPa with a ratio of strength ($f_u/f_{y)}$ of 1.21. The process of corrosion of reinforcement was electrochemically accelerated to reach targeted levels of corrosion in reasonable time. For the selected specimen, tension bars were intentionally corroded with direct current impressed on the individual sets of bars. A water tank containing sodium chloride solution and a stainless steel cathode were fixed to the concrete cover along 600 mm at mid span (see Figure 3.10-a); for the selected specimen, the current intensity was 0.9 mA/cm^2 applied for 60 days.

Figure 3.10-b shows the load versus mid-span deflection relationships from the proposed NLFEA compared to the test results of undamaged and corrosion-damaged beams. The figure shows that the proposed model slightly underestimates the ultimate load. The results show that the proposed NLFEA conservatively gives softer behavior reflecting lower stiffness than that shown in the test results. This can be explained by the conservative simulation of the nonlinear material properties of both the concrete and the steel where: (i) the concrete contribution to the sectional stiffness using the secant modulus gives underestimation of the stiffness; and (ii) the tri-linear stress strain relationship of the steel could result in softer behavior in the range of stresses.

In both case studies III and IV, the convergence is satisfied in all the cases of damaged and undamaged beams. The capability of the proposed model to capture the ultimate load and deformations and its numerical stability and fast convergence enhance the confidence to use it in more complex applications.

3.5.3 Application of the proposed NLFEA on the case of a beam-column subjected to combined eccentric load and reinforcement corrosion

In case study V, the proposed NLFEA is applied to investigate the structural behavior of a slab-on-girder bridge column subjected to axial load with variable eccentricity combined with reinforcement corrosion. Figure 3.11-a shows a typical slab-on-girder pier formed from several columns. The columns are usually supported by a rigid strip foundation with or without piles depending on the soil conditions and the columns are usually connected at the top by a “cap” beam normal to the traffic direction. This cap beam provides continuity in the direction normal to the traffic and a base for the bridge superstructure, as shown in the figure. A pin support is usually assumed in the direction of the traffic. Slab-on-girder bridge columns are typically designed to support low eccentricity; however, in this case study, high eccentricity is assumed for an aged bridge structure to investigate extreme loading conditions that could result from progressive damage in the superstructure as well as in the substructure.

Figure 3.11-b-i shows typical critical corrosion zones on slab-on-girder bridge columns. Figure 3.11-b-ii (a) shows the possible worst scenario for the location of a corrosion zone in an intermediate bridge column in a highway overpass due to splashing of de-icing water from traffic from both directions. In this case study, it is assumed that the corrosion would affect the middle third of the 6.0m height column. Figure 3.11-b-ii (b) shows the typical details of the longitudinal

and lateral reinforcement of such column, while Figure 3.11-b-ii (c) shows the details of the column cross section where the larger amount of longitudinal reinforcement is provided in the traffic direction.

The bridge column under consideration is under high axial load and external moment due to the load eccentricity, and hence the level of the concrete confinement is of major interest in evaluating the structural behavior and residual capacity of the column. Several possible corrosion damage states that can be observed by visual inspection are identified in this case study, as shown in Figure 3.11-c. The figure shows six possible damage states that are typically observed and directly related to different structural performance states. These are: (a) corrosion-induced cracks together with flexural and lateral expansion cracks, with corrosion growth on the longitudinal and lateral reinforcement with the consequent losses of the steel cross-sectional areas; (b) concrete cover spalling off one side and partial loss of cover from two orthogonal sides and high reduction of steel area and ductility; (c) added to the concrete and steel loss in (b) above, a possible rupture of one lateral reinforcement tie/stirrup; (d) spalling of concrete cover all-around the column in the corrosion affected zone together with steel losses of longitudinal and lateral reinforcement and rupture of one stirrup/tie; (e) spalling of concrete cover all-around the column together with steel losses of longitudinal and lateral reinforcement and rupture of two stirrups/ties; and (f) spalling of concrete cover all-around the column together with significant steel losses of longitudinal and lateral reinforcement, rupture of three stirrups/ties together with local loss of confinement and longitudinal bar buckling.

Figure 3.11-d shows the finite element idealized column with twelve elements, thirteen nodes and fixed-pin support condition. The column is subjected to load increment up to ultimate capacity. An eccentricity ranged from zero to 5H is assumed in all the load steps in the present

case study, where H is the depth of the column cross section in the traffic direction. This range of eccentricity is assumed here to cover all possible extreme loading cases resulting from progressive damage of different parts of aging bridges. It also enables the demonstration of the capability of the proposed NLFEA in modelling a wide range of structural behavioral cases, covering pure axial compression, pure flexure, and any combination of axial compression and bending moment in beam-columns. Figure 3.11-d also shows the distribution of lateral displacement over the column height when high eccentricity is assumed. The figure shows the lateral displacement for the case of no corrosion or undamaged column (UC) versus the case of a corrosion damaged column (CO). Extreme corrosion deterioration is assumed in the analysis, which entails spalling of the concrete cover all-around the column together with massive steel losses of longitudinal and lateral reinforcement (assuming a steel mass loss of 30% which is equivalent to 10 years of corrosion with a corrosion current density of $1\mu A/cm^2$), rupture of three stirrups, loss of confinement prior to the possible occurrence of buckling of longitudinal reinforcement. For both the undamaged column (UC) and corrosion-damaged column (CO), Figure 3.11-d, shows the lateral displacement over the height for three load cases; (a) below yield, at a moment equal to 3,000 kN.m, with axial load of 833 kN; (b) after yield and below ultimate, at a moment equal to 6,000 kN.m, with axial load of 1,667 kN, and (c) at ultimate, for UC: a moment equal to 8,200 kN.m, with axial load of 2,280 kN and for CO: a moment equal to 6750 kN.m, with axial load of 1,875 kN. The figure shows the overall increase in lateral displacement for the case of corrosion-damaged column versus the non-corroded column specifically at ultimate loads. It is also observed that the region of maximum displacement is moved upward to the zone affected by corrosion (see the two curves UC-c versus CO-c). This may lead to a general conclusion that critical sections identified in design stage could not

necessarily remain critical sections for the evaluation of aged structures. Hence, a preliminary parametric study would be essential to identify the critical “evaluation” sections.

In Figures 3.11-e and 3.11-f, the focus is on the nonlinear structural behavior at the mid-height region. In Figure 3.11-e, the effects of the eccentricity on the nonlinear behavior of the undamaged column are investigated. Figure 3.11-e (a) shows the capability of the proposed NLFEA to reflect the significant drop in the axial strength and elasto-plastic axial-deformation capacity of the column with the increase in the load eccentricity e. Conversely, Figure 3.11-e (b) shows the effects of the axial load eccentricity increase on the moment-lateral deformation relationship. The figure shows significant increase in the ultimate moment and the ultimate lateral deformation (assuming no global buckling of the column and ignoring the P-Δ effects). Of-course, the increases in the moment and lateral deformation are correlated with the decrease in axial capacity. This reflects the load-moment interaction of the column as required in design, evaluation, and seismic analysis.

On the other hand, Figures 3.11-f (a) and (b) show (for the case of high eccentricity, i.e. e = 5 H) the effect of two corrosion-induced damage states the axial load versus displacement relationship, and on the moment versus lateral displacement relationship, respectively. Both figures show an intermediate corrosion damage case (loss of cover on the tensile face) and an extreme corrosion damage case (loss of three stirrups and confinement). In Figure 3.11-f (a) up to 25% reduction in the axial strength is observed together with similar percentage of reduction of the axial deformation capacity. The reduction in moment and lateral deformation capacities is more evident as shown in Figures 3.11-f (b).

This case study shows the general capabilities of the proposed NLFEA in estimating the ultimate capacity of the strengths and deformations of beams, columns, and beam-columns (noting that

the presented results are for the nominal capacities). The model can be easily integrated with (i) a model for nonlinear dynamic analysis of the effects of traffic on the bridge structure due to a corrosion-damaged bridge columns (see chapter 4; Mohammed et al. 2014c); and (ii) a model for seismic analysis of the corrosion damaged bridge columns (see chapter 5; Mohammed et al. 2013d).

3.6 Conclusions

In this chapter, a numerically efficient nonlinear finite element analysis is proposed as part of a semi-quantitative assessment approach to evaluate the structural performance and residual capacities of slab-on-girder bridge columns subjected to combined external loads and reinforcement corrosion. The model adopts an innovative "displacement field tuning convergence, DFTC" to ensure fast convergence and numerical stability in all the examined cases with minimum tuning trials. The model is capable to analyze the nonlinear structural behavior of corrosion-damaged aged beam-columns with any possible loading. The proposed NLFEA uses the sectional analysis proposed in Chapter 2, visual inspection and any necessary material testing to estimate the columns sectional rigidities, from which the elements and structure stiffness are calculated by a trial and error ensuring equilibrium at the sectional, element, and structural levels at each load step. The displacement field tuning convergence or DFTC uses single- or multiple- corrections phases until a displacement tolerance is satisfied. The results of the case studies lead to a general conclusion that critical sections identified in the design stage do not necessarily remain critical sections for the evaluation of an aged structure. Hence, a preliminary parametric study is essential to identify the critical "evaluation" sections.

The efficiency and accuracy of the proposed NLFEA is verified through four case studies, which are compared to experimental and numerical results from previous studies on both undamaged and corrosion-damaged beam-columns. The procedure is comprehensively applied on a typical slab-on-girder bridge column and gives trends of structural behavior and results as expected. The procedure proves to be numerically efficient and insensitive to values of the controlling parameters of the nonlinear analysis. Therefore, it can then be used as part of a nonlinear static or dynamic analysis of damaged bridge columns or framed structures, and it can be integrated with a semi-quantitative assessment approach.

Table 3.1: Case study I: variation of convergence tuning parameter α verses load step ΔP (Rashid & Dinno, 1994a).

	ΔP (kN)									
α	1	2	3	4	5	6	7	8	9	10
4	S^{**}	S^{**}	S^{**}	F^{*}	S^{**}	F^{*}	S^{**}	F^{*}	F^{*}	F^{*}
6	S^{**}	F^{*}	S^{**}	F^{*}	F^{*}	F^{*}	F^{*}	F^{*}	S^{**}	F^{*}
8	F^{*}	F^{*}	F^{*}	F^{*}	F^{*}	F^{*}	F^{*}	S^{**}	F^{*}	F^{*}
10	S^{**}	F^{*}	S^{**}	F^{*}	S^{**}	F^{*}	S^{**}	F^{*}	F^{*}	F^{*}

F^{*}: Fast Convergence; S^{**}: Slow Convergence

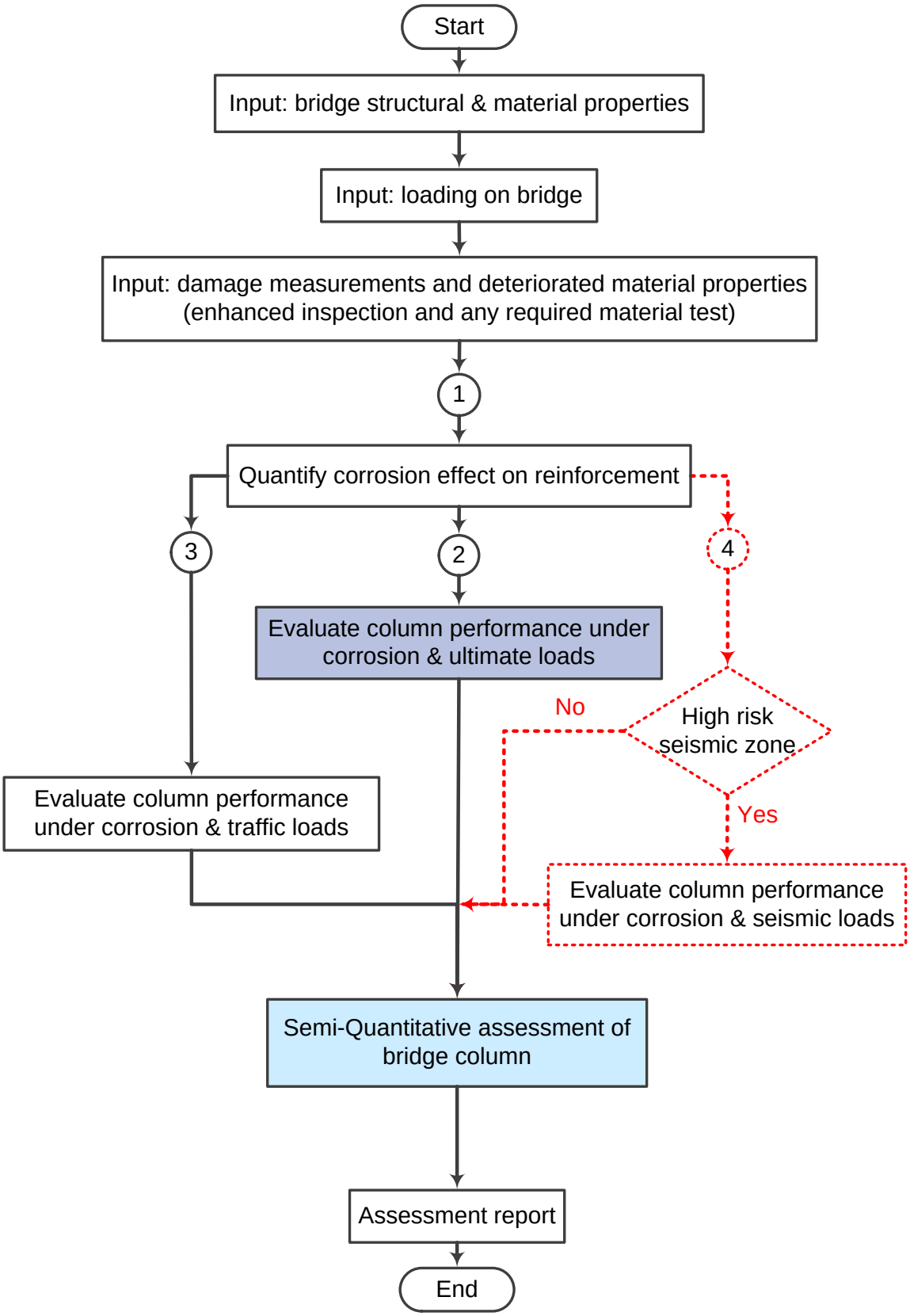

Figure 3.1: The proposed SQAF of aging RC bridge columns.

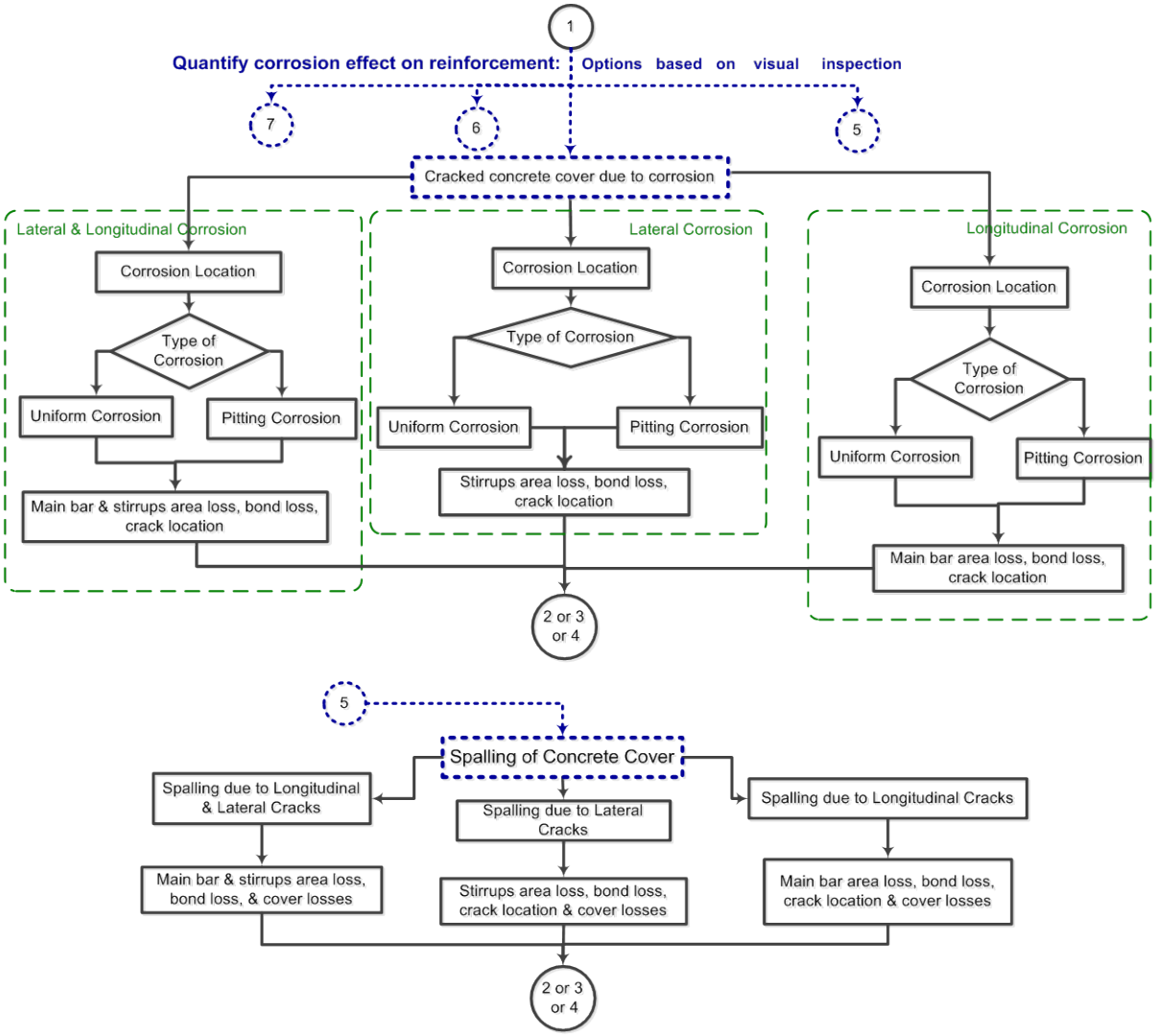

Figure 3.2: Evaluation of column performance under corrosion & ultimate loads.

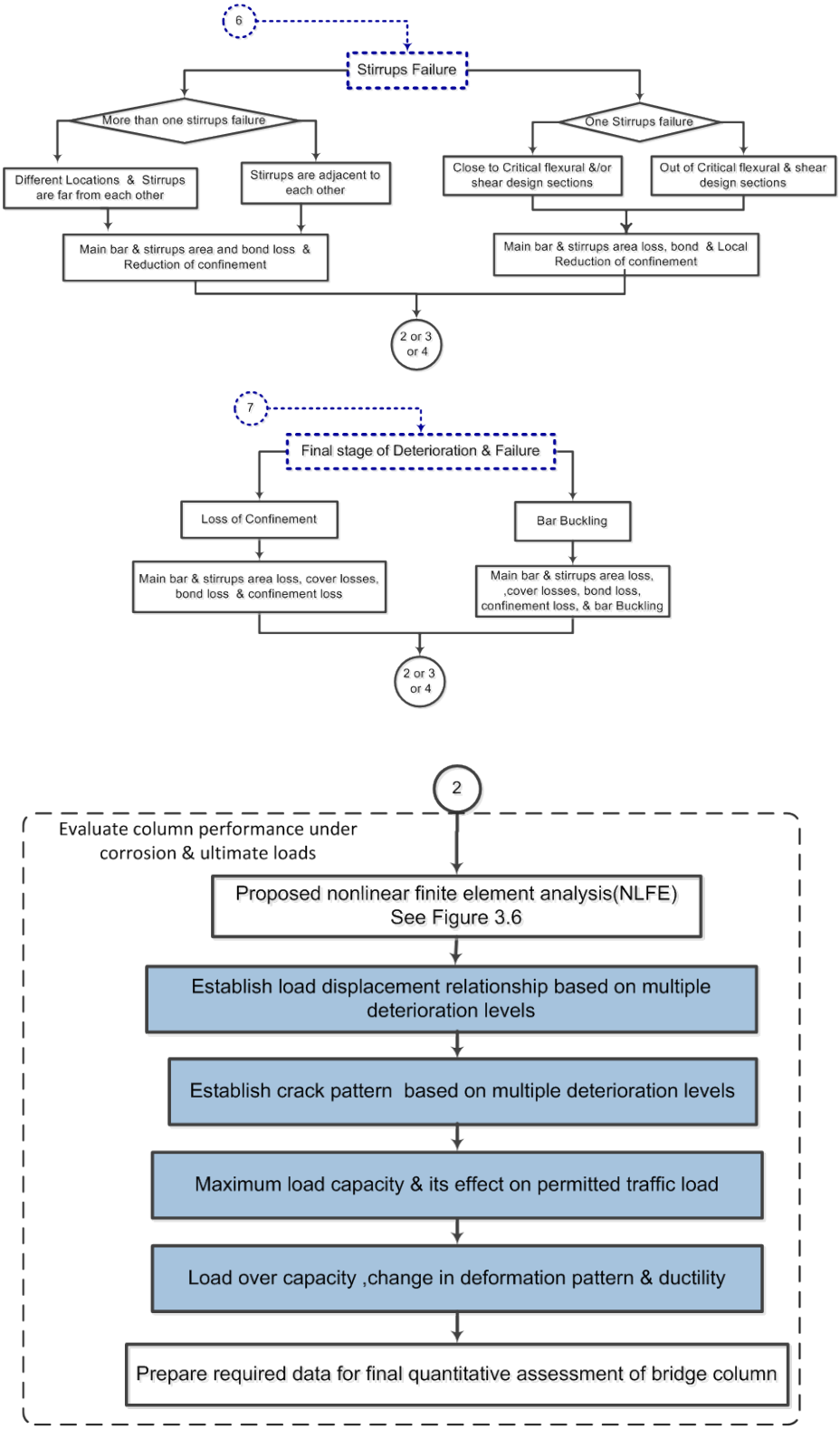

Cont'd. Figure 3.2: Evaluation of column performance under corrosion & ultimate loads.

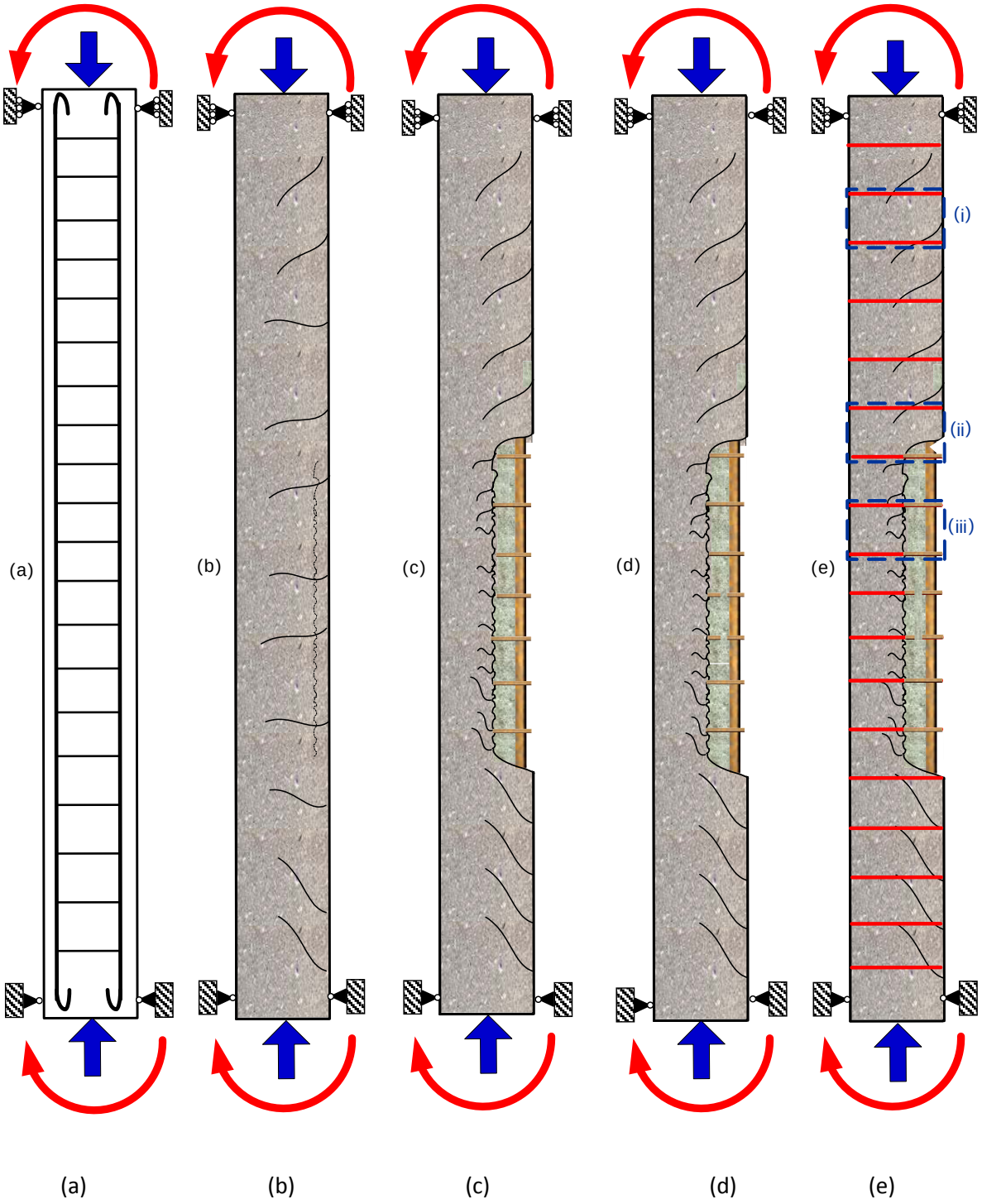

Figure 3.3 : Possible damage and failure modes of an RC beam-column due to combined gravity loads and corrosion; (a) schematic drawing; (b) flexural and corrosion cracks; (c) spalling on tension side; (d) stirrups failure;(e) beam-element discretization: (i) no corrosion damaged zone,(ii) partially-corrosion damaged zone,(iii) fully-corrosion damaged zone.

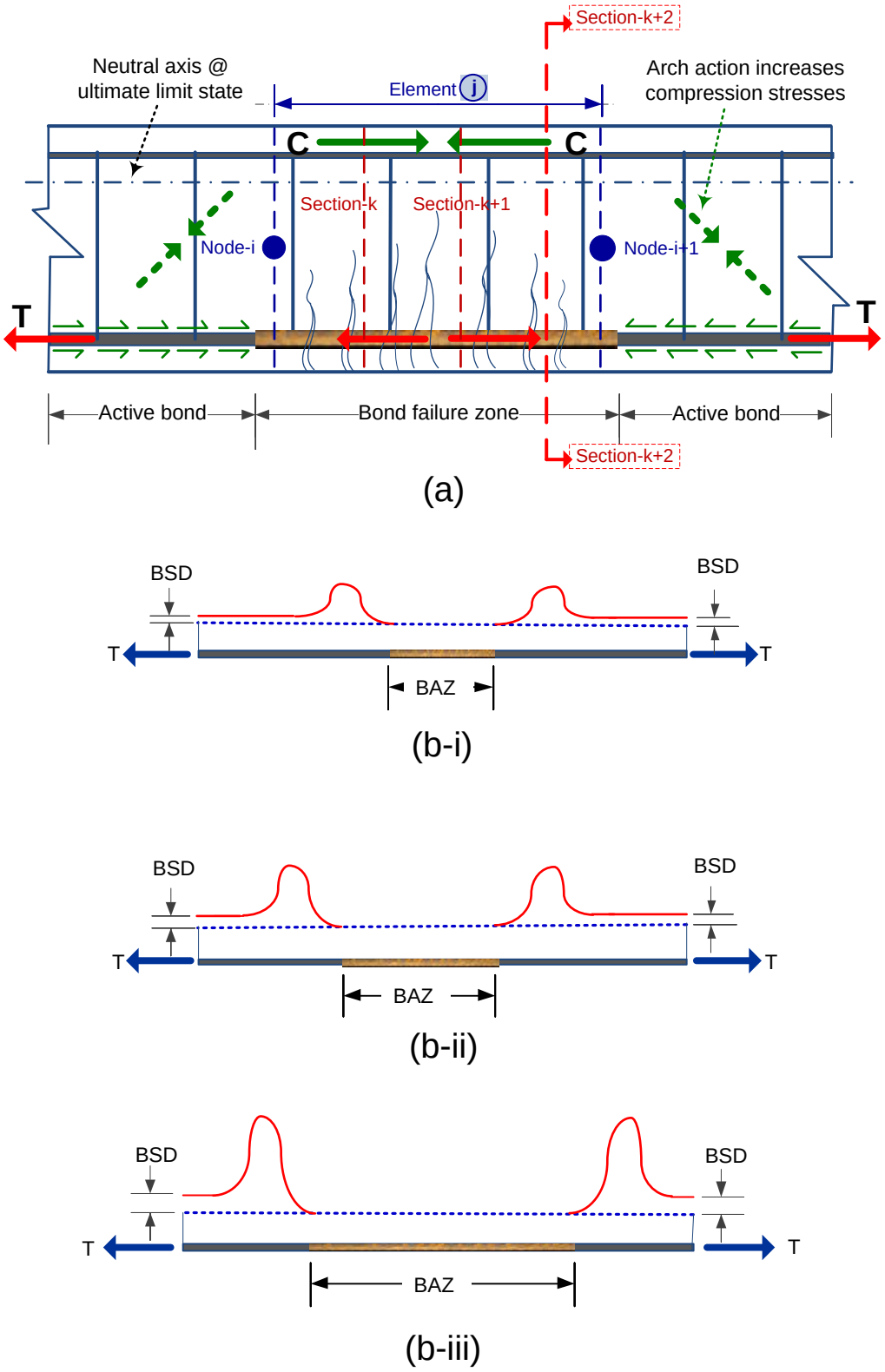

Figure 3.4: Formation and migration of bond stress “wave” throughout formation and progression of local bond failure due to corrosion.

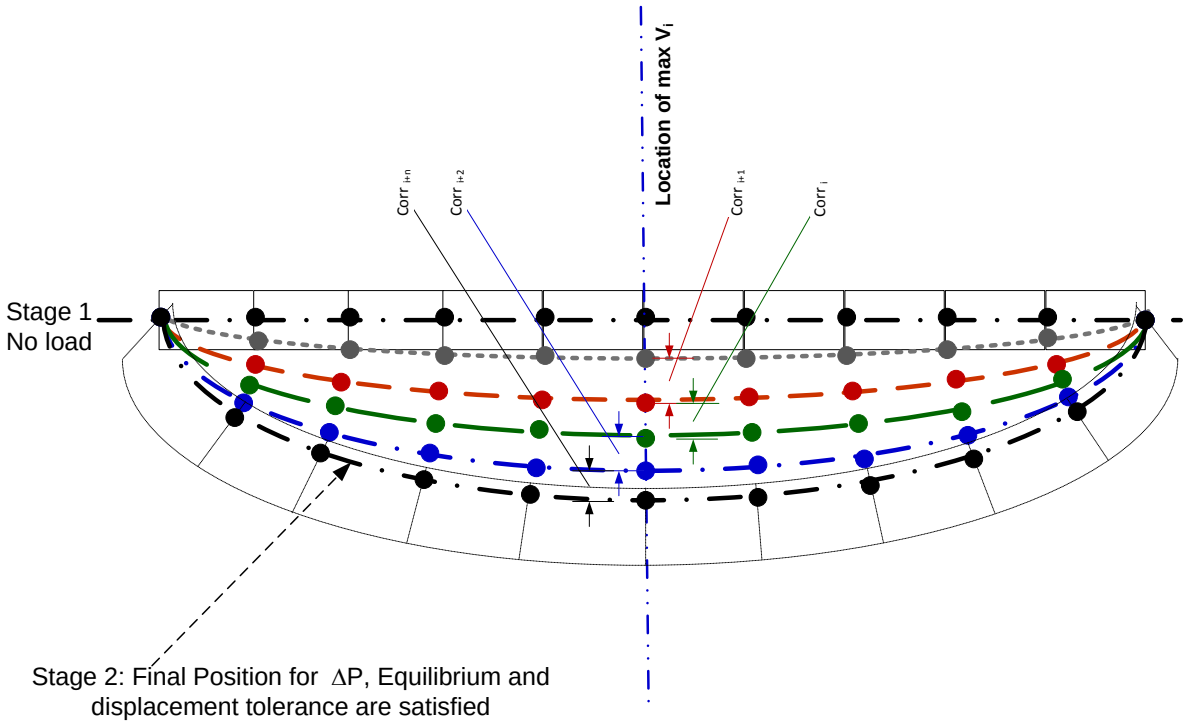

Figure 3.5: Displacement field tuning convergence in the proposed nonlinear finite element analysis procedure.

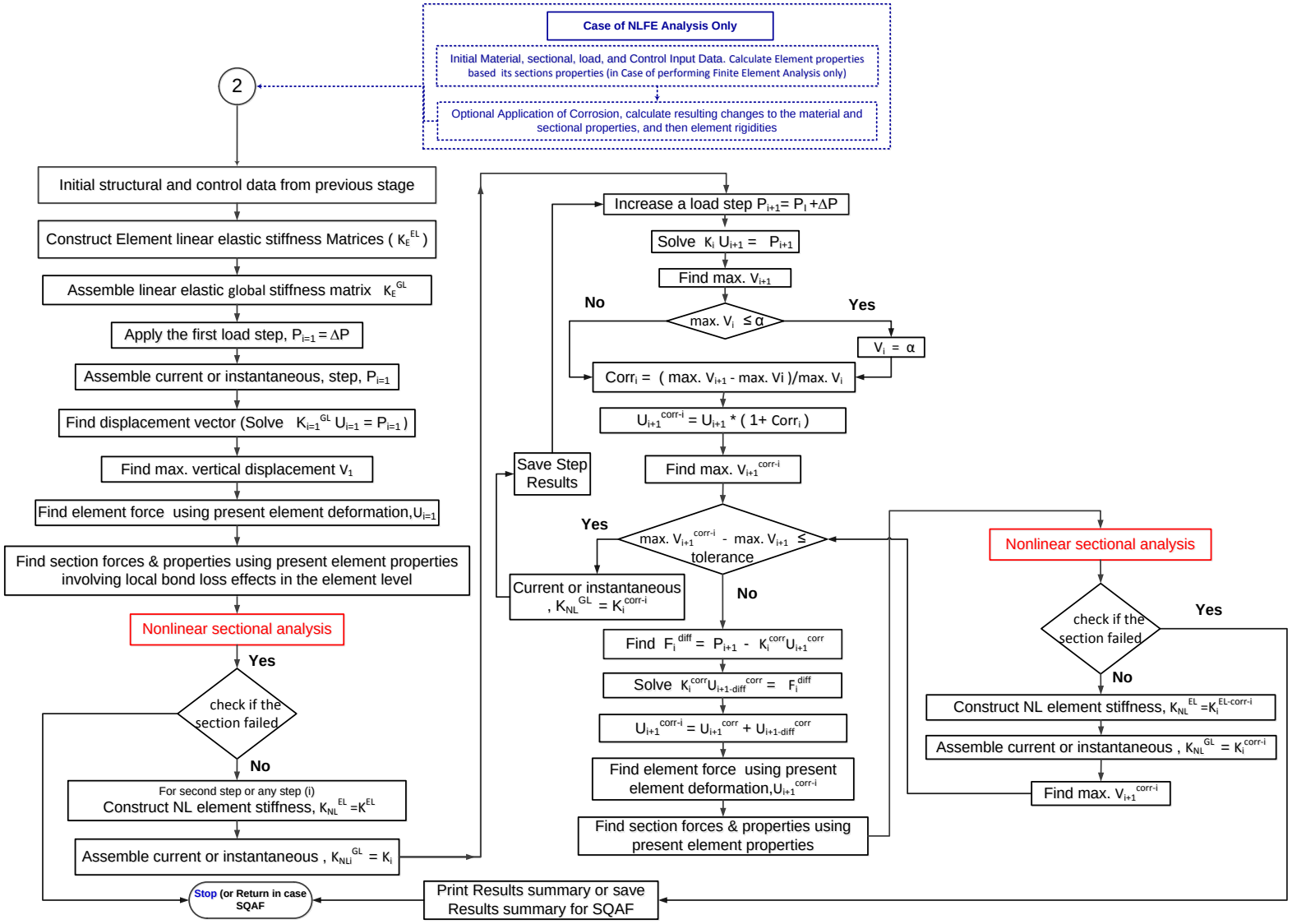

Figure 3.6: Proposed nonlinear finite element analysis approach.

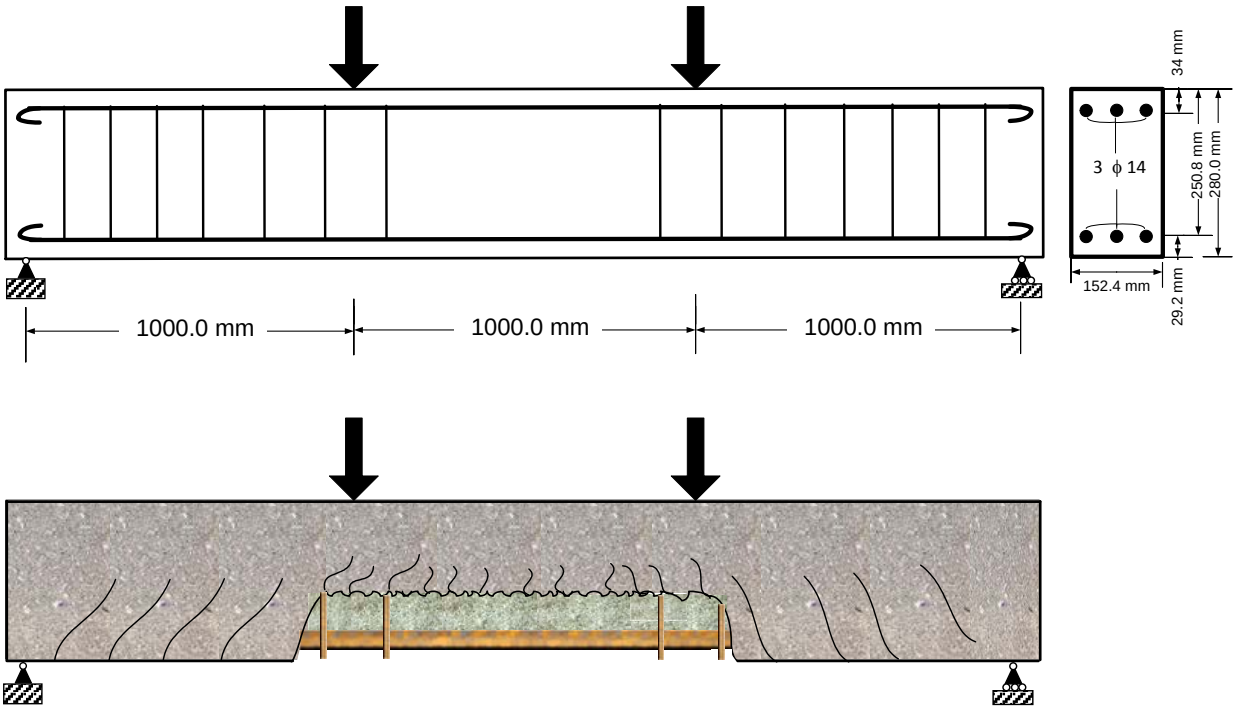

Figure 3.7-a: Case study I: beam under four points loading (Rashid & Dinno 1994a) subjected to corrosion over the middle one-third of the span.

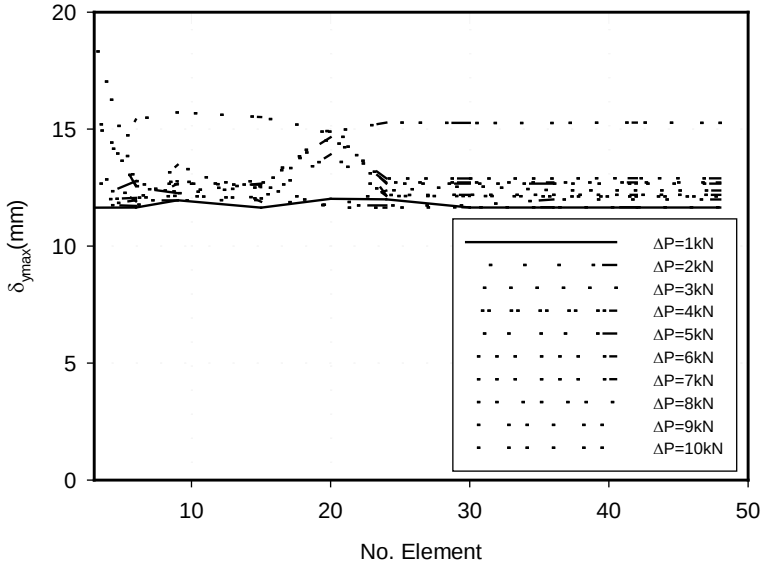

Figure 3.7-b: Case study I: Maximum displacement versus number of elements (NEL) for different load increments (ΔP) for simply-supported beam subjected to four-point loading (undamaged).

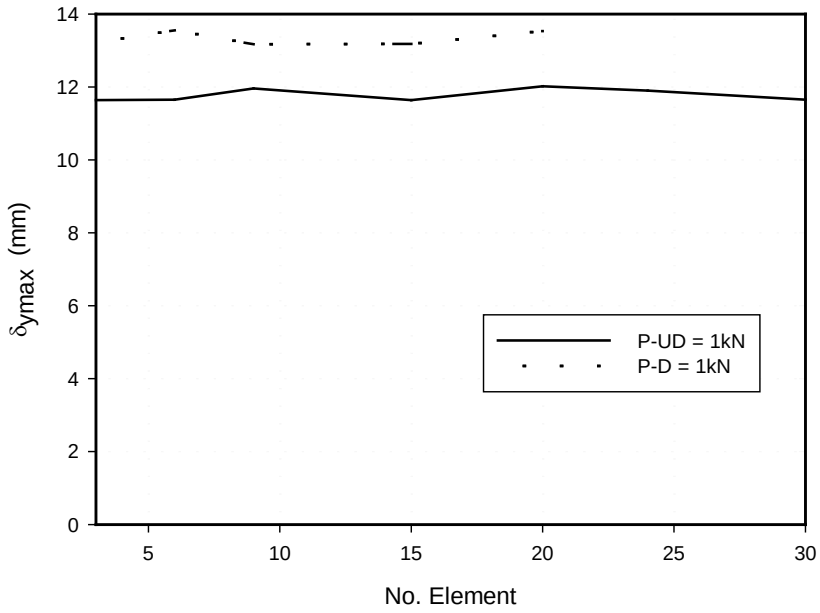

Figure 3.7-c: Case study I: variation of No. of elements (NEL) and applied load increment (ΔP) for an undamaged (UD) and a damaged (D) beam.

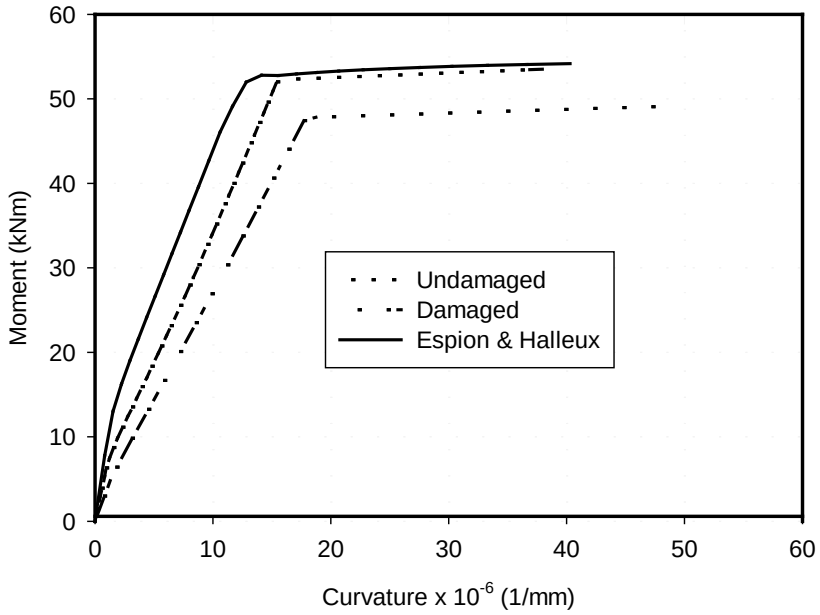

Figure 3.7-d: Case study I: Load versus mid-span curvature for an undamaged and a damaged beam ;(Espion and Halleux 1988).

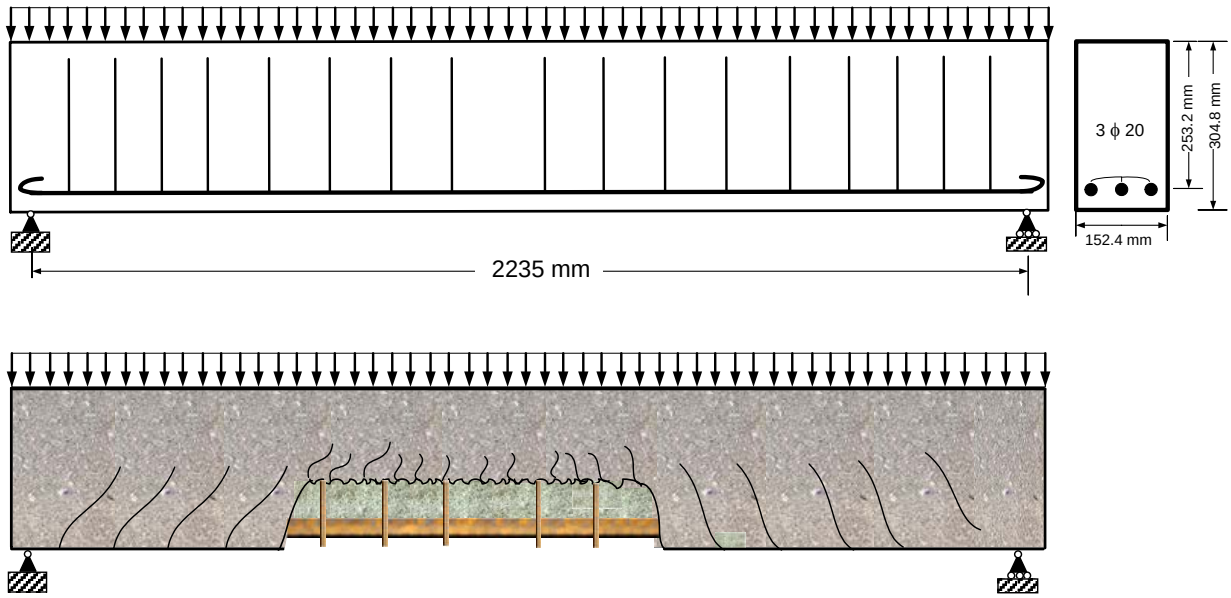

Figure 3.8-a: Case study II: simply-supported beam under uniformly distributed load (De Cossio-Siess (1960) and Rashid & Dinno (1994b)) subjected to corrosion over the middle one-third of the span.

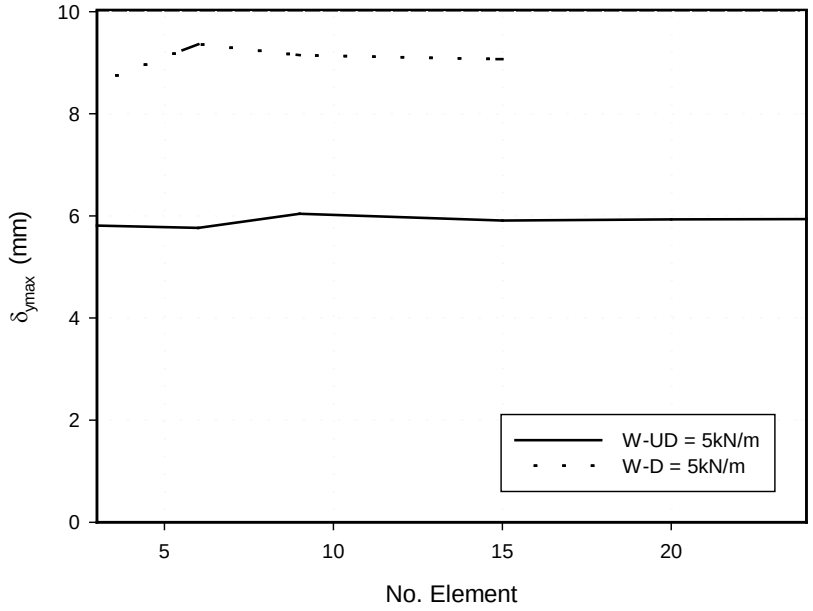

Figure 3.8-b: Case study II: variation of No. of elements (NEL) and applied load (ΔW) for an undamaged (UD) and damaged (D) beams.

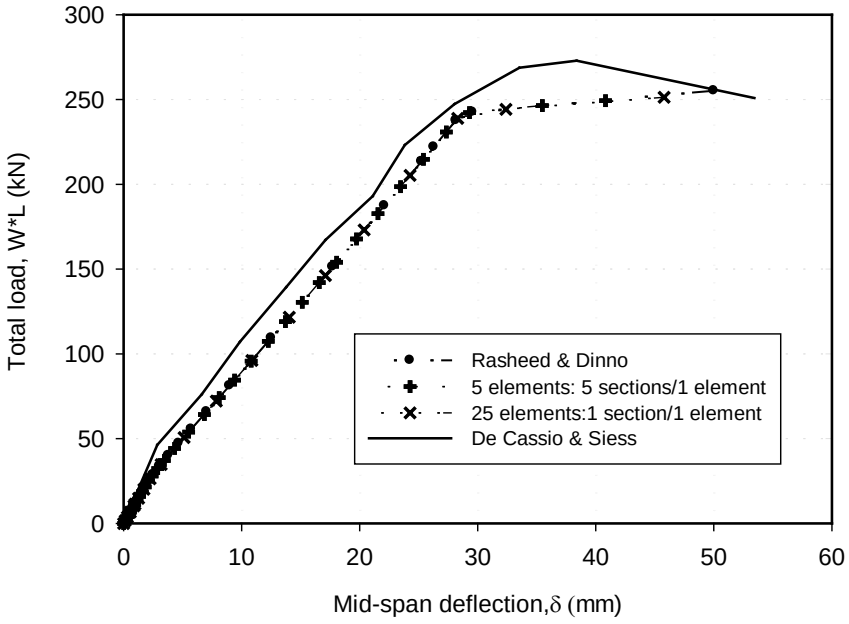

Figure 3.8-c: Case study II: Load versus mid-span deflection of a simply-supported beam subjected to uniform distributed load (UDL); (De Cossio-Siess (1960) and Rashid & Dinno (1994b)).

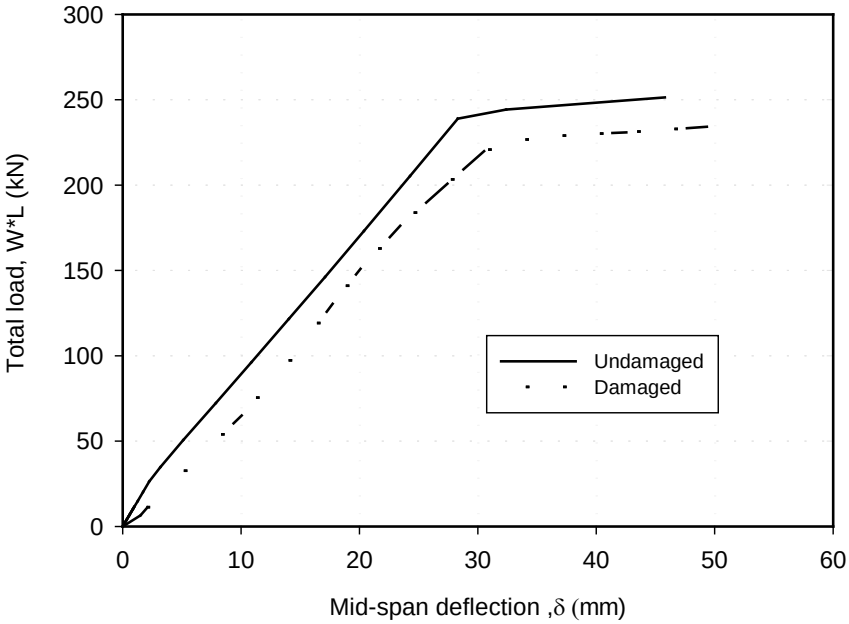

Figure 3.8-d: Case study II: Load versus mid-span deflection for the beam when subjected to UDL only (Undamaged) or when subjected to reinforcement corrosion at mid-span as well (Damaged).

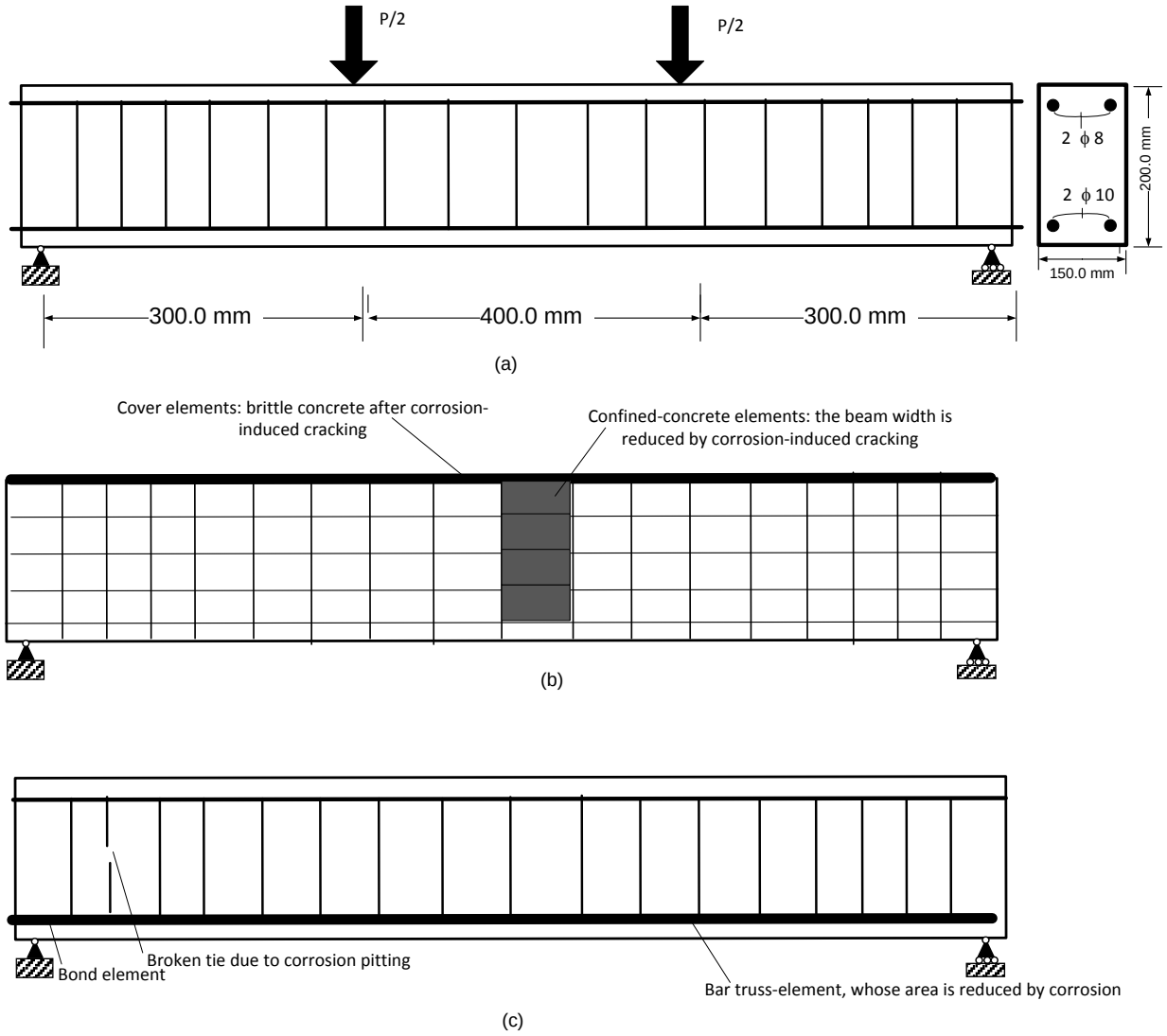

Figure 3.9-a: Case study III: simply-supported beam under points load and corrosion (Coronelli & Gambarova 2004); (a) reinforced concrete beam geometry and reinforcement ;(b &c) finite element of a reinforced concrete beam taking into account the mechanical effects of corrosion.

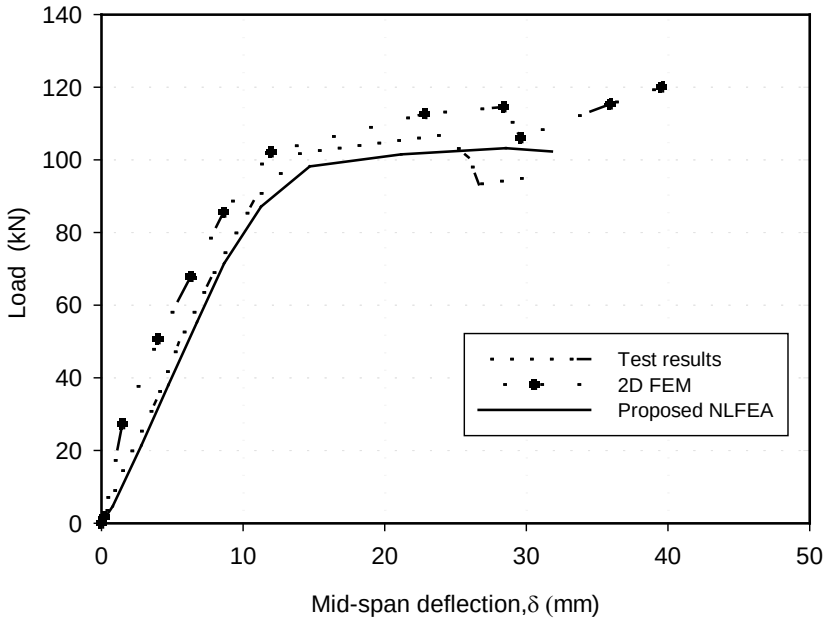

Figure 3.9-b: Case study III: comparison of the proposed NLFEA results to experimental and numerical results of Rodríguez et al. (1996) and Coronelli & Gambarova (2004), respectively.

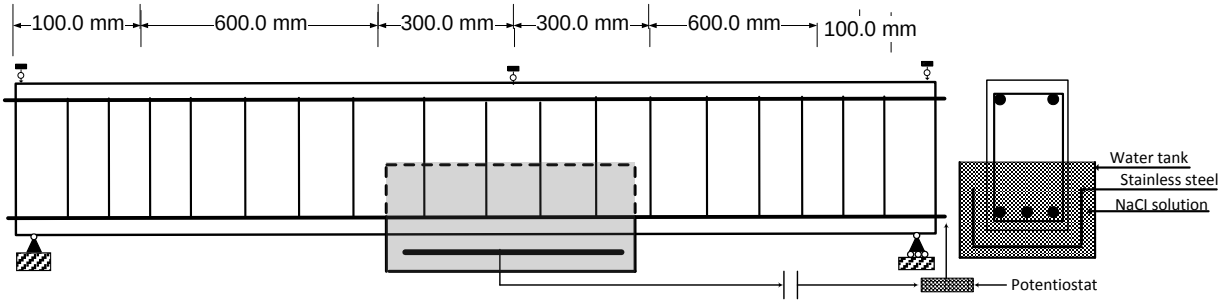

Figure 3.10-a: Case study IV: simply-supported beam under points load and corrosion (Yingang et al. 2007).

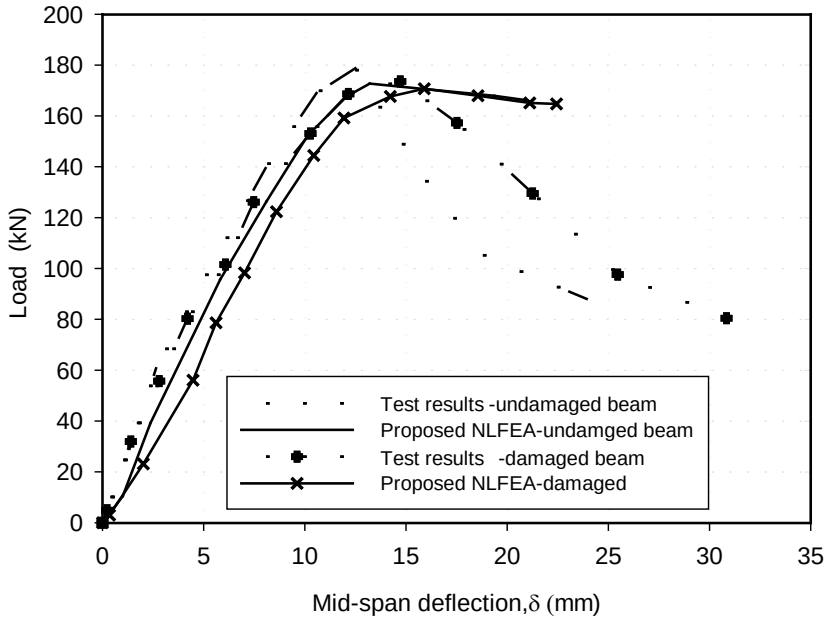

Figure 3.10-b: Case study IV: comparison of the proposed NLFEA results to experimental results from Yingang et al. (2007).

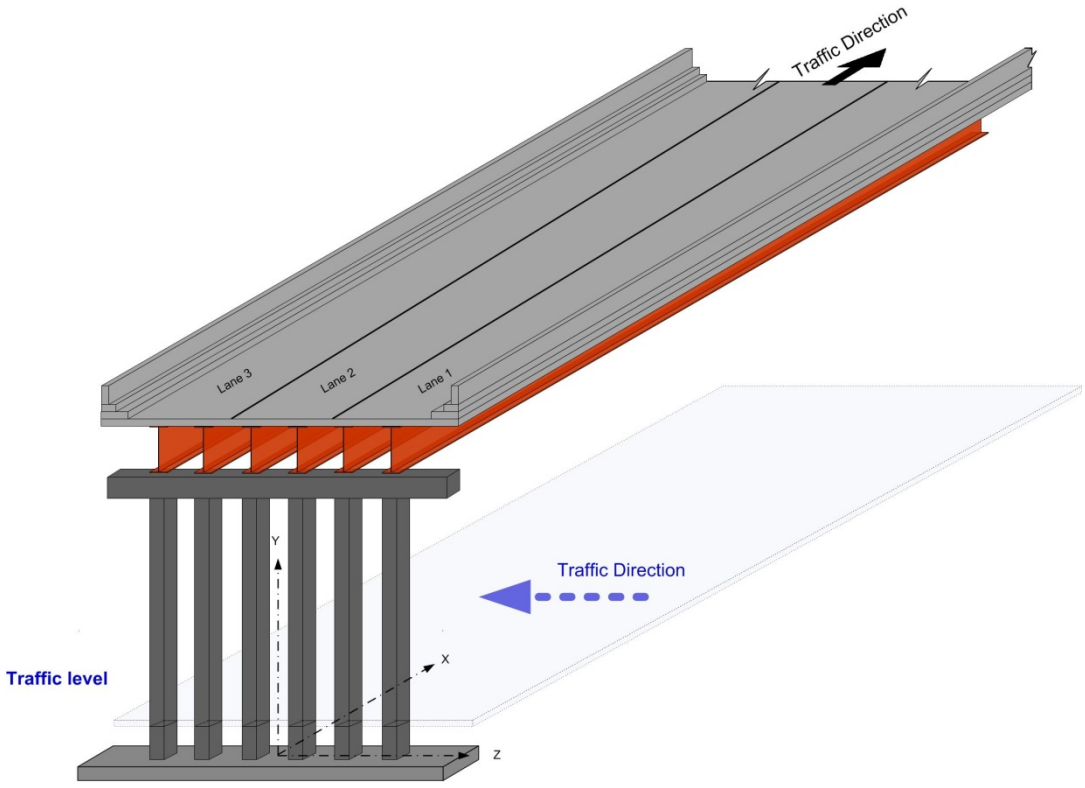

Figure 3.11-a: Case study V: bridge columns of slab-on-girder bridge subjected to local corrosion.

Figure 3.11-b-i: Case study V: sample slab-on-girder bridges with partial corrosion damage (Gardiner Parkwey-Expy, Toronto, Canada).

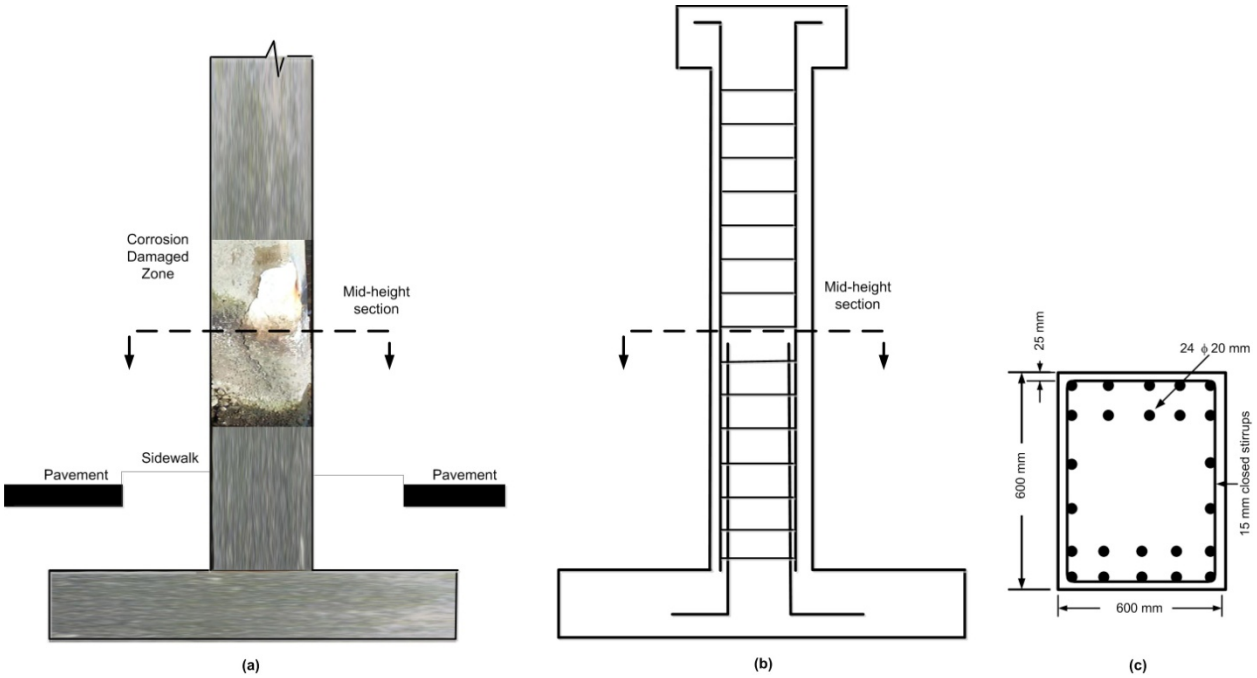

Figure 3.11-b-ii: Case study V: (a) most affected corrosion zone on a slab-on-girder bridge column; (b) column reinforcement and location of mid-height section; (c) column cross-section details.

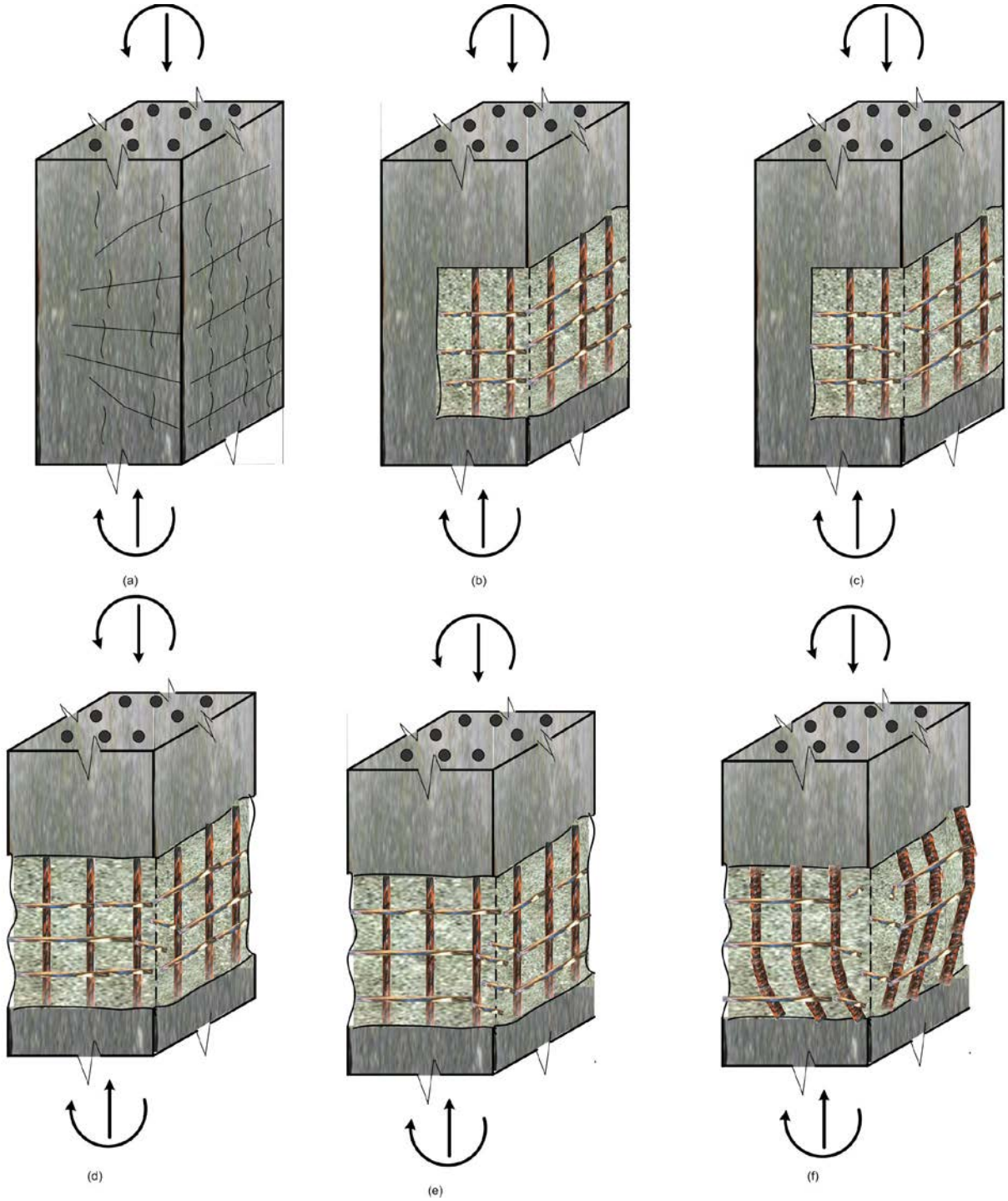

Figure 3.11-c: Case study V: possible damage of RC beam-column subjected to combined external loads and corrosion; (a) flexural and corrosion cracks; (b) initial spalling; (c) one stirrup failure; (d) spalling on all sides; (e) two stirrups failure; (f) loss of confinement and possible buckling.

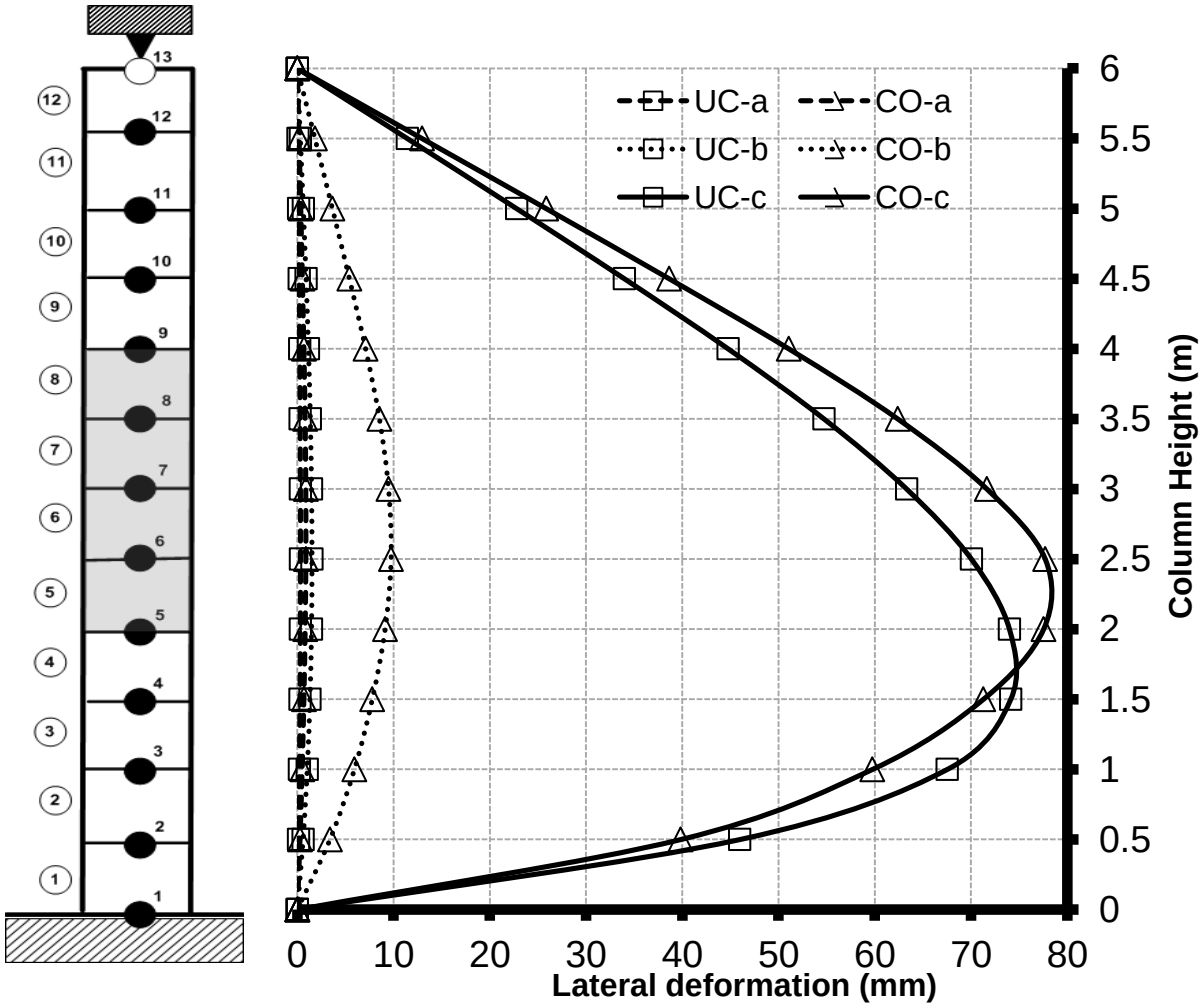

Figure 3.11-d: Case study V: FE disctitization of the column and lateral displacement of un-corroded (UC) and corroded (CO) column, both with (e = 5H), for (a) below yield load (M = 3000 kN.m); (b) after yield and below ultimate (M = 6000 kN.m); and (c) at ultimate load (M_{UC} = 8200 kN.m and M_{CO} = 6750 kN.m).

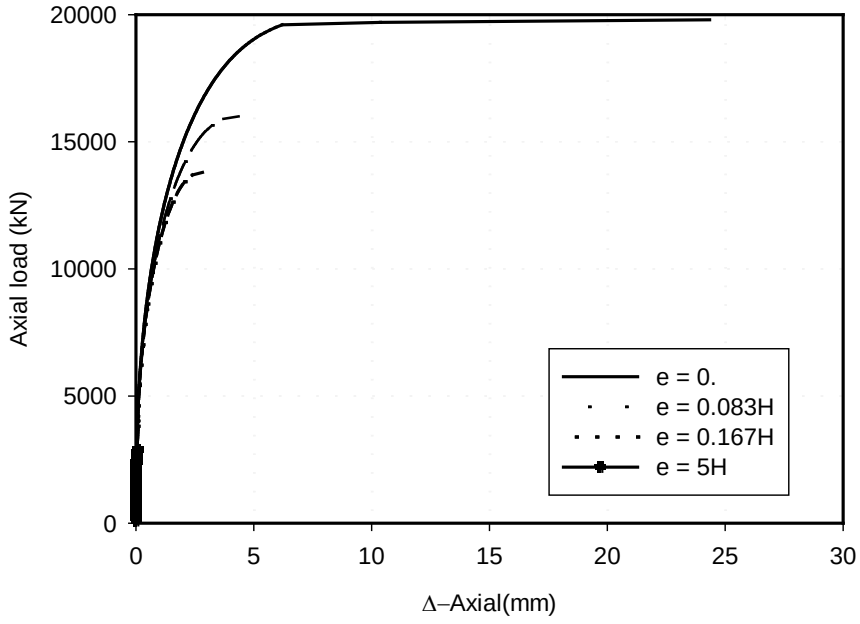

(a)

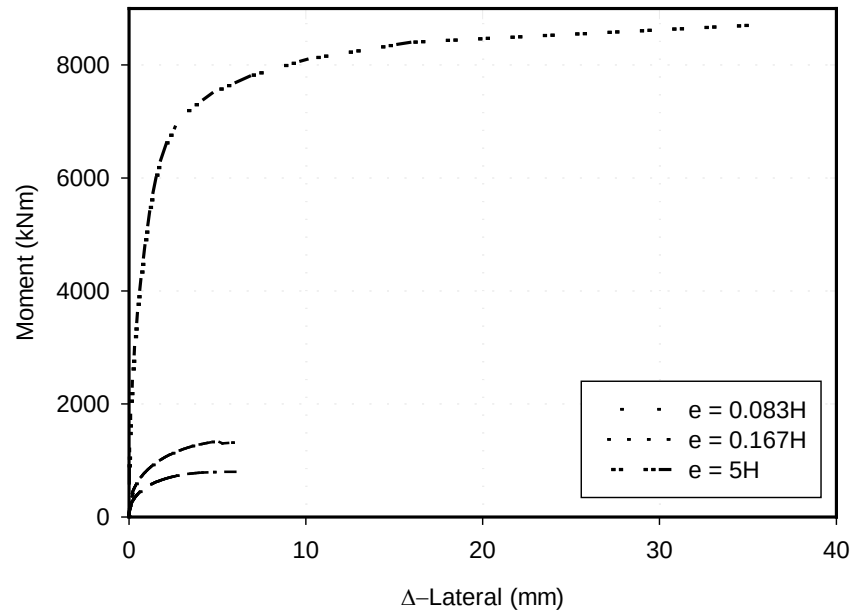

(b)

Figure 3.11-e: Case study V: (a) P-Δ_{axial} & (b) M-$\Delta_{lateral}$ at the mid-height section of the column where NO corrosion load is applied, for (e = 0 to 5H).

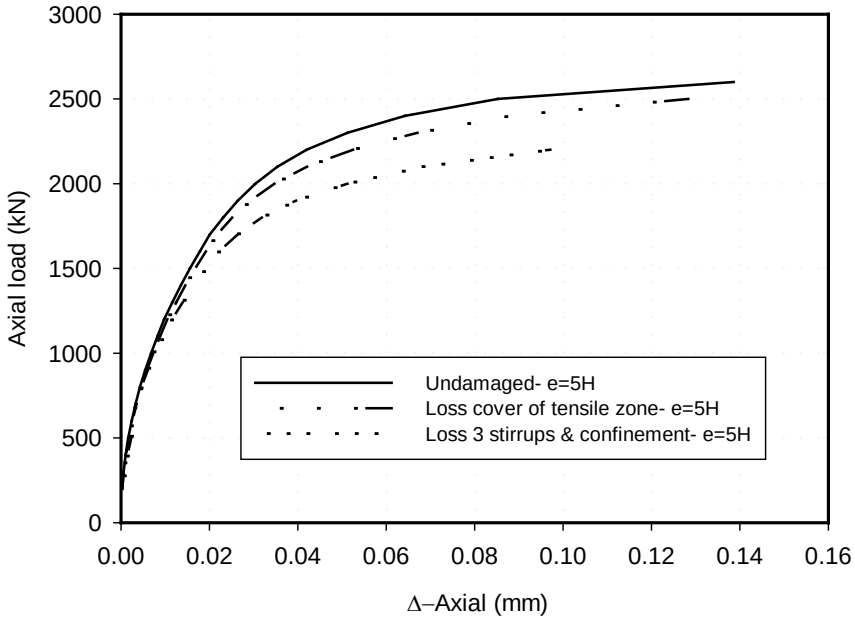

(a)

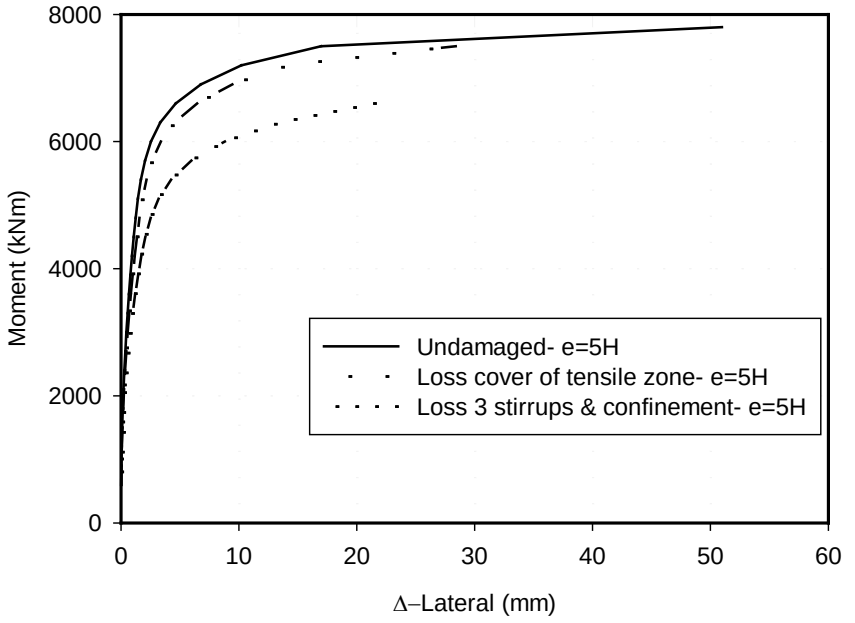

(b)

Figure 3.11-f: Case study V: (a) P-Δ_{axial} & (b) M-$\Delta_{lateral}$ at the mid-height section of the column where the corrosion load is applied, for (e =5h) and for different corrosion cases.

3.7 References

American Association of State Highway and Transportation Officials, AASHTO LRFD Bridge Design Specifications SI Units (4th Edition); 2007.

Almansour, H., The structural analysis of partially buttressed reservoir walls using finite element method. M.Sc. Thesis. University of Basrah, Basrah, Iraq; 1988.

Canadian Standards Association, Canadian Highway Bridge Design Code, S6-06, A;2006.

Coronelli, D. And Gambarova P., Structural assessment of corroded reinforced concrete beams: modeling guidelines. Journal of Structural Engineering; 2004,130(8)1214-1224.

De Cossio, R. and Siess P., Behavior and strength in shear of beams and frames without web reinforcement. J. Am. Conc. Inst.; 1960,56,695-735.

Espion B., and Halleux P. Moment curvature relationship of reinforced concrete sections under combined bending and normal force. Material and Structural.1988;21:341-351.

Lounis, Z., Vanier, D.J., Daigle, L., Sadiq, R., Almansour, H., Framework for Assessment of State, Performance and Management of Core Public Infrastructure, NRC Canada, Project 5332-Final Report; 2010.

Mohammed, A., Almansour, H., Martín-Pérez, B., State-of-the-Art in nonlinear modeling of concrete frame structures under the combined effect of ultimate loading and reinforcement corrosion. CSCE 3rd International Structural Specialty Conference, Edmonton, Alberta, 2012,June 6 to 9.

Mohammed, A., Almansour, H., Martín-Pérez, B., Nonlinear flexural analysis of reinforced concrete beam-column subjected to ultimate gravity loads combined with reinforcement corrosion, Part I: Sectional Analysis. Structure and Infrastructure Engineering, submitted, ID NSIE-2014-0014; 2014a.

Mohammed, A., Almansour, H., Martín-Pérez, B., Evaluation of dynamic of slab-on-girder-bridge under moving trucks with corrosion-damaged columns", Engineering Structures, (6), 159-172;2014c.

Mohammed, A., Almansour, H., Martín-Pérez, B., Seismic performance of aged reinforced concrete bridge columns subjected to reinforcement corrosion. Journal of Bridge Engineering (ASCE), to be submitted; 2014d.

Mohammed, A., Almansour, H., Martín-Pérez, B., A semi-quantitative assessment framework for aging reinforced concrete bridge columns. Engineering Failure Analysis; to be submitted; 2014e.

Rasheed, H., and Dinno, K., An efficient nonlinear analysis of RS sections. Computer and Structures; 1994a, 53(3)613-623.

Rasheed, H., and Dinno, K., An improved nonlinear analysis of reinforced concrete frames. Computer and Structures; 1994b, 53(3)625-636.

Rodríguez, J., Ortega, L. M. and Casal, J., Load bearing capacity of concrete columns with corroded reinforcement. Corrosion of Reinforcement in Concrete Construction, Royal Society of Chemistry; 1996, 220-230.

Oyado, M., Saito, Y., Yasojima, A., and Kanakubo, T., Structural Performance of corroded RC column under seismic Load. First International Workshop on Performance, Protection & Strengthening of Structures under Extreme Loading, Whistler, Canada; 2007.

Yingang, D., Leslie, A., and Chan, A., Impact of reinforcement corrosion on ductile behaviour of reinforced concrete beams. ACI Structural Journal; 2007,104(28),285-293.

Chapter 4

Evaluation of Dynamic Deformations of Slab-on-Girder Bridge under Moving Trucks with Corrosion Damaged Columns as Part of Semi-Quantitative Assessment Framework

4.1 Introduction

Evaluating the dynamic performance of a bridge structure under service loads is a major component of bridge design requirements as well as of assessment of aging bridges. At present, qualitative assessment approaches are used in most of North American states and provinces. With the lack of accuracy of existing assessment approaches, there is a need to develop a more efficient assessment approach that can quantitatively evaluate the bridges structural performance when safety critical elements (the bridge columns, for instance) are partially damaged. A semi-quantitative assessment approach has been proposed in Chapter 3 (see Mohammed et al. 2014b), introducing a limit states evaluation (LSE) approach in parallel to the limit states design (LSD) approach in North American bridge design codes (CSA S6-06/ CHBDC 2006, and AASHTO LRFD Bridge Design Specifications, 2007). The major evaluation limit states are: evaluation ultimate limit state (ULS), evaluation serviceability limit state (SLS) and evaluation earthquake limit state (ELS). The focus of this chapter is on the evaluation serviceability limit state, which is mainly based on evaluating the maximum static and dynamic deformations when an aging structure is under service loads.

The requirements for a quantitative assessment of the serviceability of aging bridges address the importance of estimating, measuring and monitoring the changes in bridges dynamic characteristics for different critical levels of corrosion damage. The damages that result from reinforcement corrosion of the bridge column, such as spalling of concrete cover, reduction in

reinforcement section, fracture of one or more stirrups, etc, can be defined as critical damage levels. As a transition stage preceding the development of a time-dependent quantitative assessment approach, visual inspection can be employed as major source of input to the proposed quantitative assessment framework.

It is thought that the changes in basic dynamic characteristics, such as the natural frequencies of bridge systems (or bridge elements), can be used as an accurate measure to identify and quantify their state of damage. This is based on the observed reductions of the stiffness and the mass of the affected bridge members. However, the natural frequencies are proportional to the square root of the structural element stiffness-to-mass ratio, and hence they are not apparently affected by the discretization approach or to the variation of the finite element characteristics. Most bridge columns are conservatively designed (over-designed) and their service-load-over-capacity ratios (SLOCR) are usually low or sometimes very low (usually 25% to 50%). For aging bridges, the increase in the truck load, traffic density, frequency and speed, in addition to the reduction in the load capacity of corrosion-affected columns, could apparently increase their SLOCR. Higher design SLOCRs are targeted for newly constructed bridges, to reduce the initial cost or to satisfy aesthetical needs, for the increasing use of high performance (HP) materials, and for performance-based design and structural optimization approaches. On the other hand, the design truck load, traveling velocity, number of truck axels, and the average number of trucks passing over bridges have been extensively increased in the past four decades. This has raised the concern about the possible increase of the vibration and dynamic deformation of bridges, which could exceed the acceptable limits in the bridge design codes.

Bridge design codes in North America (CSA S6-06/ CHBDC 2006, and AASHTO LRFD Bridge Design Specifications, 2007) limit the vibration amplitude to an acceptable level as part of the

serviceability limit state checks. Depending on the slenderness, damping, and continuity of the bridge superstructure and its integration with the bridge substructure, the vibration of the bridge could be sensitive to the dynamic excitation of the traffic load. For short and medium span bridges, the significant changes in the superstructure or substructure stiffness and mass due to reinforcement corrosion of the bridge columns can result in distinguished changes of the vibration amplitude and/or mode shape. Corrosion-related damages to bridge substructures could result in significant reduction in their structural capacities and safety. However, it has not been reported whether the changes in bridges substructures (columns) capacity to a critical level result in a similar critical change in the dynamic characteristics of the bridge superstructure under traffic load. Such changes in the bridge dynamic characteristics are of major interest to bridge owners and those involved in their maintenance as a basis for the development of health monitoring and/or non-destructive evaluation techniques. On the other hand, many observations of the change in vibration amplitude of bridge superstructures related to the reinforcement corrosion of the deck slab or girders or both are reported (Cremona 2004).

With the progress of reinforcement corrosion in affected zones, the bridge column capacity is reduced, and hence the load-over-capacity ratio of the substructure (bridge columns) is increased. Although the service load is lower than the ultimate capacity, and the structural behaviour is mostly in the elastic range when subjected to traffic loads, reinforcement corrosion and its effects on the concrete strength and confinement could shift the elastic behavior of the column to the plastic region. Many researchers have also observed that the ductility of the reinforcement is also reduced with the progression of corrosion (Rodríguez et al. 1996). Typically, linear dynamic finite element analysis is used to evaluate bridge vibration. However, with the shift of the structural behaviour of bridge columns to the plastic region, the material nonlinearity should be

taken into account in estimating the instantaneous element stiffness in the corrosion-affected zone. Hence, nonlinear modeling of the substructure should be essential.

The objective of this chapter is to develop a simplified hybrid linear/nonlinear dynamic finite element analysis (SHDFEA) that enables an accurate evaluation of the vibrations of aging bridges when the bridge columns are subjected to severe reinforcement corrosion as part of the proposed semi-quantitative assessment framework. The emphasis is on: (i) the numerical efficiency and stability of the analysis approach; (ii) the approach capability to capture the characteristics changes in dynamic deformation distributions over the superstructure and the substructure; (iii) the approach ability to determine the changes in the dynamic load allowance (or the impact factor); and, (iv) exploring the cases where the simplified linear dynamic finite element analysis (SLDA) is adequate.

4.2 Simplified hybrid linear/nonlinear dynamic finite element analysis (SHDFEA) as a part of semi-quantitative assessment framework (SQAF)

Figure 4.1 shows the proposed SQAF, which has six major parts: (I) data input; (II) quantifying reinforcement corrosion and its effects; (III) evaluating columns performance under combined corrosion and ultimate loads (evaluation-ULS); (IV) evaluating columns performance under combined corrosion and service (or traffic) loads (evaluation-SLS); (V) evaluating columns performance under corrosion and seismic loads (evaluation-ELS) (only in high risk seismic zones); and, (VI) semi-quantitative assessment and reporting. In North American bridge codes (CSA S6-06/ CHBDC 2006, and AASHTO LRFD Bridge Design Specification, 2007), the serviceability limit state is a major limit state to be verified for bridge design. Nonlinear dynamic finite element analysis is the basis for the evaluation serviceability limit state of the proposed

semi-quantitative assessment framework (SQAF). The evaluation of the column structural performance under combined reinforcement corrosion and ultimate loads, and the evaluation of the column structural performance under combined reinforcement corrosion and seismic loads are respectively presented in Chapters 3 and 5 (Mohammed et al. 2014b&d).

The first part of the proposed SQAF includes three data-input tasks: (I-a) the structural material and geometrical data including boundary conditions; (I-b) the loading data; and, (I-c) the enhanced in-depth visual inspection (or enhanced inspection) and any required material test. In the first task, the data are collected from the original design information/report and shop drawings (if available), and from field tests on the materials in their current state (if possible). The difference between the original design loads and the present loads on the bridge column under consideration are to be determined. Visual inspection (see Chapter 6; Mohammed et al. 2014e) can provide important measurements and details that can identify the affected zone, state of corrosion and the resulting local damage. Further tests following the visual inspection are necessary to quantify the major factors essential to estimate the material properties if detailed testing program is not an economical option. The deterioration of the structural parameters is then re-evaluated quantitatively through the NLFEA as presented in Chapter 3 and shown in Mohammed et al. (2014b).

The proposed SQAF identifies four major damage cases due to reinforcement corrosion, which are: (a) cracking of concrete due to corrosion; (b) spalling of the concrete cover; (c) rupture of one or more stirrups; and, (d) in a more advanced state of corrosion damage, structural failure of the column through complete loss of confinement and/or rebar(s) buckling. The details of each of these major possible deterioration states are shown in Figure 4.2.

The evaluation SLS is integrated with the proposed SQAF (see step IV above) in Figure 4.1, where quantifying the effects of reinforcement corrosion for each major case is taken into account. The flowchart shows the link to one of the three major evaluation limit states: ULS, SLS, which is discussed in detail in this chapter, and ELS. The simplified hybrid linear/nonlinear dynamic finite element analysis (SHDFEA) is the basis of four tasks of the evaluation-SLS, which are: (a) establishing the static mid-span deflection when the truck is moving very slowly over the bridge length; (b) establishing the dynamic deflection of the bridge superstructure under front axle for maximum truck speed and for extreme corrosion damage; (c) establishing the dynamic load allowance DLA as per CHBDC or the impact factor (IF) as per AASHTO for different states of damage of the column; and, (d) establishing the dynamic lateral displacement of the bridge columns versus the truck location for different cases of damaged and undamaged columns. These four tasks of evaluation-SLS end with the preparation of the required data for the SQAF. The details of the proposed SQAF are presented in Chapter 6 (Mohammed et al. 2014e).

4.3 Appropriate dynamic analysis approach of slab-on-girder bridge subjected to traffic combined with reinforcement corrosion

The focus of this chapter is on the effects of local corrosion damage in slab-on-girder bridge columns on the vibrations of the bridge superstructure and columns themselves. It is believed that for the purpose of the development of the dynamic analysis approach, the bridge columns represent the most general members under axial load and moment in addition to their boundary conditions. Columns also represent the most critical elements for the bridge safety, and developing a tool to quantify their damage effects on the bridge vibrations is of high interest to bridge owners, practicing engineers and researchers. In order to avoid the interaction of the corrosion damage effects of different zones of the bridge superstructures and columns on the

bridge vibration, the bridge superstructure is assumed to be in a good condition with no corrosion damage. Figure 4.3-a shows a highway overpass where a three-lane slab-on-steel-girder (superstructure) is supported by a typical multi-column reinforced concrete (RC) pier with a RC cap beam (substructure). Aging slab-on-girder bridges are affected by corrosive aggressive environment due to the use of deicing-salt over the long winter in Canada and the Northern states of the United States. Figures 4.3-a and 4.3-b show the traffic directions over and under the bridge, and they show a typical road configuration in the highway overpass. The splash of salty water affects the bridge columns above the traffic level, where corrosion damage usually develops at approximately the middle-third of the column height (see Figure 4.3-b).

When a heavy truck passes over the bridge superstructure as shown in Figure 4.3-b, the truck load is transferred to the two bridge substructures based on the location of the truck with respect to the two piers. As the truck passes over the left column (assuming the traffic direction is from left to right), the load transferred to that column is the maximum possible load. When the truck moves away from the left column, the load on the left column is decreased and reaches its minimum level as the truck leaves the bridge. As shown in Figure 4.3-c, for example, the truck front axle at point B_i gives lower load on the left column than the load when the truck front axle is at point A_i. As the bridge is designed to satisfy ultimate and serviceability limit states, the bridge column is assumed to have enough safety at ultimate limit state, and it would always behave in the elastic range when subjected to service loads. As shown in Figure 4.3-d, and right after the bridge construction is completed, the maximum ultimate load B_{iu} results in elastic deformation, while the ultimate load A_{iu} results in plastic deformation well below the failure load (as per typical conservative design of bridge columns). When reinforcement corrosion and related damage occur, the strength, stiffness and deformability range of the columns are reduced

as shown in Figure 4.3-d. For a severe level of corrosion damage, it is possible that when an overloaded truck is in a critical location of the bridge, the bridge load capacity could be lower than the applied load. Even under a typical truck load (service level), the column deformation could be in the non-elastic region. Hence, nonlinear analysis has to be used in the development of the dynamic analysis of the bridge column subjected to traffic load combined with reinforcement corrosion. In the case a bridge column is overdesigned and continues to behave elastically under all levels of service loads, even with a severe level of corrosion damage, and then elastic dynamic analysis gives an economical solution.

4.4 Proposed simplified hybrid linear/nonlinear dynamic finite element analysis (SHDFEA)

The proposed SHDFEA approach is developed to estimate the vibration of different components of the slab-on-girder bridge: the superstructure, as well as the damaged columns themselves. The effects of corrosion damage in the bridge column on the vibration of the superstructure are more interesting than the vibration of the columns, because: (i) its vibration amplitude is limited by code requirements; (ii) the direct contact between the vehicle and the superstructure results in the highest possible dynamic response to be in the superstructure; and, (iii) the hinge and roller connecting the superstructure to the substructure (in addition to the dampers) reduce the dynamic load transferred to the columns. It is important to mention that the proposed dynamic analysis approach is developed for two-axle trucks; however, it is extendable to any multi-axle truck with any configuration when the basic dynamic characteristics of the truck are available.

Figure 4.4 shows a brief flowchart of the proposed SHDFEA, where both the static and the linear/nonlinear time history analysis of the traffic load are performed. The input data of SHDFEA is transferred from earlier stages of the semi-quantitative assessment framework

(SQAF), which includes the visual inspection data and the quantification of the effects of reinforcement corrosion as shown earlier (see Figures 4.1 and 4.2). As mention in the previous section, the finite elements of the bridge superstructure are assumed to behave linearly elastic under the traffic load (service load), as no corrosion damage is assumed in the superstructure. The bridge columns, on the other hand, are subjected to high axial load, and their behaviour could change from pure compression to combined axial compression and bending depending on the level of applied load and the location of the corrosion-damaged zone. The elements stiffness, mass and damping matrices of the corrosion-damaged columns are formulated using the nonlinear finite element analysis (NLFEA) approach proposed in Chapter 3 (see Mohammad et al. 2013b).

The SHDFEA procedure proposed in this chapter employs a non-linear time-history analysis of the bridge under traffic load, where the stiffness, mass and damping matrices of the column elements are successively updated at each new truck location. As the truck moves, the loads on the columns vary, and hence the material properties in the damaged and no damaged zones of the columns also vary. The sectional rigidities, the elements stiffness, mass and damping matrices are variables and dependent on the load and state of corrosion damage as observed by the visual inspection. It is assumed that at each truck location, a nonlinear static analysis is performed on the column to estimate the element stiffness and mass, and hence estimate the damping as it is assumed proportional to the stiffness and mass. The instantaneous nonlinear global dynamic matrices are then assembled into the equation of motion in every integration step of the time history analysis.

At each step of the time history analysis, a large amount of data is generated in the sub-processes of the nonlinear analysis to derive the instantaneous stiffness and mass of different elements. An

interactive data filing system has been developed and used to manage the data transferred between the Random Access Memory (RAM) and the external memory. The data filing system enables fast access to the data when needed in the instantaneous assembly process of the time history analysis. The data for each element matrix are transformed into a vector of a higher-order matrix and saved as parallel records. A file-name is generated for each record and saved for reference, and the record is saved randomly on the external drive. The symmetry of the matrices is taken into account to minimize the mathematical operations, the memory use and the time required for data processing and transfer. The convergence in three different levels (sectional, element and dynamic-time-history analysis) is checked and ensured. The filing system together with the displacement field tuning convergence used in the NLFEA (see Chapter 3 and Mohammed et al.2014b) enable the generalization of the approach to be used in more complicated structural systems with many structural elements.

As an example, at any step of the time history analysis, the instantaneous global stiffness matrix has the following general form, where it includes parts derived from the linear formulation and other parts derived from the nonlinear formulation:

$$\begin{bmatrix} [K_{Left\ column}]NL & & \\ & [K_{superstructre}]L & \\ & & [K_{Right\ column}]NL \end{bmatrix} \quad (4.1)$$

4.4.1 Modeling the bridge structure and traffic load

Over the past three decades, several attempts have been conducted to model the effects of dynamic interaction between vehicles and a bridge system. It is usually considered as two dynamic systems that are introduced by deriving the equation(s) of motion of the interaction

system. In almost all previous studies (except Mohammed et al. 2010, see Appendix B), only the bridge superstructure is modeled, while the substructure and the superstructure-to-substructure connection (or internal boundary conditions) are ignored.

Lin and Trethewey (1990) presented a finite element formulation of beams subjected to different types of moving loads (a moving concentrated force and moving one and two-foot long dynamic "systems"). Their objective was to derive the governing equations for the beam and the moving dynamic system interaction, whereas cubic Hermitian polynomials were employed as interpolation functions of the finite element formulation. The Rung-Kutta method was used to solve the governing equations and hence obtain the dynamic response of both, the beam and the moving load (or "system"). Law and Zha (2004), Zambrano et al. (2008) and Asnachinda et al. (2008) presented analytical solutions for simply supported and continuous beams with uniform cross sections under moving loads. The main objective of Law and Zha (2004) and Zambrano et al. (2008) studies was to determine the dynamic damage of the concrete bridge under moving vehicular loading. Asnachinda et al. (2008) performed analytical and experimental work to investigate the dynamic axle-load identification of multiple vehicles from the bridge bending strain response. In these studies, the vehicle is modeled as a moving single or multi-degree-of-freedom system, and the bridge is modeled as a simply supported Euler-Bernoulli beam. In order to analyze the interaction of the vehicle-bridge system, two sets of equations of motion are presented; one is for the vehicle, and the other one is for the bridge structure. Then the equations of motion of the interactive-system are solved to obtain its dynamic response.

Ali (1999) extended the application of the finite strip method to the dynamic analysis of bridge structures under moving trucks. He studied single-span slab-on-girder bridges, box-girder bridges, and multi-span slab bridges. The study considered several modeling approaches of the

vehicles, such as moving load, moving mass, sprung mass and un-sprung mass connected together by elastic springs and a dash-pot, and a two-axle vehicle.

Gong and Cheung (2008) studied the dynamic response of long-span box-girder bridges under moving loads using finite strip method. Their study concluded that (i) the dynamic response of a bridge depends mainly on the bridge superstructure dynamic characteristics, which include the natural frequencies and vibration mode shapes, and (ii) the vehicles-bridge structure interaction might be influenced by vehicle mass, traveling speed, damping ratio of the vehicles, and the ratio of the vehicle mass to the bridge mass.

Mohammed et al. (2010) proposed a linear dynamic finite element analysis approach for slab-on-girder bridges under moving vehicle when the columns are subjected to time dependent corrosion damage. The bridge structure is modelled as a static and dynamic system using the direct stiffness method. Three types of analysis are performed: (i) static analysis, wherein the traffic load is defined by a static truck load positioned to induce maximum static response; (ii) free vibration analysis; and, (iii) linear time-history analysis. The approach enables evaluating the effects of the current deterioration of bridge concrete columns on the dynamic performance of the bridge superstructure compared to its dynamic performance when no corrosion takes place.

4.4.2 Modeling the bridge structure

A typical slab-on-girder bridge is simply supported on columns (piers) or abutments (see Figures 4.3-a and 4.3-b). The focus of this study is on developing the SHDFEA based on the bridge structure-traffic dynamic interaction and on exploring the effects of columns' reinforcement corrosion damage on the dynamic behaviour of the bridge. Hence, it is essential to model both

the superstructure and substructure as one structural system. The SHDFEA is required to integrate the components of the slab-on-girder bridge, the superstructure and the columns, into one structural system involving an internal hinge and a roller. Since there is no load or expected response/deformation in the bridge lateral direction orthogonal to the traffic direction (or Z-direction as shown in Figure 4.3-a), the bridge structure can be modelled as a two-dimensional frame (in the X-Y plane as shown in Figure 4.3-b). The frame in the SHDFEA is formed of a beam, representing the superstructure, and two columns, representing the substructure. The connections between the beam and the columns are represented by an "internal" hinge on one side and an "internal" roller on the other side of the beam. The model also accounts for any possible eccentricity in both connections. The bases of the two columns are assumed fully fixed.

The columns sections are considered as reinforced concrete "composite" sections for the purpose of the nonlinear analysis. The sectional rigidities that lead to the estimation of elements stiffness, mass and damping matrices of the corrosion-damaged columns are formulated using the nonlinear sectional analysis and the nonlinear finite element analysis (NLFEA) approaches proposed in Chapters 2 and 3, respectively (see Mohammed et al. 2014a&b). The superstructure is formed from either slab-on-steel girders or slab-on-prestressed concrete girders. The slab is assumed to be compositely integrated to the girders. The distribution of the traffic loads (truck or lane load) in the lateral direction (Z) are assumed to follow the CHBDC load distribution approach. In the proposed SHDFEA, the composite beam and the columns are introduced as two-node frame elements with three degrees of freedom at each node. The self weight of the bridge elements is included as a uniform load. The instantaneous damping matrices are derived assuming that the damping is linearly proportional to the elements mass and stiffness.

As mentioned earlier, the beam-column joints are modeled as an internal hinge in one side and as an internal roller in the other side of the bridge system. The fulfillment of the boundary conditions at the beam-column joints is considered as follows:

Hinge: (i) continuity in the vertical displacement V, i.e., beam and column have the same V; (ii) continuity in the horizontal displacement; (iii) discontinuity in the rotations, i.e., beam and column have independent rotations θ, or $\theta_{beam} \neq \theta_{column}$.

Roller: (i) continuity in the vertical displacement; (ii) discontinuity in the horizontal displacement U, or $U_{beam} \neq U_{column}$; (iii) discontinuity in the rotations, or $\theta_{beam} \neq \theta_{column}$.

Incorporating the above internal boundary conditions (McGuire et al. 2000), the overall stiffness matrix of the modeled frame is:

$$\begin{Bmatrix} F_e \\ F_o \end{Bmatrix} = \begin{bmatrix} K_{ee} & K_{eo} \\ K_{oe} & K_{oo} \end{bmatrix} \begin{Bmatrix} \Delta_e \\ \Delta_o \end{Bmatrix} \tag{4.2}$$

where $\{F_e\}$ is the vector of applied forces on the free nodes, $\{F_o\}$ is the vector of forces on the roller and hinge nodes; $[K_{ee}]$ is the stiffness matrix associated to degrees of freedom of free nodes; $[K_{oe}] = [K_{eo}]$ are the interaction stiffness matrices; $[K_{oo}]$ is the stiffness matrix associated to degrees of freedom of roller and hinge nodes; $\{\Delta_e\}$ is the vector of deformations associated to free nodes; and $\{\Delta_o\}$ is the vector of deformations associated to the roller and hinge nodes. Expanding the lower partition of Eq. (4.2) results in:

$$K_{oe}\Delta_e + K_{oo}\Delta_o = F_o \tag{4.3}$$

Likewise, expanding the upper partition of Eq. (4.2) results in:

$$K_{ee}\Delta_e + K_{eo}\Delta_o = F_e \quad (4.4)$$

From Eq. (4.4):

$$\Delta_o = K_{oo}^{-1}F_o - K_{oo}^{-1}K_{oe}\Delta_e \quad (4.5)$$

By subsisting Eq. (4.5) into Eq. (4.2), the overall stiffness matrix and load vector of the modeled frame are:

$$[K] = [[K_{ee}] - [K_{eo}][K_{oo}]^{-1}[K_{oe}]] \quad (4.6)$$

$$\{F\} = \{\{F_e\} - \{[K_{eo}][K_{oo}^{-1}]\{F_o\}\} \quad (4.7)$$

where $[K]$ is the overall stiffness matrix of the bridge structure, and $\{F\}$ is the overall load vector of the bridge structure.

4.4.3 Modelling the vehicle

The vehicle is modelled as a dynamic system with two degrees of freedom: the vertical displacement (y) and the rotation (θ), as shown in Figure 4.5. It is assumed that the two axles of the vehicle remain in contact with the surface of the bridge superstructure. Only vertical vibration is considered. The governing equations of the moving dynamic system and the bridge are adopted from Lin and Trethewey (1990), where the overall vehicle-bridge system is presented as follows:

$$\begin{bmatrix} [M] & \sum_{i=1}^{2}[N_i]^T f_{yi} & \sum_{i=1}^{2}[N_i]^T f_{\theta i} \\ [0] & m_1 & 0 \\ [0] & 0 & I_\theta \end{bmatrix} \begin{Bmatrix} \{\ddot{d}\} \\ \{\ddot{y}\} \\ \{\ddot{\theta}\} \end{Bmatrix} + \begin{bmatrix} [C] & \{0\} & \{0\} \\ \sum_{i=1}^{2} -c_i[N_i] & \sum_{i=1}^{2} c_i & \sum_{i=1}^{n}(-1)^{i+1} c_i b_i \\ \sum(-1)^i b_i c_i[N_i] & \sum(-1)^{i+1} c_i b_i & \sum_{i=1}^{2} c_i b_i^2 \end{bmatrix} \begin{Bmatrix} \{\dot{d}\} \\ \{\dot{y}\} \\ \{\dot{\theta}\} \end{Bmatrix} + \begin{bmatrix} [K] & \{0\} & \{0\} \\ \sum_{i=1}^{2}(-c_i \dot{x}[N_i]_x - k_i[N_i]) & \sum_{i=1}^{2} k_i & \sum_{i=1}^{n}(-1)^{i+1} k_i b_i \\ \sum(-1)^i (b_i c_i \dot{x}[N_i]_x + b_i k_i[N_i]) & \sum(-1)^{i+1} k_i b_i & \sum_{i=1}^{2} k_i b_i^2 \end{bmatrix} \begin{Bmatrix} \{d\} \\ \{y\} \\ \{\theta\} \end{Bmatrix} = \begin{Bmatrix} \sum_{i=1}^{2}[N]^T f_i \\ 0 \\ d_1 F(t) \end{Bmatrix} \quad (4.8)$$

where [M], [K], [C] are respectively the structural mass, stiffness, and damping matrices of the bridge, $\ddot{d}$, $\dot{d}$, d are the nodal acceleration, velocity and displacement vectors, respectively, f_i is the magnitude of a concentrated force, [N] is the shape function, m_1, k_i, c_i are respectively the spring mass, stiffness, and damping of an axle of the moving system, $\ddot{y}$, $\dot{y}$, y are respectively the vertical displacement, velocity and acceleration of the spring mass, and b_i is the vehicle axle position from its center of gravity.

The vehicle dynamic system is first integrated with the bridge superstructure, and then it is integrated with the proposed beam- column system. The combined equations of the vehicle–bridge system given by Eqs. 4.6&4.8 are solved by the step-by-step integration method. The dynamic response of the bridge under the moving vehicle is expressed as a function of the transverse displacement of the structure w(x,t), i.e., w = [N]{d}.

4.5 Modelling of Corrosion Load

Field surveys have shown that RC bridge columns in cold climates are among the bridge elements with highest observed corrosion related damage. The most critical column zones that are suffering from corrosion are the top (superstructure drain zone) and mid-height “splash zone” (Andersen 1997). Reinforcement corrosion is a continuous long-term process, leading to

reduction in cross sectional area of the affected steel bars and loss of concrete section as a result of longitudinal cracking and spalling. Hence, reinforcement corrosion may cause significant changes in the bridge column capacity and safety. One of the most detailed experimental studies was performed by Rodríguez et al. (1996), in which the effects of steel corrosion on the RC column behavior were examined by considering the concrete section reduction, concrete cover cracking and spalling, and the corrosion of longitudinal and tie reinforcement. From their results, it was observed that the ultimate load was reduced due to the effect of corroded reinforcement on the concrete column performance, and the compressive stiffness of the column at service load was reduced as well. Also, the ultimate axial force value was estimated by considering the reduced steel section and decreasing the concrete section by assuming that one or more concrete covers had delaminated. Further, it was observed that reinforcement corrosion introduced a load eccentricity due to spalling of the concrete cover and led to buckling of the longitudinal reinforcement due to premature loss of one or more columns ties.

Tapan and Aboutaha (2009) presented a methodology to evaluate the load carrying capacity of deteriorated concrete bridge pier columns (by constructing the full P-M interaction diagrams), considering the need to individually evaluate each bridge substructure. The presented methodology incorporates the actual material properties of deteriorated columns, and accounts for the amount of corrosion and exposed corroded bar length, concrete loss, loss of concrete confinement and strength due to stirrups deterioration, bond failure, and type of stress in the corroded reinforcement.

Chapters 2 and 3 (Mohammed et al. 2014a&b) have introduced a NLFEA approach based on visual inspection to identify the state of damage from which the nonlinear behaviour of aged bridge columns is simulated. The approach is developed to take into account corrosion of both

longitudinal and lateral (stirrups/ties) reinforcement, concrete spalling, the effects of stirrups loss on the core concrete confinement, reinforcement ductility, progressive change in load eccentricity, and the effects of local loss of bond on the structural behaviour at both sectional and element levels. Chapter 3 (Mohammed et al. 2014b) has shown that the critical evaluation zones for shear and flexure could be different from the critical design zones based on the location of the corrosion affected zone and the state of damage. The NLFEA approach estimates, with high accuracy, the current sectional and element (finite elements) instantaneous characteristic properties based on the observed state of damage (from visual inspection) and the required material tests. Some tests that follow the visual inspection are to estimate the corrosion effect on the steel and the material properties if detailed testing program is too expensive. The NLFEA approach is integrated with the SHDFEA approach, as mentioned earlier, enabling engineers to have integrated tools in their everyday bridge assessment work.

4.6 Validation of the proposed model

4.6.1 Case study: Moving truck on slab-on-steel-girder bridge

The proposed SHDFEA is validated through a case study of a concrete slab-on-steel girder bridge (called Bridge A throughout this study) with center-to-center span of 61.31 m, selected from the Virginia State Bridge Inventory (Hevener 2003, and Nutt et al. 1998). The bridge is simply-supported on RC piers formed from eight square 600 x 600 mm columns, connected from the top to a cap beam where the bridge superstructure girders rest on hinge or roller joints (see roller support in Figure 4.6 (a)). The 6-m height columns are assumed to have full fixity at the foundation level, and the reinforcement is detailed as shown in Figure 4.6 (b) and 4.6 (c). The bridge superstructure consists of a concrete slab compositely casted on steel girders, as shown in

Table 4.1. The bridge was built in the 1970's, and the current concrete compressive strength f'_c for all the bridge components, the superstructure and the columns is assumed equal to 35 MPa. Details of the slab thickness, girder geometrical properties, girder spacing, bridge width and number of girders are given in Table 4.1.

The present case study involves studying the structural dynamic performance when the bridge is subjected to different static and dynamic loads using a two-axle truck of a total mass of 34,400 kg, where the body mass is 30,189 kg, the front axle mass is 2,806 kg, and the rear axle mass is 1,403 kg. The truck mass moment of inertia is 263,052 kg.m^2, the stiffness of each axle is 5,363,163 N/m and the axle spacing is 6.19 m (Ali 1999). Since the proposed model is a two-dimensional model and the variation through the bridge width perpendicular to the traffic direction is ignored, the reported results (stiffness, mass, and damping) are average values per traffic lane/per column. It should be noticed in this case study, the slab-on-steel girder has been selected for its low stiffness and mass per lane, so its stiffness-to-mass ratio is relatively high, which should lead to the bridge being more sensitive to vibrations.

4.6.2 Convergence study

To verify the validity of the proposed SHDFEA approach when performing static and/or dynamic analysis, it is necessary to ensure the correct implementation of the internal hinge and roller at the beam-column joints. A static analysis of the slab-on-steel girders bridge under the two-axle truck (see above section for details) is performed, where the front axle location on the superstructure changes representing the truck movement from one side of the bridge to the other in the static mode. The analysis is performed on two cases: (i) simply-supported beam (SSB); and (ii) beam on a two-column system (BOTC) with internal hinge and roller. Depending on the

column stiffness, the deformations of the bridge superstructure are expected to increase in the case of the beam on two columns (BOTC) frame compared to the case of the simply-supported beam. Figure 4.7 shows that modeling the bridge as BOTC gives slightly higher deflections than modeling the bridge superstructure as SSB.

Two convergence studies were conducted on the dynamic analysis part of the proposed SHDFEA. For both convergence studies, the truck speed is equal to 100 km/h. In the first convergence study, the number of elements (NE) is assumed to be fixed (NE = 60), and the number of integration points (NI) varies from 5 to 100. Figure 4.8-a shows the dynamic deflection under the front axle of the truck along the span of Bridge A for different NI. It is found that after NI = 24, the change in the deflection becomes negligible. In the second convergence study, the number of integration points is set constant (NI = 50), and the number of elements varies from 6 to 80. It is found that after NE = 30 the results become stable and the change in the dynamic deflection due to the increase in the number of elements is negligible (see Figure 4.8-b).

For nonlinear modeling of the columns, the convergence is to optimize different variables that lead to a stable solution at the section and element levels (see Chapters 2 & 3 ;Mohammed et al. 2014a&b), such as: (i) load step; (ii) element size; and, (iii) number of sections per element. By compromising the accuracy within an acceptable range and the computation time of the step-by-step nonlinear dynamic time-history analysis, the convergence can be further accelerated by eliminating the secondary correction cycles of the “displacement field tuning convergence” used in the NLFEA, provided that equilibrium is satisfied at both sectional and structural levels.

In order to show the proposed SHDFEA capability, a severe corrosion-damage state of the columns is assumed in this case study. Corrosion-induced damage is estimated assuming a steel mass loss of 30%, and assuming that the concrete cover of the columns has spalled off and there is local loss of the lateral reinforcement. For the two-axle truck moving over the bridge at a speed of 100 km/h, Fig. 9 shows a marginal increase in the dynamic deflection of the superstructure although all studied damage scenarios reinforcement corrosion of both side columns.

4.7 Results and Discussion

4.7.1 Static deflection versus dynamic deflection of the bridge superstructure

Figure 4.10 shows the dynamic deflection of the superstructure of Bridge A under the front axle for different truck speeds. The figure shows that the dynamic deflection increases as the truck speed increases. The location of maximum deflection is also shifted towards the roller side with high truck speeds. The dynamic load allowances (DLA) (or the impact factors in AASHTO LRFD) are calculated from the ratio of the maximum dynamic deflection to the maximum static deflection, which range between 1.013 to 1.5, as shown in Table 4.2.

4.7.2 Effect of using nonlinear versus linear analysis of columns on dynamic deformations of bridge components

For the bridge in this case study (Bridge A), Figure 4.11-a and 4.11-b show respectively the dynamic deflection of the bridge superstructure and the maximum lateral displacement of the bridge columns when the given two-axle truck passes over the bridge superstructure with a speed of 100 km/h. It is observed that the axial deformations of the columns are very small for the load of the moving traffic in this study. Linear and nonlinear analysis alternatives are preformed using

the proposed SHDFEA approach. It is clear that an insignificant difference in the dynamic deflections of the superstructure is observed when either linear or nonlinear analysis is used, Figure 4.11-a. However, Figure 4.11-b shows that the nonlinear option of the SHDFEA gives higher lateral displacement of the left column (with internal hinge) than that obtained from the linear analysis, while the nonlinear analysis gives slightly higher lateral displacement of the right column (with internal roller) than that obtained from the linear analysis.

Figure 4.12 shows the load-displacement curve of one column of the bridge pier using the NLFEA, where the corrosion-induced damage (as described earlier) results in a high reduction of the load capacity in the two loading cases: (i) concentric loading (e = 0); and (ii) eccentric loading with an eccentricity equal to 15% of the column cross-section depth. The figure shows that the maximum un-factored load applied on the column (which equals to 634 kN for Bridge A) is very low compared to the load capacity of the column even in the elastic range. Also, the figure shows that the axial load capacity of the column is reduced by around 30% when the load eccentricity is increased to 15% of the column cross-section depth (H). This shows that the bridge columns are overdesigned. When a severe corrosion state is considered (well below the collapse level), the bridge load capacity is reduced, and the reduction in the strength is very high when the applied load approaches the ultimate load capacity of the columns (in both cases: with or without eccentricity). Since the applied traffic load is very low compared to the load capacity, even in the case when severe corrosion is assumed, the changes of the performance major parameters show very low changes due to reinforcement corrosion. With the service (traffic) loading level, the differences between the linear and nonlinear analysis are negligible in most of the structural performance parameters.

4.7.3 Effect of the bridge span length on dynamic deflection of bridge superstructure

As mentioned earlier, the focus of the current study is on the combined effect of traffic load and reinforcement corrosion applied on the bridge columns at high exposure zones on the dynamic behaviour of the bridge. The proposed SHDFEA is used to investigate three more bridges with spans shorter than the span of Bridge A. The major difference between the selected bridges (Bridges A to D in Table 4.1) is the unsupported span length; however, the spacing girder, skew angle and transverse width are similar. All the four bridges columns are designed with load over capacity of 50% (i.e., the applied ultimate load divided by the bridge load capacity is equal to 0.5). Corrosion-induced damage is assumed to present the worst scenario of the column deterioration (but not at full damage or close to the collapse state), where stirrups and confinement are partially lost. For the investigated bridge spans of 15, 30, 36, and 60 m, Figure 4.13 shows that the dynamic deflection is different from one bridge to another depending on its span. It is observed that with a truck speed of 100 km/hr (usual design speed for highway bridges), the maximum dynamic deflection under the front axle is located close to the bridge mid-span, similar to the case of static analysis. However, the maximum dynamic deflections in the cases of longer bridge span lengths (36 m and 60 m) are shifted towards the column with an internal roller. It is also clear that the maximum dynamic deflection is highly increased with the increase of the span. The influence of having corrosion damage in the bridge columns is negligible on the dynamic deflection for all bridge spans. It should be noticed that the bridge with span length 30 m has prestressed concrete girders instead of steel girders; however, this has not a large impact on the trend of the dynamic deflection of the superstructure. This can be explained by the fact that the higher mass and higher stiffness of the prestressed concrete girders over the steel girders together with the girders spacing have not shifted the natural frequency of

the composite superstructure of Bridge C from the range of natural frequencies of the other three bridges in the group.

4.7.4 Nonlinear static versus nonlinear dynamic analysis of various bridge span lengths

In this section, comparisons of nonlinear static analysis using the NLFEA versus nonlinear dynamic analyses using the SHDFEA of undamaged and damaged bridge columns of various bridge span lengths are presented. The nonlinear static behaviour of the columns when loaded up to ultimate static load and their nonlinear dynamic behaviour when they are loaded dynamically by a moving truck (traffic load) are investigated. All the bridges columns are assumed to be exposed to the same states of damage as shown in Section 4.6.2. The purpose of this investigation is to explore whether safety critical damage states of the columns due to reinforcement corrosion can be captured by the change of any of the bridge dynamic parameters that is easy to be observed and measured. Hence, it would be possible to develop a sensing technique that can predict any critical safety and stability states of the columns from the characteristic changes of the bridge dynamic behavior under traffic. Figures 4.14-a and 4.14-b show the load versus axial deformation relationship for the columns of the four bridges (Bridge A through Bridge D) for the case of concentric axial load and the case of 0.15 H eccentricity of the axial load, respectively. When the load is concentric, both the load capacity and the ductility (measured as the ratio of the ultimate displacement divided by the yield displacement) are decreased when the column is subjected to local corrosion damage (for instance at the column mid-height). When the load is eccentric by 0.15 H, the load capacity is decreased when the columns are subjected to severe reinforcement corrosion; however, the ductility is increased in some cases (for instance, L=60 m & L= 15 m). Figure 4.14-c shows the applied moment versus

the lateral displacement relationship, where the moment capacity is reduced for the columns of all bridges when they are subjected to severe corrosion damage.

Figures 4.15-a and 4.15-b show the distribution of the static axial displacement and the static lateral displacement, respectively, over the column height for the four bridges, Bridges A through D. Both figures show the change of the location of the maximum displacement when the columns are subjected to severe reinforcement corrosion. It is important here to mention that the bents (or kinks) of the axial displacement distribution over the damaged-column height in Figure 4-15-a are located the end of the damaged zone (4 m from the base). The reduction of axial stiffness and the column boundary conditions and the location of the damaged zone contributed to this change in the axial displacement.

As mentioned earlier, the service (or traffic) load magnitude is well below the ultimate static capacity of the column, and hence even with severe local corrosion damage in the columns, their static behaviour remains in the elastic range or in the early plastic range. This may explain the low sensitivity of the dynamic parameters of the bridge structures to the corrosion damage of the columns, although they could be in a critical safety and stability state. Figures 4.16-a and 4.16-b show that for all studied bridges (Bridges A through D) and when both the right and left columns of each bridge are subjected to severe local corrosion damage, there are no observed changes in their dynamic lateral displacement related to the truck front axle location on the bridge superstructure.

Appendix C shows that even for extreme loading or design alternatives, the sensitivity of the dynamic response of the bridge superstructure or substructure remains low. The two extreme

cases shown in the appendix are: (i) very high axial load eccentricity, and (ii) very high load over capacity ratios for performance-based designed columns.

4.8 Conclusion

A major part in the evaluation serviceability limit state is to ensure that dynamic deflections of the bridge superstructure when the bridge is under service (or traffic) loads are within the allowable limits defined by North American Highway Bridge design codes (CHBDC and AASHTO LRFD). In this chapter, a simplified hybrid linear/nonlinear dynamic finite element analysis (SHDFEA) is proposed to evaluate the dynamic characteristics and behavior of slab-on-girder bridges under moving trucks when their columns are subjected to severe corrosion damage. The proposed SHDFEA uses NLFEA to evaluate the damaged columns stiffness, mass and damping throughout the step-by-step time history analysis.

It is found that the proposed SHDFEA is numerically efficient and stable in all the studied cases. Although the nonlinear analysis presents the appropriate selection to evaluate the possible effects of the corrosion damage of the column on the dynamic behaviour of the bridge, linear dynamic analysis is found to be a more economical alternative when the columns are overdesigned. It is also found that when the traffic load magnitude is well below the ultimate static capacity of the columns, even with severe local corrosion damage in the columns, their static behaviour mostly remain in the elastic range. This leads to a low sensitivity of the dynamic parameters of the bridge structure to corrosion damage of the columns, even when they could be in a state of critical safety and stability.

Table 4.1: Properties of selected bridges (Hevener 2003, based on Nutt et al., 1988, NCHRP Report 12-26)

Name	Span (m)	Type of girder	Year Built	Skew Angle (^{o})	Girder Spac-ing (m)	Girder Properties			Trans-verse width (m)	Slab Thick-ness (m)	No. of Girders
						A (m^2)	I (m^4)	H (m)			
A	61.31	Steel	1977	0.0	2.644	.0462	.01739	2.898	20.49	0.216	8
B	36.91	Steel	1978	0.0	2.46	0.0071	0.0017	1.119	19.59	0.229	8
C	30.81	Prestressed	1981	7.0	2.1	0.359	0.0782	1.601	22.57	0.158	7
D	15.83	Steel	Unknown	6.43	1.69	0.0323	0.0044	0.915	21.35	0.191	8

Table 4.2: Impact factors under two-axle moving truck.

Velocity (km/h)	Impact Factor Nonlinear
20	1.013
40	1.011
60	1.38
80	1.53
100	1.51

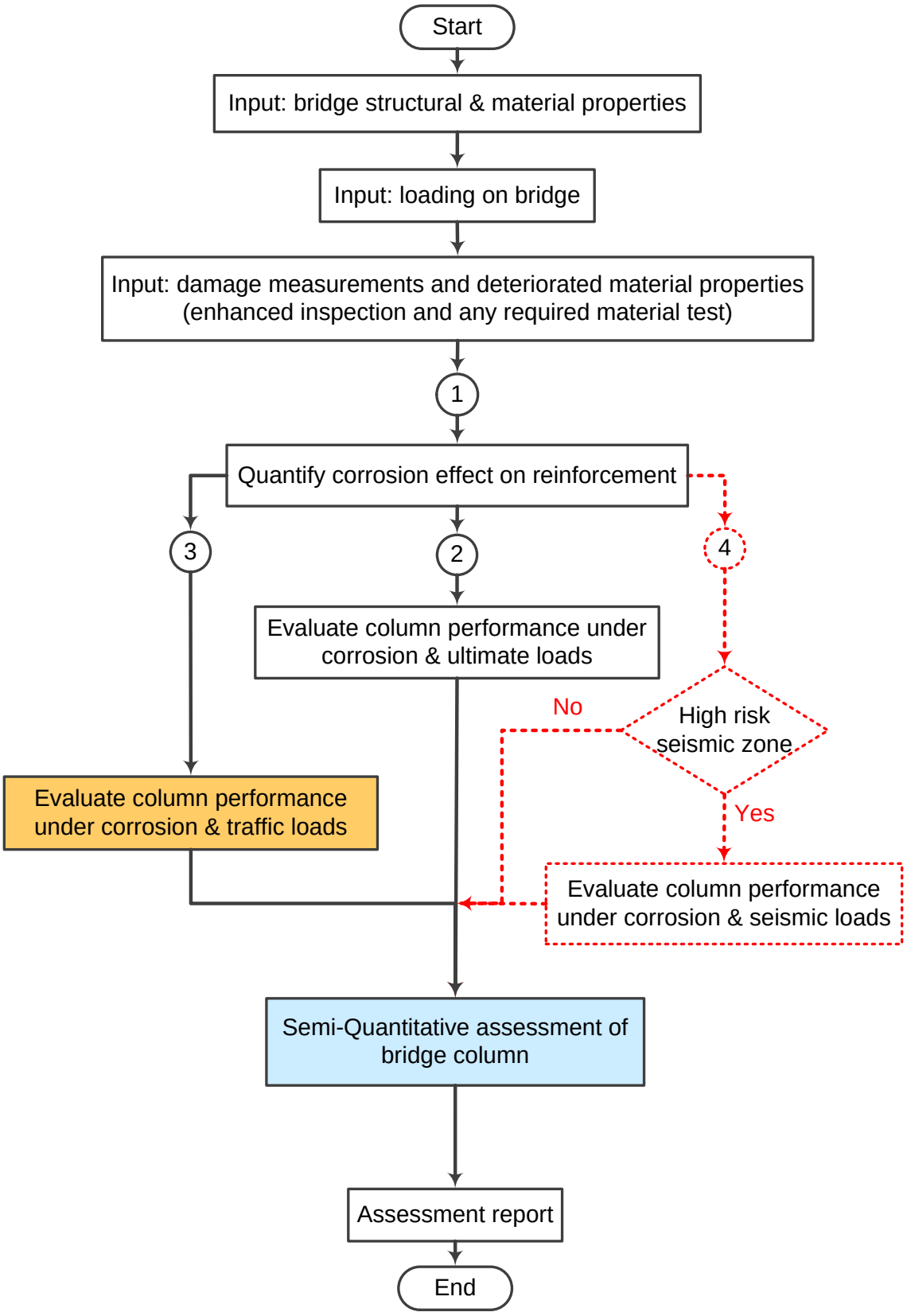

Figure 4.1: The proposed SQAF of aging RC bridge columns.

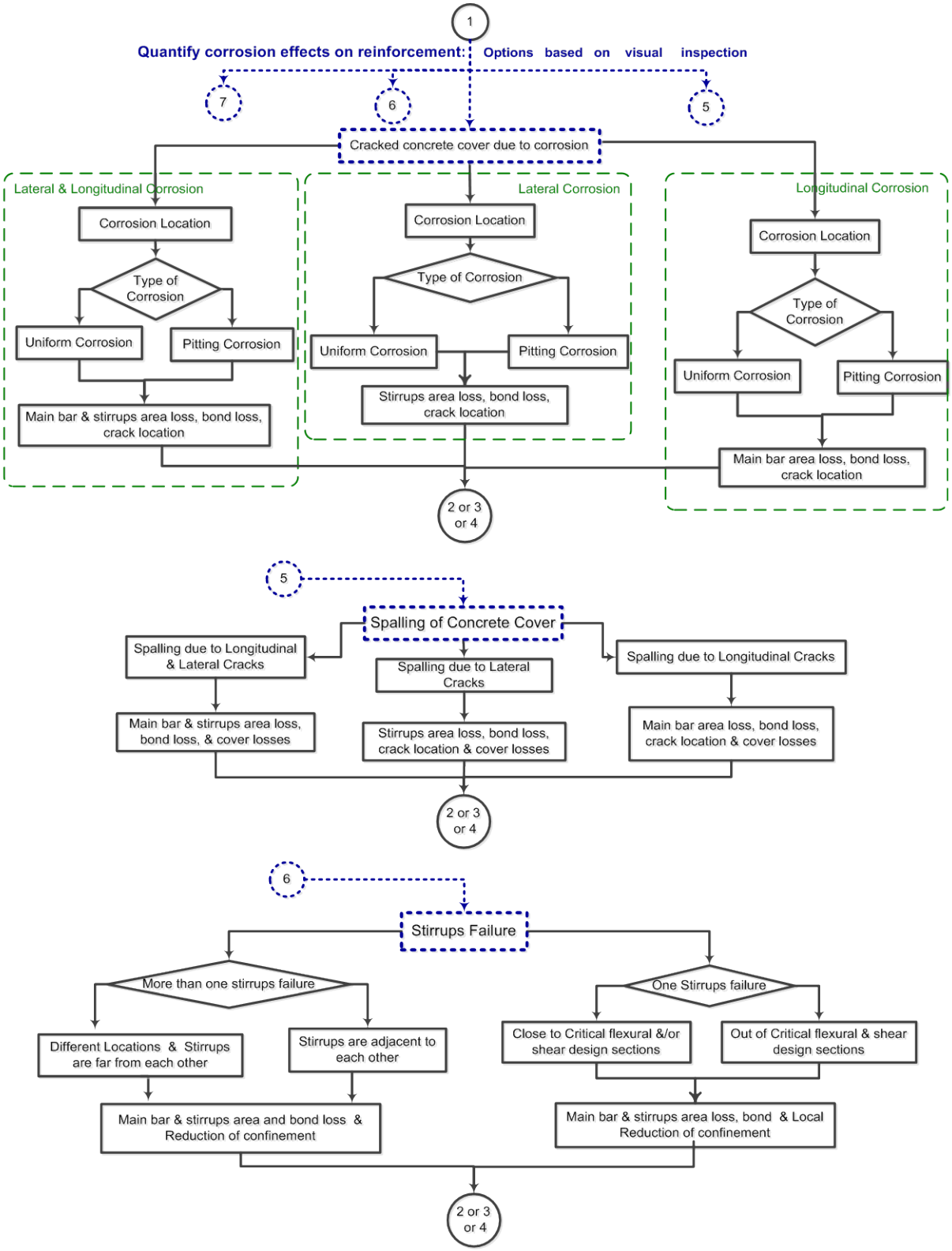

Figure 4.2: Evaluation of column performance under corrosion & ultimate loads.

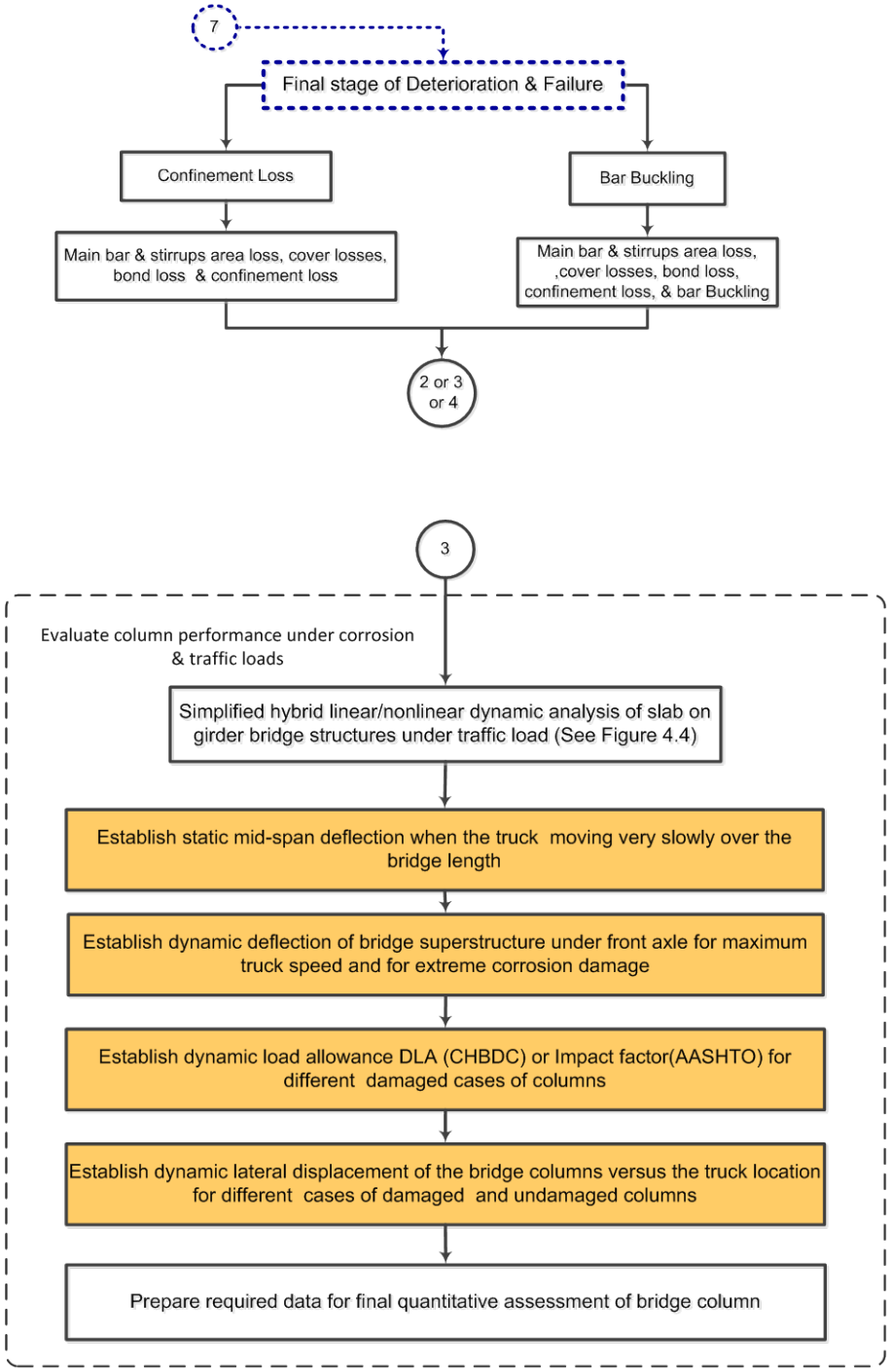

Cont'd. Figure 4.2: Evaluation of column performance under corrosion & ultimate loads.

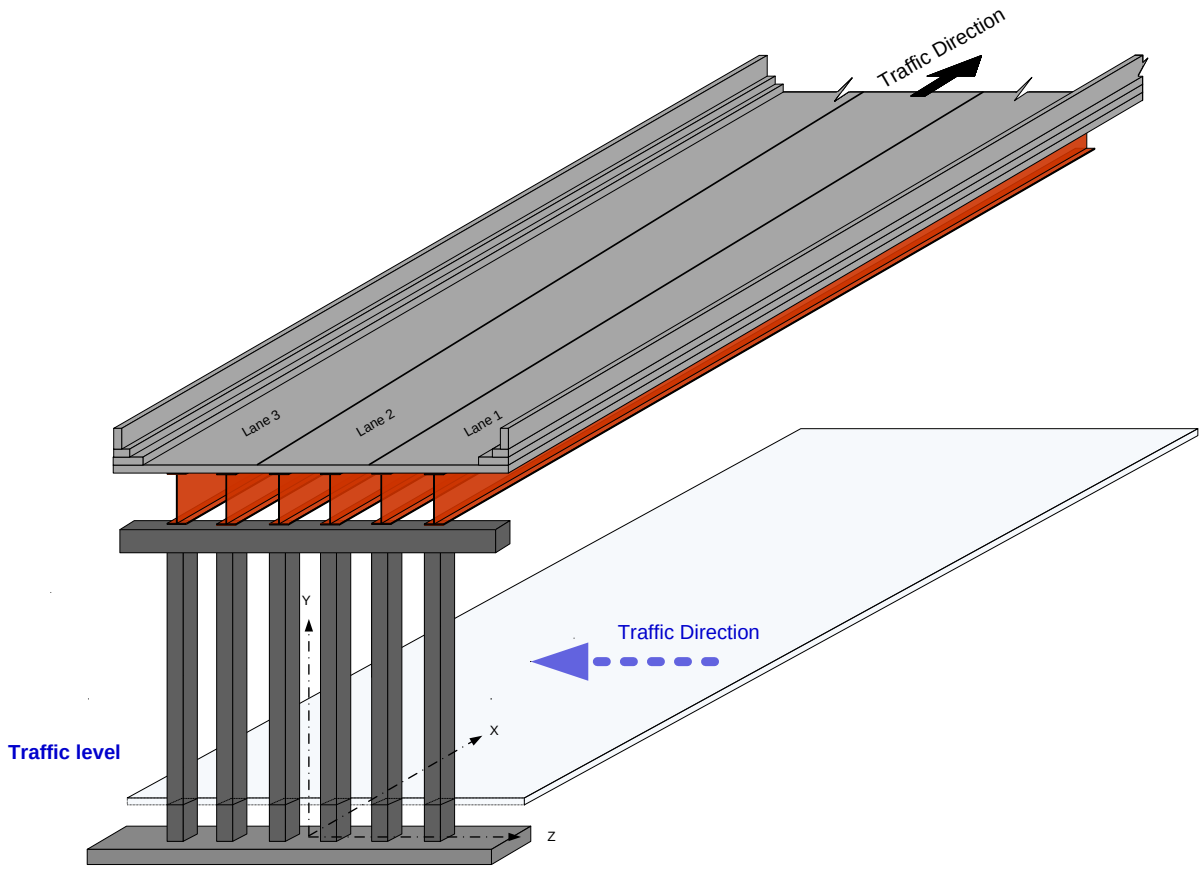

Figure 4.3-a: Typical slab-on-steel-girder bridge columns.

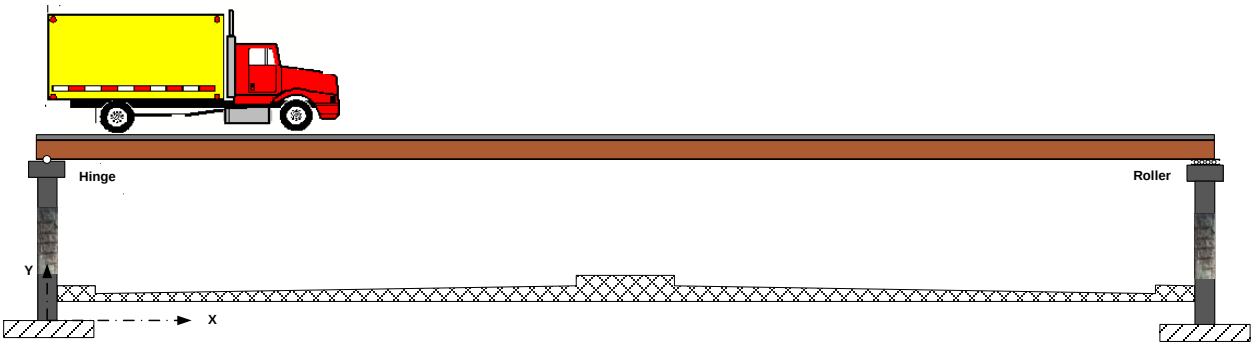

Figure 4.3-b: A truck moving on an aged slab-on-girders bridge over a highway. Possible damaged zones and boundary conditions are shown.

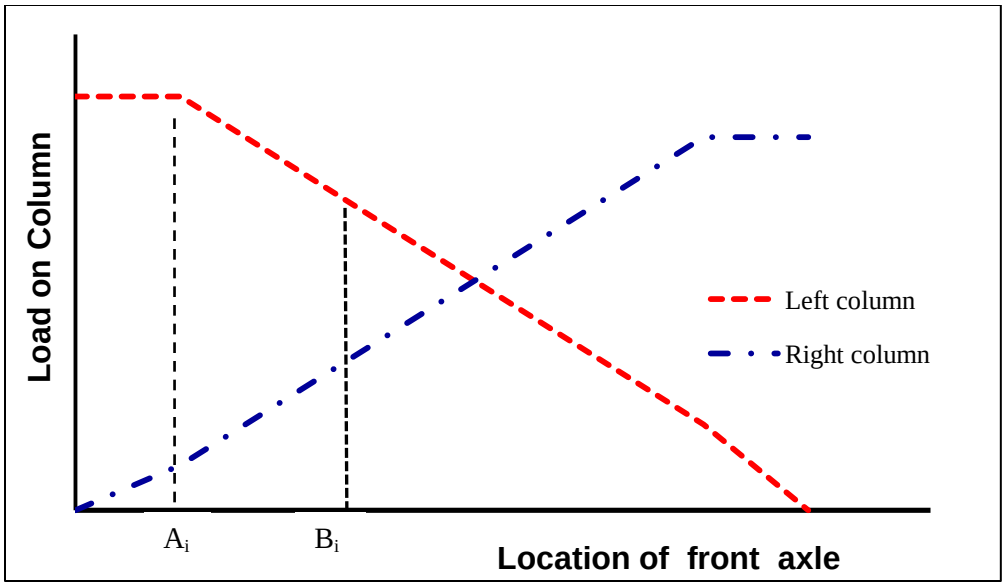

Figure 4.3-c: Variation of load on each column relative to the location of front axle of a two-axle moving truck.

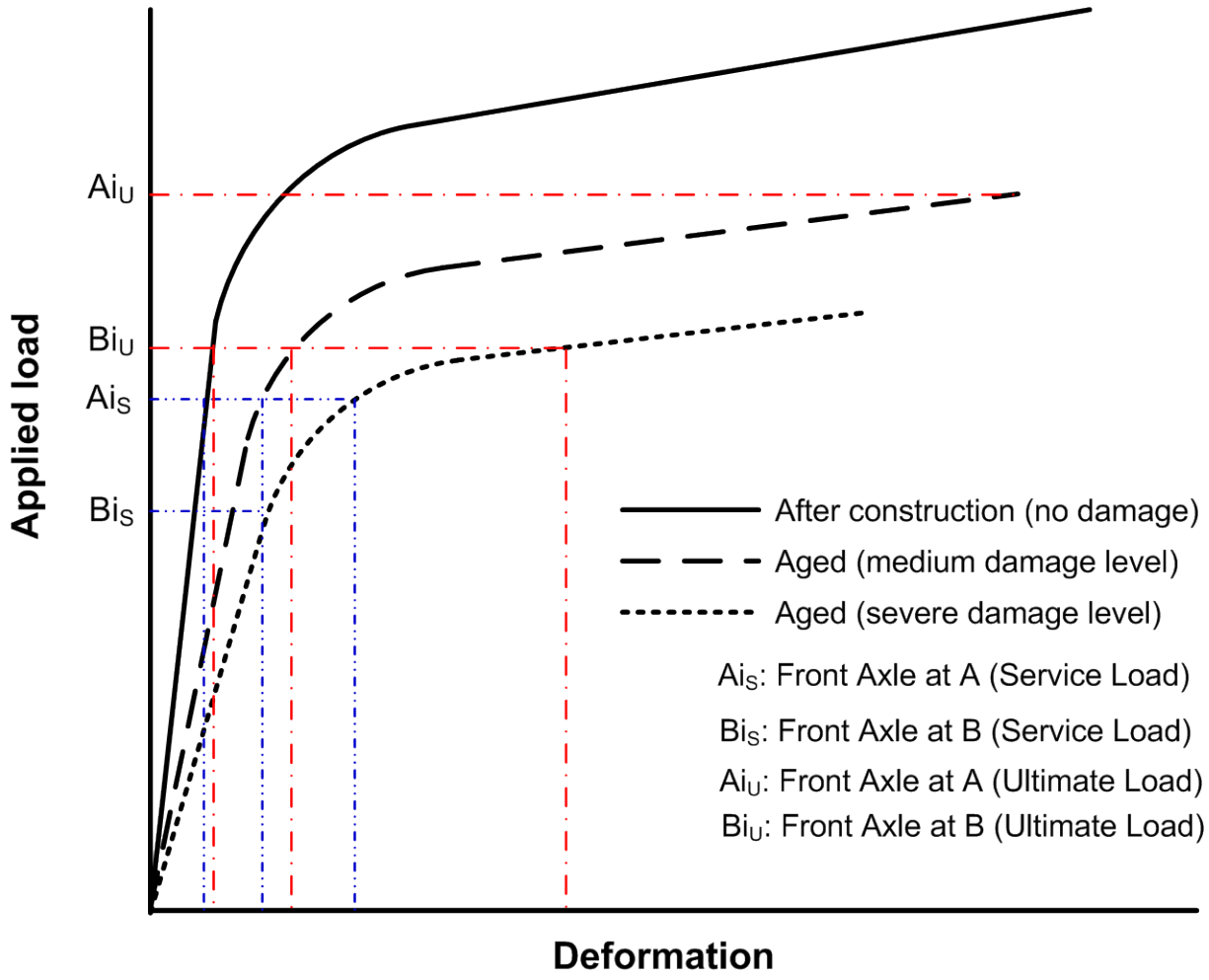

Figure 4.3-d: Applied ultimate or service loads vs. deformation for new and aged bridge columns.

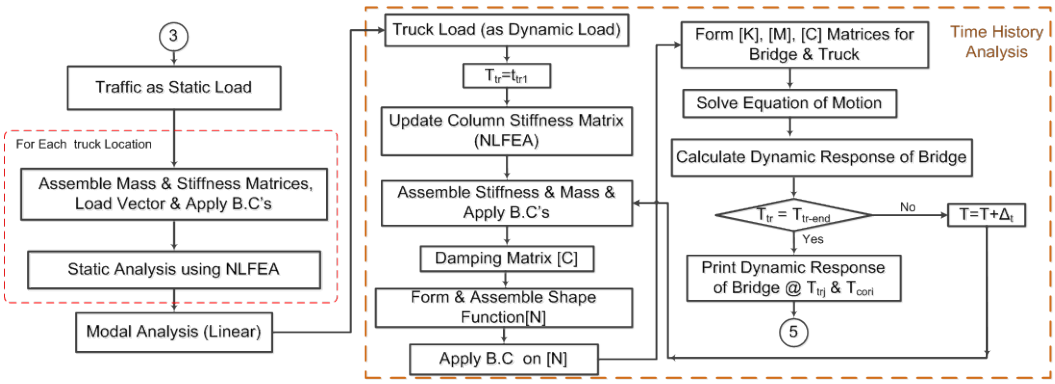

Figure 4.4: Proposed simplified hybrid linear/nonlinear dynamic analysis of slab-on-girder bridge structures under traffic load.

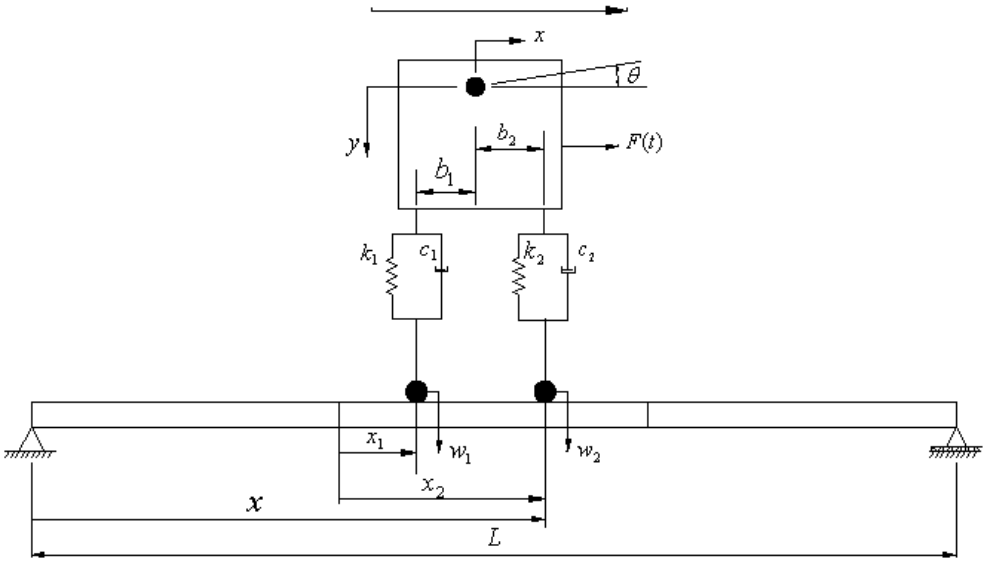

Figure 4.5: Vehicle model (after Lin and Trethewey, 1990).

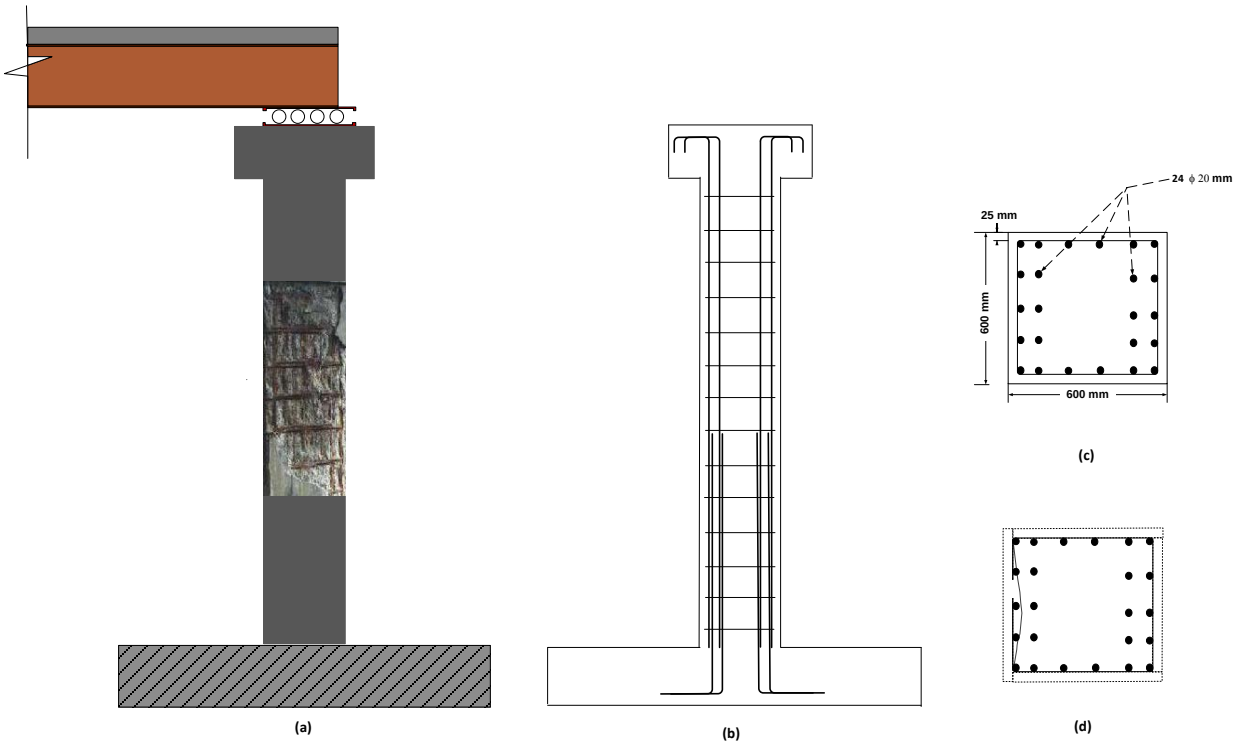

Figure 4.6: Column design, reinforcement details and damage due to corrosion in critical corrosion zone.

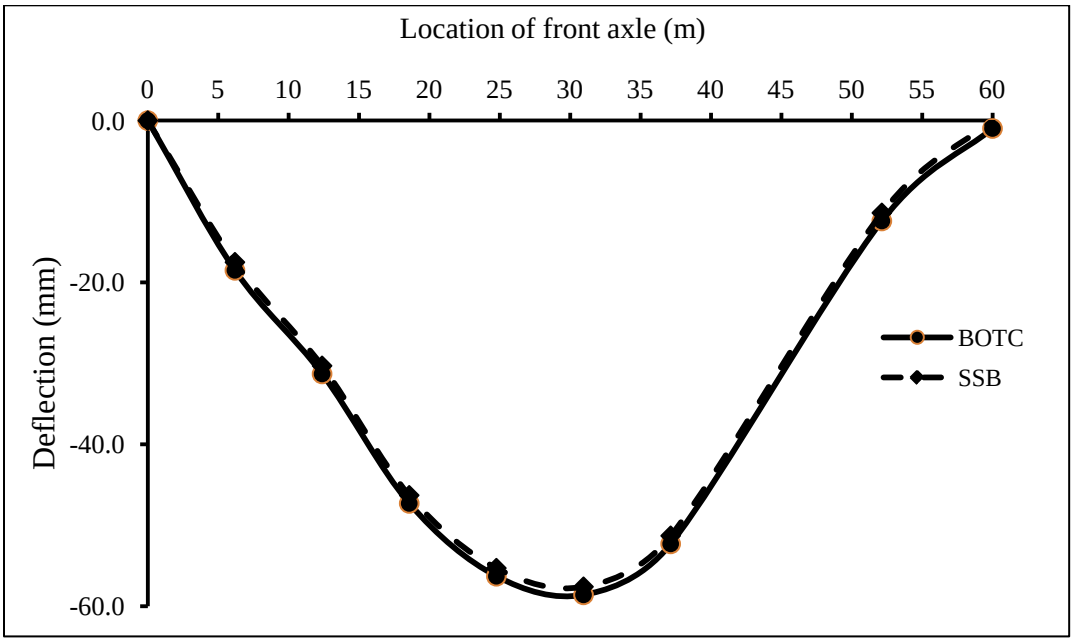

Figure 4.7: Mid-span deflection of BOTC compared to SSB under truck load for nonlinear model.

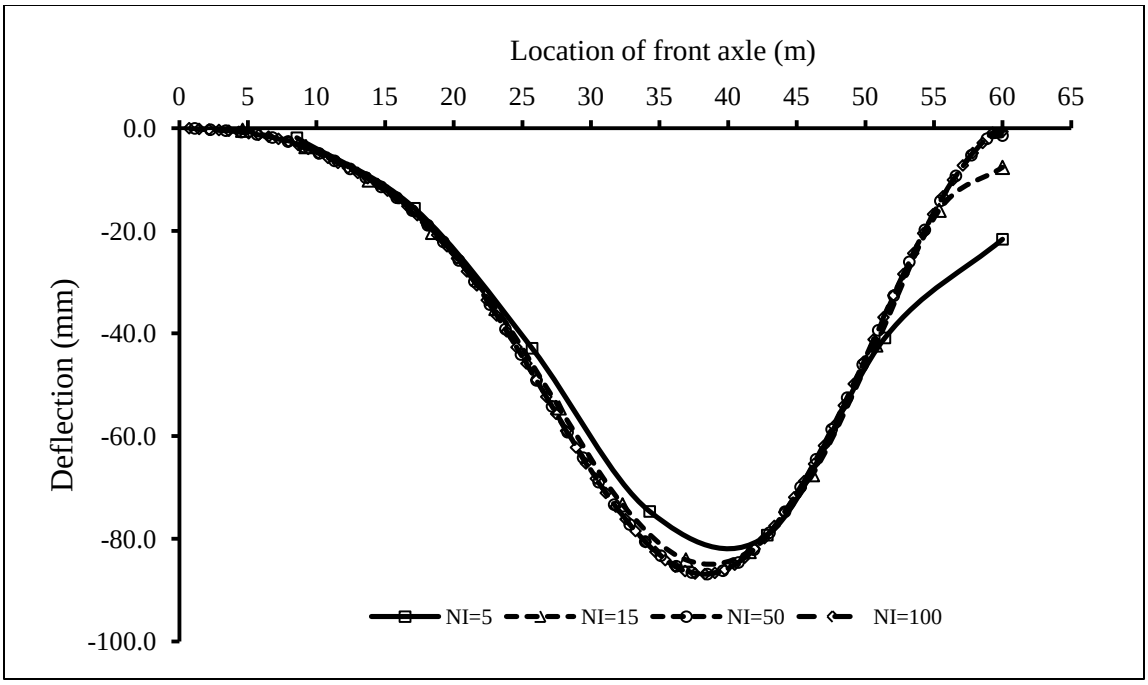

Figure 4.8-a: Convergence study 1: number of elements NE = 60 and truck speed = 100 km/h for different number of integration points (NI).

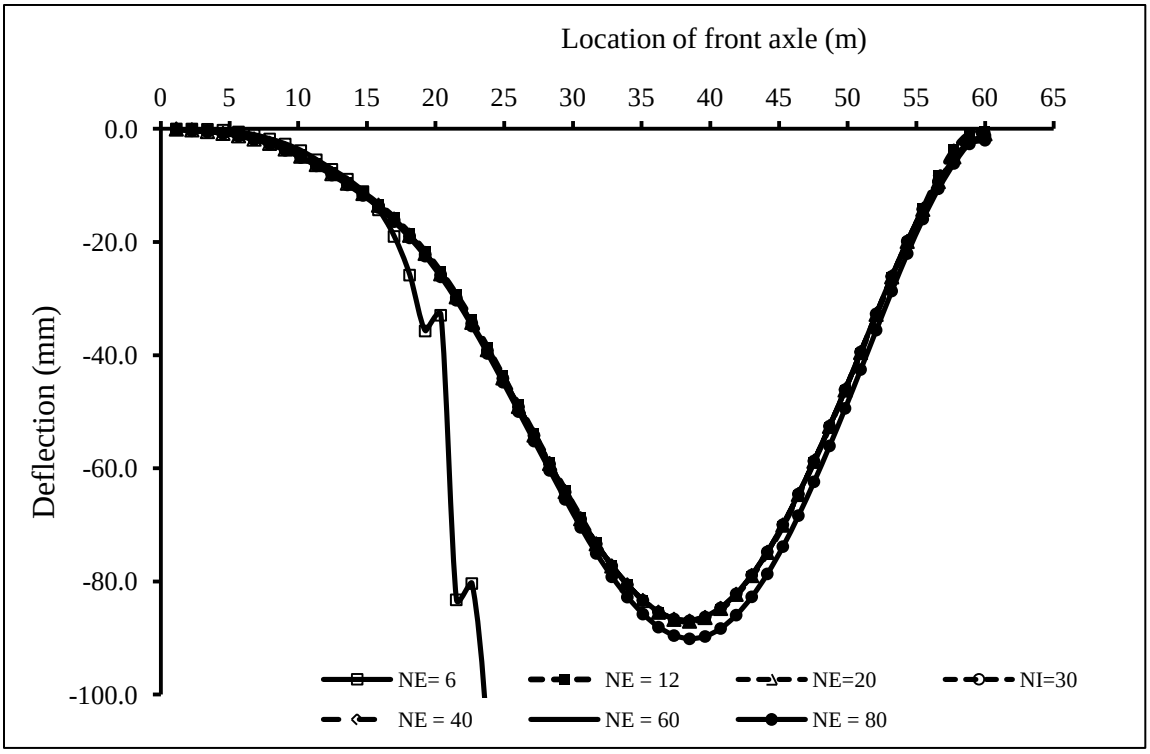

Figure 4.8-b: Convergence study 2: number of integration points NI = 50 and truck speed = 100 km/h for different number of elements (NE).

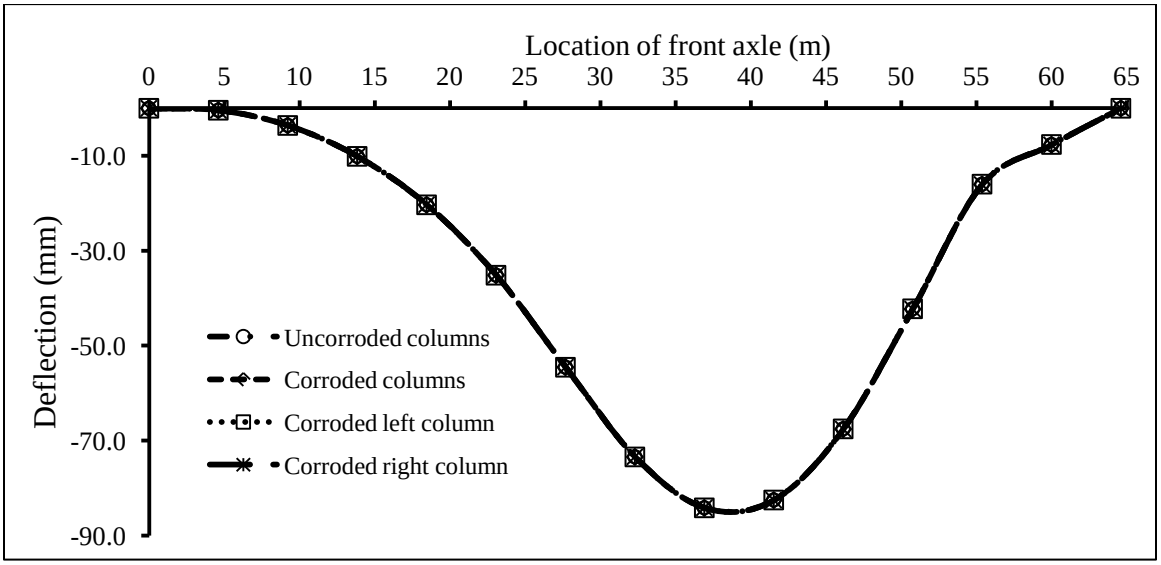

Figure 4.9: Comparison of dynamic deflections of superstructure under traffic load only and combined traffic and corrosion loads.

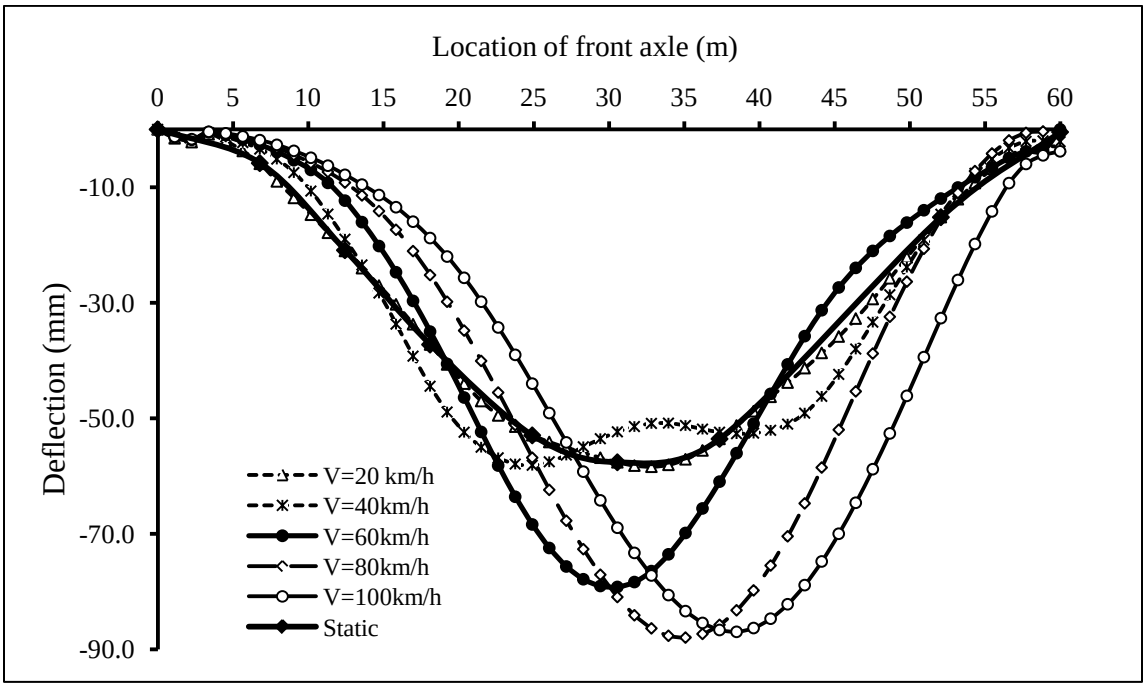

Figure 4.10: Dynamic deflection of BOTC under front axle for different truck speeds using the proposed SHDFEA.

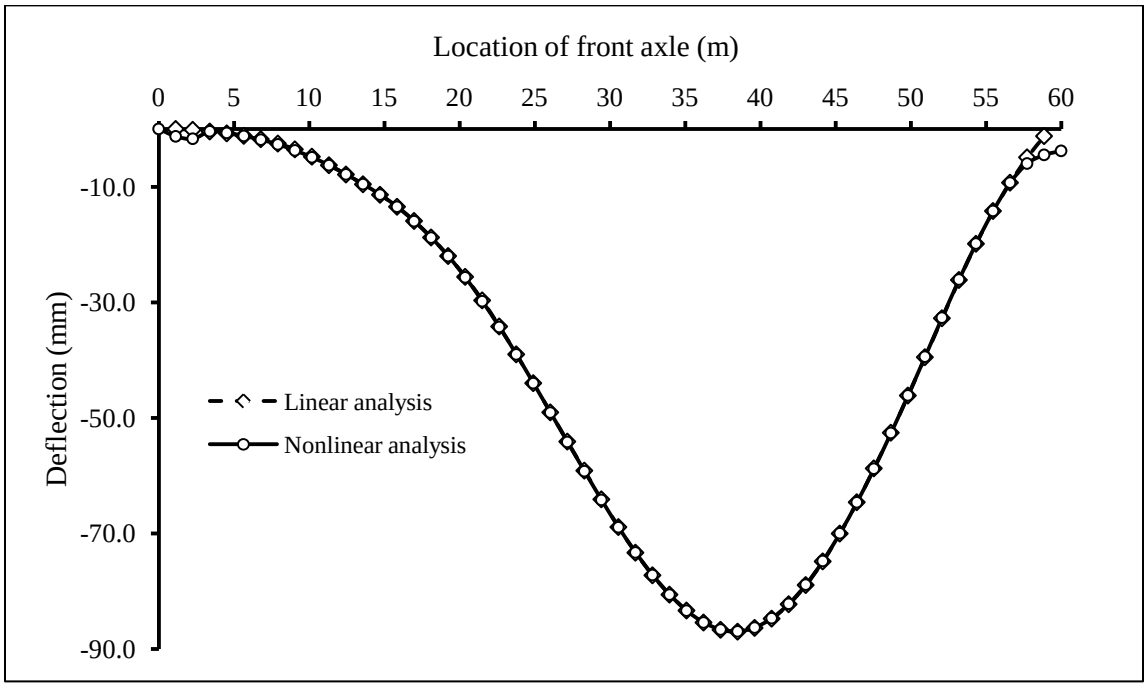

Figure 4.11-a. Comparison of dynamic deflection due to linear and nonlinear analysis of the columns.

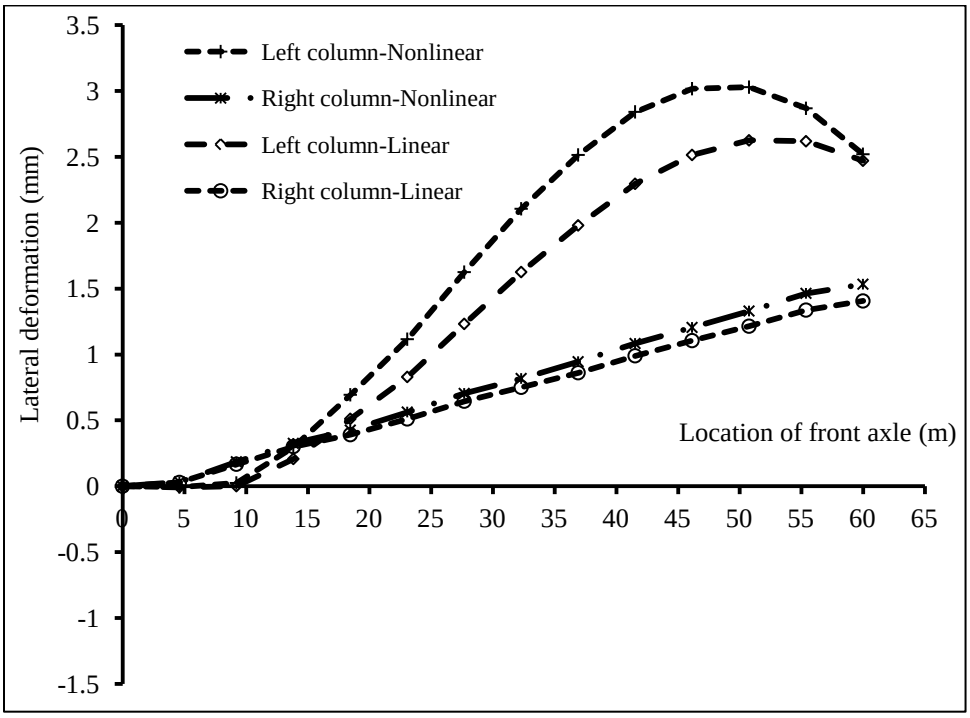

Figure 4.11-b: Comparison of maximum linear and nonlinear lateral deformation of the bridge columns.

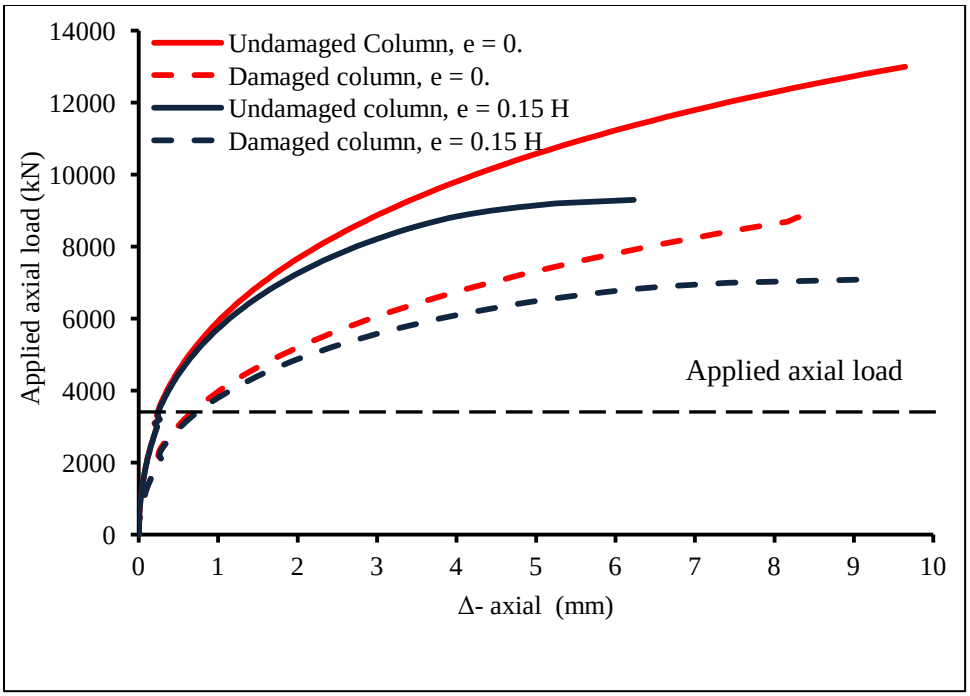

Figure 4.12: Applied axial load vs. axial displacement of the top section of the bridge column (right before static failure load).

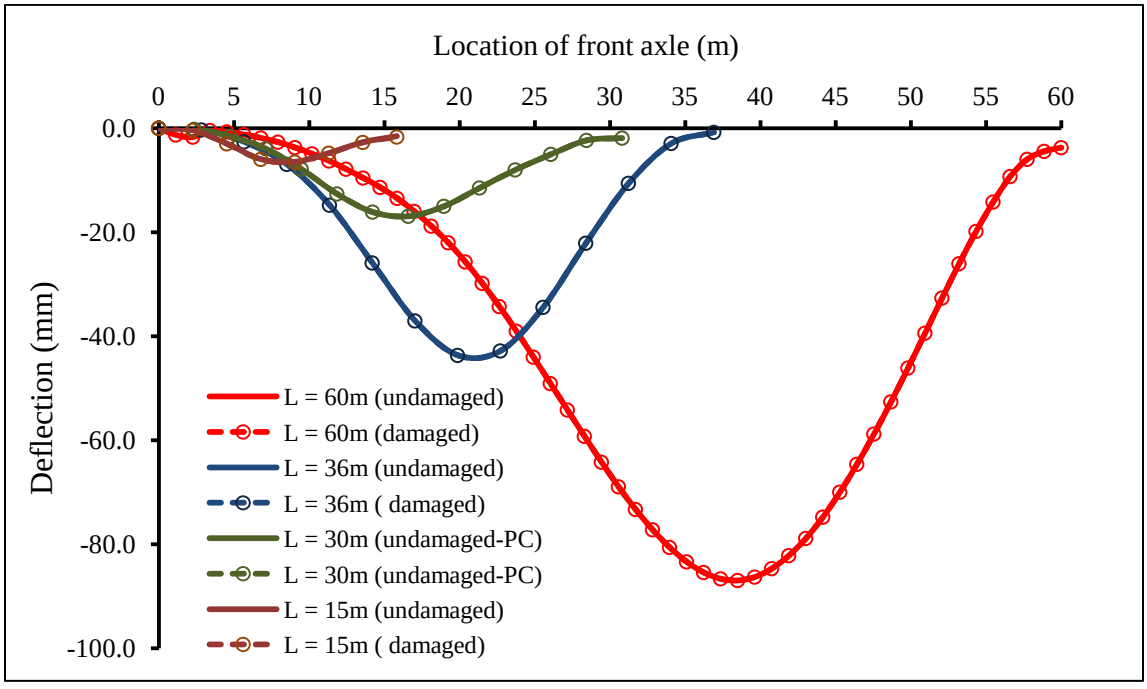

Figure 4.13: Comparison of dynamic deflections of superstructure under traffic load only and combined traffic and corrosion loads for different bridge lengths.

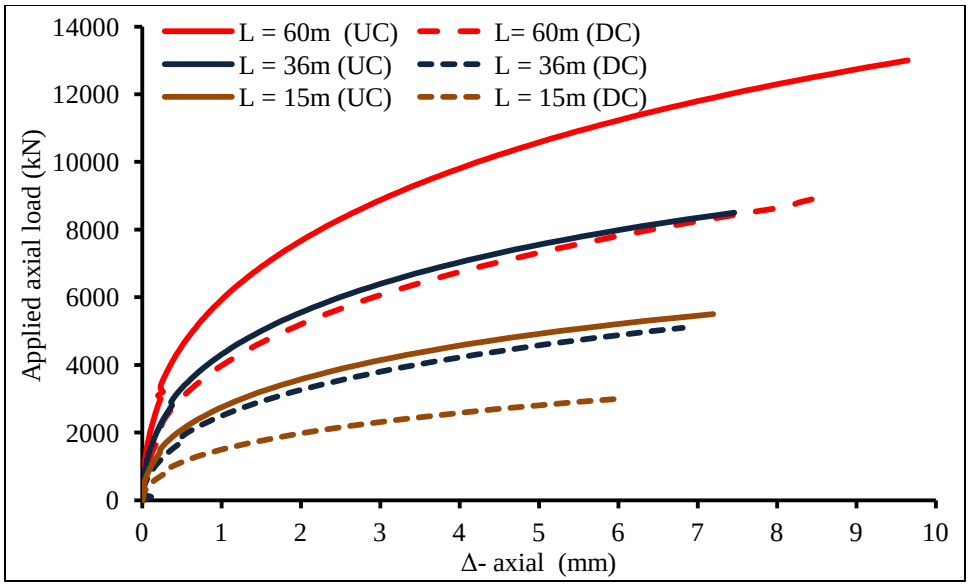

Figure 4.14-a: Applied axial load vs. axial displacement of the top section of the bridge column (right before static failure load) with zero eccentricity; UC: undamaged column; DC: damaged column.

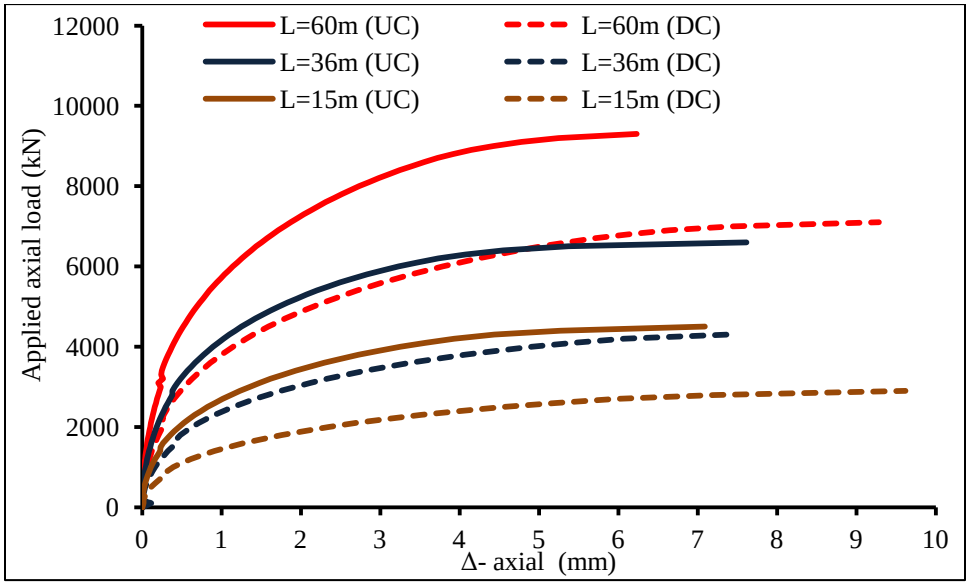

Figure 4.14-b: Applied axial load vs. axial displacement of the top section of the bridge column (right before static failure load) with 0.15H eccentricity; UC: undamaged column; DC: damaged column.

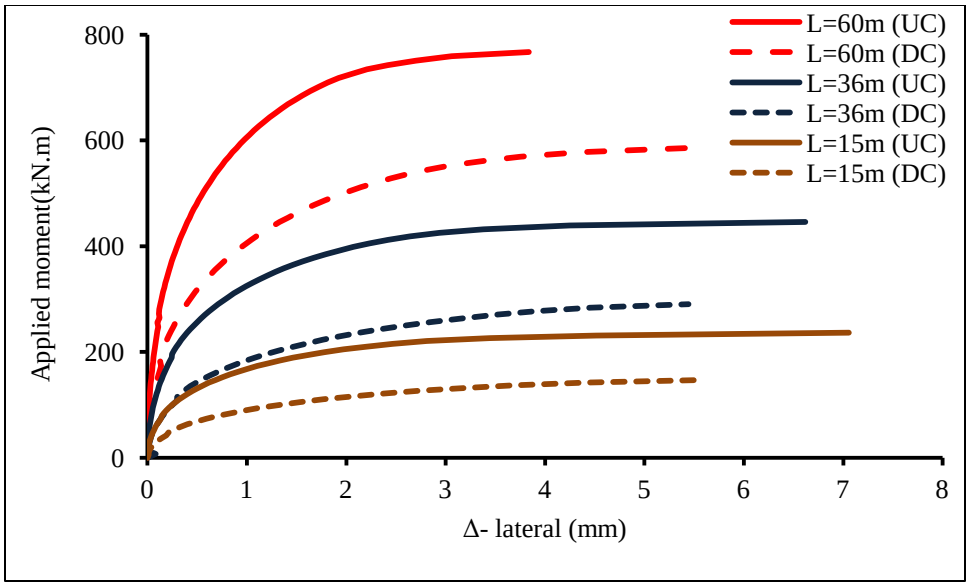

Figure 4.14-c: Applied moment vs. lateral displacement of the top section of the bridge column right before static failure load; UC: undamaged column; DC: damaged column.

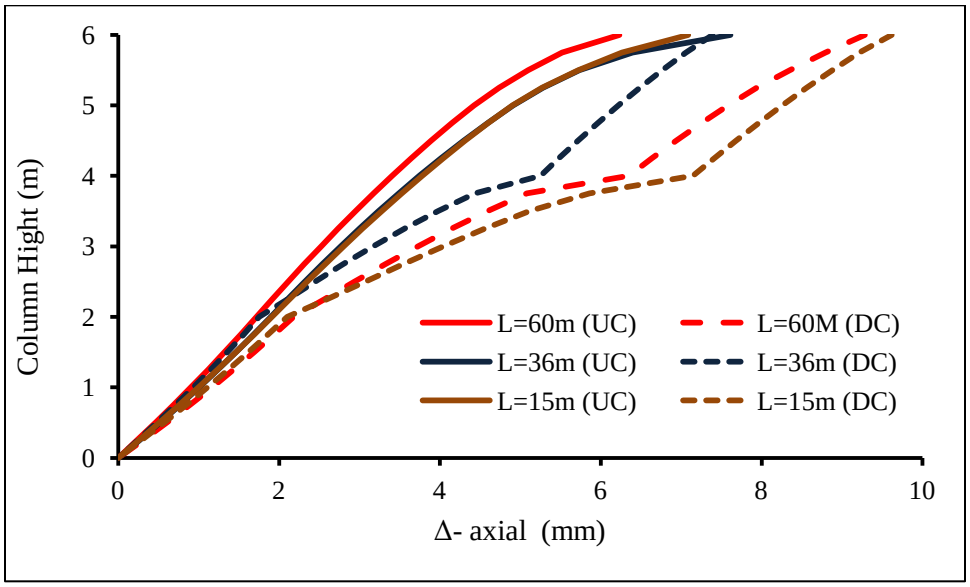

Figure 4.15-a: Column height vs. axial displacement of the bridge column at failure load; UC: undamaged column; DC: damaged column.

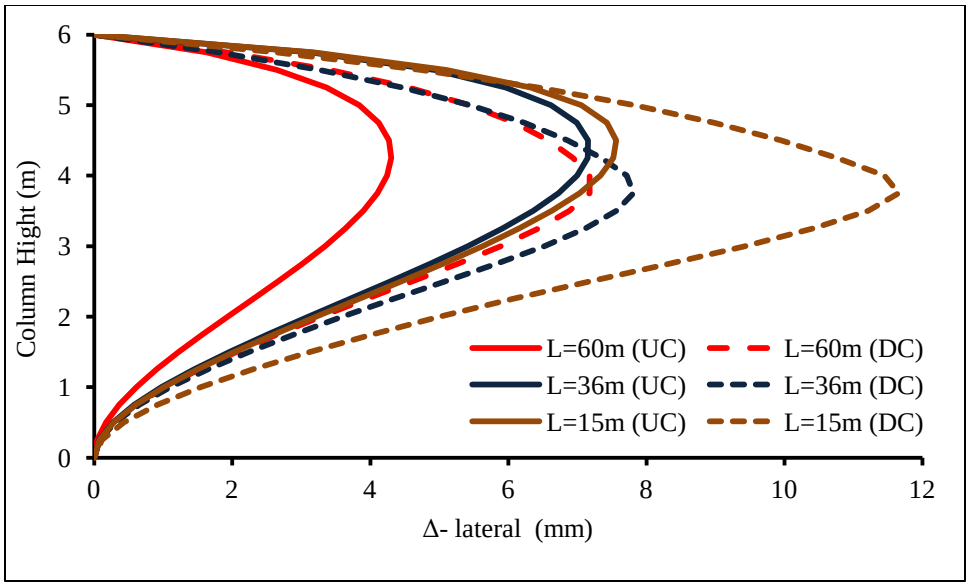

Figure 4.15-b: Column height vs. lateral displacement of the bridge column at failure load; UC: undamaged column; DC: damaged column.

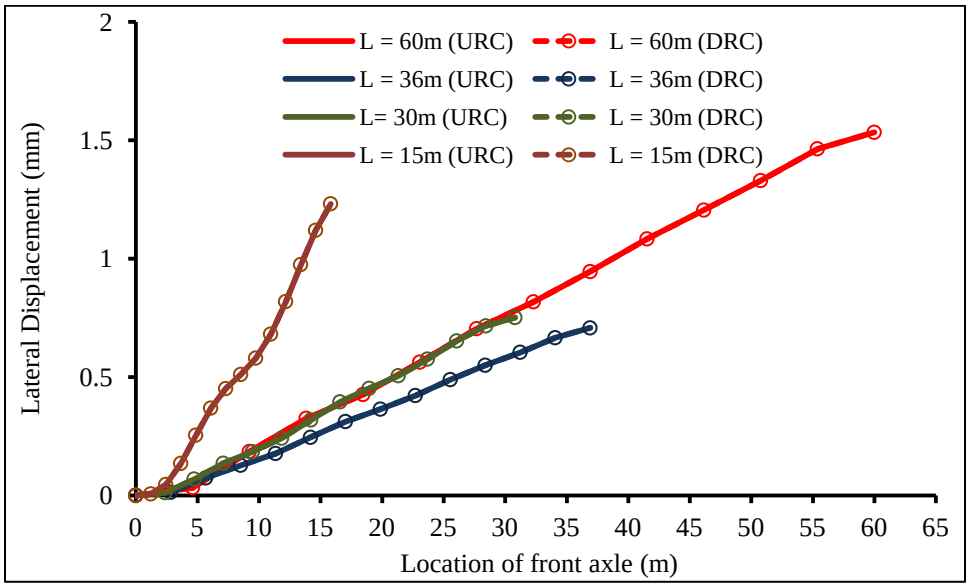

Figure 4.16-a: Truck position vs. maximum lateral deformation of the right column for different bridge lengths; URC: Undamaged right column; DRC: Damaged right column.

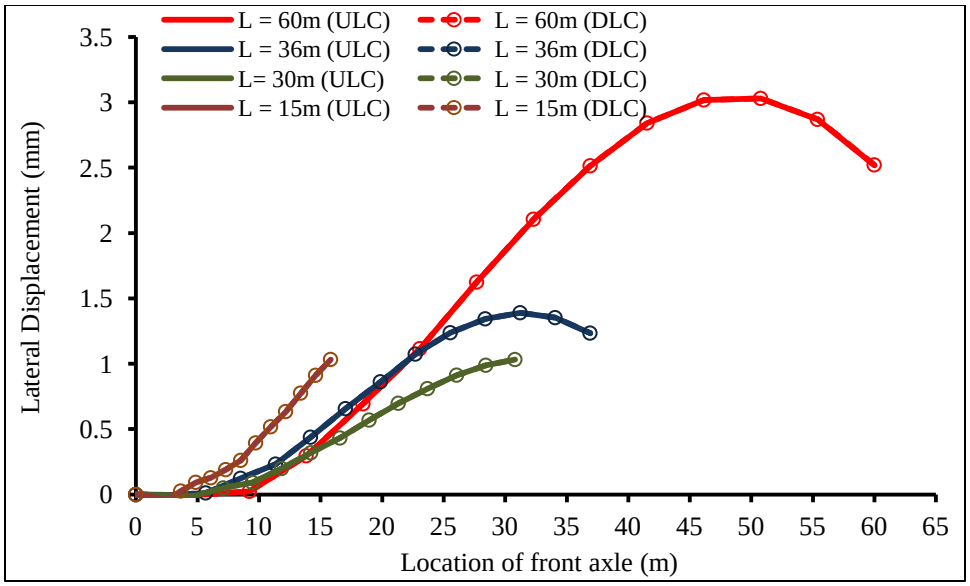

Figure 4.16-b: Truck position vs. maximum lateral deformation of the left column for different bridge lengths; ULC: Undamaged left column; DLC: Damaged left column.

4.9 References

Ali, A., Dynamic Analysis of Bridges Using the Finite Element Strips Method. Ph.D. Thesis, Dept. of Civil Engineering, University of Ottawa, Ottawa, Canada; 1999, 213 pages.

American Association of State Highway and Transportation Officials, AASHTO LRFD Bridge Design Specifications SI Units (4th Edition); 2007.

Andersen, A., HETEK, Investigation of Chloride Penetration into Bridge Columns Exposed to De-Icing Salt. Copenhagen, Denmark;1997.

Asnachinda P., Pinkaew T. and Laman J.A., Multiple Vehicle Axle Load Identification From Continuous Bridge Bending Moment Response. Engineering Structures; 2008,30(10): 2800-2817.

Canadian Standards Association, Canadian Highway Bridge Design Code, S6-06, A;2006.

Cremona, C., Dynamic monitoring applied to the detection of structural modifications: a high-speed railway bridge study.Prog. Struct. Engng Mater; 2004, 6:147–161.

Gong, L. and Cheung, M., Computer Simulation of Dynamic Interactions between Vehicle and Long Span Box Girder Bridge. Tsinghua Science and Technology; 13(SUPPL. 1), 71-77.

Hevener, W., Simplified live-load moment distribution factors for simple span slab on I-girder bridges. MSc. Thesis, Dept. Civil and Environmental Engineering, University of West Virginia, Morgantown,West Virginia,USA;2003, 151pages.

Law, S. and Zhu, X. 2004. Dynamic Behaviour of Damaged Concrete Bridge Structures Under Moving Vehicular Loads. Engineering Structures;2004,26(9): 1279-1293.

Lin, Y.H. and Trethewey, M.W., Finite Element Analysis of Elastic Beams Subjected to Moving Dynamic Loads. Journal of Sound and Vibration;1990,136(2): 323-342.

McGuire, W., Gallagher, R. H., Matrix structural analysis. John Wiley & Son. Inc., New York, NY, 2000.

Mohammed, A., Almansour, H., Martín-Pérez, B., Modelling RC bridge columns under the combined effects of traffic and reinforcement corrosion. 8th International Conference on Short & Medium Span Bridges, Niagara Falls, Ontario, Canada, 2010, Paper 168, 10 pp.

Mohammed, A., Almansour, H., Martín-Pérez, B., Nonlinear flexural analysis of reinforced concrete beam-column subjected to ultimate gravity loads combined with reinforcement corrosion, Part I: Sectional Analysis. Structure and Infrastructure Engineering, submitted, ID NSIE-2014-0014; 2014a.

Mohammed, A., Almansour, H., Martín-Pérez, B., Nonlinear flexural analysis of reinforced concrete beam-column subjected to ultimate gravity loads combined with reinforcement

corrosion, Part II: finite element analysis. Structure and Infrastructure Engineering, submitted, ID NSIE-2014-0015; 2014b.

Mohammed, A., Almansour, H., Martín-Pérez, B., Seismic performance of aged reinforced concrete bridge columns subjected to reinforcement corrosion. Journal of Bridge Engineering (ASCE), to be submitted; 2014d.

Mohammed, A., Almansour, H., Martín-Pérez, B., A semi-quantitative assessment framework for aging reinforced concrete bridge columns. Engineering Failure Analysis; to be submitted; 2014e.

Nutt, R. V., Schamber, R.A, and Zokaie, T., Distribution of wheel loads on highway bridges. Final report for national cooperative highway research program;1988.

Rodríguez, J., Ortega, L. M. and Casal, J., Load Bearing Capacity of Concrete Columns with Corroded Reinforcement. Corrosion of Reinforcement in Concrete Construction, Royal Society of Chemistry;1996. 220-230.

Tapan, M., and Aboutaha, R., Load carrying capacity of deteriorated reinforced concrete columns. Computer and Concrete Construction;2009,6(6):473-492.

Zambrano, A., Rauci, M. and Malngone, P.,Vehicle-Structure Interaction to Analyse the Primary Dynamic Aspects of Railway Bridges. Structure and Infrastructure Engineering;2008, 4(2): 107-121.

Chapter 5

Evaluation of Seismic Performance of Aged Reinforced Concrete Bridge Columns Subjected to Reinforcement Corrosion as Part of Semi-Quantitative Assessment Framework

5.1. Introduction

Reinforced concrete (RC) bridge columns represent the most critical elements for the bridge safety, and developing a tool to quantify their damage effects on the bridge stability when subjected to earthquake load is of high interest. Bridges in cold regions are affected by chloride-induced reinforcement corrosion, generated mainly from the application of de-icing salts in winter. The development of a cost effective and simplified evaluation approach that enables fast and accurate assessment of the structural capacity of corrosion damaged RC bridges presents a major challenge to practicing engineers as well as infrastructure owners.

Significant percentage of the stiffness and the strength of these critical elements can be lost due to severe reinforcement corrosion and damage in the concrete. The interactive effects of corrosion-induced damage and the repeated traffic load cycles can result in accelerated deterioration of critical structural elements. In high risk seismic zones, the dynamic response of corrosion affected RC columns could significantly change. The locations of critical evaluation sections could move to corrosion-damaged zones from the typical seismic-design sections. Hence, the drop in stiffness and strength of the corrosion-damaged zones could result in a serious drop of the overall seismic capacity of the structural elements, and the collapse mechanism of these elements could also change.

Estimating the structural capacity and the dynamic performance of the element and the overall bridge structural system when subjected to seismic loads is a major component of the assessment of aging bridges. At present, qualitative assessment approaches are used in most of North

American states and provinces. With the lack of accuracy of existing assessment approaches, there is a need to develop an efficient assessment approach that can quantitatively evaluate the structural performance of bridges when safety critical elements (the bridge columns, for instance) are partially damaged. A semi-quantitative assessment approach is proposed in Chapter 6 (see Mohammed et al. 2013e), introducing a limit states evaluation (LSE) approach in parallel to the limit states design (LSD) approach in North American bridge design codes (CSA S6-06/ CHBDC 2006, and AASHTO LRFD Bridge Design Specifications, 2007). The major evaluation limit states are: evaluation ultimate limit state (ULS), evaluation serviceability limit state (SLS) and evaluation earthquake limit state (ELS) (which is the focus of this chapter; Mohammed et al. 2013d).

In order to estimate the instantaneous seismic capacity of a bridge beam-column, it is important to identify the changes in the geometrical and material properties of the corrosion-damaged zones for different critical damage levels. Mohammed and Almansour (2013), see Appendix D, shows that it is possible to simulate the staged failure mechanism developed in RC concrete columns subjected to quasi-static or cyclic loads. The collapse is further accelerated and the structural capacities are further deteriorated when severe reinforcement corrosion damage states take place. However, the staged failure mechanism takes analogous patterns to those staged failure patterns of non-corrosion damaged elements, but with lower strength and significant changes in their ductility and hysteretic behavior. Different types of reinforcement corrosion-induced damage in bridge columns, such as spalling of concrete cover, reduction in reinforcement section, fracture of one or more stirrups, etc, can be defined as critical damage levels. As a transition stage preceding the development of a time-dependent quantitative assessment approach, visual inspection and additional measurements and material tests on the

corroded reinforcement can be employed as major source of input to the proposed semi-quantitative assessment framework.

Most bridge columns are conservatively designed (over-designed) and their service-load-over-capacity ratio (SLOCR) range between 25% and 50%. The SLOCR is increased in aging bridge columns due to the increase in the truck loads, number of axles, traffic density, frequency and traffic speed, in addition to the reduction of the column ultimate capacity due to reinforcement corrosion. On the other hand, higher design SLOCRs are targeted for newly constructed bridges, mainly because: (i) it could result in reducing the initial cost; (ii) smaller column sections are required for aesthetical needs; and (iii) of the use of high performance materials. There can be two possible scenarios for the interactive effects of reinforcement corrosion on the seismic resistance of RC columns: (i) an earthquake load is applied where reinforcement corrosion is in progress and maybe in an advanced stage; or (ii) a bridge column survived a medium size earthquake with some damage in the form of cracks, which could accelerate the initiation and/or the progress of the corrosion process. Whereas the first case is important in evaluating the safety and capacity of the bridge column as presented in this chapter, the second case is important for post disaster inspection/maintenance process.

Numerous studies have experimentally shown that reinforcing steel corrosion could result in a reduction of the static capacity of RC structural elements (e.g. Rodríguez et al. 1996). However, limited efforts have been directed to study the structural behaviour of corrosion affected RC columns when subjected to seismic load. It is worthy to present here three recent studies focused on the seismic performance of existing RC structures that are affected by corrosion, in which both strength and stiffness degradation are observed: (1) Saito et al. (2007) and Oyado et al. (2007), (2) Choe et al. (2008), and (3) Berto et al. (2009). Saito et al. (2007) and Oyado et al.

(2007) conducted a number of tests to evaluate the strength and deformation capacities of RC columns with reinforcement corrosion subjected to static and cyclic loads. In their study, two set of columns were tested: (i) columns subjected to only axial compression; and (ii) columns subjected to axial compression and lateral cyclic load. They observed that the corrosion of longitudinal bars and hoops reduce the column deformation capacity. They proposed a stress-strain model and corresponding deformation capacity by considering only the reduction of the rebars cross section. The study did not consider the effects of corrosion on the reduction of steel ductility, the reduction of the core concrete compressive strength when one or more stirrups are damaged, and the spalling of the concrete cover. Choe et al. (2008) developed probabilistic drift and shear force capacity models by integrating the effects of the deterioration of structural elements affected by reinforcement corrosion into a structural capacity estimation model. In their study, a numerical analysis was performed using the OpenSees software to obtain the fragility estimate of a given column, which was modeled by fiber-discretized cross sections, where the material of each fibre is modeled as a uniaxial inelastic material. Also, the probabilistic model for reinforcement corrosion (corrosion initiation, corrosion rate, and loss of cross-section area) was carried out to characterize the prediction of the service life of existing and new structures. Berto et al. (2009) conducted an analytical investigation to assess the corrosion effects on the seismic behaviour of RC structures. They considered two major parameters: the reduction of the rebar section and the loss of concrete cover. A nonlinear static analysis was performed using MIDAS Gen software considering gravitational and seismic loads. Choe et al. (2008) and Berto et al. (2009) studies considered only the reduction of reinforcement cross-sectional area, while they did not consider the impact of stirrups damage on the concrete confinement and hence the concrete strength.

Mohammed et al. (2011), see Appendix E, proposed a nonlinear elasto-plastic numerical analysis approach to simulate bridge columns under the combined effects of reinforcement corrosion and seismic excitation. The approach addressed the diversity in time between the two processes, the progress of the reinforcement corrosion and the sudden or "flash" attack of earthquake load. The instantaneous seismic load-capacity of an aging column subjected to reinforcement corrosion as a time dependent process is evaluated. Reinforcement corrosion is simulated in an external time-dependent-cycle, while the seismic load is simulated in an internal cycle of elasto-plastic time-history analysis. The seismic time-history analysis is activated at each major level of corrosion damage that was identified based on assuming constant rate of corrosion. The approach is based on assuming ideal conditions that result in constant rate of corrosion and does not include the effect of inspection and possible maintenance/rehabilitation interventions on the bridge columns.

The objective of this chapter is to develop a simplified nonlinear seismic analysis (SNLSA) as part of the semi-quantitative assessment framework (SQAF) proposed in chapter 6 (see Mohammed et al. 2013e). The proposed SNLSA provides a practical tool that enables the evaluation of the residual seismic capacity and the seismic behaviour of slab-on-girder bridge columns subjected to local damage due to reinforcement corrosion. The emphasis is on: (i) the numerical efficiency and stability of the analysis approach; (ii) the staged failure mechanism simulation and the hysteretic diagram envelope simulation; and (iii) the approach capability to capture the characteristics changes in time history behaviour.

5.2. Simplified nonlinear seismic analysis (SNLSA) as a part of semi-quantitative assessment framework (SQAF)

Figure 5.1 shows the proposed SQAF, which has six major parts: (I) data input; (II) quantifying reinforcement corrosion and its effects; (III) evaluating columns performance under combined

corrosion and ultimate loads (Evaluation-ULS); (IV) evaluating columns performance under combined corrosion and service (or traffic) loads (Evaluation-SLS); (V) evaluating columns performance under corrosion and seismic (earthquake) loads (Evaluation-ELS); and, (VI) semi-quantitative assessment and reporting. In North American bridge codes (CSA S6-06/ CHBDC 2006, and AASHTO LRFD Bridge Design Specification, 2007), the earthquake limit state is a major limit state to be verified for bridge design in high risk seismic zones. As shown in the following sections, the nonlinear sectional analysis (NLSA) presented in Chapter 2 (see Mohammed et al. 2013a) is the basis for the evaluation seismic limit state of the semi-quantitative assessment framework (SQAF) proposed by the authors as mentioned earlier. The evaluation of the column structural performance under combined reinforcement corrosion and ultimate loads, and the evaluation of the column structural performance under combined reinforcement corrosion and traffic loads are presented in Chapters 3 and 4, respectively (Mohammed et al. 2013b&c).

The first part of the proposed SQAF includes three data-input tasks: (I-a) the structural material and geometrical data including boundary conditions; (I-b) the loading data; and, (I-c) the enhanced inspection and reinforcement corrosion data. In the first task, the data are collected from the original design information/report and shop drawings (if available), and from field tests on the materials in their current state (if possible). The difference between the original design loads and the present loads on the bridge column under consideration are to be determined.

In task I-c, the enhanced in-depth visual inspection (or enhanced inspection) is used in the proposed semi-quantitative assessment framework to provide detailed field measurements on the dimensions of the damaged concrete zone, the volume of concrete spalling of the corrosion affected zone (FHWA-RD-01-020, 2001). Determining the state of corrosion damage of the

rebars and their mechanical properties that used in the model is more complicated. In this study, a hybrid approach to find the steel rebars properties is suggested. Out of all the columns of the bridge pier under assessment, the most damaged one is selected, and the damage status and size and the material properties can be generalized over the other columns of the pier for a conservative assessment of the substructure. The most damaged rebars are then identified, and samples of suitable size and number are collected. In the lab tests of the steel rebars, a precise measurement of the maximum reduction of rebar diameter or the reduction in the reinforcing steel thickness is found for each sample (using different available techniques ranged from hand cleaning and measurement to the use of recent technology of 3D laser scanner). Assuming a constant rate of corrosion, the corrosion current density and the time elapsed to generate the measured reduction in the reinforcing steel thickness are then found using the data of different samples and the empirical equations shown in Chapter 2 (see Mohammed et al.2013a). Using the evaluated reinforcement corrosion parameters and empirical formulae (for example, see Lay and Schiebl 2003 and Cairns et al. 2005) the loss of strength and ductility of the reinforcement subjected to corrosion attack can be estimated. On the other hand, the strength and ductility of the reinforcement can be evaluated by tensile tests if the corroded rebar samples can be available in suitable length. The deterioration of the structural ultimate and earthquake capacities are then respectively quantified using the nonlinear finite element analysis, NLFEA, (see Chapter 3; Mohammed et al. 2013b) and the simplified nonlinear seismic analysis, SNLSA, proposed in this chapter.

The proposed SQAF identifies four major damage cases due to reinforcement corrosion, which are: (a) cracking of concrete due to corrosion; (b) spalling of the concrete cover; (c) rupture of one or more stirrups; and, (d) in a more advanced state of corrosion damage, structural failure of

the column through complete loss of confinement and/or rebar(s) buckling. It is important to mention here that the focus is on the last three damage cases, where the damage case (a) can be considered as part of damage case (b), in which the impact on the structural behaviour is more apparent. The details of each of these major possible deterioration states are shown in Figure 5.2.

The evaluation ELS is integrated with the proposed SQAF (see step V above and Figure 5.1), wherein quantifying the effects of reinforcement corrosion for each major case is taken into account. The flowchart shows the link to one of the three major evaluation limit states; E-ULS, E-SLS and E-ELS. The simplified nonlinear seismic analysis, SNLSA, is the basis of the E-ELS four tasks (see Figure 5.2), which are: (a) establishing the nonlinear load-displacement relationship for critical sections and for different states of corrosion damage; (b) establishing the load-displacement hysteretic relationship based on states of corrosion damage; (c) establishing the time-history relationships of lateral displacement of critical sections; and, (d) establishing the interaction diagram for different states of corrosion damage. These four tasks of E-ELS end with the preparation of the required data for the final SQAF. The details of the proposed SQAF are presented in Chapter 6 (Mohammed et al. 2013e).

5.3. Proposed Simplified Non-Linear Seismic Analysis (SNLSA) for Corrosion Damaged Beam-Columns

Reinforcement corrosion is a continuous long-term time-dependent process that is affected by several environmental and operational parameters. It could lead to significant changes in the mechanical properties of the structural element, in which ultimate and seismic capacities could severely drop. Hence evaluating the safety, serviceability and durability of the affected structural elements is essential. For bridges located in seismic regions, the main concerns are the structural capacity of the column in terms of residual strength and ductility, the level of damage after a

major earthquake, and the collapse mechanisms compared to columns that are not affected by reinforcement corrosion (or right after construction). The seismic response of corrosion-damaged bridge columns depends on their original design, the level of corrosion damage/deterioration and the characteristics of the earthquake load. The focus of this chapter is on the effects of local corrosion damage in slab-on-girder bridge columns on their seismic response.

Figure 5.3 shows a highway overpass where a three-lane slab-on-steel-girder (superstructure) is supported by a typical multi-column reinforced concrete (RC) pier with an RC cap beam (substructure). Aging slab-on-girder bridges are usually affected by an aggressive corrosive environment due to the use of deicing-salt over the long winter in Canada and the Northern states of the United States. Figure 5.3 also shows the traffic directions over and under the bridge with a typical road configuration. The figure also shows the possible seismic excitation applied in the direction of the traffic over the bridge. The splash of salty water affects the bridge columns above the traffic level, where corrosion damage usually develops at approximately the middle-third of the column height (Andersen 1997). Figure 5.4 shows the assumed location of the column corrosion affected zone relative to the seismic excitation, which corresponds to the middle third of the column height.

The proposed simplified non-linear seismic analysis (SNLSA) for corrosion-damaged beam-columns is briefly presented in this section. The analysis approach is based on four major steps: (i) the semi-quantitative assessment framework (SQAF); (ii) the simplified nonlinear sectional analysis (NLSA) (see chapter 2, or Mohammed et al. 2013a); (iii) the dynamic inelastic analysis of plane RC structures (DRAIN-RC; (Alsiwat 1993 and Shoostari 1998)); and, (iv) Takeda hysteretic model (Cheng 2000). Corrosion-induced damage on the steel reinforcement (cross section loss and ductility decrease) and on the concrete section in the damaged zone is evaluated

in the SQAF as explained in detailed in Chapter 6 and in Figure 5.2. The nonlinear behavior at the sectional level of the corrosion-damaged section is evaluated using NLSA. The time-history analysis of the RC columns based on the sectional analysis is then performed using DRAIN-RC. The hysteretic response of the column at the critical section of the damaged zone is then established using Takeda's model.

5.3.1. Nonlinear modelling and time history analysis

The computer program that integrates the three background programs (namely, NLSA, DRAIN-RC, and Takeda) with the preliminary part of the SQAF involves: (i) data preparation; (ii) enhanced inspection and any required tests; and (iii) the quantification of the corrosion effect on the steel and concrete sections. The computer program DRAIN-RC is used in the proposed SNLSA mainly to perform inelastic dynamic history analysis, as shown in Figure 5.2. The original version of the program (DRAIN-2D) was developed by Kanaan and Powell (1973) to conduct dynamic analysis of inelastic plane structures. The program was modified by Alsiwat (1993) and Shoostari (1998) by adding new features such as inelastic static analysis (push-over) and P-Δ effects. In this program, the structure is discretized into a number of elements with three degrees of freedom at each node, two translations and one rotation. The global stiffness of the structure is assembled from individual element stiffness using the direct stiffness method, while the mass of the structure is assumed lumped at the joints resulting in a diagonal mass matrix. Damping can be specified as either mass dependent or stiffness dependent Raleigh damping. Ground motion is entered as accelerations specified at constant time intervals and can differ for horizontal and vertical directions.

The dynamic response is determined using the step-by-step integration technique assuming constant average acceleration during each time step(t). In assembling the stiffness matrix, the tangent stiffness at the start of an integration step is assumed to remain constant throughout that step. The stiffness of each element is updated at the beginning of each step, and if the nonlinear analysis option is selected, errors due to possible overshooting are corrected by applying a corrective load at the beginning of the following step.

5.3.2. Modeling the effects of reinforcement corrosion on the steel rebars and the concrete

As mentioned earlier, the proposed analysis approach employs visual inspection and any required material testing as the major source of the input data of the corrosion damage and material properties for the proposed analysis approach. Hence, it is not the purpose of the proposed analysis approach to study, identify or simulate how the corrosion grew up, what the real corrosion rate was, or whether the corrosion rate was constant or variable. The focus is only on quantifying the effects of the ongoing corrosion process on the material properties, the distribution of the damage or its size, and the integrity of the RC element in the damaged zone at the inspection/assessment time. In order to prepare the data for the analysis approach, a uniform rate can be assumed, where the observed level of damage at the time of the inspection can be matched, and hence the instantaneous material properties can be estimated.

In Chapter 2 (NLSA), the effects and modeling of the corrosion on the reinforcement, the concrete section, and the composite action between the concrete and the steel are presented in detail. The three major effects of the corrosion on the state of damage are: (i) the reduction of the reinforcement cross-sectional area and ductility; (ii) loss of concrete cover; and (iii) the local bond loss of tensile steel reinforcement (see Mohammed et al. 2013a).

5.3.3. Load combinations

The load combinations for the nonlinear seismic analysis in this study are considered according to the extreme possibilities of the combinations of the traffic and the seismic load. The three scenarios of the load combination on an aging bridge during an earthquake are: (i) the earthquake occurs when there is no traffic on the bridge; (ii) earthquake occurs during the rush hour; and, (iii) the earthquake occurs when one truck is moving on the bridge. In all the three load combination scenarios, the traffic load is considered as a static load.

5.3.4. The integration and data flow between the SNLSA programs

In the proposed SNLSA, as illustrated in Figures 5.1 and 5.2, the preparation and transferring of the data and the results from any analysis step to the other steps are done through the main program. Each of the three "supporting" programs run inside the main program reading the required input data from an instantaneous data file issued in the preceding step. After the completion of running the supporting program, the output of that step is saved in another file, and so on. The main program prepares the data input for the NLSA and controls the running of the supporting programs (NLSA, DRAIN-RC, and Takeda), and then it extracts each program's results and re-circulates them if required in the seismic analysis. The main program accumulates the required results for the final semi-quantitative assessment of the bridge column.

5.4. Case Studies, Results and Discussions

The results of four case studies are discussed in this section. The first case study is a comparative study with selected RC column specimens from the series of tests performed by Oyado et al. (2007). The other three case studies are done on three columns subjected to the same loads, but they have different cross-sections dimensions and reinforcement ratios. All the three columns are

designed for seismic resistance as per CSA-S6-2006 (CHBDC), but with low, medium and high load-over-resistance ratios.

5.4.1 Staged failure mechanism under cyclic loads

An RC bridge column is usually subjected to different levels of gravity loads when an earthquake event occurs. The loads applied on the bridge columns are a combination of self-weight of the bridge superstructure and the equivalent traffic loads (static load magnified by a dynamic load allowance, or impact load factor and a reduction factor to account for multi-lane loading). For slab-on-girder bridges simply supported on columns, the loads of the superstructure are applied eccentrically. When the column suffers from corrosion damage, the load eccentricity could be further increased in the damaged zones, resulting in additional local and global flexural deformations. When an earthquake attacks an aging column, a large lateral seismic load is then applied on the column. Figure 5.5 shows several states of local corrosion damage and the general loads applied on the columns. The most important damage states are: (a) flexural and corrosion cracks; (b) initial (or partial) spalling; (c) one stirrup failure (with partial spalling); (d) all-sides spalling; (e) two stirrups failure (with all-sides spalling); (f) loss of confinement and possible buckling.

5.4.2 Case study verification

In this case study the SNLSA results are compared with results of tests performed on reinforced concrete columns by Oyado et al. (2007). Figure 5.6 shows the column specimen design and reinforcement details. The column is reinforced with 16.0-mm diameter longitudinal rebars, with a reinforcement ratio of $\rho_{sl} = A_s/A_g = 2.5\ \%$, and with 10-mm diameter hoop reinforcement, with a reinforcement ratio of $\rho_{sh} = 2.5\ \%$, where ρ_{sl} A_s is the total longitudinal reinforcement,

and A_g is the gross area of the concrete column. The column was subjected to accelerated corrosion on two opposite faces over a length of 200 mm (starting at 350 mm and ending at 550 mm from the foundation face). The comparison between the proposed model results and the test results focuses on the control specimen (no corrosion, specimen 1 of Oyado et al. 2007) and one of the corroded specimens (specimen 4).

Figures 5.7 shows the results of the NLSA for the main damage states of an uncorroded column loaded quasi-statically up to failure. The damage states during the test are identified as: concrete cover spalling, one stirrup failure, two stirrups failure, and loss of confinement. The path of the staged failure is established (dotted line) with the guidance of the test results (red line). The NLSA results show a slight underestimation of the strength and stiffness in general. Figure 5.8 shows only the test results and the proposed staged failure path. In Figure 5.9, the envelope of the experimental load-displacement hysteretic relationship and the envelope of the load-displacement hysteretic relationship generated by the SNLSA are compared to the load-displacement relationships of Oyado's corroded specimen (4) for different states of corrosion-induced damage as generated directly by the NLSA. A good match is observed between the NLSA results and the staged failure path developed as an envelope by the SNLSA load-displacement hysteretic relationship. Hence, NLSA could be used directly to establish the envelope of the hysteretic relationship saving large efforts with an acceptable approximation. Figure 5.10 compares the envelopes of the load-displacement hysteretic relationship for column specimens 1 and 4 from the test results (Oyado et al. 2007) and from the proposed NLSA. The figure shows that a good match between the proposed approach and the test results is obtained. It also shows that the different stages of corrosion-induced damage result in a large drop of the column load and displacement capacities.

Following a similar approach, the staged failure path of the hysteretic load-displacement relationship of Oyado's non-corroded specimen (specimen 1) is established using Takeda's model as part of the proposed SNLSA. In each cycle of the response, the damage state is changed from undamaged to spalling, to one and two stirrups failure, up to the loss of confinement (see Figure 5.11). The nonlinear behaviour is evaluated using the NLSA as part of the SNLSA transferring the sectional behavior results of the column in each damage state to Takeda's model program. The SNLSA results again slightly underestimate the test results, but with good accuracy. The staged failure path of the hysteretic load-displacement relationship of Oyado's corroded specimen (specimen 4) is also established (see Figure 5.12). The proposed SNLSA gives a larger underestimation of strength capacity than in the case of non-corroded column. This can be explained by the conservative input data for material properties. Comparison of the results in Figures 5.11 and 5.12 shows the shrinkage in the hysteretic relationship, which indicates a significant drop in the energy absorption capacity due to corrosion damage.

5.4.3 Slab-on-girder bridge column with variable load-over-capacity ratio

This section discusses three case studies where the column design is variable according to an assumed load-over-capacity ratio. The aim of this investigation is to show the capability of the proposed SNLSA to estimate the structural behaviour of bridge columns with a variety of possible design alternatives. A slab-on-steel girder bridge with center-to-center span of 61 m and width of 20.5 m constructed in 1977 (Hevener 2003) is selected. The bridge is simply supported on RC piers formed from eight square columns. The 6.0-m height columns are assumed to have full fixity at the foundation level. The bridge superstructure consists of a concrete slab

compositely casted on steel girders. The girders spacing is 2.64 m, their cross-sectional area is 0.05 m^2, and the concrete slab thickness is 0.22 m.

The load combination for earthquake design in accordance to CHBDC 2006 (CAN/CSA-S6-06) assumes only 50% of the equivalent traffic load is acting on the bridge. Three design cases of the bridge column are discussed here based on three assumed load over capacity ratio (LOCR), which are: (i) 25% (or low) for a conservative design case, (ii) 40% (or medium) for regular design, and (iii) 60% (or high) for design controlled by aesthetic considerations. The concrete compressive strength ($f_c^{'}$) is assumed to be 35 MPa. For LOCR = 25%, the cross sectional dimensions are 700 mm x 700 mm, the longitudinal reinforcement ratio is $\rho_{sl} = A_s/A_g = 3.46$ %, with rebar diameter of 20 mm and hoops of 15 mm diameter at 30 mm c/c. For LOCR = 40% , the cross sectional dimensions are 600 mm x 600 mm, the longitudinal reinforcement ratio is $\rho_{sl} = A_s/A_g = 2.0$ %, with rebar diameter of 20 mm and hoops of 15 mm diameter at 30 mm c/c (see Figure 5.4 for details of the design). For LOCR = 60%, the cross sectional dimensions are 500 mm x 500 mm, the longitudinal reinforcement ratio is $\rho_{sl} = A_s/A_g = 2.5$ %, with rebar diameter of 20 mm and hoops of 10 mm diameter at 20 mm c/c.

The corrosion damage is assumed to affect the mid-height zone of all the three columns (see Figure 5.4). Figure 5.13 shows the load displacement relationships for different states of damage, including cover spalling, loss of one and two stirrups, and the loss of confinement, for LOCR = 40% when no corrosion is applied (i.e., no loss of reinforcement cross section and ductility), while Figure 5.14 shows the same relationships but when corrosion is applied (assuming a corrosion current density of 1 μA/cm^2). It should be pointed out that in this case study, it is assumed that with 5 % reduction of steel cross-sectional area due to reinforcement corrosion

would result in concrete cracks, 15% reduction would result in concrete spalling, 20% reduction would result one stirrup failure and 30% reduction would result two stirrups failure. These assumptions are approximate and based on generalization of the lab tests done by Oyado et al. (2007). The reason behind these assumptions here case is to show how to apply the present analysis approach. In field investigations, accurate measurements of the reduction of the steel and concrete are required, however, for approximate evaluation empirical equations could reduce the number of tests and samples required to prepare the data input. Figure 5.15 shows the load-displacement hysteretic relationship of the uncorroded column (LOCR = 40%) and the envelope when the column is subjected to cyclic load up to failure, while Figure 5.16 shows the same relationships when corrosion is applied. Figure 5.17 shows a comparison of the envelopes of the moment-displacement hysteretic relationships for the three columns when no corrosion is accounted for and when corrosion is applied. Similar to the first case study, the comparisons of the different figures and different cases show that corrosion-induced damage results in a large drop of the column load and displacement capacities. Comparisons also show the shrinkage in the hysteretic relationship, which indicates a significant drop in the energy absorption capacity due to corrosion damage. From Fig. 5.17, it is observed that corrosion-induced damage becomes less significant on the envelop of the load-displacement hysteretic relationship when the LOCR increases. However, this observation cannot be generalized as in the present case studies, the lateral reinforcement does not varies with variation of the LOCR, and further investigation on this point is needed.

In the four case studies, the behaviour of corrosion-damaged columns is compared to the behavior of non-damaged columns. It is found that for all columns, it is possible to simulate the staged degradation of capacity up to collapse or the “staged failure mechanism” when the

columns are subjected to quasi-static loading up to failure or to cyclic loading (hysteretic relationship) using only the NLSA developed in Chapter 2 (see for example Figures 5.7 through 5.17, and more details are also shown in Appendix F).

5.4.4 Time-History of Displacement of Uncorroded and Corroded Bridge Columns

The data of a short earthquake record in Ottawa, Ontario is used as shown in Figure 5.18 to study the time history behaviour of the three bridge columns in the second to fourth case studies above. As the steel area and concrete cover of the column at the critical cross section are reduced due to the corrosion process and resulting damage, the column stiffness is reduced. Depending on the inelastic behaviour of the column, the corroded section on the column will have less deformation capacity than the non-corroded sections. With the reduction in the column flexural stiffness and the reduction in the reinforcing steel ductility, the lateral displacement history of the corroded section is increased when the bridge is subjected to seismic load. Although the observations show that the middle height zone of the column is the most corrosion affected zone (see Mohammed et al. 2013b), in the parametric study of the displacement time history presented in the following, corrosion damage is considered to be located on the column top and bottom sections as well.

Figures 5.19 and 5.20 show the time history of the lateral displacement for the top, mid-height and bottom sections of the column with LOCR= 40% for the uncorroded and corroded sections, respectively; it is assumed that corrosion attacks one section at a time. Table 5.1 defines the acronyms used in the figures. As expected for the given boundary conditions of the columns, the figures show that the top section has the maximum deformation than the other sections for all the cases. It is also observed that the non corroded column can continue to deform up to and after the

loss of one stirrup, while the corroded column develops the same level of deformation only up to the spalling of the concrete cover, followed by the collapse of the column. In Figure 5.21 the staged failure path in the time history is established based on the level of deformation correlated to each damage state in the earlier analysis steps (NLSA and load displacement hysteric analysis). Each state of damage is identified in the figure by different color. From the figure, it is clear that the corroded columns develop larger deformation at earlier states of damage. For instance, with LOCR = 40% and at the same seismic excitation and time frame, the corroded column with only spalling of the cover deforms more than the non-corroded column with one stirrup broken. The same observation is recorded with other LOCRs as shown in Figures 5.22 and 5.23. However, the columns with large LOCR have no ability to develop an acceptable time history deformation when an advanced state of corrosion-damage is applied. Figures 5.22 and 5.23 compare the time history of the columns for different LCOR and the three selected sections (top, middle height, bottom). Based on Figures 5.19 through 5.23 (and Figures (F-9) to (F-15) of Appendix F), it is concluded that for seismic critical zones, low load over capacity ratio (LOCR < 40%) or "overdesign" of the columns are recommended in seismic critical zones. On the other hand, it is found that the time history analysis of the corrosion damaged columns is complicated and not recommended. However, a cost and time effective structural evaluation can be achieved by the NLSA and/or the hysteretic analysis.

Figure 5.24 shows the interaction diagram of corrosion damaged RC columns versus undamaged columns for different LOCR. The state of corrosion damage is assumed to be severe, resulting in local loss of the concrete confinement after losing two stirrups (see Appendix F for the interaction diagrams of the three types of columns and for all major states of corrosion damage). The figure shows significant contraction of the column interaction capacity when subjected to

severe corrosion damage for all load over capacity ratios. It is observed that the percentage reduction is very high when the column is conservatively designed or designed with a high LCOR. Compared to the applied service axial load with an eccentricity of 15% of the column depth in the direction of the traffic over the bridge, it is found that the interaction relationship is reduced to highly unsafe levels when the corrosion damage is applied and the column is designed for an LOCR of 60%. Figure F-15 of Appendix F shows that this type of column becomes unsafe even after only concrete spalls off the four column faces. Figures F-13 and F-14 show that for conservative or medium LCOR's, the interaction envelope is higher than the applied service load-and-moment by a large margin. This significant impact of reinforcement corrosion on the axial load-moment interaction relationship enhanced the previous recommendation on the need to conservatively design the bridge columns with low LCOR's in the critical seismic zones when reinforcement corrosion is expected.

5.5. Conclusions

In this chapter, a simplified non-linear seismic analysis (SNLSA) approach is proposed as part of a semi-quantitative assessment framework (SQAF). The approach is based on the nonlinear sectional analysis (NLSA) proposed in Chapter 2, DRAIN-RC nonlinear time history analysis program, and Takeda's hysteretic analysis. The approach is capable to match experimental results with acceptable accuracy.

It is found that the staged failure mechanism of the columns subjected to quasi-static load and cyclic load up to failure can be simulated with high accuracy using only the NLSA. It is also found that corrosion-induced damage results in a large drop of the column load and displacement capacities, and a large shrinkage in the hysteretic relationship, which indicates a significant drop in the energy absorption capacities of the different columns. From the time history analysis, it is

found that at the same seismic excitation and time frame, the corroded column deforms more than the non-corroded column at earlier stages of damage. Based on the given results, it is concluded that for seismic critical zones, overdesign of the columns is recommended. On the other hand, it is found that the time history analysis of the corrosion-damaged columns is complicated and not recommended. However, a cost and time effective structural evaluation can be achieved by the NLSA and/or the hysteretic analysis. Significant contraction of the column interaction capacity when subjected to severe corrosion damage for all load over capacity ratios is observed. The interaction relationship is reduced to unsafe levels when the corrosion damage is applied and the column is designed for an LOCR of 60%. This significant impact of reinforcement corrosion on the axial load-moment interaction relationship highlights the need to conservatively design the bridge columns in the critical seismic zones when reinforcement corrosion is expected.

Table 5.1: Acronyms definition for Figures 5.19– 5.23 and F-9–F-15 in Appendix F.

No	Definition	Acronyms	No	Notation	Acronyms
1	Load over capacity ratio	LOCR	20	Loss confinement- IS-NC	LC-IS-NC
2	Top section	TS	21	Loss confinement--BS-NC	LC-BS-NC
3	Intermediate section	IS	22	Flexural cracks- TS-C	CC-TS-C
4	Bottom section	BS	23	Flexural cracks- IS-C	CC-IS-C
5	Uncorroded	NC	24	Corrosion cracks- BS-C	CC-BS-C
6	Corroded	C	25	Spalling- TS-C	S-TS-C
7	Undamaged-TS-NC	UN-TS	26	Spalling- IS-C	S-IS-C
8	Undamaged-IS-NC	UN-IS	27	Spalling- BS-C	S-BS-C
9	Undamaged-BS-NC	UN-BS	28	1 stirrup failure- TS-C	OSF- TS-C
10	Spalling-TS-NC	S-TS-NC	29	1 stirrup failure- IS-C	OSF- IS-C
11	Spalling-IS-NC	S-IS-NC	30	1 stirrup failure- BS-C	OSF- BS-C
12	Spalling-BS-NC	S-BS-NC	31	2 stirrups failure- TS-C	TSF- TS-C
13	1 stirrup failure-TS-NC	OSF-TS-NC	32	2 stirrups failure- IS-C	TSF- IS-C
14	1 stirrup failure-IS-NC	OSF-IS-NC	33	2 stirrups failure- BS-C	TSF- BS-C
15	1 stirrup failure-BS-NC	OSF-BS-NC	34	Loss confinement- TS-C	LC-TS-C
16	2 stirrups failure-TS-NC	TSF-TS-NC	35	Loss confinement- IS-C	LC-IS-C
17	2 stirrups failure-IS-NC	TSF-IS-NC	36	Loss confinement- BS-C	LC-TS-C
18	2 stirrups failure-BS-NC	TSF-BS-NC	37	Applied moment	AM
19	Loss confinement- TS-NC	LC-TS-NC			

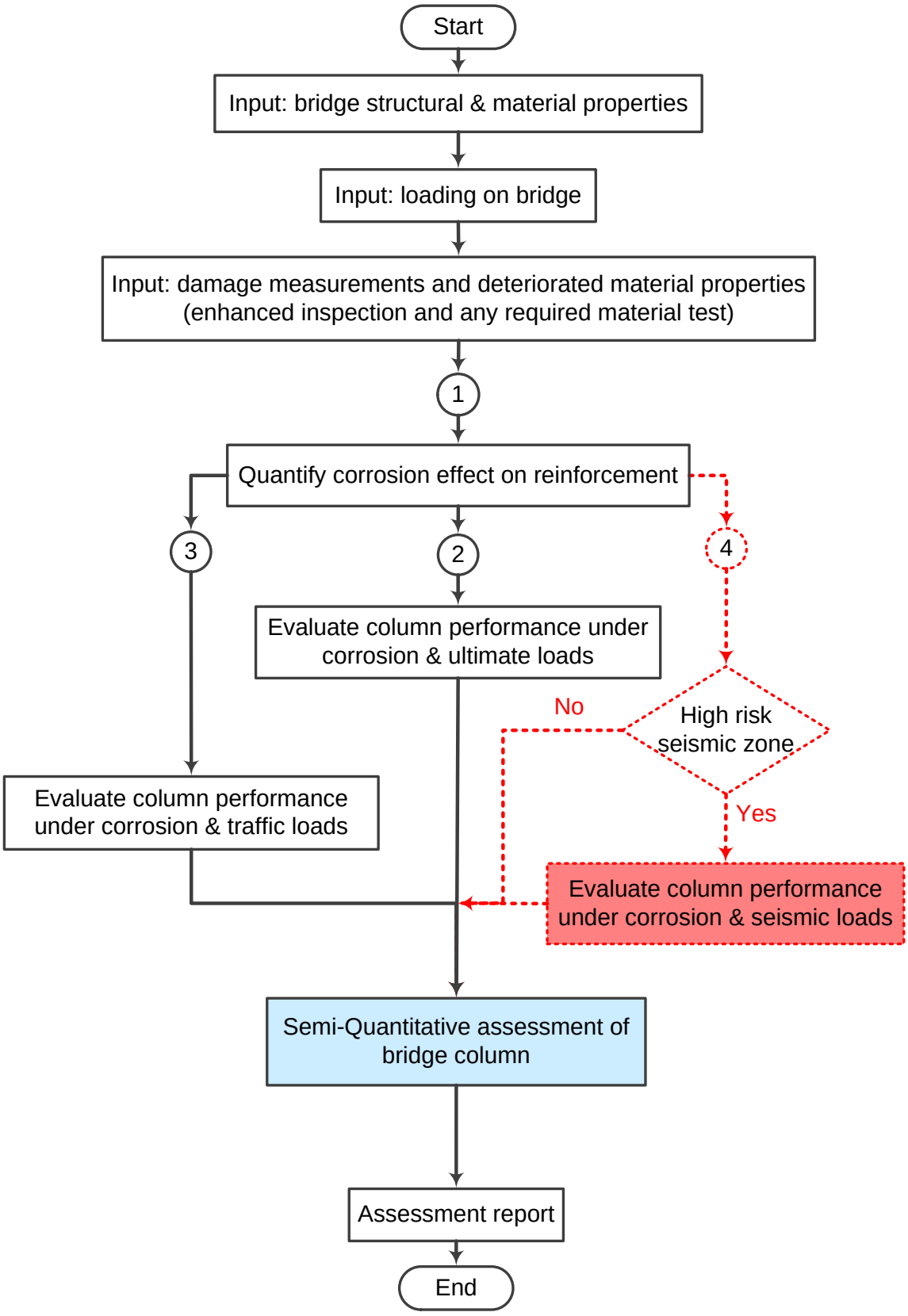

Figure 5.1: The proposed SQAF of aging RC bridge columns.

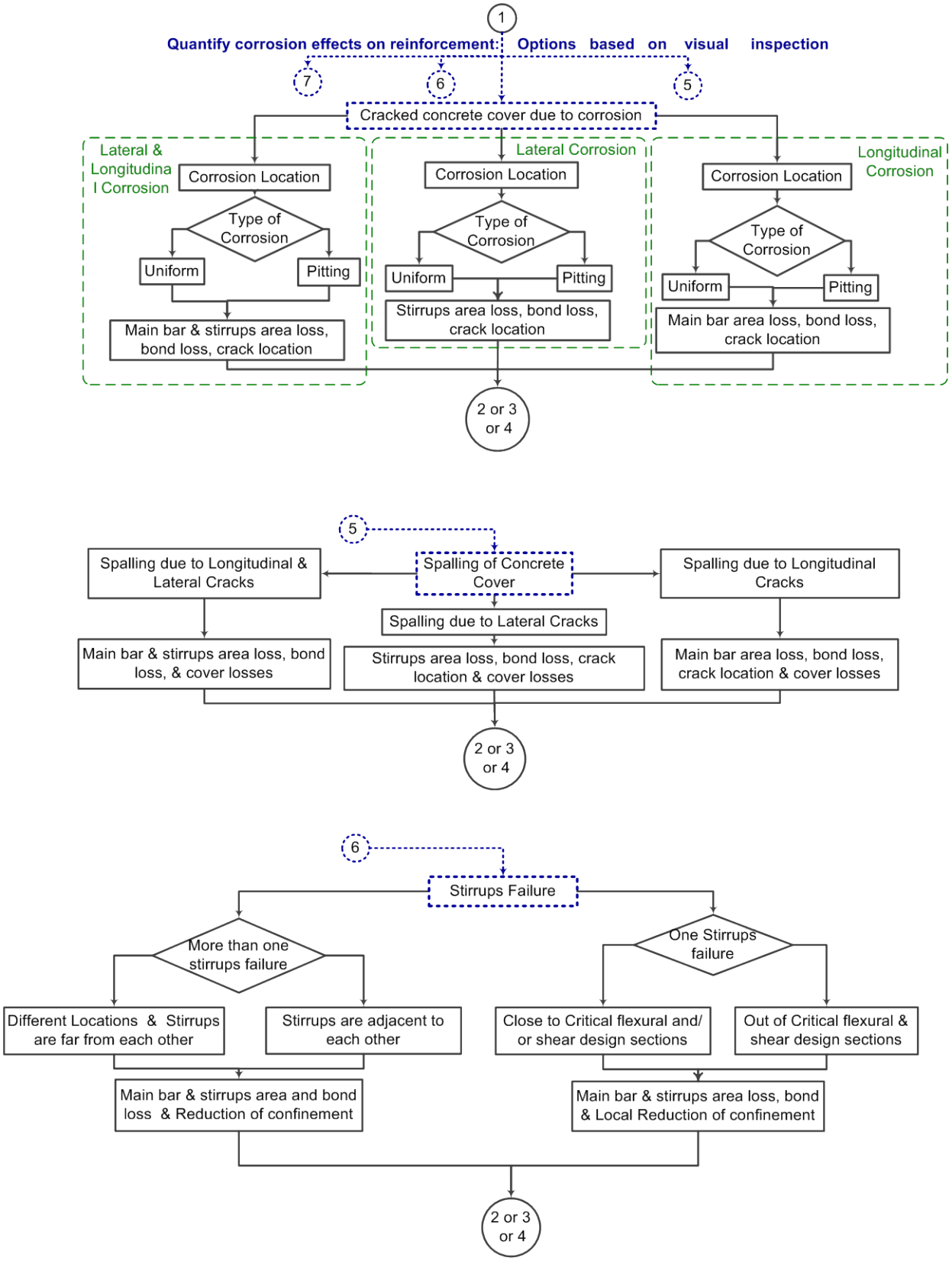

Figure 5.2: Evaluation of column performance under corrosion & seismic loads.

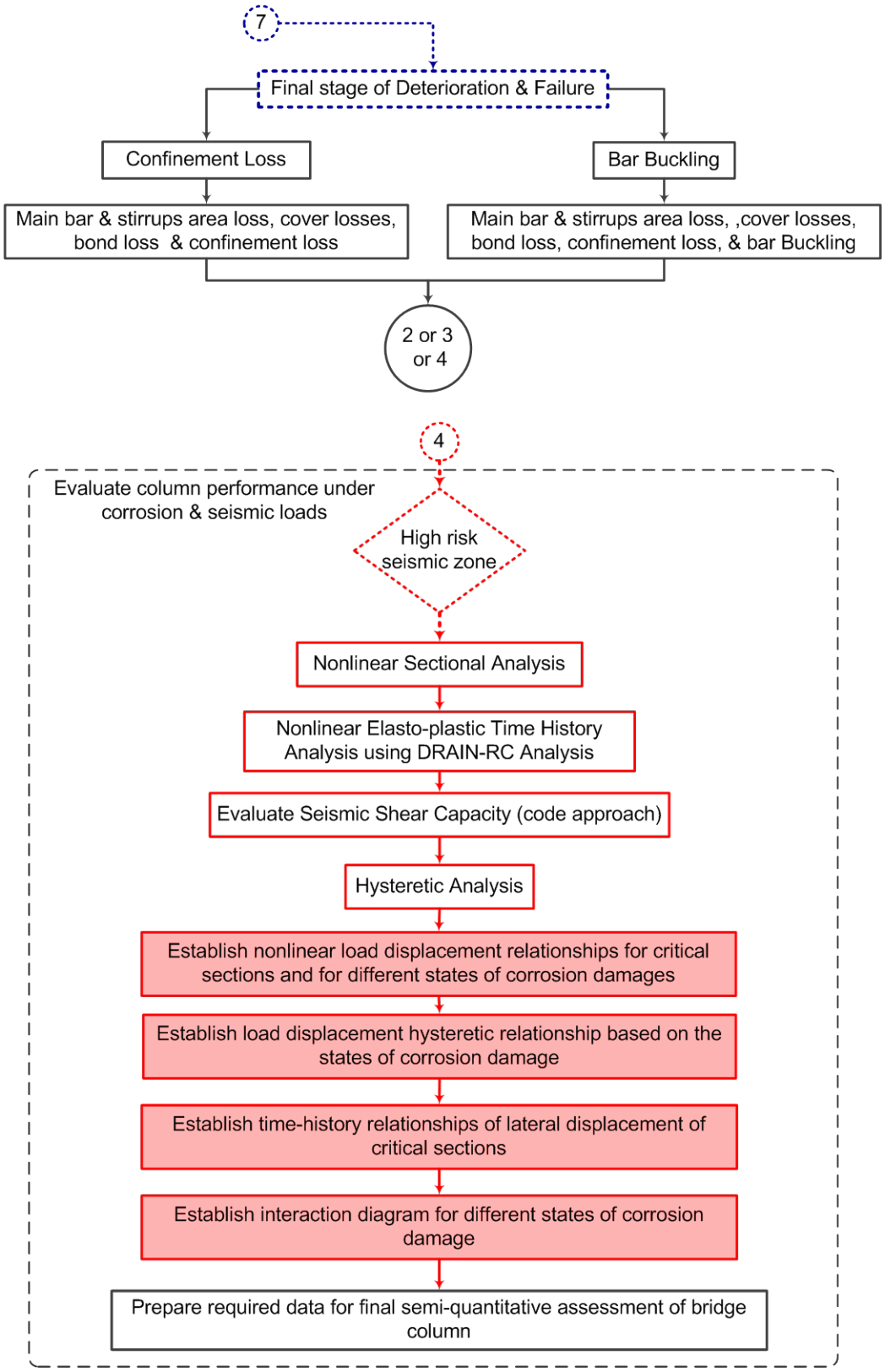

Figure 5.2 Cont'd.: Evaluation of column performance under corrosion & seismic loads.

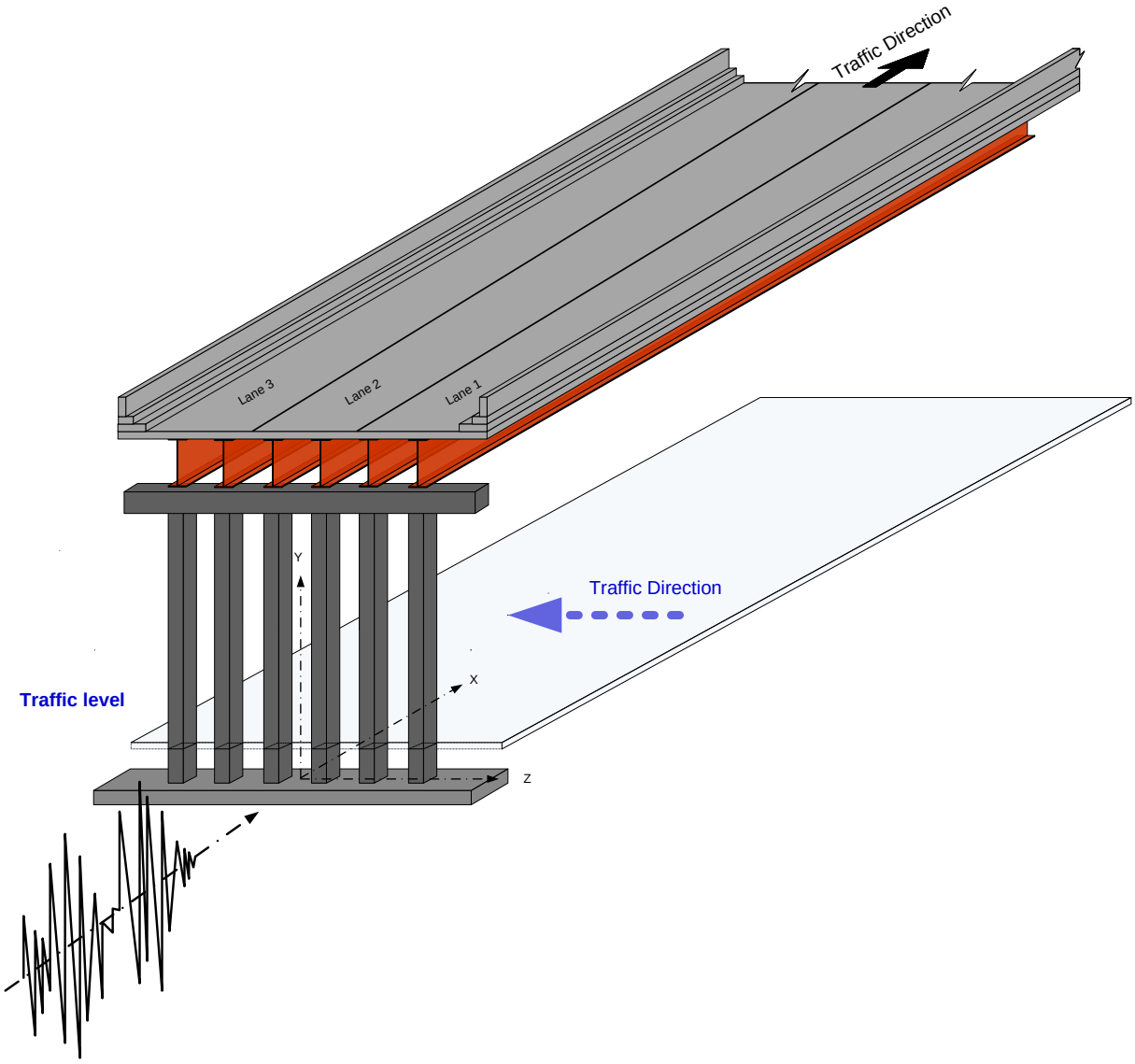

Figure 5.3: Slab-on-girder bridge with traffic configuration and under seismic load.

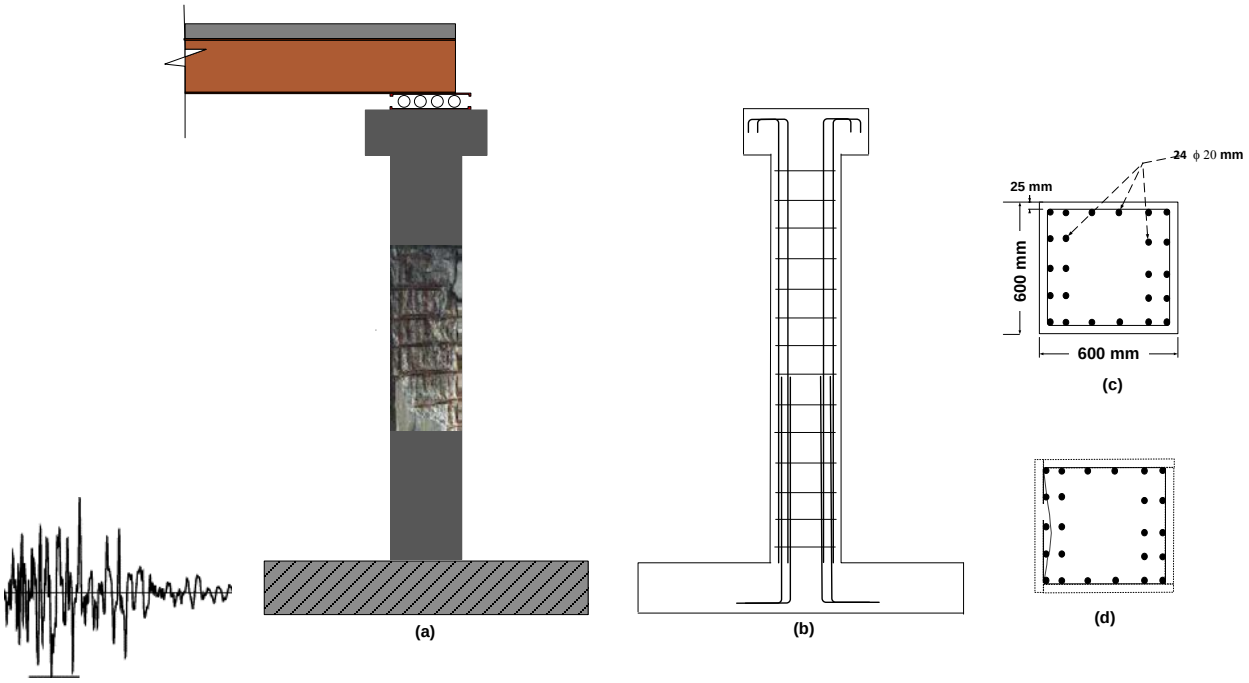

Figure 5.4: Most possible critical corrosion-damaged zone of slab on girder bridge column subjected to corrosion and seismic load, column design, and reinforcement details and damage due to corrosion in critical corrosion zone.

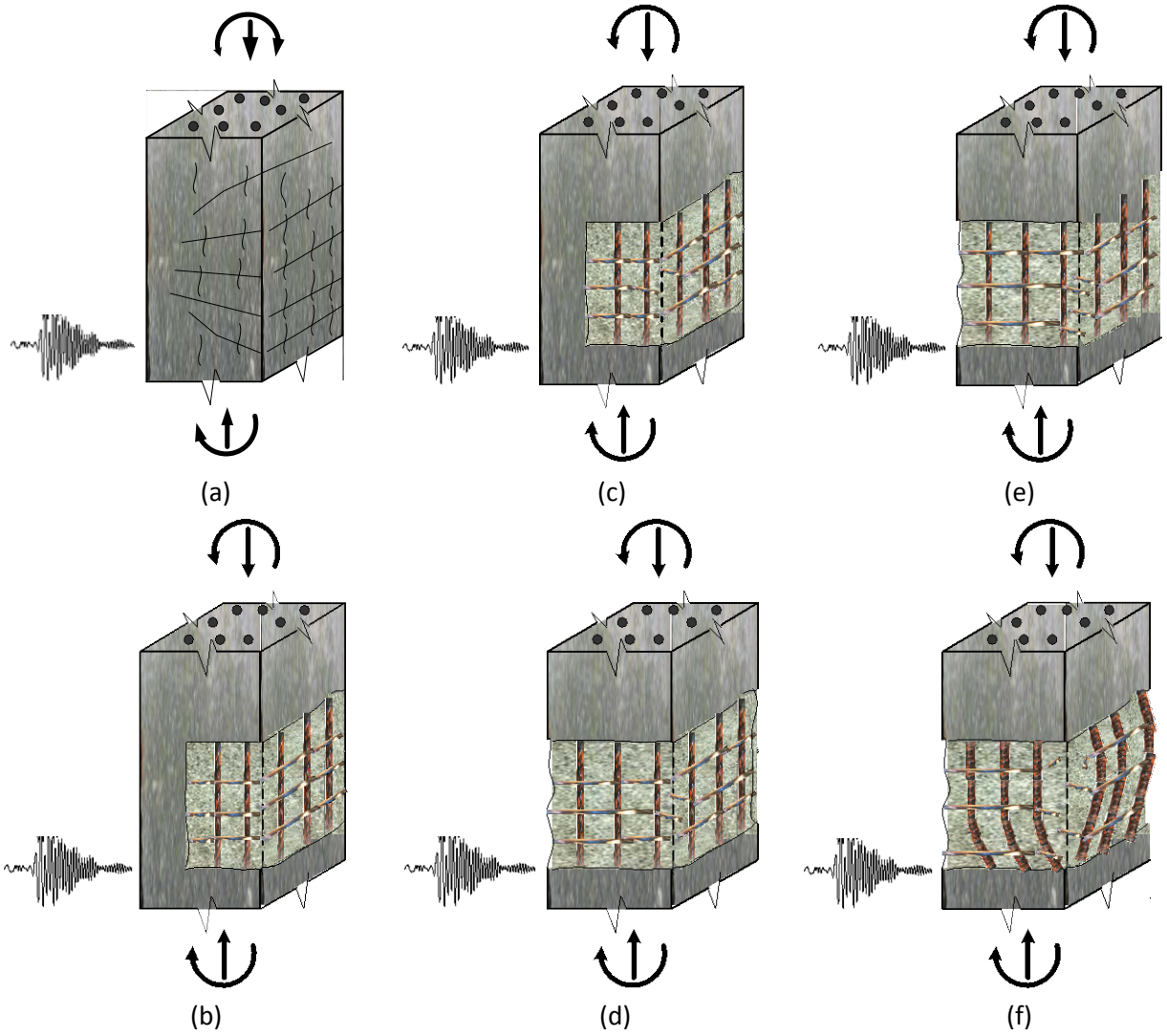

Figure 5.5: Possible damage and failure modes of RC columns due to combined gravity loads, seismic loads and reinforcement corrosion; (a) flexural and corrosion cracks; (b) initial spalling; (c) one stirrup failure; (d) spalling on all sides; (e) two stirrups failure; (f) loss of confinement and possible buckling.

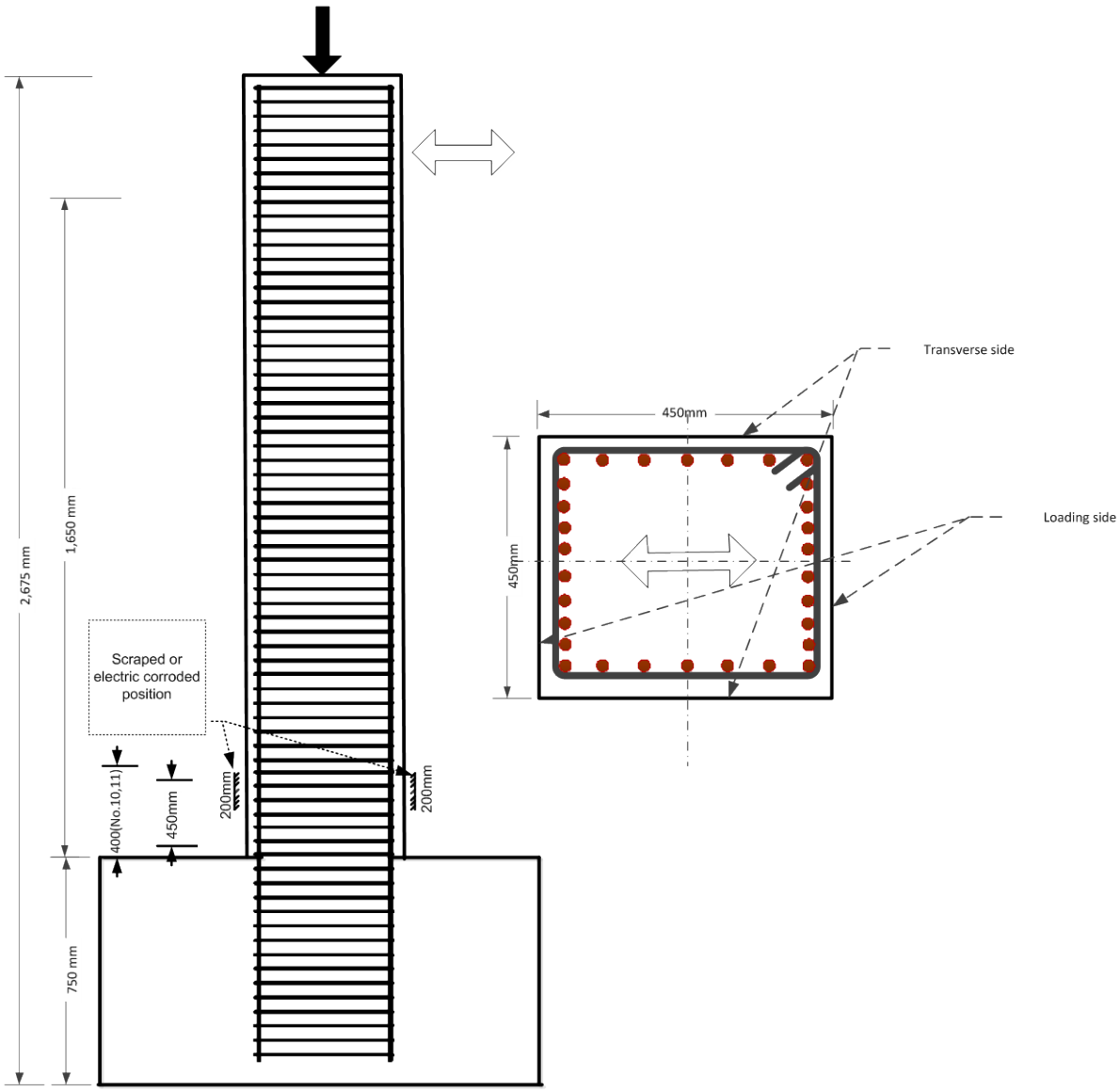

Figure 5.6: Case study verification: specimen details (Oyado et al. 2007).

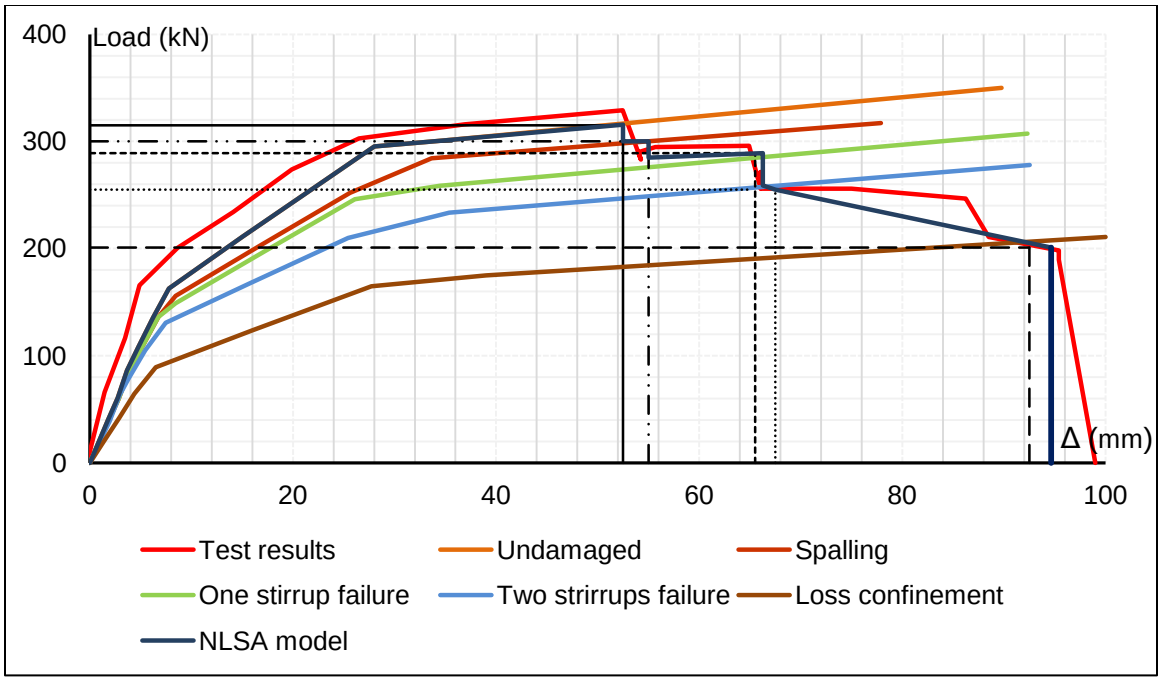

Figure 5.7: Envelope of load-displacement relationships for different damage levels using NLSA proposed by the authors (Mohammed et al. 2013a) versus test results (Oyado et al. 2007, specimen number 1).

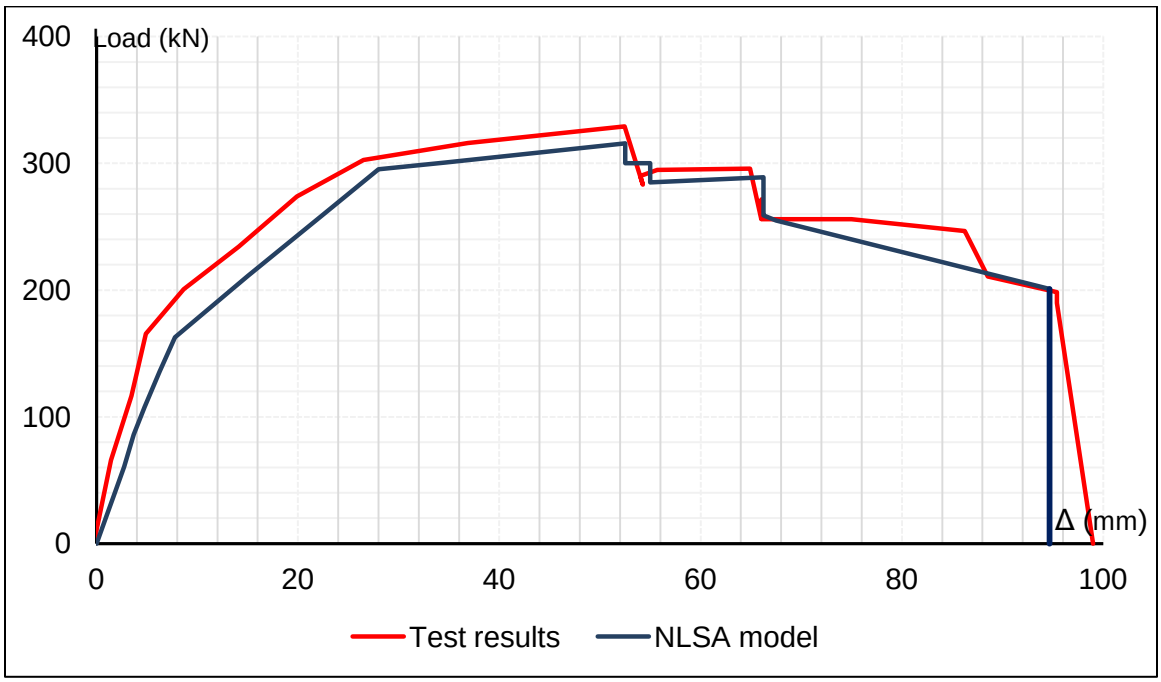

Figure 5.8: Load-displacement relationship of uncorroded specimen loaded up to failure (Oyado et al. 2007, specimen number 1) versus envelope of load-displacement relationships for different damage levels using NLSA.

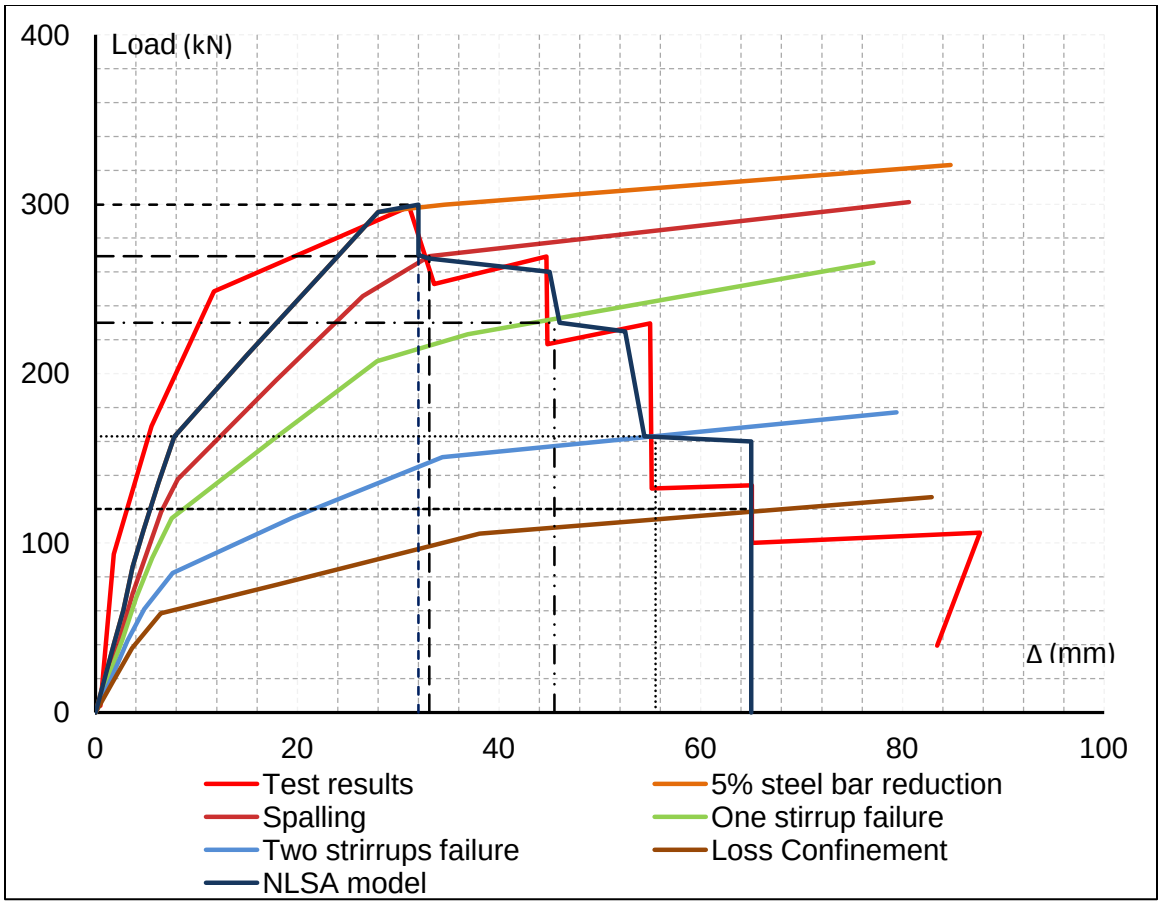

Figure 5.9: Envelope of load-displacement relationships for different damage levels using NLSA versus test results (Oyado et al.2007, specimen number 4).

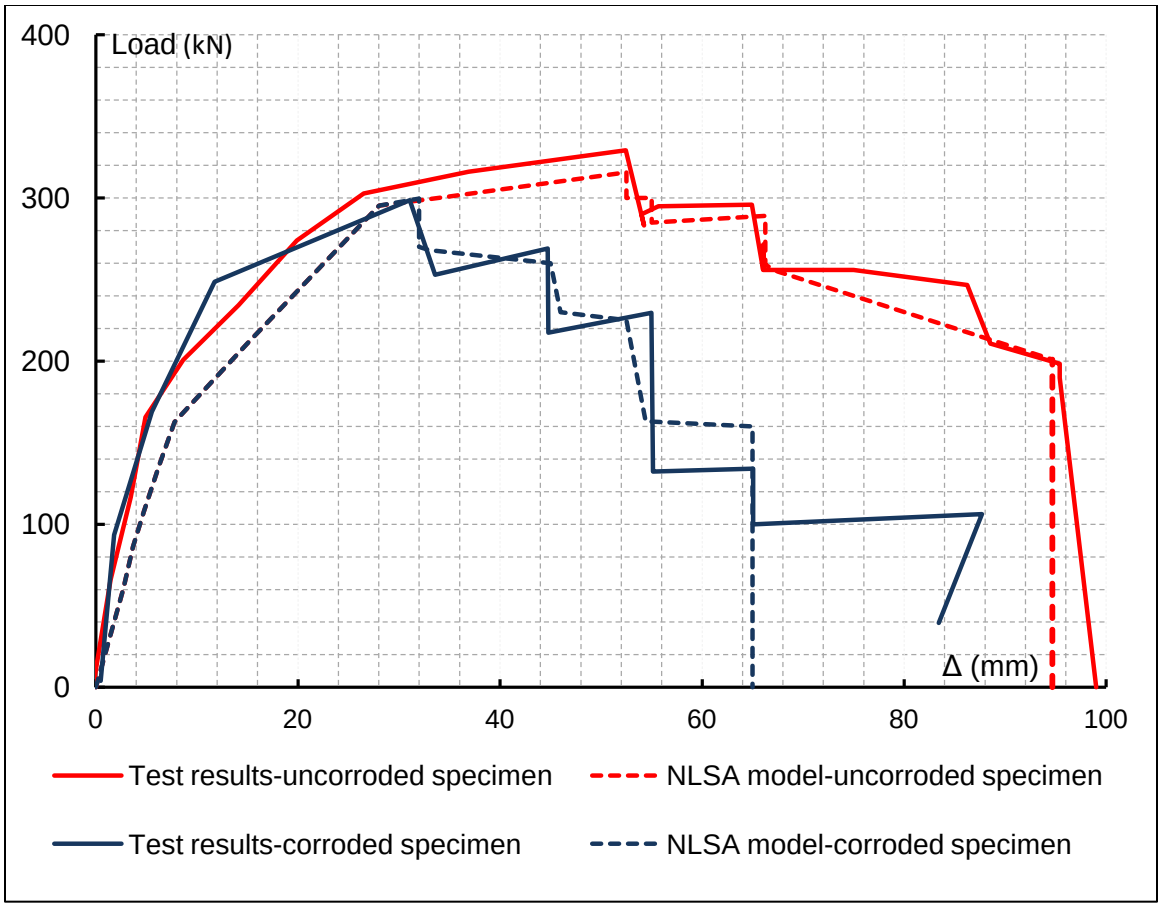

Figure 5.10: Envelope of load-displacement relationships using NLSA versus test results (Oyado et al. 2007) for uncorroded and corroded specimens.

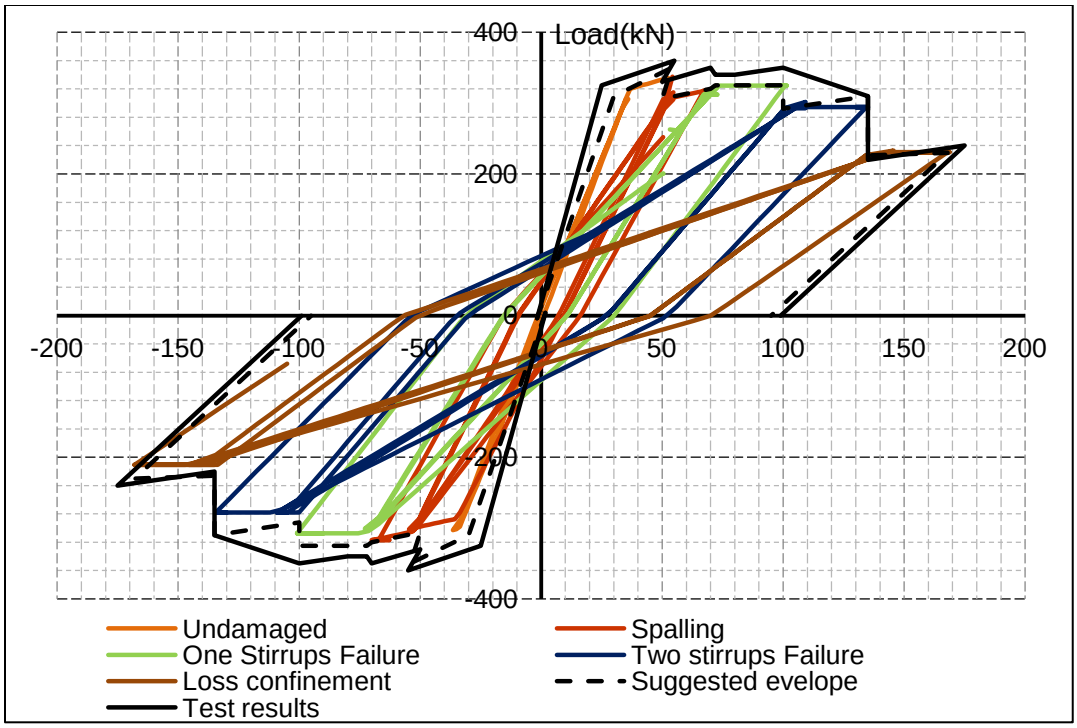

Figure 5.11: Envelopes of load-displacement hysteretic relationship of uncorroded specimen under cyclic load up to failure (Oyado et al. 2007; specimen number 1).

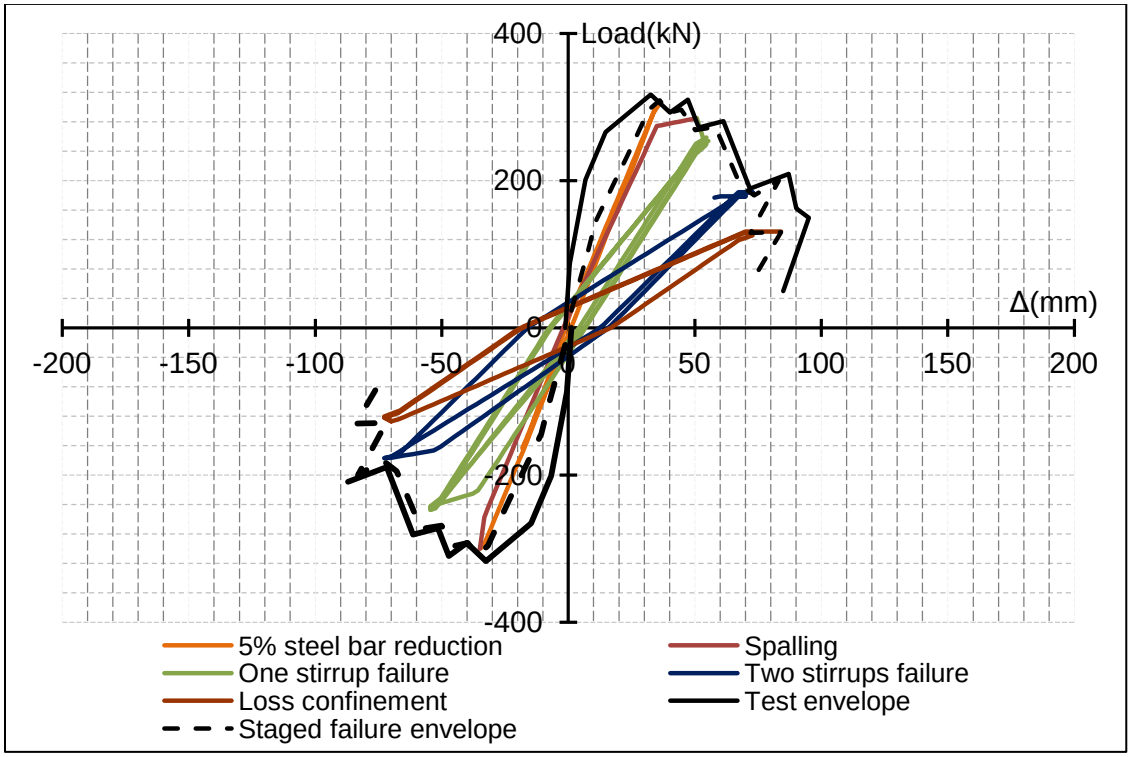

Figure 5.12: Envelopes of load-displacement hysteretic relationship of corroded specimen under cyclic load up to failure (Oyado et al. 2007; specimen number 4).

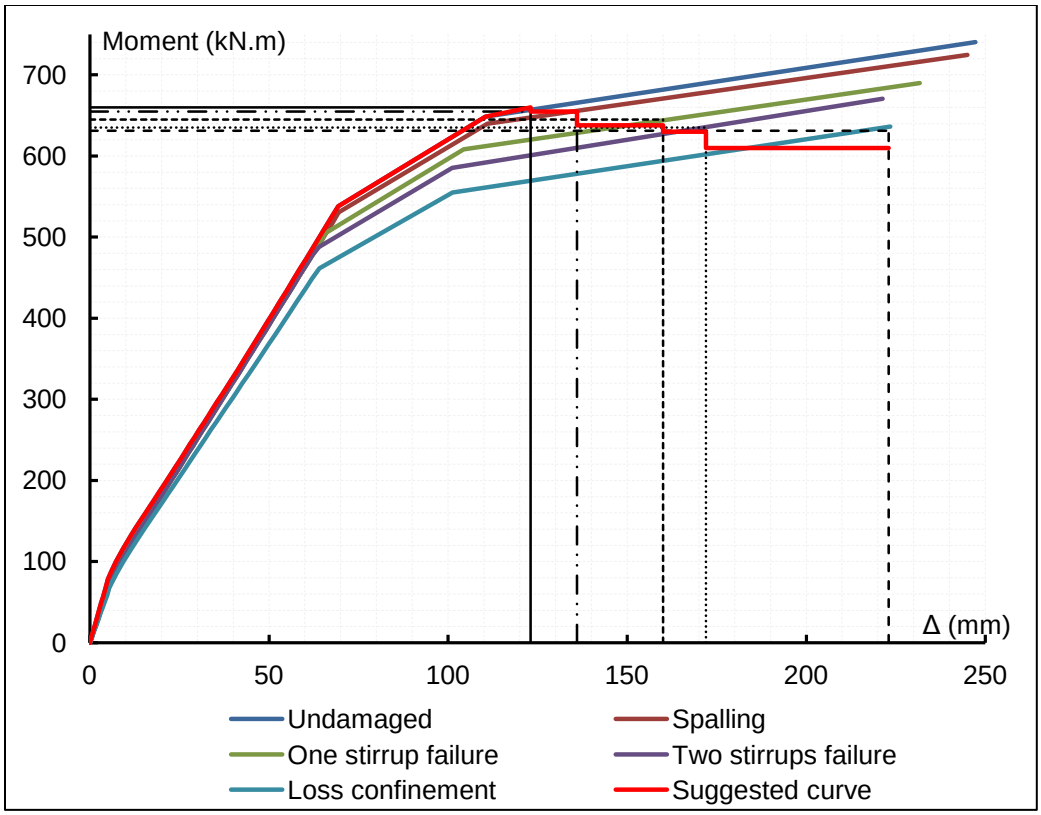

Figure 5.13: Envelope of load-displacement relationships of uncorroded column (LOCR = 40%) using NLSA.

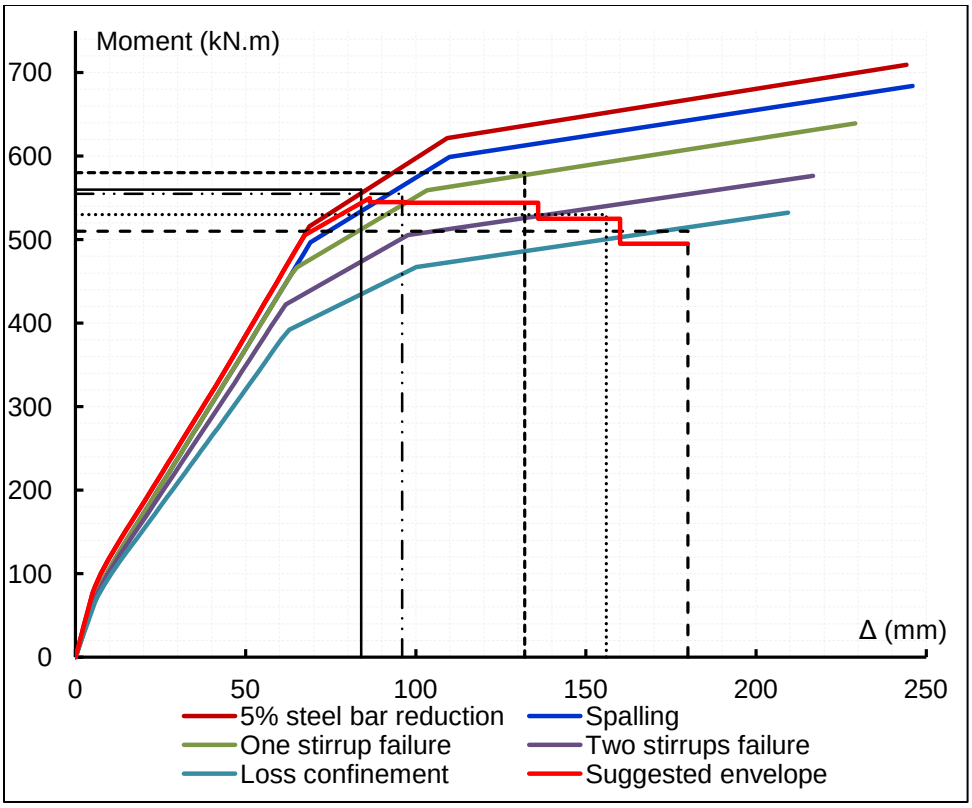

Figure 5.14: Envelope of load-displacement relationships of corroded column (LOCR = 40%) using NLSA.

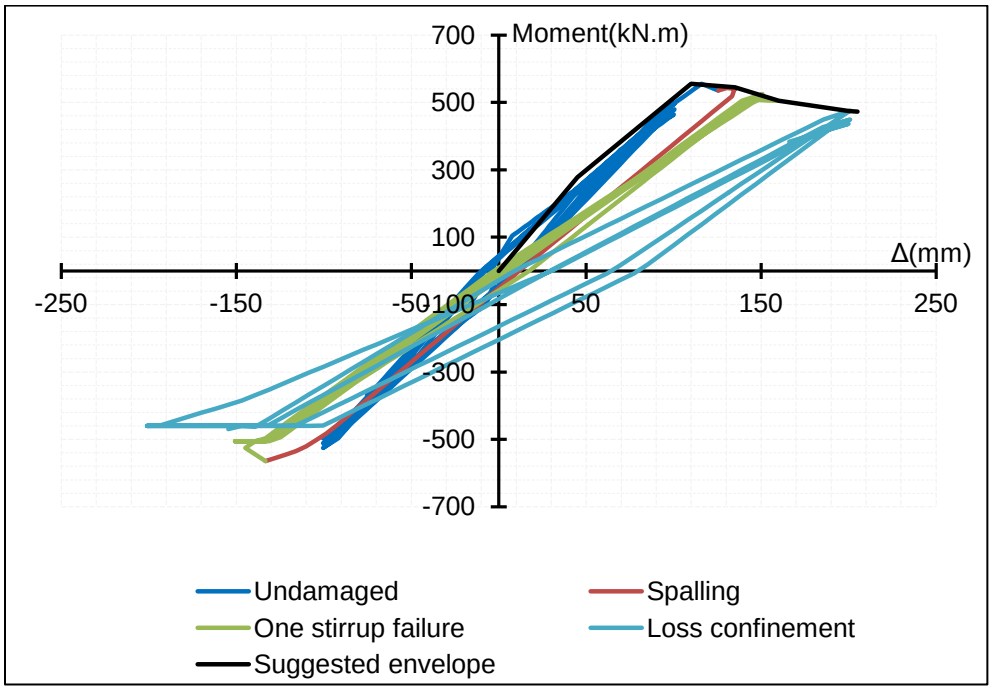

Figure 5.15: Envelope of load-displacement hysteretic relationship of uncorroded column (LOCR = 40%) under cyclic load up to failure.

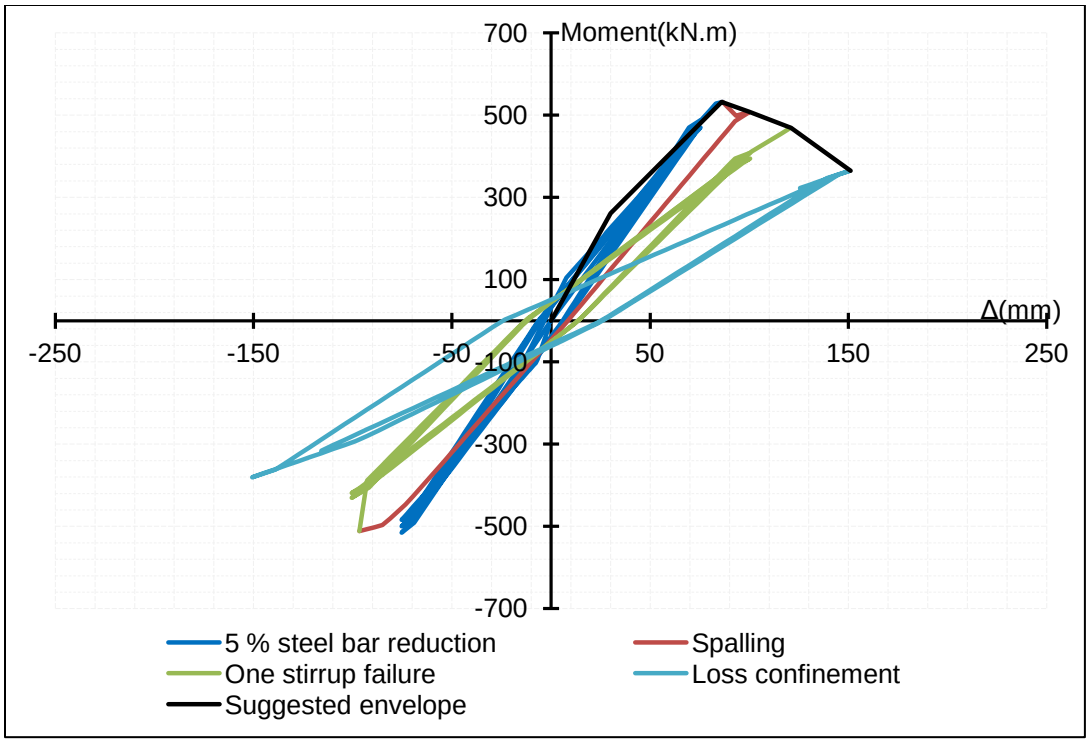

Figure 5.16: Envelope of load-displacement hysteretic relationship of corroded column (LOCR = 40%) under cyclic load up to failure.

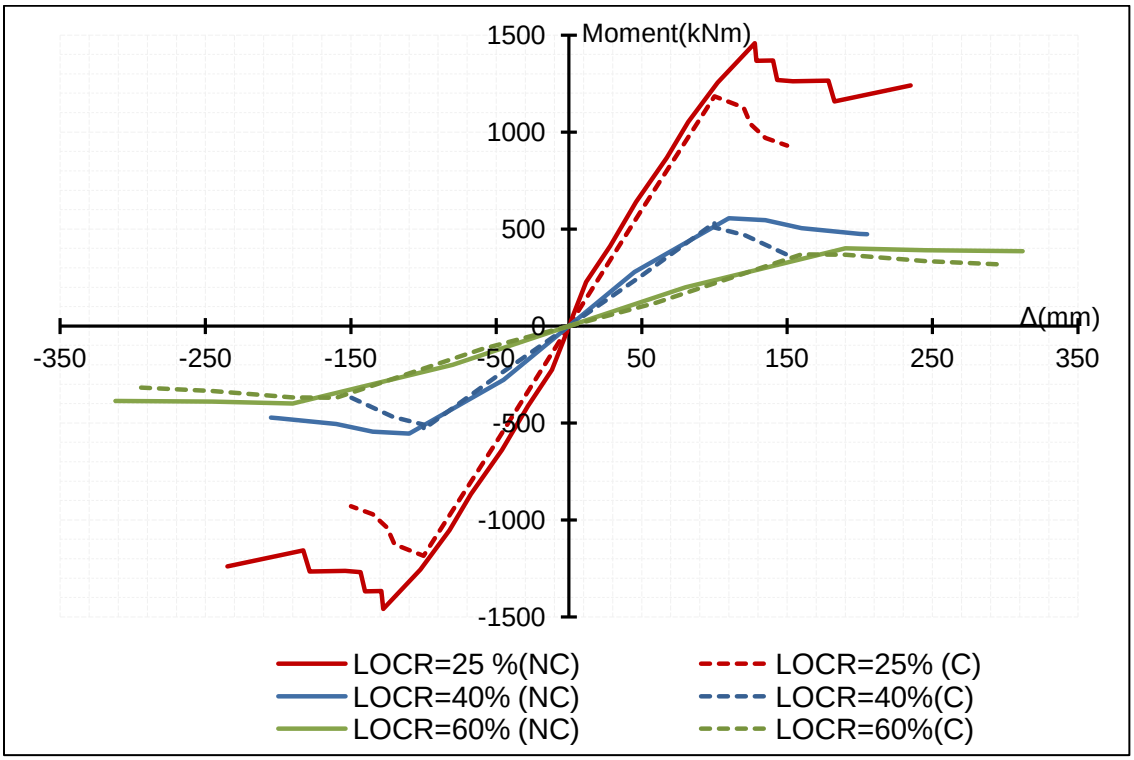

Figure 5.17: Envelope of load-displacement hysteretic relationship of corroded column (different LOCR percentages) under cyclic load up to failure.

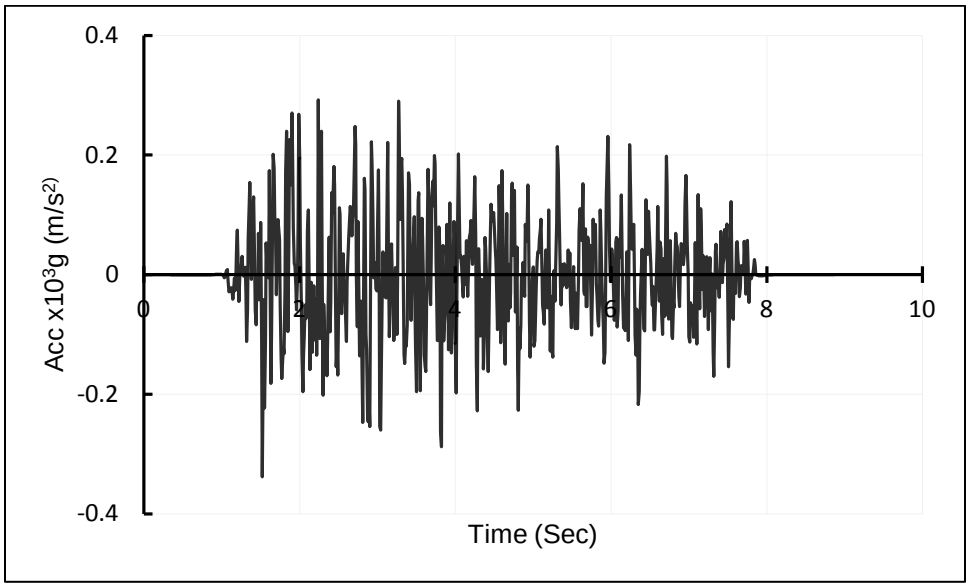

Figure 5.18: Artificial ground acceleration time histories used.

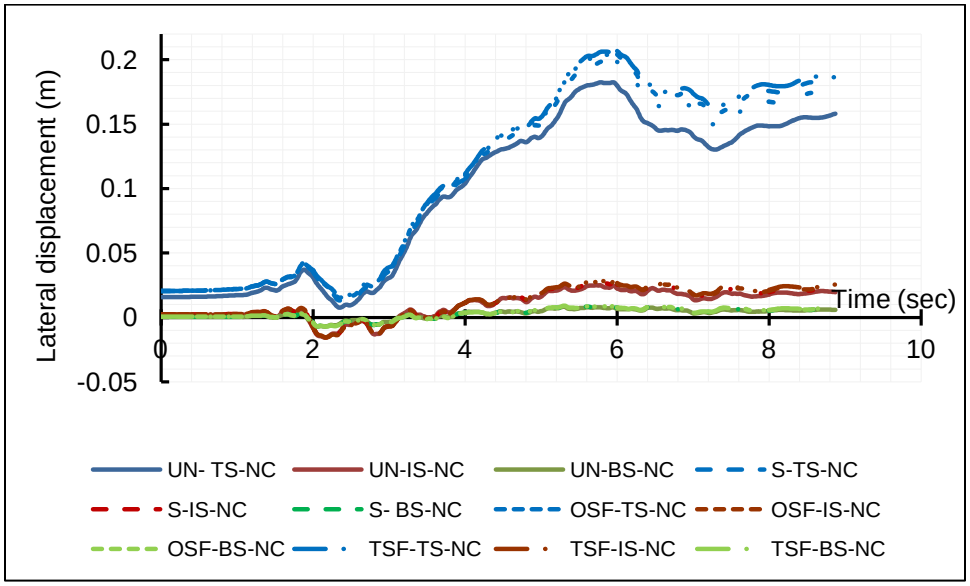

Figure 5.19: Time history of lateral displacement for different sections of un-corroded column with LOCR = 40%.

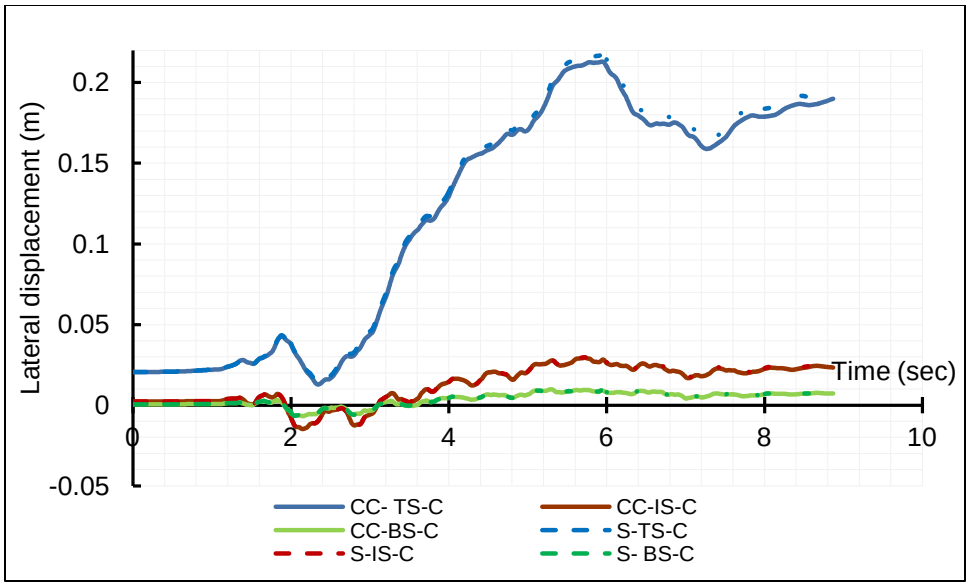

Figure 5.20: Time history of lateral displacement for different sections of corroded column with LOCR = 40%.

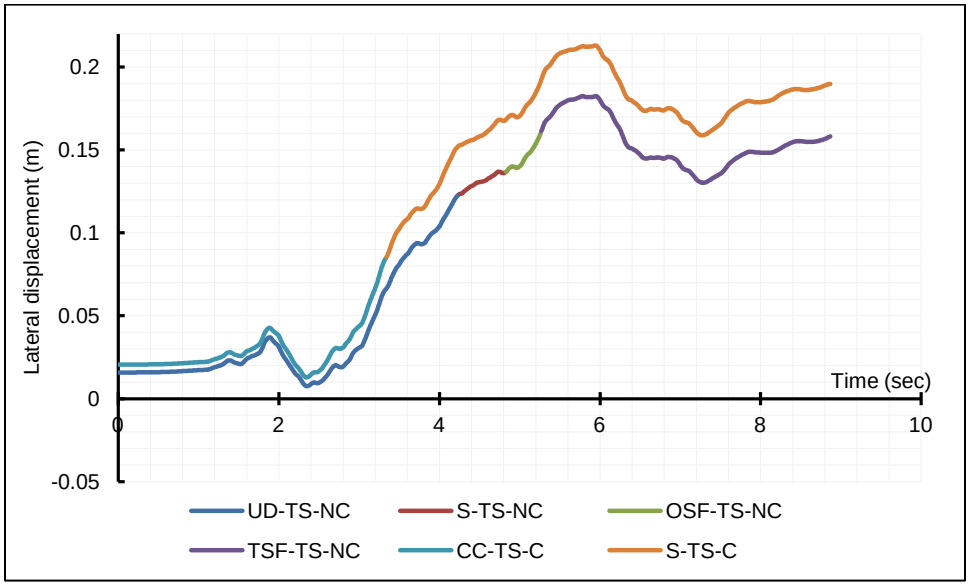

Figure 5.21: Time history of lateral displacement of top-section of un-corroded and corroded column with LOCR = 40%.

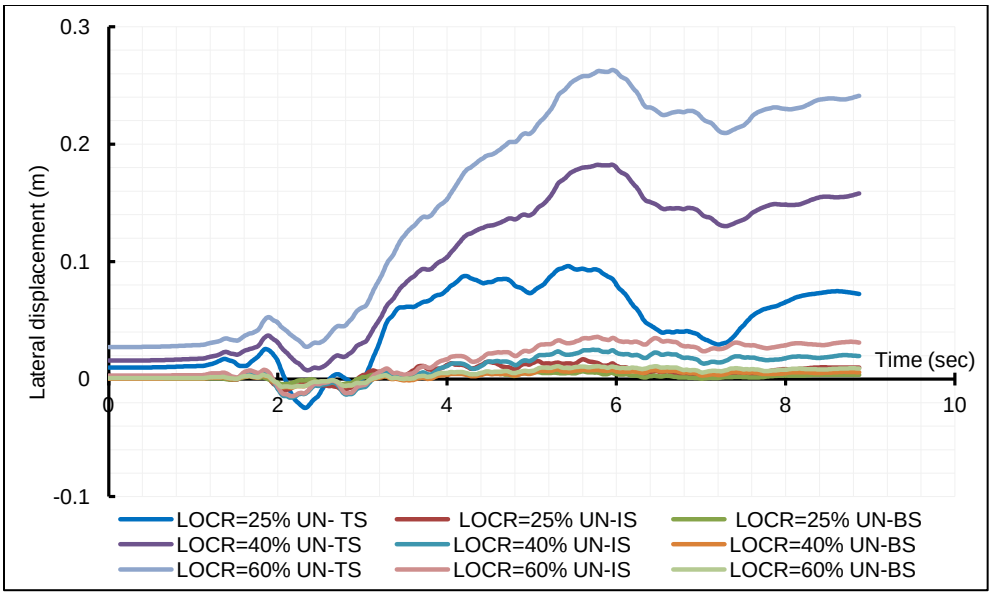

Figure 5.22: Time history of lateral displacement for different sections of uncorroded columns with different LOCR.

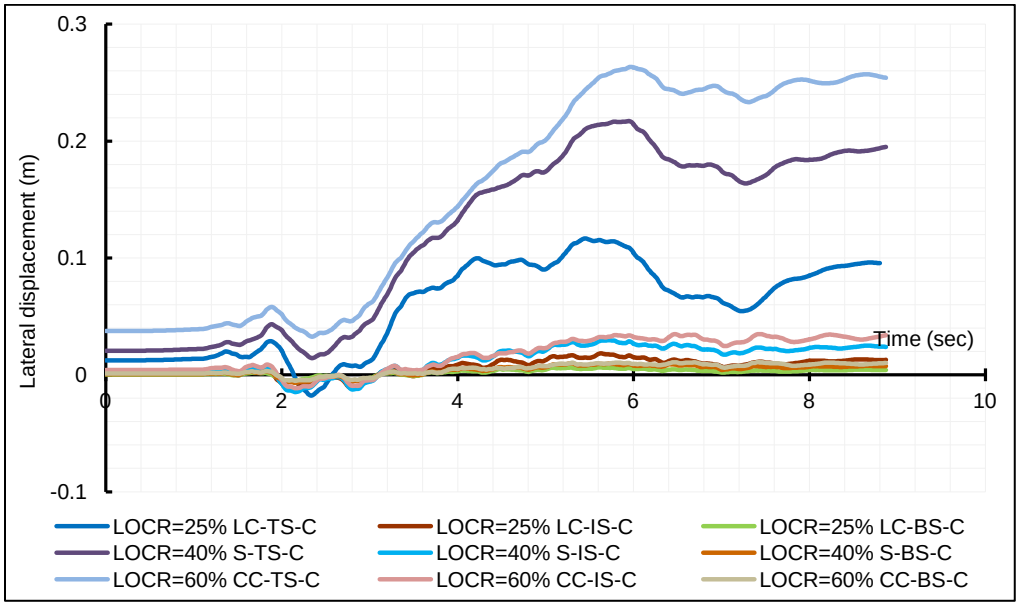

Figure 5.23: Time history of lateral displacement for different sections of corroded columns with different LOCR.

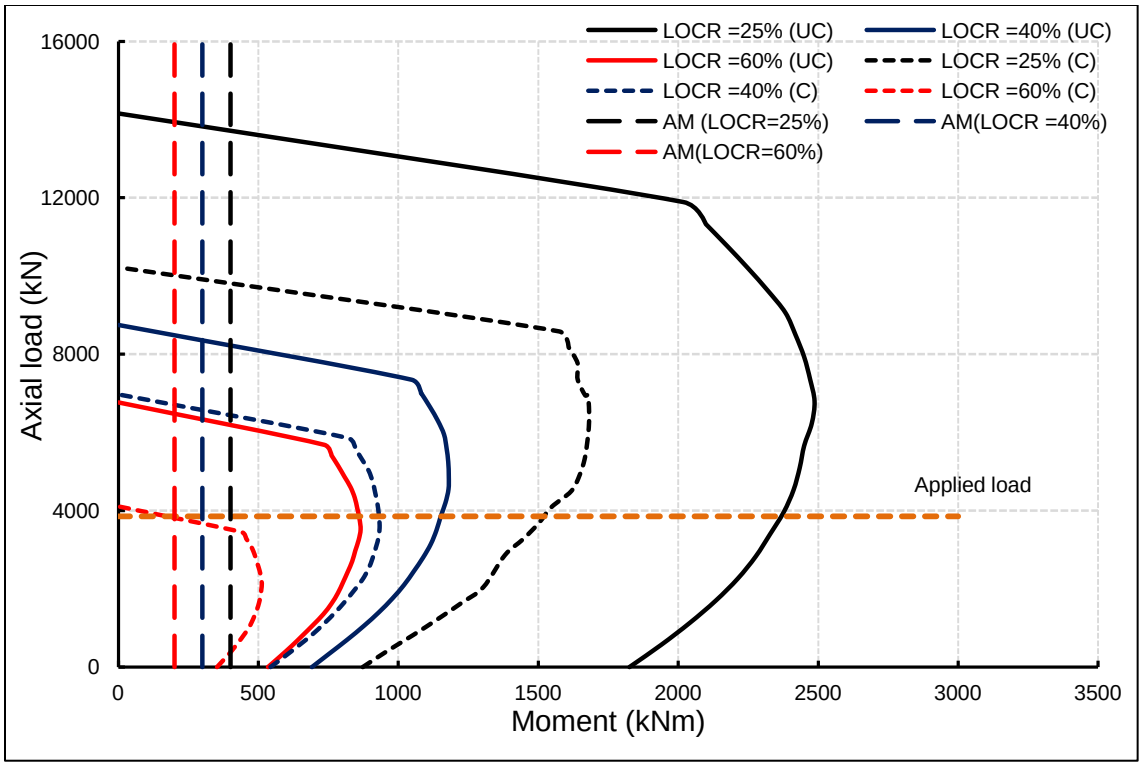

Figure 5.24: Interaction diagrams of uncorroded and corroded columns with different LOCR.

5.6 References

Alsiwati, J., Effect of anchorage slip and inelastic shear on seismic response of reinforced concrete frames. Ph.D. Thesis, Dept. of Civil Engineering, University of Ottawa, Ottawa, Canada; 1993, 367 pages.

American Association of State Highway and Transportation Officials, AASHTO LRFD Bridge Design Specifications SI Units (4th Edition); 2007.

Andersen, A., HETEK, Investigation of Chloride Penetration into Bridge Columns Exposed to De-Icing Salt. Copenhagen, Denmark; 1997.

Berto, L., Vitaliani, R., Saetta, A., and Simion, P., Seismic assessment of existing structures affected by degradation phenomena. Structural Safety; 2009, 31(4): 284-297.

Cairns, J., Plizzari, G., Du,Y., Law, D., Franzoni, C., Mechanical properties of corrosion reinforcement. ACI Materials Journal; 2005, 102(4): 256-264.

Canadian Standards Association, Canadian Highway Bridge Design Code, S6-06, A; 2006.

Cheng, F.Y., Matrix analysis of Structural Dynamics. Marcel Dekker, Inc., New York .Basel, 2001.

Choe, D.-F., Gardoni, P., Rosowsky, D., Haukaas, T., Probabilistic capacity models and seismic fragility estimates for RC columns subject to corrosion. Reliability Engineering and System Safety; 2008, 93(3): 383-393.

Federal Highway Administration, Reliability of visual inspection for highway bridges, volume I: final report, FHWA-RD-01-020; June, 2001.

Hevener, W., Simplified live-load moment distribution factors for simple span slab on I-girder bridges. MSc. Thesis, Dept. Civil and Environmental Engineering, University of West Virginia, Morgantown,West Virginia,USA;2003, 151pages.

Kanaan, A., E., and Powell, G. H. Drain-2D User's Manual, Earthquake Engineering Research Center, Report No. EERC 73-22, University of California, Berkeley, USA; 1973.

Lay, S. and Schiebl, P., Life cycle management of concrete infrastructures for improved sustainability. European Community Fifth Framework Program: GROWTH; 2003.

Mohammed, A., Almansour, H., Martín-Pérez, B., Combined effect of reinforcement corrosion and seismic loads on RC bridge columns: modelling. CSCE 2nd International Engineering Mechanical and Materials Specialty Conference, Ottawa, Ontario, Canada; 2011, June 14 to 17.

Mohammed, A., Almansour, H., Simplified non-linear FE model to predict staged capacity deterioration of RC columns subjected to combined ultimate or seismic and reinforcement

corrosion loads. CSCE 3rd Specialty Conference on Material Engineering and Applied Mechanics, Montréal, Québec, Canada; 2013, May 29 to June1.

Mohammed, A., Almansour, H., Martín-Pérez, B., Nonlinear flexural analysis of reinforced concrete beam-column subjected to ultimate gravity loads combined with reinforcement corrosion, Part I: Sectional Analysis. Structure and Infrastructure Engineering, submitted, ID NSIE-2013-0261; 2013a.

Mohammed, A., Almansour, H., Martín-Pérez, B., Nonlinear flexural analysis of reinforced concrete beam-column subjected to ultimate gravity loads combined with reinforcement corrosion, Part II: finite element analysis. Structure and Infrastructure Engineering, submitted, ID NSIE-2013-0262; 2013b.

Mohammed, A., Almansour, H., Martín-Pérez, B., Evaluation of dynamic of slab-on-girder-bridge under moving trucks with corrosion-damaged columns", Engineering Structures, (6), 159-172;2014c.

Mohammed, A., Almansour, H., Martín-Pérez, B., Evaluation of seismic performance of slab-on-girder bridge columns subjected to reinforcement corrosion damages. Journal of Bridge Engineering (ASCE); to be submitted 2013d.

Mohammed, A., Almansour, H., Martín-Pérez, B., Semi-quantitative assessment framework for aging RC bridge columns. Engineering Failure Analysis; to be submitted 2013e.

Rodríguez, J., Ortega, L. M. and Casal, J. Load bearing capacity of concrete columns with corroded reinforcement. Corrosion of Reinforcement in Concrete Construction, Royal Society of Chemistry; 1996, 220-230.

Saatcioglu, M. and Razvi, S., Strength and ductility confined concrete. Journal of Structural Engineering; 1992, 1590-1607.

Saito, Y., Oyado, M., Kanakubo, T. and Yamamoto, Y. Structural performance of corroded RC column under uniaxial compression load. First International Workshop on Performance, Protection & Strengthening of Structures under Extreme Loading, Whistler, Canada; 2007.

Shooshtari, A. Seismic drift demands of reinforced concrete building. Ph.D. Thesis, Dept. of Civil Engineering, University of Ottawa, Ottawa, Canada; 1998, 285 pages.

Oyado, M., Saito, Y., Yasojima, A., and Kanakubo, T. Structural performance of corroded RC column under seismic Load. First International Workshop on Performance, Protection & Strengthening of Structures under Extreme Loading, Whistler, Canada; 2007.

Chapter 6

A Semi-Quantitative Assessment Framework for Aging Reinforced Concrete Bridge Columns

6.1 Introduction

Among more than seven hundred thousand bridges in North America, a large percentage is reported deficient and in urgent need for rehabilitation or replacement (Lounis et al. 2010). The increase in the traffic intensity and truck loads in the past four decades and the decline of the resources available for rehabilitation or replacement have accelerated the deterioration and deficiency of these bridges (Lounis et al. 2010). Due to the substantial role of the bridges in transportation networks and the limited funding available for bridge management, remediation strategies have to be prioritised. A conservative bridge assessment will result in unnecessary actions, such as expensive bridge strengthening. On the other hand, any bridge maintenance negligence and delayed actions may lead to extensive future costs or irrevocable degradation of bridge elements. The accuracy of bridge rating and management decisions of bridge engineers relies on the accuracy of the bridge condition assessment (Rashidi 2012), which is mainly based on different levels of visual inspection. Different bridge management systems recognise many types of visual inspection such as the typical visual inspection (VI), in-depth VI; enhanced in-depth VI (or enhanced inspection, as referred in this chapter) (see FHWA-RD-01-020, 2001; MTO- OSIM, 2008; and AASHTO- MCEB, 1994). Bridge rating systems are usually based on a very subjective procedure and are associated with uncertainty and personal prejudice (Rashidi 2012). The lack of a practically simple and cost effective quantitative assessment approach that is capable to accurately determine the state of the performance in terms of safety and serviceability of critical bridge elements is now identified as a major research gap.

Visual inspection is probably the most important of all non-destructive tests. It can often provide valuable information to the well trained eye. Visual features may be related to workmanship, structural serviceability, and material deterioration. It is particularly important that the inspector or the evaluating engineer is able to differentiate between various signs of distress which may be encountered. These include for instance, cracks, pop-outs, spalling, disintegration, colour change, weathering, staining, surface blemishes and lack of uniformity. Extensive information can be gathered from visual inspection to give a preliminary indication of the condition of the structure and allow formulation of a subsequent in-depth inspection and testing programme (International Atomic Energy 2002).

Historically, the inspections were usually done as a consequence of warnings received from sources very often outside the bridge network system, or as a result of an obvious inadequacy of the bridge that did not allow it to fulfill the expected function (Branco and Brito 2004). In the past five decades, the Visual Inspection (VI) method has become the predominant non-destructive evaluation (NDE) technique used for bridge inspections and serves as the baseline with which many other NDE techniques may be compared. Since implementation of the National Bridge Inspection Standards (NBIS) of the US in 1971 and the OSIM of Ontario in 1985, which define the frequency with which each bridge must be inspected and prescribe minimum qualifications for inspectors, a complete study of the reliability of VI as it relates to bridge inspections has not been undertaken until recently (FHWA-RD-01-020, 2001and MTO- OSIM, 2008). It is worthy to mention here that the bridge management systems (BMS) in North America and many other countries around the world are based on identification of four general condition states where the bridge elements are categorized under. The four condition states are

(i) Excellent, (ii) Good; (iii) Fair; and (iv) Poor (see MTO- OSIM, 2008 and AASHTO- MCEB, 1994).

FHWA study on the reliability of VI concluded that the National Bridge Inspection Standards Condition Rating system definitions may not be refined enough to allow for reliable routine visual inspection (RI) results. It also stated that with the exception of some bridge management software, Condition Rating values are generally not assigned through the use of a rational approach. This general conclusion is based on the inconsistencies found in the collected data on the Condition Rating during the mentioned FHWA study (FHWA-RD-01-020, 2001). Consequently, the arbitrary nature of data collected from the routine visual inspection and its dependency on the personal training and experience of inspectors result in high uncertainty in the existing qualitative assessment approaches and hence the efficiency of the BMS. Therefore, it is clear that the accuracy of the condition assessment relies heavily on the quality of the inspection, and if quantitative assessment tools are integrated with the existing inspection, a significant improvement of the BMS could be achieved.

The comparison of bridge inspection standards between various international organisations indicates that each organisation has a different approach to bridge inspection in terms of the types of inspection, the frequency of the inspections, the definition of the various inspection types and the type of personnel that undertake the inspections (Brown et al. 2010). Among cost-effective counteractive approaches are extensive inspectors' training, the consistent use of enhanced inspection (FHWA-RD-01-020, 2001), and if possible, the preparation of visual catalogues correlating the damage/deterioration to the structural performance (e.g., California Department of Transportation, CDT 2006). For example, according to MTO-OSIM (2008), the "Enhanced OSIM inspection" should typically be done for structures that are over 30 years old

with critical components in “Poor” condition. However, it is not expected that the mentioned improvement approaches will always lead to accurate evaluations of the bridge elements state without the use of comprehensive structural analysis approaches based on accurate damage measurements and material tests results.

Lounis et al. (2010) presented a comprehensive critical review of the state of the art in the area of performance assessment and management of bridge infrastructure. The authors indicated that there are several condition rating scales that are not easily comparable. They also addressed the need for more quantitative or improved qualitative deterioration approaches that can forecast the deterioration of bridges under the effects of changing climate loads. Furthermore, they indicated the need for more mechanistic or quantitative condition assessment that can predict the serviceability and strength of bridges under changing traffic loading and maintenance conditions. The report highlighted the research gap and identified the strong need for the development of accurate quantitative assessment/evaluation tools that would save many potential fatalities (due to the collapse of aging bridges) and reduce the management cost for Canada's aging infrastructure.

Reinforcement corrosion has been identified as the major cause of RC infrastructure deficiency (deterioration/damage). However, the initiation and progression of corrosion in reinforcing steel can have unlimited number of scenarios that are yet not fully understood or modeled. It is very challenging to develop practical time-dependent analytical models that are capable to accurately estimate the effects of different reinforcement corrosion scenarios on the structural behavior of damaged RC elements. Instead, detailed measurements of the damaged zones together with any required material testing can be performed during the enhanced inspection of aged bridge elements, which usually follows the routine visual inspection in most international BMS (see

FHWA-RD-01-020, 2001; MTO- OSIM, 2008; and AASHTO MCEB, 1994). The results of the enhanced inspection can be used in the semi-quantitative assessment framework (SQAF) proposed in this chapter, which presents an intermediate step towards the development of a quantitative assessment framework (QAF). The proposed SQAF addresses the three major evaluation limit states of corrosion-damaged bridge elements that are consistent with existing bridge design codes: ultimate limit state (ULS), serviceability limit state (SLS), and earthquake limit state (ELS) (CHBDC 2006/ CAN/CSA-S6-06, or AASHTO-LRFD, 2007). All the three limit states are based on simplified non-linear static and dynamic finite element analysis approaches presented in the previous chapters, where the combined effects of mechanical loads and measured corrosion damage on structural performance are quantitatively evaluated.

The objective of this chapter is to present the semi-quantitative assessment framework (SQAF) of aged and damaged bridge columns based on enhanced inspection, any required material testing and simplified static and dynamic nonlinear analysis approaches of the three major evaluation limit states developed in the previous chapters (see Mohammed et al. 2013b,c &d). The focus is on the structural behavior of aged slab-on-girder bridge columns (or beam-columns) because: (i) slab-on-girder bridges are the most common types of bridges in North America; (ii) the columns are the most critical elements for the stability and robustness of the slab-on-girder bridges; and, (iii) beam-column elements are the most general frame elements that simulate the behavior of beams, columns, or beam-columns, and hence they can be adopted in modeling buildings as well (e.g., parking garages).

6.2 Proposed Semi-Quantitative Assessment Framework

Figure 6.1 shows the flowchart of the proposed semi-quantitative assessment framework (SQAF). The proposed SQAF aims at improving the enhanced inspection through simplified

tools that can quantitatively identify the state of structural performance. The framework involves six major steps: (I) data input; (II) quantification of reinforcement corrosion and its effects; (III) evaluation of columns performance under combined corrosion and ultimate loads (evaluation ultimate limit state: E-ULS); (IV) evaluation of columns performance under combined corrosion and traffic loads (evaluation serviceability limit state: E-SLS); (V) evaluation of columns performance under corrosion and seismic loads, which is only applicable in high-risk seismic zones (evaluation earthquake limit state E-ELS); and, (VI) the semi-quantitative assessment and reporting. Following is brief description of each of the first five steps, while the sixth step is discussed in more detail in the following sections.

6.2.1 Data input:

The first part of the proposed SQAF includes three data-input tasks: (I-a) the structural material and geometrical data including boundary conditions; (I-b) the loading data; and, (I-c) the damage measurements and deteriorated material properties through an enhanced inspection and the related material tests as required, to prepare the input data for the properties of the corroded reinforcement. In task I-a, the data is collected from the original design information/sketches (if available), and the field tests on the materials (if required). The difference between the original design loads and the present loads on the bridge column under consideration is to be determined.

In task I-c, the enhanced in-depth visual inspection (or enhanced inspection) is used in the proposed semi-quantitative assessment framework to provide detailed field measurements on the dimensions of the damaged concrete zone, the volume of concrete spalling of the corrosion-affected zone (FHWA-RD-01-020, 2001). Determining the state of corrosion damage of the rebars and their mechanical properties that are used in the model is more complicated. In this study, a hybrid approach to find the steel rebars properties is suggested. Out of all the columns of

the bridge pier under assessment, the most damaged one is selected, and the damage status and size and the material properties can be generalized over the other columns of the pier for a conservative assessment of the substructure. The most damaged rebars are then identified, and samples of suitable size and number are collected. In the lab tests of the steel rebars, a precise measurement of the maximum reduction of rebar diameter or the reduction in the reinforcing steel thickness is found for each sample (ASTM G1-03, 2011). Assuming a constant rate of corrosion, the corrosion current density and the time elapsed to generate the measured reduction in the reinforcing steel thickness are then found using the data of different samples and the equations shown in Chapter 2 based on Faraday's law (see Mohammed et al.2013a). Using the evaluated reinforcement corrosion parameters and empirical formulae given by Eqs. (2.4, 2.5 and 2.6)(for example, see Lay and Schiebl 2003 and Cairns et al. 2005), the loss of strength and ductility of the reinforcement subjected to corrosion attack can be estimated. On the other hand, the strength and ductility of the reinforcement can be evaluated by tensile tests if the corroded rebar samples are available in suitable length.

6.2.2 Quantification of reinforcement corrosion and its effects

The proposed SQAF identifies four major damage cases due to reinforcement corrosion, as shown in details in chapters 3, 4 and 5 (Mohammed et al.2013b,c &d), which are: (a) flexural cracking of concrete due to reduction of reinforcement bars and their ductility; (b) spalling of concrete cover; (c) failure of one or more stirrups; and, (d) more advanced state of corrosion damage, which may lead to the structural failure or collapse of the column through complete loss of the confinement or rebar buckling.

6.2.3 Evaluation ultimate limit state: E-ULS

The ULS is interactively integrated with step (II) of the semi-quantitative assessment framework, where at each major damage case due to reinforcement corrosion, the nonlinear finite element analysis NLFEA can quantify the ultimate residual capacity, ductility, and the load-deformation or moment-curvature relationships of the column (see Chapter 3; Mohammed et al.2013b). The evaluation of the deterioration of the load capacity compared to the initial undamaged state and the evaluation of the deterioration of the structural ductility are quantitatively assessed.

6.2.4 Evaluation serviceability limit state: E-SLS

The SLS is assessed using the simplified hybrid linear/nonlinear dynamic finite element analysis (SHDFEA) presented in Chapter 4 (Mohammed et al.2013c). The program is capable to evaluate the dynamic characteristics and the behaviour of the slab-on-girder bridges (both the superstructure and the substructure elements) under moving trucks when the columns are subjected to different levels of corrosion damage. The SHDFEA uses the NLFEA (developed in Chapter 3; Mohammed et al.2013b) to evaluate the damaged columns stiffness, mass and damping through a step-by-step time history analysis.

6.2.5 Evaluation earthquake limit state E-ELS

The ELS is evaluated (as an option for evaluation required in high-seismic risk zones) using the simplified non-linear seismic analysis (SNLSA) approach presented in Chapter 5 (Mohammed et al. 2013d). The approach is based on the nonlinear sectional analysis (NLSA) presented in Chapter 2 (Mohammed et al. 2013a), the DRAIN-RC nonlinear time history analysis program, and Takeda's hysteretic analysis. The approach is capable of evaluating the effects of corrosion-induced damage on seismic and energy absorption capacities and the interaction relationship of the column.

6.3 The Semi-Quantitative Assessment of the Bridge Column

One of the major steps of the proposed framework is the semi-quantitative assessment, and it is the major focus of this chapter (Mohammed et al. 2013e). Based on the three evaluation limit states mentioned earlier, the semi-quantitative assessment involves three assessment steps (see Figure 6.2), which are (i) assessment of the ultimate capacity; (ii) assessment of the serviceability; and, (iii) assessment of the seismic capacity only if the bridge is located in a high-risk seismic zone.

In the bridge management system, it is essential to define operational performance limits (or thresholds) for each major performance parameter (or measure). For example, the ultimate strength and deformation capacities can be defined at different ages and for different levels of services, etc. Figure 6.3 shows three possible thresholds for the ultimate limit capacity (TH_{ULC1}, TH_{ULC2} & TH_{ULC3}) of a beam-column plotted on the load-deformation relationship of a new structure and an aged structure. The performance relationship shown in this conceptual figure can be established using the nonlinear finite element analysis proposed in Chapter 3. The performance relationships of both the undamaged and the corrosion-damaged structural elements are compared to the thresholds, hence identifying the state of performance of that element and leading to take suitable management decisions accordingly (maintenance, retrofitting, etc).

Figure 6.4 proposes an assessment approach based on the ultimate capacity of the corrosion-damaged column as estimated by the NLFEA (see Chapter 3; Mohammed et al. 2013b). If the calculated ultimate load capacity is more than the load capacity required by the design code (RLC), then the column is safe and no management action is required. On the other hand, if the required ultimate capacity is not matched, and the column appears to have less than the required capacity by the transportation network, then a management decision is required. By comparing

the calculated ultimate capacity (ULC) of the column at the inspection date to the three thresholds (shown in Figure 6.4), which are defined by the bridge management or the owner, a decision is made based on a quantitative comparison and not a qualitative decision stemming only from visual observation. The figure shows, for example, three threshold column load capacities (TH_{ULC}): (i) if the current ultimate limit capacity (ULC) is above TH_{ULC1} and below RLC, then minor maintenance is required; (ii) if the ULC is above TH_{ULC2} and below TH_{ULC1}, then major maintenance is required; and, (iii) if the ULC is above TH_{ULC3} and below TH_{ULC2}, then major maintenance is required in addition to retrofitting and/or reduction of the allowable service (or truck) load. If the lowest threshold (TH_{ULC3}) is not met, then reconstruction could be required.

Several approaches have been proposed in the literature to monitor the serviceability of aged and damaged bridges such as: (i) monitoring the change in the natural frequency; (ii) comparing the instantaneous ratio of dynamic-to-static load (RDTS) with the dynamic load allowance (DLA, of the CHBDC), or the impact factor (of the AASHTO-LRFD); or, (iii) comparing directly the dynamic deformations of the damaged bridge with those of an undamaged bridge and the allowable deformations established by the design code. In this study, the proposed serviceability assessment is based on the direct comparison of the dynamic deformations.

Figure 6.5 proposes an approach for the serviceability assessment of a slab-on-girder bridge with corrosion damaged column(s) based on the results of the simplified hybrid dynamic finite element analysis (SHDFEA) presented in Chapter 4. As shown in Chapter 4, the use of linear dynamic analysis could be adequate in most of the cases because of: (i) the conservative column design in most of aging bridges; (ii) the simple joints connecting the superstructure to the substructure; and, (iii) the use of dampers. However, it is suggested here that the selection

between using nonlinear dynamic or linear dynamic analysis be left to the user or to the BMS team. For example, if the columns are slender and designed for high load-over-capacity ratios and/or the bridge has a long span and a slender superstructure, then nonlinear dynamic analysis could give a better estimation of the dynamic performance indicators. In Figure 6.5, the assessment of the serviceability starts after selecting the type of analysis of the SHDFEA to calculate the maximum dynamic deformation (MDD) of the superstructure and the columns. For a quantitative assessment, it is required to compare MDD with the allowable maximum dynamic deformation (AMDD) according to the type of bridge and the bridge design code, and to compare MDD with the required operational deformations limits (or threshold service limits) TH_{SL}. If MDD is less or equal to AMDD, then no action is required as the deformations of bridge elements are acceptable under traffic or service loads. This range of acceptable deformation can practically extend up to TH_{SL1} (see FHWA-RD-01-020, 2001; MTO- OSIM, 2008; and AASHTO- MCEB, 1994). If MDD is more than the first service limit (TH_{SL1}) but less than the second service limit (TH_{SL2}), then minor maintenance or improving the damping is required. If MDD is less than TH_{SL3} but more than (TH_{SL2}), then reduction of the allowable truck load on the bridge and/or major maintenance and retrofitting are required. If MDD is more than TH_{SL3} then reconstruction of the bridge could be decided.

Figure 6.6 proposes an assessment approach for the seismic capacity of a slab-on-girder bridge column subjected to reinforcement corrosion based on the results of the simplified non-linear seismic analysis (SNLSA) presented in Chapter 5 (Mohammed et al. 2013d). The calculated residual seismic capacity (RSC) is compared with the required seismic capacity (RESC). If RSC is more than or equal to RESC, then the column is safe and no maintenance is required. If RSC is less than RESC but more than the first threshold seismic capacity (strength or displacement)

(TH_{SC1} or $TH_{SC-\Delta1}$), then "basic" maintenance is required. If RSC is more than the second threshold seismic capacity (TH_{SC2} or $TH_{SC-\Delta2}$) but less than the TH_{SC1} or $TH_{SC-\Delta1}$, then "major" maintenance and retrofitting are required. If RSC is less than TH_{SC3} or $TH_{SC-\Delta3}$ then demolition and reconstruction of the columns or the whole bridge could be decided.

The results of the three evaluation limit states and the assessment are combined in one semi-quantitative assessment approach. It should be pointed out that different thresholds are identified or decided by the bridge owner or the BMS team based on the location of the bridge, its importance to the resiliency of the transportation network, its age, and the history of damage/maintenance cycles.

6.4 Case Studies, Results and Discussions

Two slab-on-girder bridges have been selected from the bridge inventory of the states of Maine and Florida in the US. The first bridge (Bridge I) is a slab-on-steel girder bridge built in 1977 with a span of 49 m, a transverse width of 20.5 m and girder spacing of 2.64 m. The second bridge (Bridge II) is a slab-on-prestressed concrete girder bridge built in 1973 with a span of 39 m, a transverse width of 13.7 m, and a girder spacing of 2.4 m. Table 6.1 shows more details of the two bridge superstructures. The design details of the substructure and their present state are not available, and hence they are designed for the purpose of this study based on the traditional material properties of bridge construction in the 1970's. The two bridges are highway bridges with design traffic speed of 100 km/hr. The concrete compressive strength is assumed equal to 30 MPa for the slab and the bridge columns, while the compressive strength of the concrete in the prestressed girders is assumed equal to 40 MPa. The substructure is assumed to be constructed from eight columns for Bridge I and six columns for Bridge II, with a total height of 6 m. The columns are assumed to be joined from the top by a cap beam normal to the direction

of the traffic. The columns of Bridge I are designed for a load-over-capacity ratio (LOCR) of 40%, while the columns of Bridge II are designed for an LOCR of 50%. The three evaluation limit states are performed for each of the two bridges using the three analysis approaches developed in Chapters 3 through 5.

Figure 6.7 shows Bridge I (with an overpass configuration) subjected to (a) traffic load and (b) seismic load. Figure 6.8 (a) shows the critical corrosion damaged zone located in the middle third of the column height of one of the two bridge sides with a roller boundary between the substructure and the superstructure. Figure 6.8 (b) shows the longitudinal reinforcement of the bridge column for both bridges. Figures 6.8 (c) and (d) show the cross section of the column of Bridge I before and after corrosion damage has taken place, respectively, and Figures 6.8 (e) and (f) show the cross section of the column of Bridge II before and after corrosion damage has taken place, respectively. Figure 6.9 shows several states of local corrosion damage and the general loads applied on the columns. The most important damage states are: (a) flexural and corrosion-induced cracks; (b) initial (or partial) spalling; (c) one stirrup failure (with partial spalling); (d) all-sides spalling; (e) two stirrups failure (with all-sides spalling); and, (f) loss of confinement and possible buckling.

In the two case studies (Bridge I and Bridge II), it is assumed that a 5% reduction of steel cross-sectional area due to reinforcement corrosion would result in concrete cracks, 15% reduction would result in concrete spalling, 20% reduction would result in one stirrup failure, and 30% reduction would result in two stirrups failure. These assumptions are approximate and based on generalization of the lab tests done by Oyado et al. (2007). The reason behind these assumptions here is to show how to apply the present analysis approach. In field investigations, accurate measurements of the reduction of the steel and concrete are required; however, for an

approximate evaluation, empirical equations (Lay and Schiebl 2003 and Cairns et al. 2005) could reduce the number of tests and samples required to prepare the data input.

The results of the analysis of the first case study (Bridge I) are shown in Figures 6.10 through 6.21. Figure 6.10 shows the load-displacement relationship for concentric loading and for the case of an eccentricity with 15% of the column width. Figure 6.11 shows the moment-displacement relationship (with 15% eccentricity) and the possible three ultimate load capacity (or strength) thresholds (TH_{ULC1}, TH_{ULC2}, TH_{ULC3}). The figure shows the reduction in the column strength when subjected to extreme reinforcement corrosion damage (loss of confinement and rebar buckling), which could result in lower strength than that established by threshold 3 (TH_{ULC3}). It is important to mention that the strength thresholds used in Figure 6.11 (and all other types of thresholds used in other figures of this chapter) are hypothetical or conjectural, and they are only presented to show how the proposed assessment approach can be applied. The decision on the threshold values is to be taken by the evaluating bridge-engineers based on BMS requirements.

Sample results of the evaluation serviceability limit state for Bridge I are shown in Figures 6.12 through 6.15. The displacement under the truck front axle (see Figure 6.12) only increases by a negligible amount when the columns are affected by reinforcement corrosion (see also Chapter 4 for more explanation). In the present example, the RDTS (ratio of maximum dynamic deformation to the maximum static deformation of the superstructure) is equal to the DLA (the dynamic load allowance in CHBDC or the impact factor in AASHTO-LRFD) for both cases with and without applying the corrosion on the columns reinforcement. However, the dynamic deformations of the columns themselves show a large increase due to the reinforcement corrosion. The maximum dynamic axial and lateral displacements are increased, and the location

of peak lateral displacement also changes with the application of corrosion damage (see Figures 6.13 and 6.14). Each of the two figures shows three thresholds on the dynamic axial and lateral displacements of the column. Figure 6.15 shows that there are no noticeable changes of the maximum lateral dynamic deformation of the corrosion-damaged bridge columns compared to undamaged bridge columns when the truck passes over the bridge.

The results of the evaluation earthquake limit state for Bridge I are shown in Figures 6.16 through 6.21. Figures 6.16 and 6.17 show respectively the moment-deflection relationships of the Bridge I column without and with reinforcement corrosion for the possible damage stages when extreme loads are applied using the nonlinear sectional analysis (see Mohammed and Almansour, 2013, and Chapters 2 & 5). As shown in Figures 6.16 and 6.17, the damage stages start with “undamaged” stage, then the spalling of the concrete cover, followed by the failure of one and two stirrups, and finally the loss of the core concrete confinement. Based on approximate strain values for each damage stage, the “staged failure path” is established. Similarly, the staged failure path is also established for the column with reinforcement corrosion damage, as illustrated in Figure 6.17. It is important to mention that the stages of the corrosion damage are similar to the general stages on damage when no corrosion is applied; however, reinforcement corrosion accelerates these stages as the stiffness and ductility of the steel, the concrete, and hence the composite section are affected.

Using the artificial ground acceleration time history shown in Figure 6.18, the seismic time history analysis of the columns of Bridge I and Bridge II of two case studies of this chapter are established for the case of non-corroded and corroded columns. Figure 6.19 shows the large increase in lateral deformation time history of Bridge I when the reinforcement of the column is subjected to severe corrosion. Table 6.2 defines the acronyms in Figure 6.19. The three

suggested deformation thresholds are shown in the figure, which could be decided according to the importance of the bridge in the transportation network, required seismic performance, and the location of the bridge on the national seismic map. Figures 6.20 and 6.21 show the load-displacement hysteretic relationships of uncorroded and corroded column sections of Bridge I, respectively. Comparing the two figures shows that a reduction in the energy dissipation capacity when reinforcement corrosion takes place. The three suggested seismic capacity thresholds (TH_{SC1}, TH_{SC2}, TH_{SC3}) are shown in Figures 6.16 and 6.17 compared to the moment-displacement relationships of non-corroded and corroded columns. In the case of the corroded column, the seismic capacity is lower, and the performance curve is located in the lower threshold zone (between TH_{SC2} and TH_{SC3}). Evaluating engineers can use the results from the hysteretic relationships, the required seismic performance, BMS necessities, etc., to establish three seismic strength and three seismic deformation thresholds for the hysteretic relationships, as shown in Figures 6.20 and 6.21.

The results of the analysis for the second case study (Bridge II) are shown in Figures 6.22 through 6.33. Figure 6.22 shows the axial load-displacement relationship for concentric loading and for eccentric loading with an eccentricity of 15% of the column width. Figure 6.23 shows the reduction in the moment strength capacity of the column under concentric loading when extreme corrosion damage is applied. It is possible to show the thresholds on the figures similar to the first case study of Bridge I; however, all the previously suggested thresholds are hypothetical and presented only for the purpose of illustration. Hence, it is found that there is no need to show them again for the second case study.

Results of the evaluation serviceability for Bridge II are shown in Figures 6.24 through 6.27. Figure 6.24 shows that there are no noticeable changes of the maximum lateral dynamic

deformation of the bridge superstructure when the bridge columns are subjected to reinforcement corrosion compared to a bridge with undamaged columns. On the other hand, the maximum dynamic axial and lateral displacements of the columns increase with the application of the corrosion damage and the location of the peak lateral displacement changes as well (see Figures 6.25 and 6.26). The dynamic displacement of the bridge superstructure under the truck front axle (see Figure 6.27) only increases marginally.

The results of the evaluation earthquake limit state for Bridge II are shown in Figures 6.28 through 6.33. Figures 6.28 and 6.29 show the moment-deflection relationships of the Bridge II columns without and with reinforcement corrosion, respectively. The figures show the relationships for the five possible damage stages, from which the "staged failure paths" are established.

Using the artificial ground acceleration time history shown in Figure 6.18, the seismic time history analysis results are established for the cases of non-corroded and corroded columns. Figures 6.30 and 6.31 shows the large increase in lateral deformation time history of Bridge II for uncorroded and corroded columns (when the reinforcements of the column are subjected to severe corrosion damage). Table 6.2 defines the acronyms in Figures 6.30 and 6.31. Figures 6.32 and 6.33 show the load-displacement hysteretic relationships of uncorroded and corroded column sections of Bridge II. Similar to the first case study, comparing the two figures also shows a reduction in the energy dissipation capacity when the reinforcement corrosion takes place.

6.5 Conclusions

This chapter presents the proposed semi-quantitative assessment framework (SQAF) of bridge beam columns subjected to reinforcement corrosion and different types of loads. The framework uses three evaluation limit states, which are the evaluation ultimate limit state (E-ULS),

evaluation serviceability limit state (E-SLS), and evaluation earthquake limit state (E-ELS). The structural analysis approaches used in each of the three limit states are developed and verified in previous chapters (Chapters 2, 3, 4, and 5). The SQAF suggests the use of thresholds, set by the evaluation engineers based on the BMS requirements and against which decisions for remedial action are taken. The SQAF proves to be comprehensive and provides a systematic assessment procedure that needs minimum numerical efforts. The approach can be integrated into a bridge management system. It provides simplified analysis tools that enable practicing engineers to improve the accuracy and the cost effectiveness of the assessment of aging infrastructure. It also presents a step toward the development of a fully quantitative assessment approach.

The framework is still dependent on the accuracy of the input data, which is dependent on the enhanced inspection and material testing. The two case studies prove that the proposed assessment framework provides an efficient analysis tool that helps to quantify the important performance parameters of aged slab-on-girder bridge columns. The quantitative comparisons between the required and existing capacities or performance measures would give the bridge owners, practicing engineers and management team an accurate evaluation, which would lead to a reduction in the maintenance/rehabilitation cost and would provide better safety. It also results in reducing the variation in the data collected using traditional inspection methods.

Table 6.1: General properties of slab-on-steel girders and slab-on-prestressed concrete girders bridges in Case Studies (BridgeI & II). (Hevener 2003, based on Nutt et al., 1988, NCHRP Report 12-26).

Type of girder	Year Built	Skew Angle ^{o}	Span Length m	Girder Spacing m	Girder Properties			Transverse width m	Slab Thickness m	No. of Girders	No. of Columns
					A m^2	I m^4	H m				
Steel	1977	10.0	49.11	2.64	0.0462	0.0187	2.898	20.487	0.2159	8	8
Prestressed	1973	0.0	39.35	2.37	0.699	0.3052	1.83	13.649	0.19	6	6

Table 6.2: Acronyms definition for Figures 6.19, 6.30, and 6.31.

No	**Definition**	**Acronyms**	**No**	**Notation**	**Acronyms**
1	top section	TS	16	flexural cracks- IS-C	CC-IS-C
2	intermediate section	IS	17	flexural cracks- BS-C	CC-BS-C
3	bottom section	BS	18	Spalling- TS-C	S-TS-C
4	uncorroded	NC	19	Spalling- IS-C	S-IS-C
5	corroded	C	20	Spalling- BS-C	S-BS-C
6	Undamaged-TS-NC	UD-TS	21	1 stirrup failure- TS-C	OSF- TS-C
7	Undamaged-IS-NC	UD-IS	22	1 stirrup failure- IS-C	OSF- IS-C
8	Undamaged-BS-NC	UD-BS	23	1 stirrup failure- BS-C	OSF- BS-C
9	Spalling-TS-NC	S-TS-NC	24	2 stirrups failure- TS-C	TSF- TS-C
10	Spalling-IS-NC	S-IS-NC	25	2 stirrups failure- IS-C	TSF- IS-C
11	Spalling-BS-NC	S-BS-NC	26	2 stirrups failure- BS-C	TSF- BS-C
12	1 stirrup failure-TS-NC	OSF-TS-NC			
13	1 stirrup failure-IS-NC	OSF-IS-NC			
14	2 stirrups failure-BS-NC	TSF-BS-NC			
15	flexural cracks- TS-C	CC-TS-C			

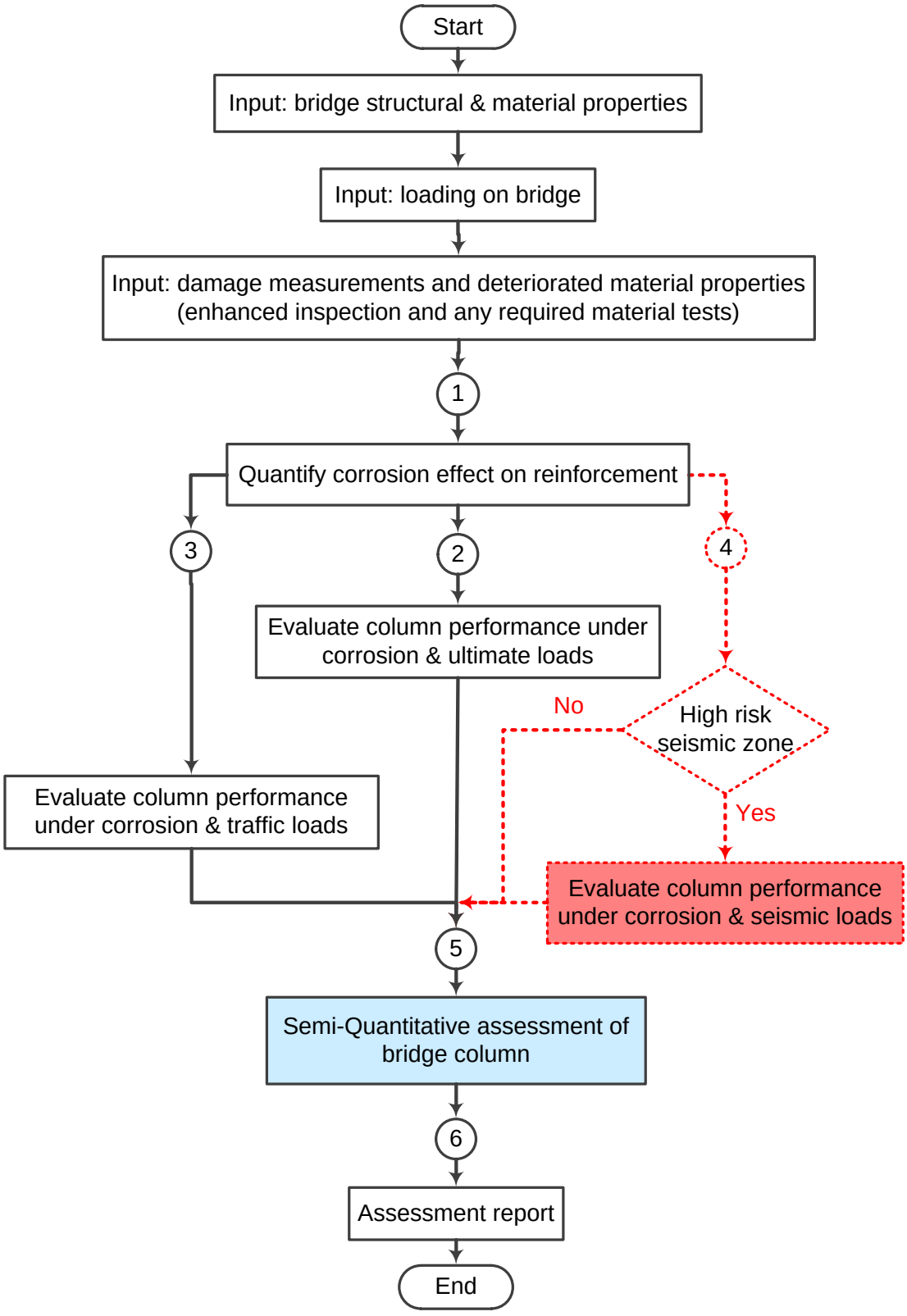

Figure 6.1: The proposed semi-quantitative assessment framework (SQAF).

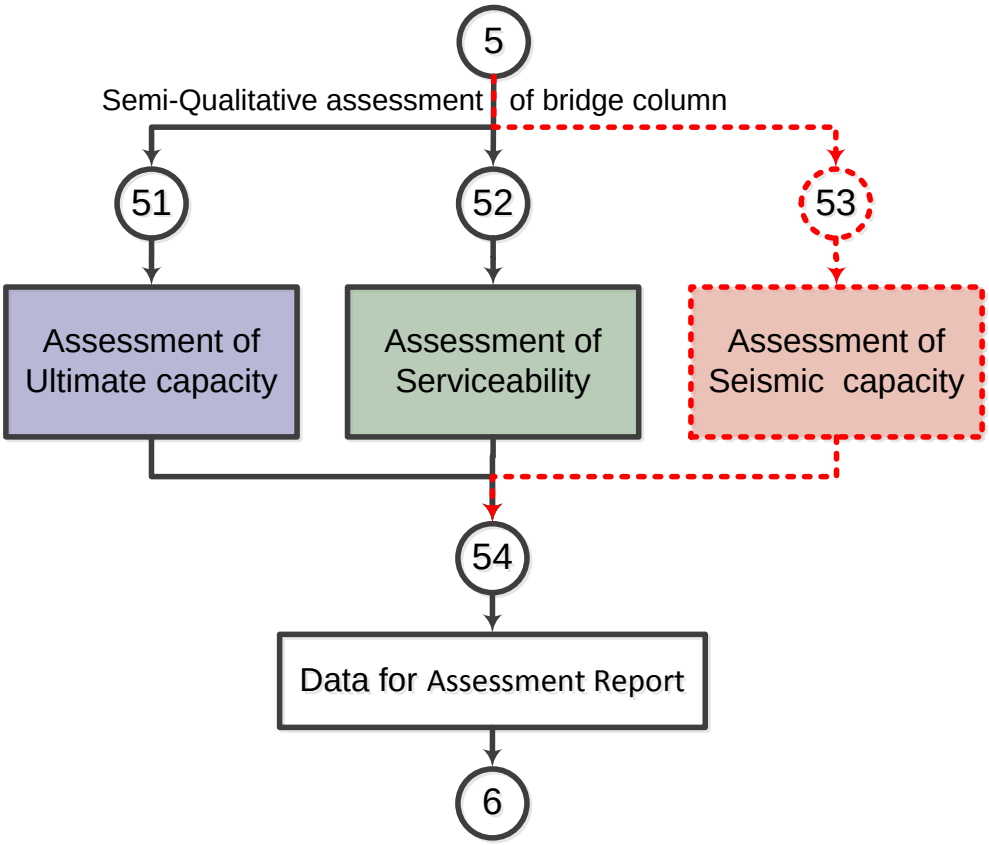

Figure 6.2: Components of the semi-quantitative assessment and reporting stage following the three evaluations limit states.

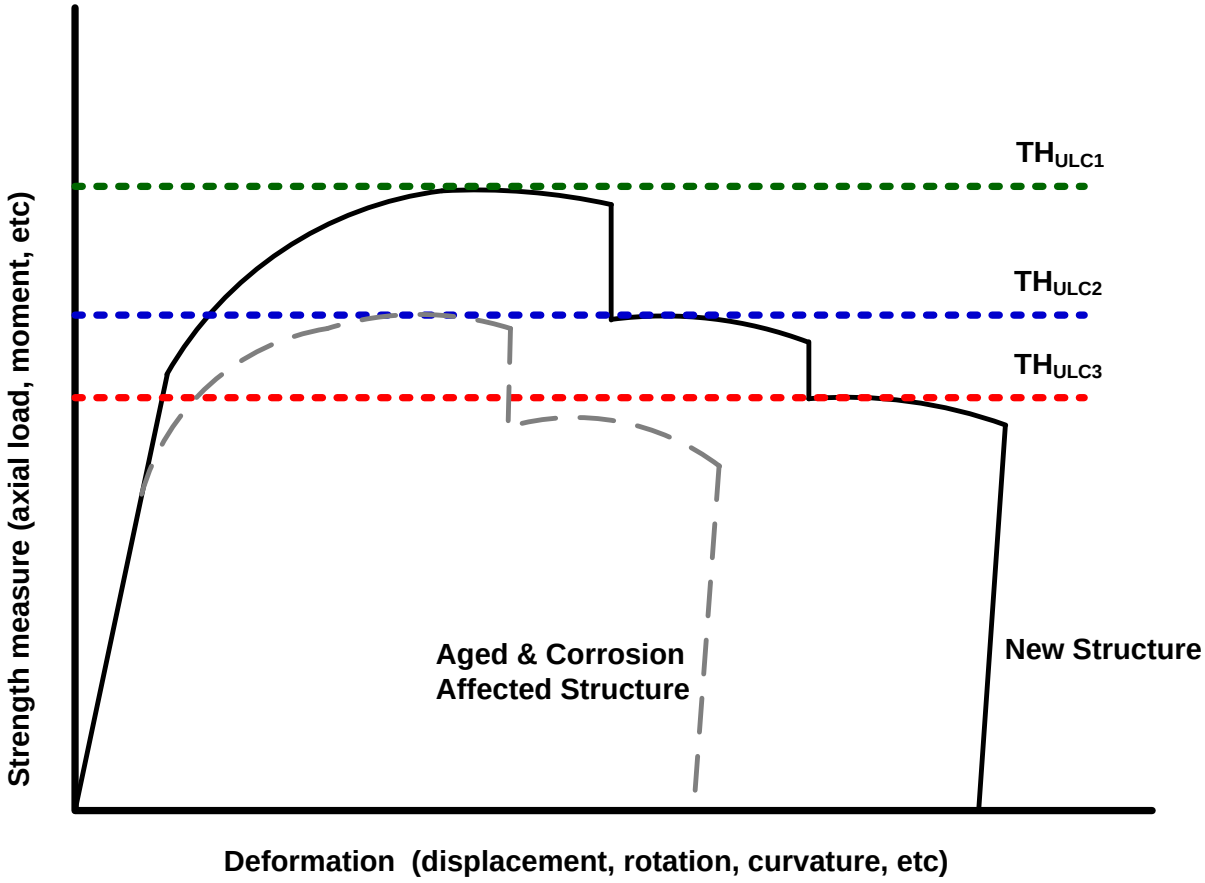

Figure 6.3: Strength and deformation thresholds projected on the performance relationship of corrosion-affected aged bridge beam-columns.

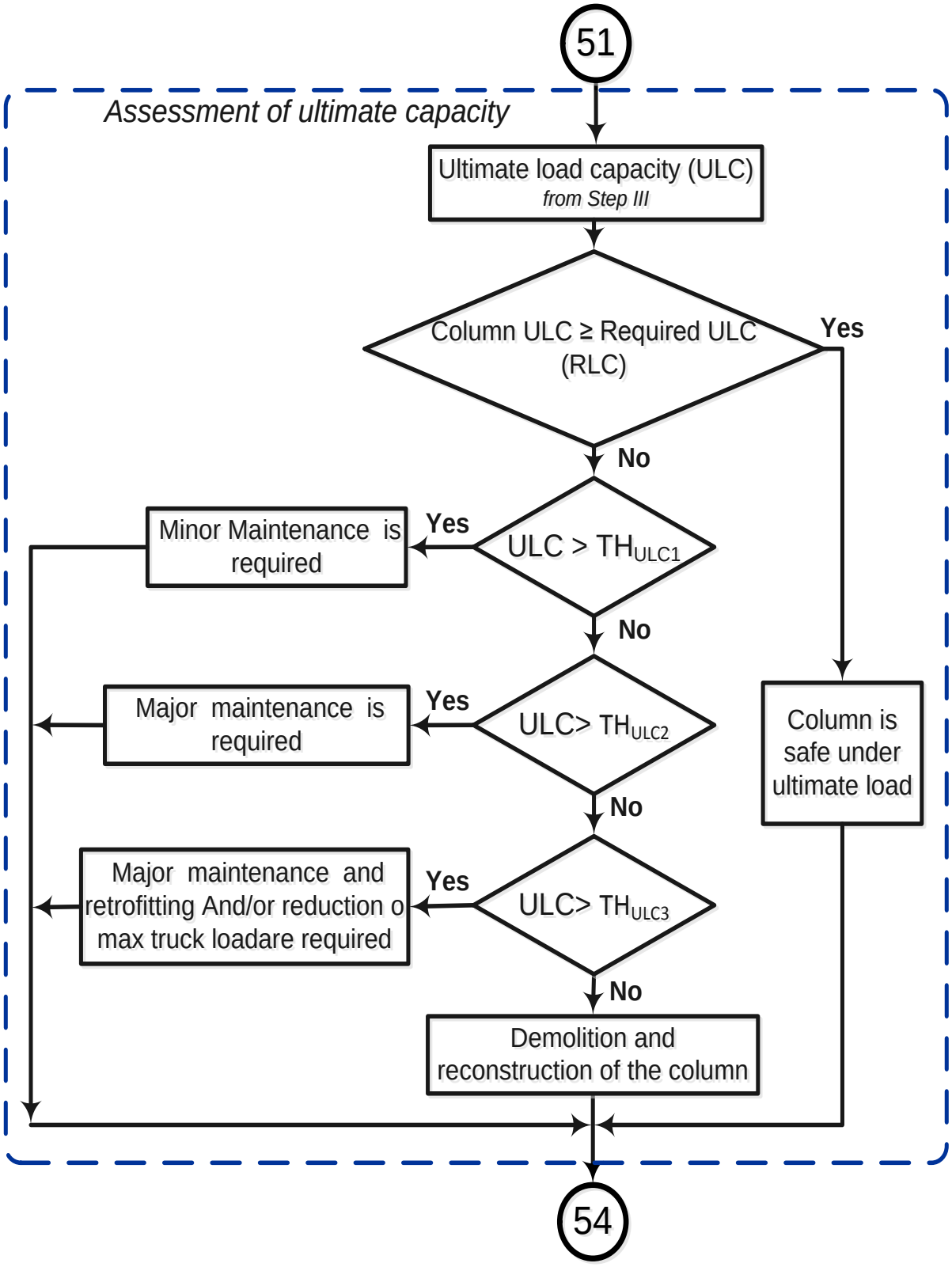

Figure 6.4: Assessment of the ultimate capacity.

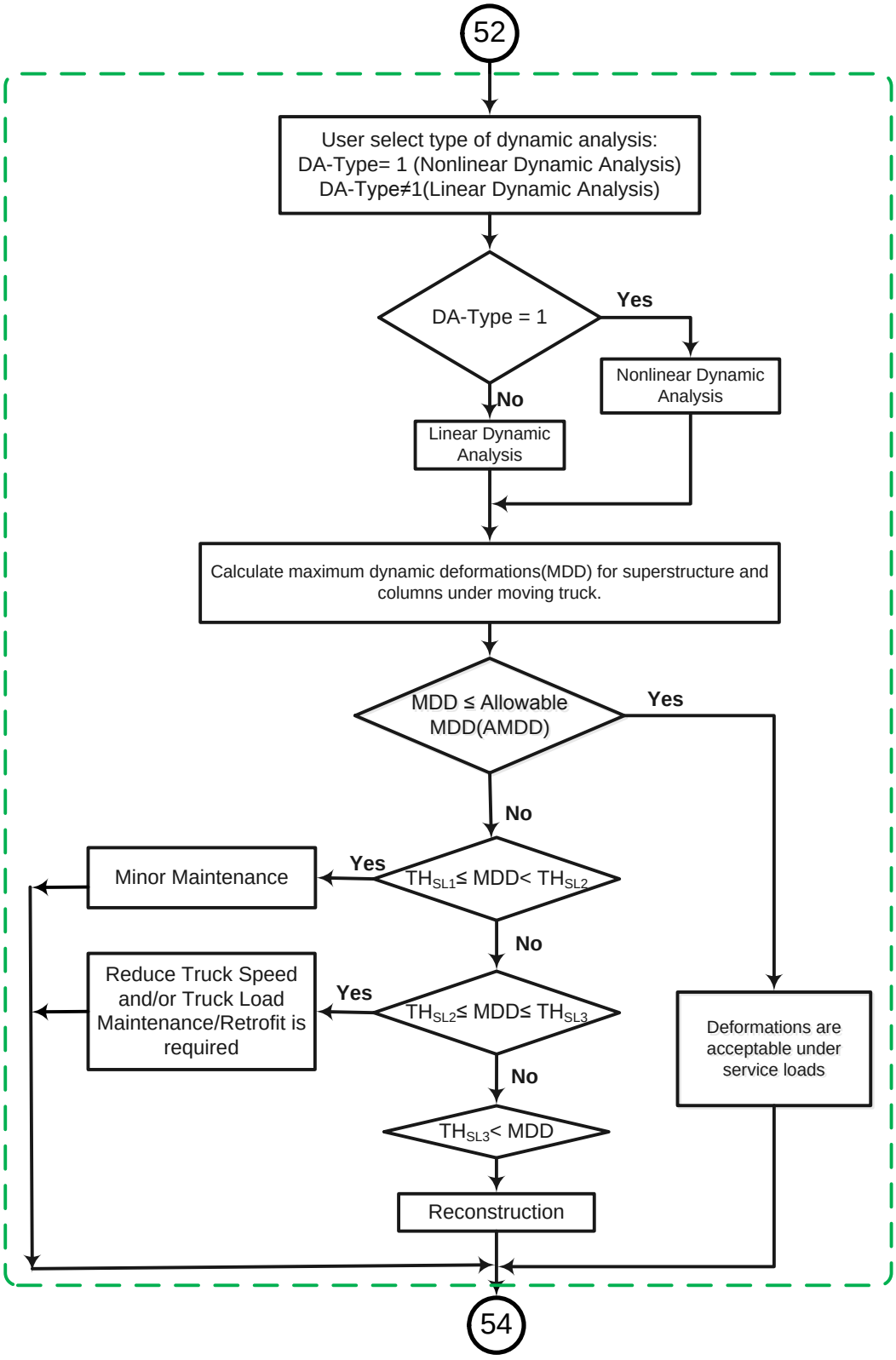

Figure 6.5: Assessment of the bridge serviceability.

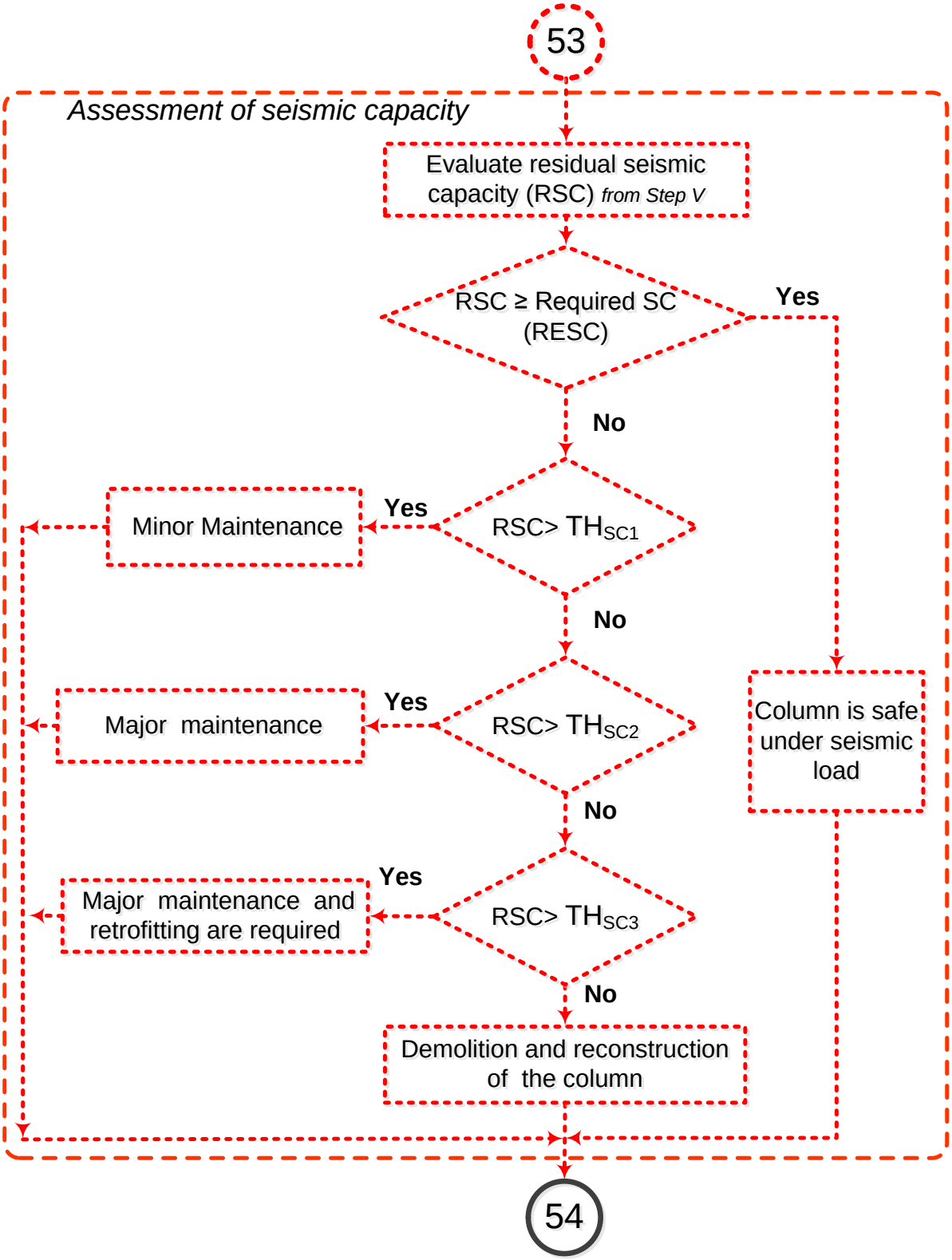

Figure 6.6: Assessment of seismic capacity.

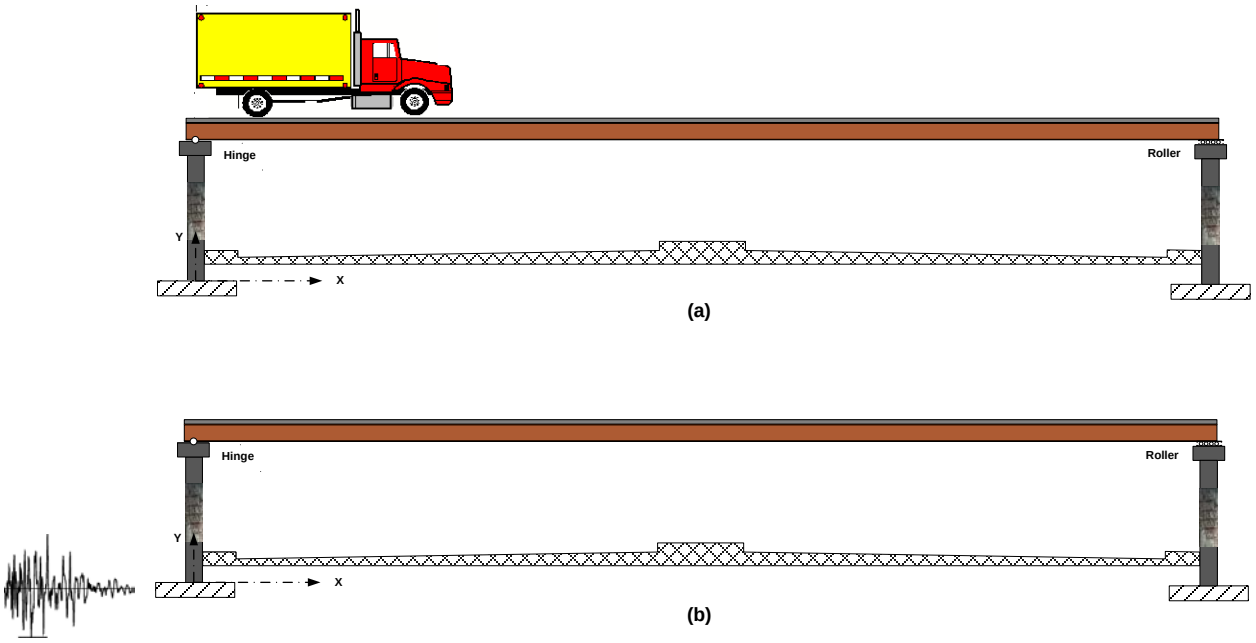

Figure 6.7: Slab-on-girder bridge under (a) traffic; and (b) seismic loads.

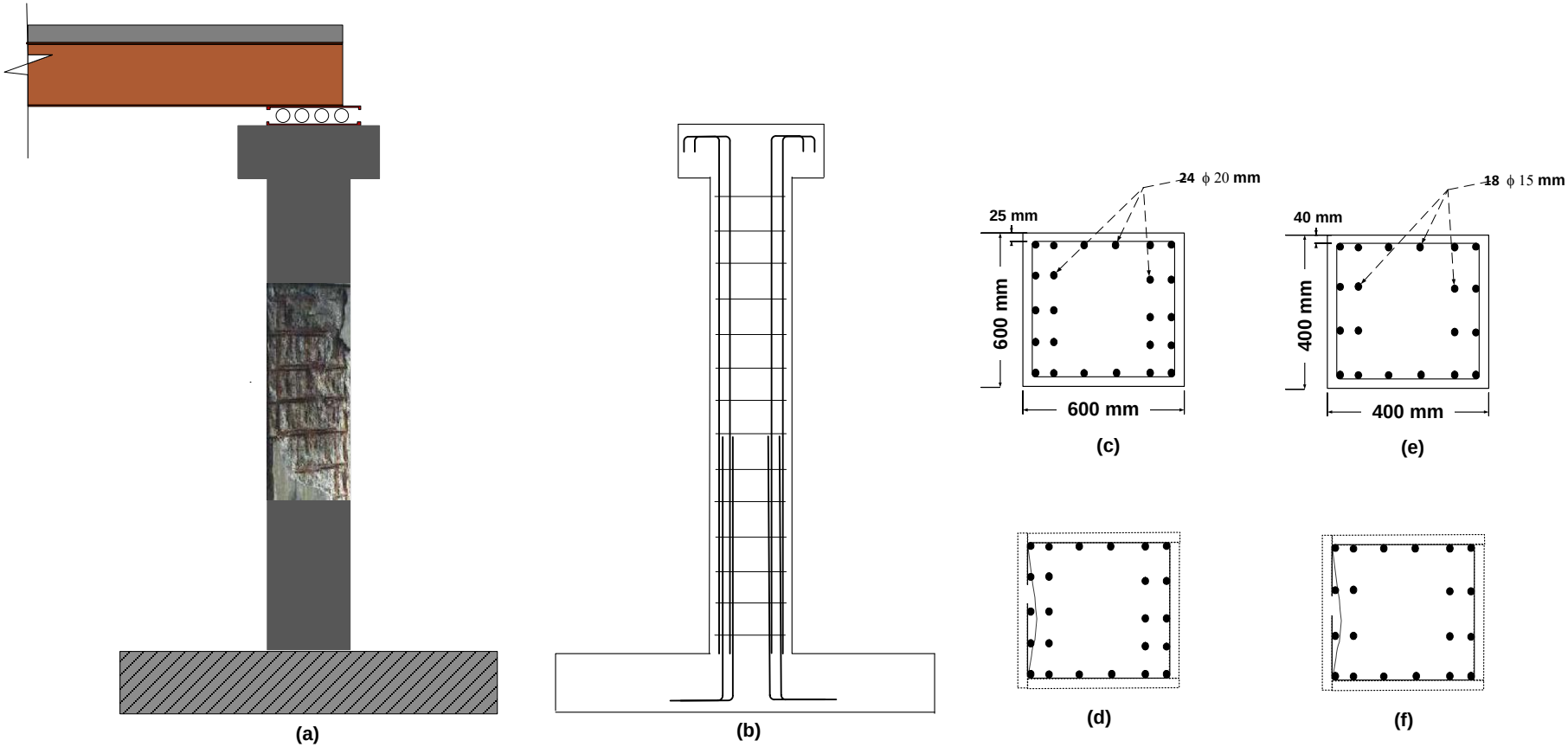

Figure 6.8: Critical corrosion-damaged zone of aged columns of the slab-on-girder bridges of the two case studies in this chapter (not-to-scale)

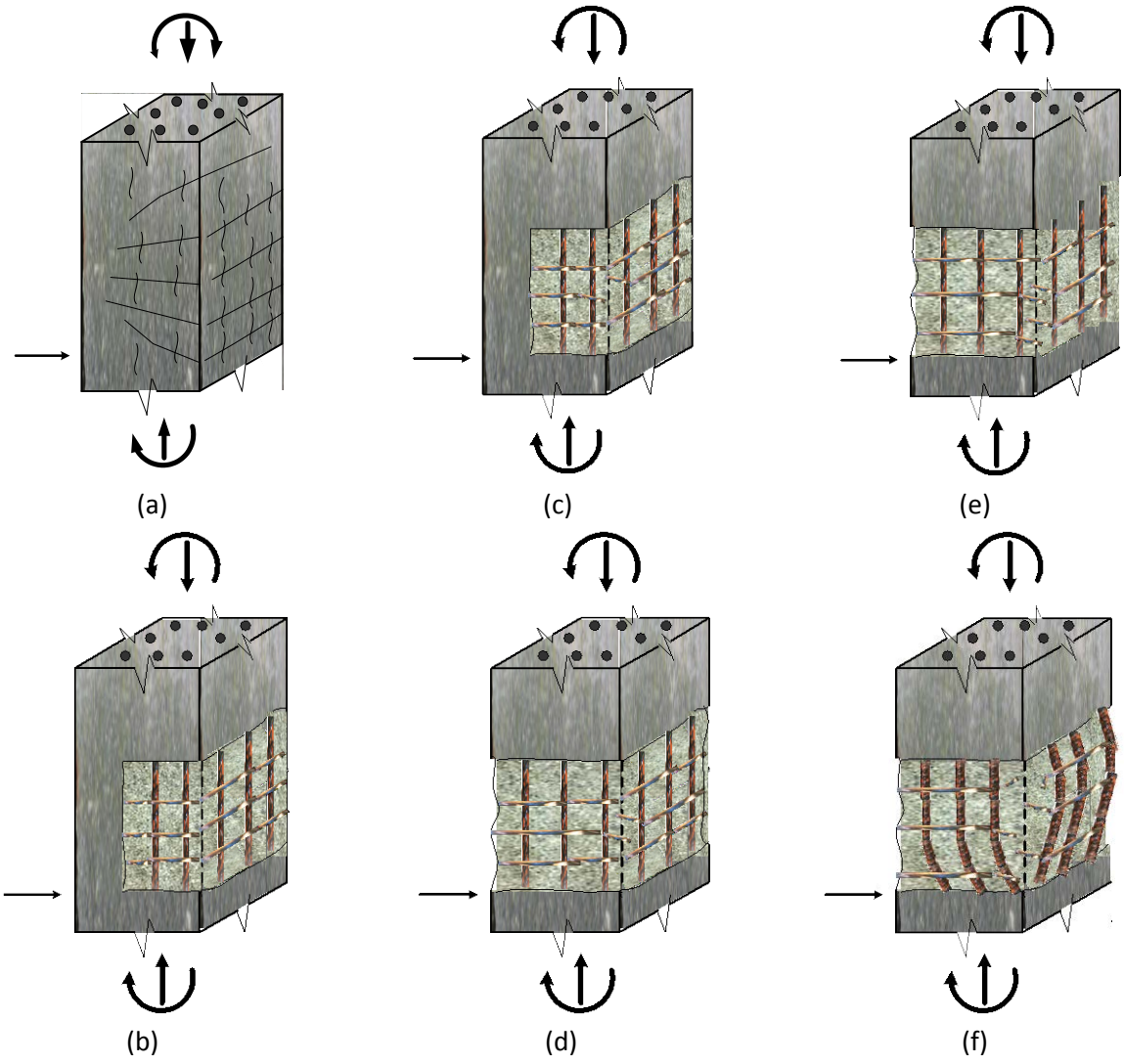

Figure 6.9: Possible damage and failure modes of RC columns due to combined gravity loads, lateral loads and reinforcement corrosion; (a) flexural and corrosion cracks; (b) initial spalling; (c) one stirrup failure; (d) spalling on all sides; (e) two stirrups failure; (f) loss of confinement and possible buckling.

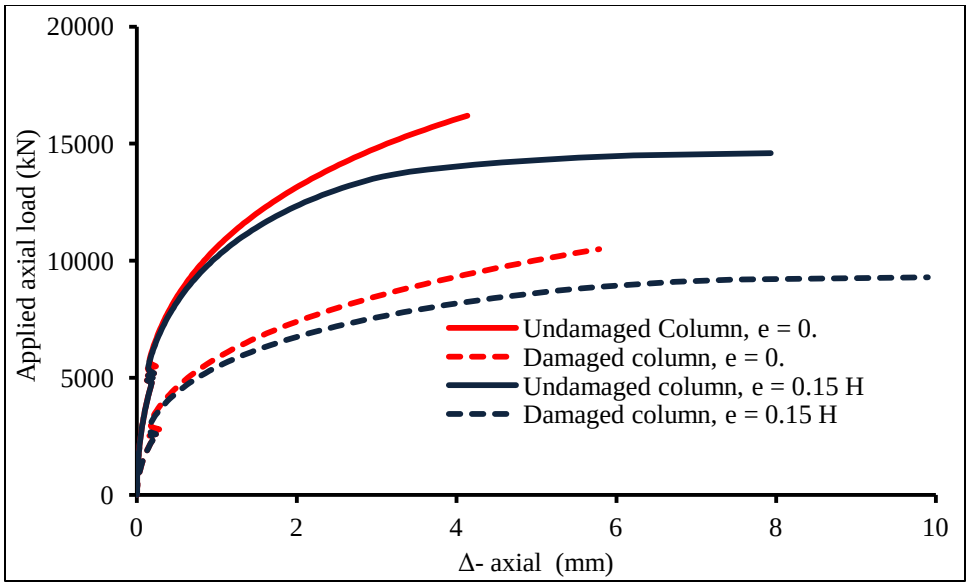

Figure 6.10: Applied axial load vs. axial displacement of the top section of the bridge column; Bridge I (right before static failure load).

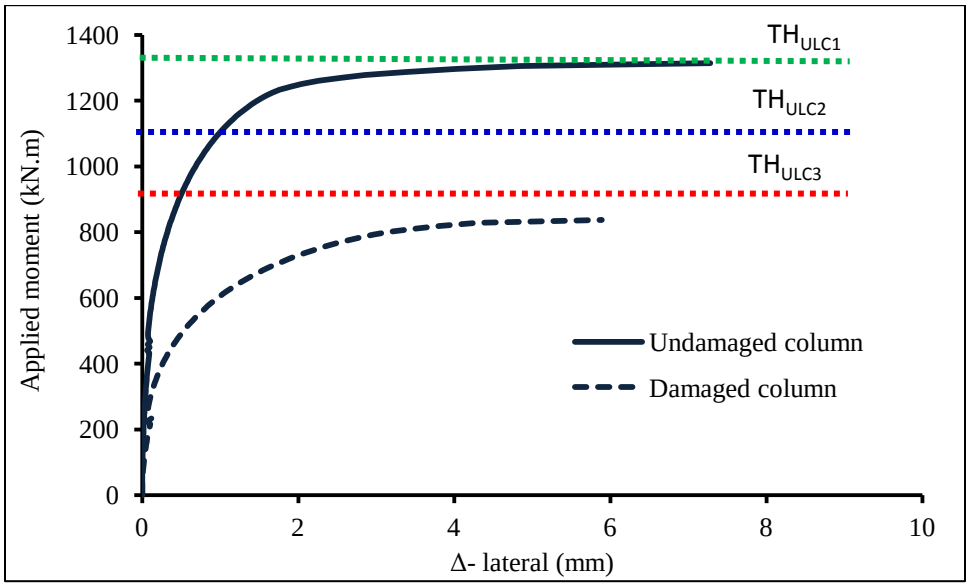

Figure 6.11: Applied moment vs. lateral displacement of the mid-height section of the bridge column right before static failure load (e = 0.15H); Bridge I.

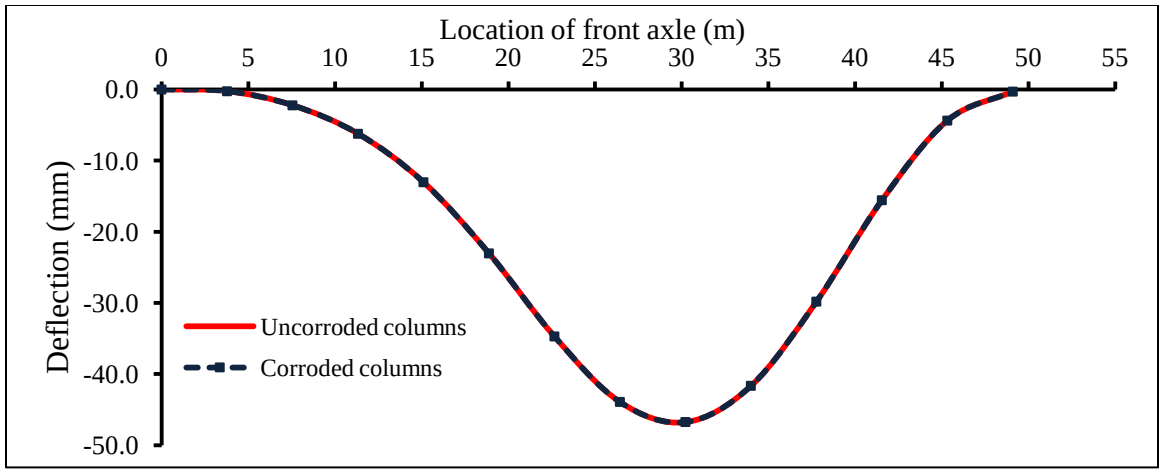

Figure 6.12: Comparison of dynamic deflections of superstructure under traffic load only and combined traffic and corrosion loads; Bridge I

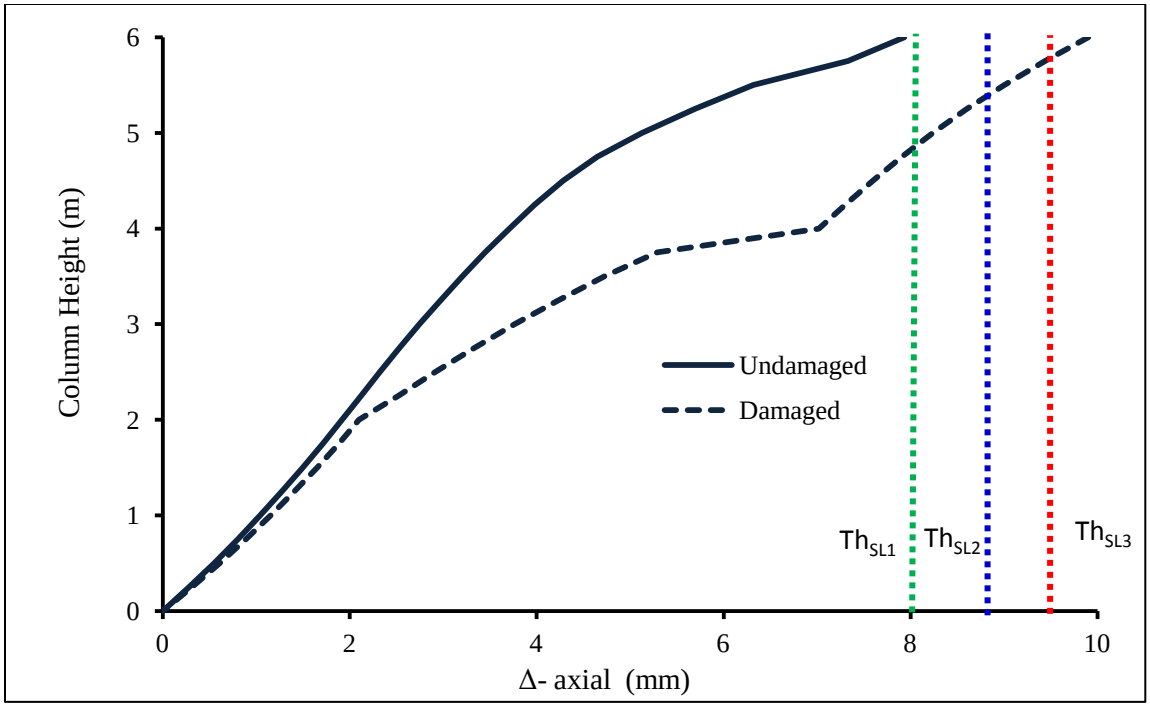

Figure 6.13: Column height vs. axial displacement of the bridge column at failure load (e = 0.15H); Bridge I.

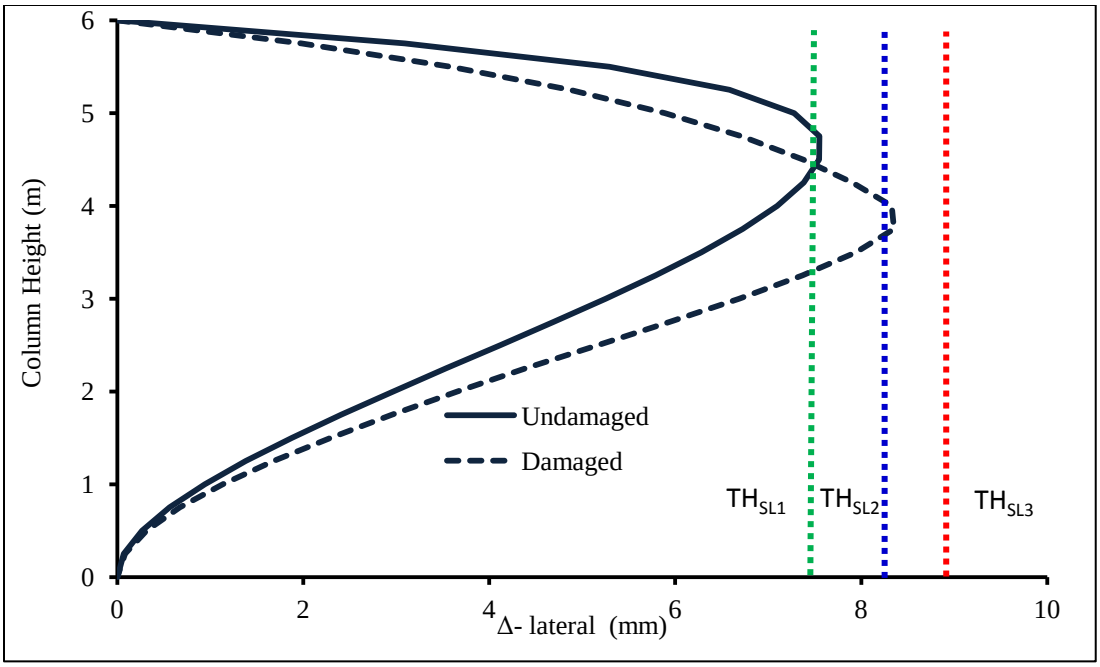

Figure 6.14: Column height vs. lateral displacement of the bridge column at failure load (e = 0.15H); Bridge I.

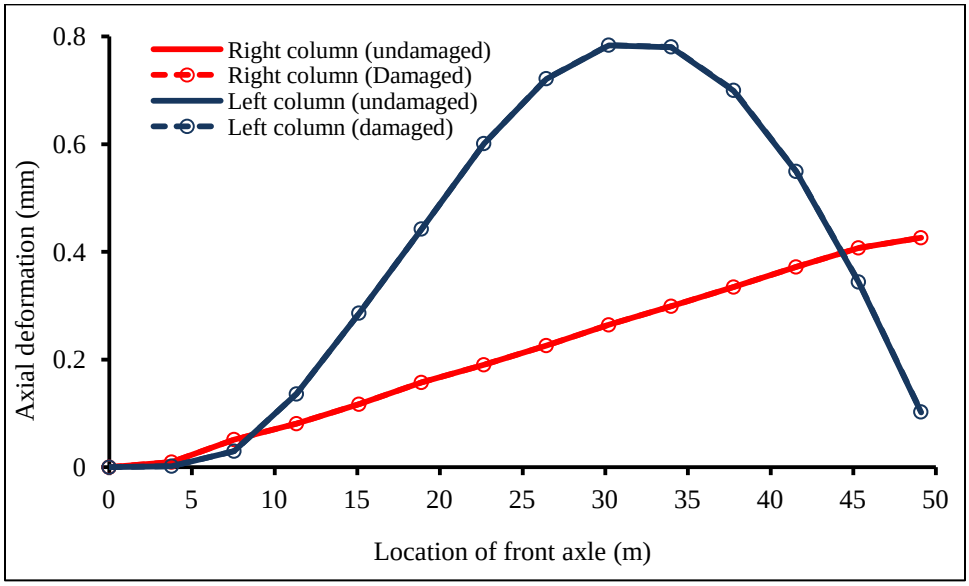

Figure 6.15: Truck position vs. maximum lateral deformation of the bridge column; Bridge I.

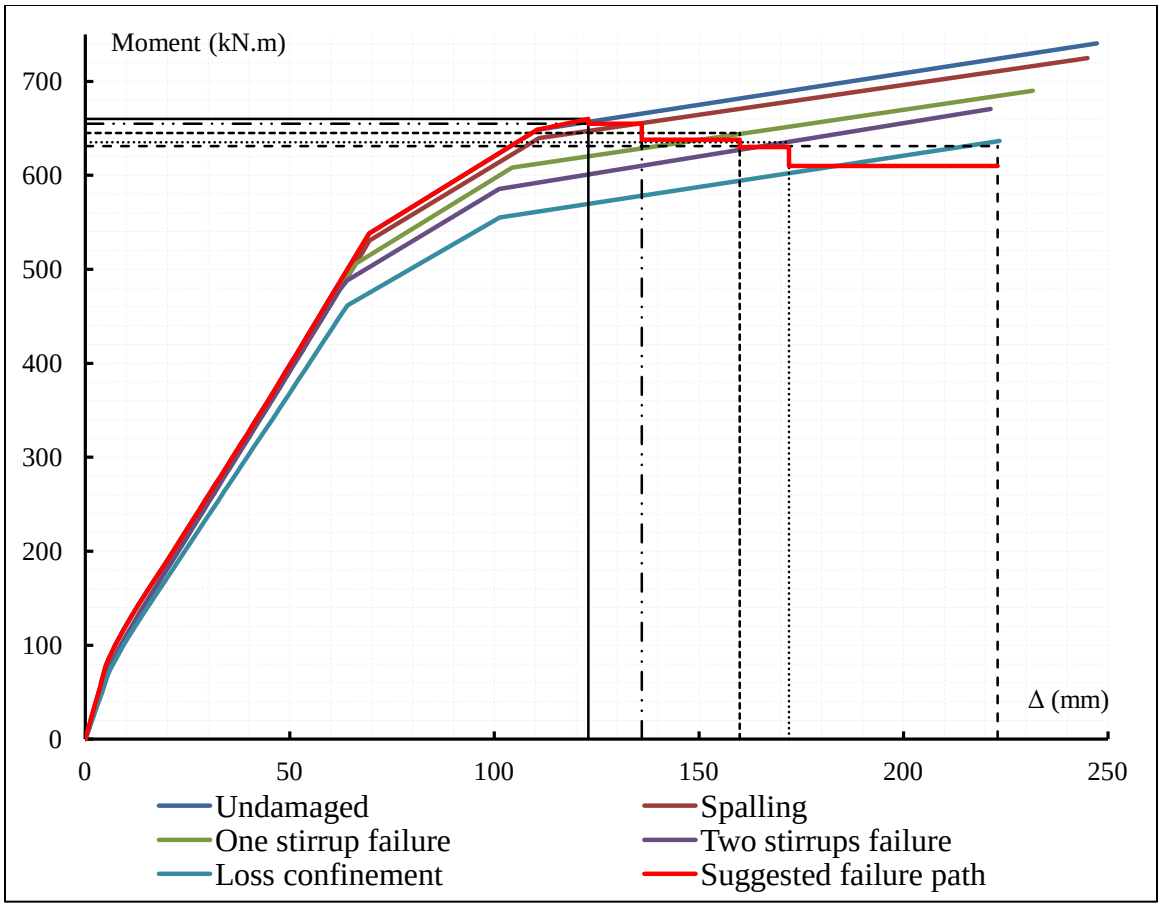

Figure 6.16: Envelope curve of load-displacement relationship of uncorroded column section; Bridge I.

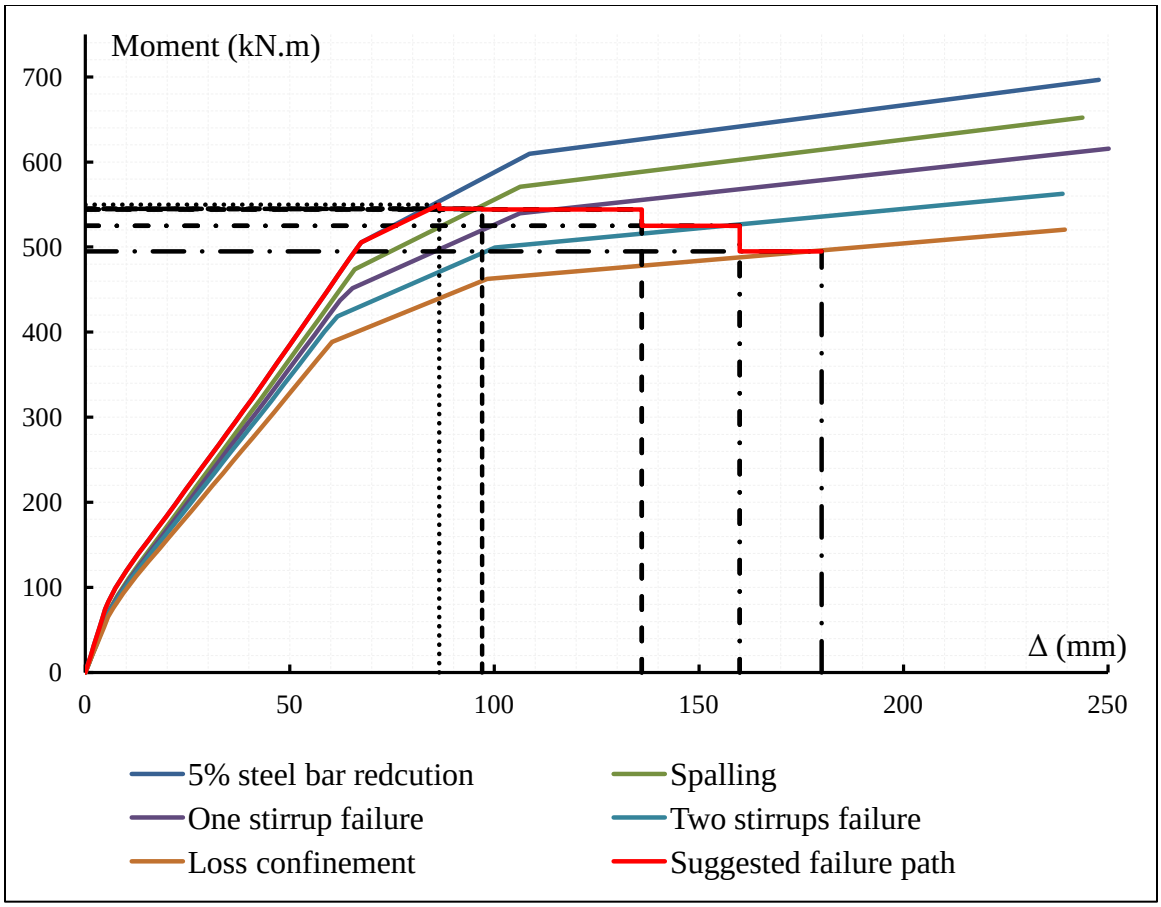

Figure 6.17: Envelope curve of load-displacement relationship of corroded column section; Bridge I.

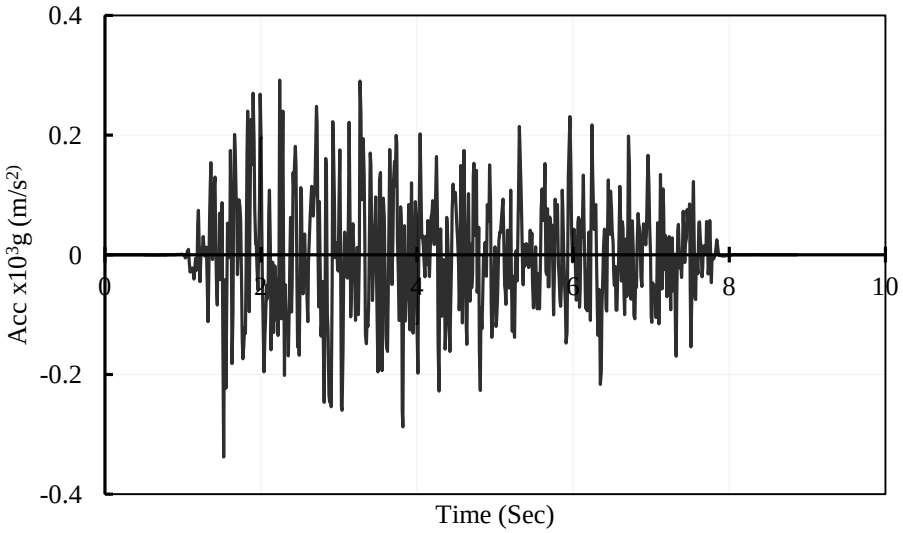

Figure 6.18: Artificial ground acceleration time history used in the seismic time history analysis.

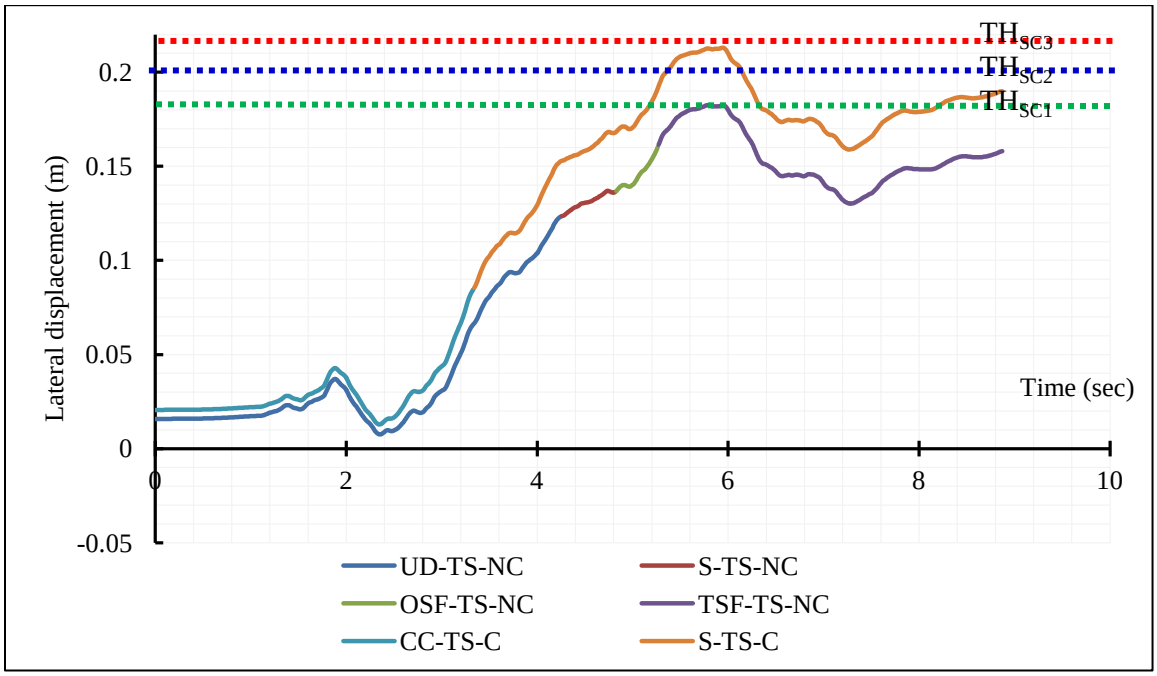

Figure 6.19: Top lateral displacement of uncorroded and corroded column; Bridge I.

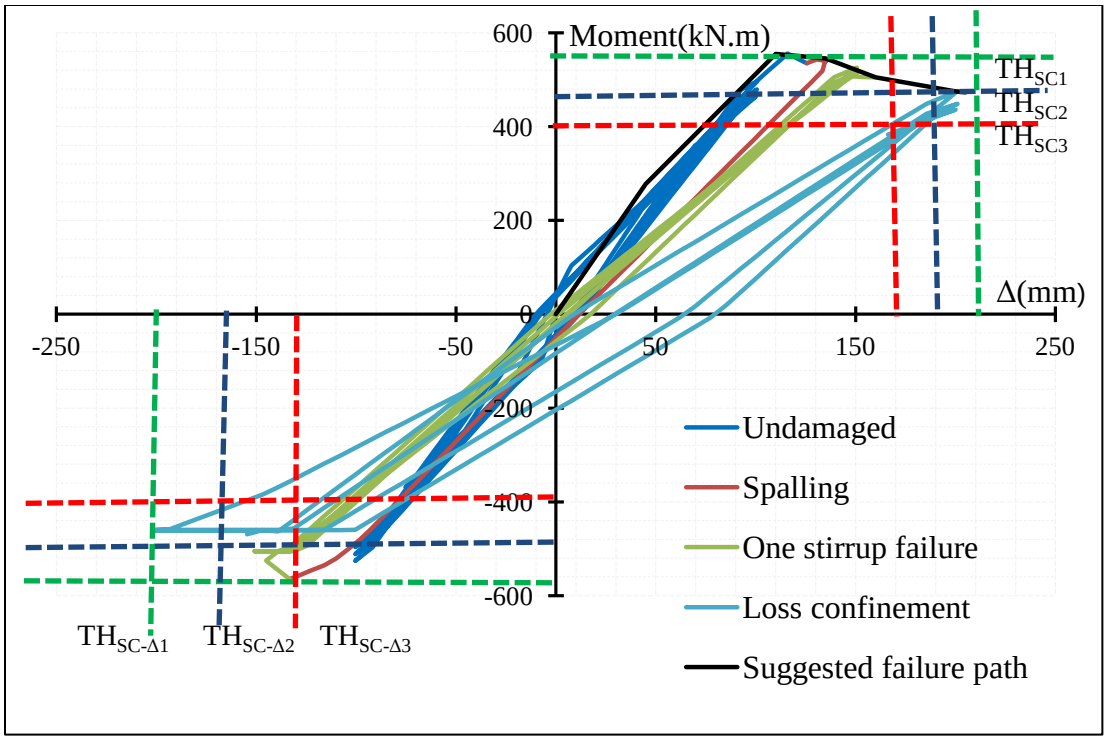

Figure 6.20: Load-displacement hysteretic relationship of uncorroded column section; Bridge I.

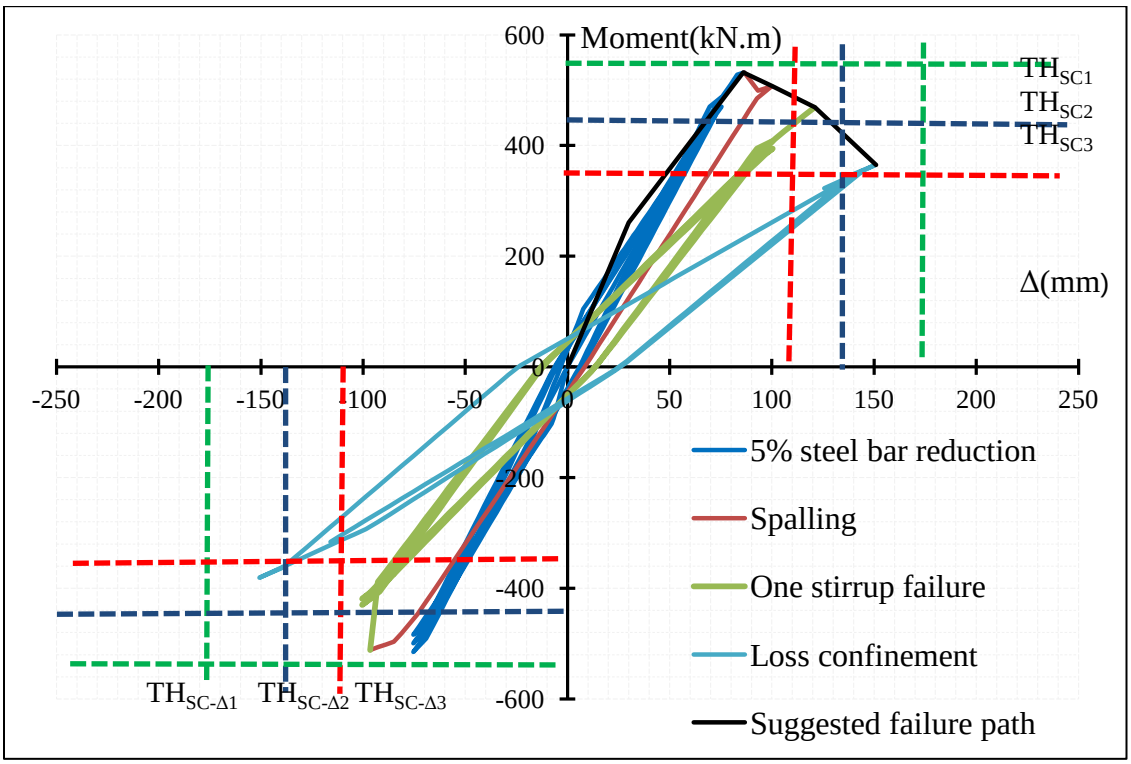

Figure 6.21: Load displacement hysteretic relationship of corroded column section; Bridge I.

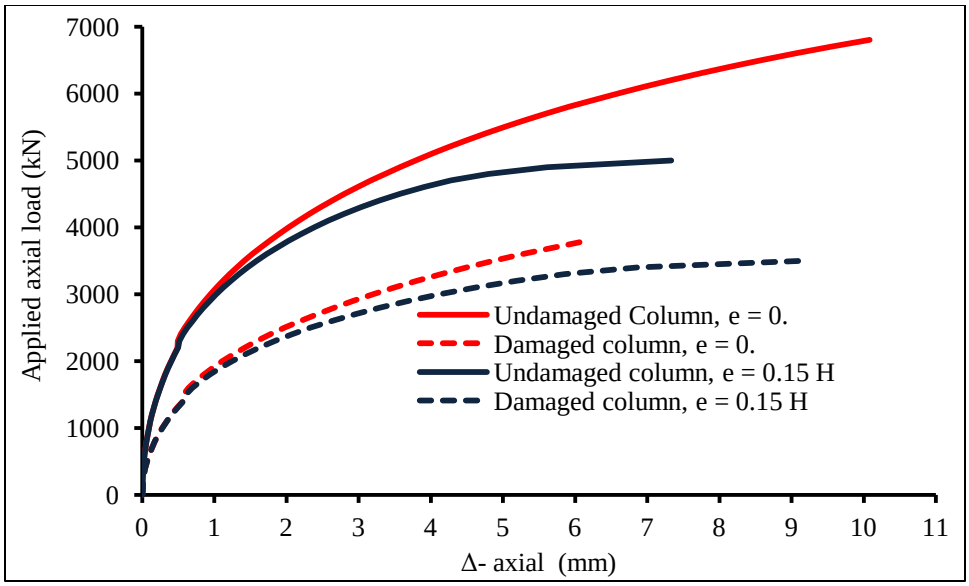

Figure 6.22: Applied axial load vs. axial displacement of the top section of the bridge column (right before static failure load); Bridge II.

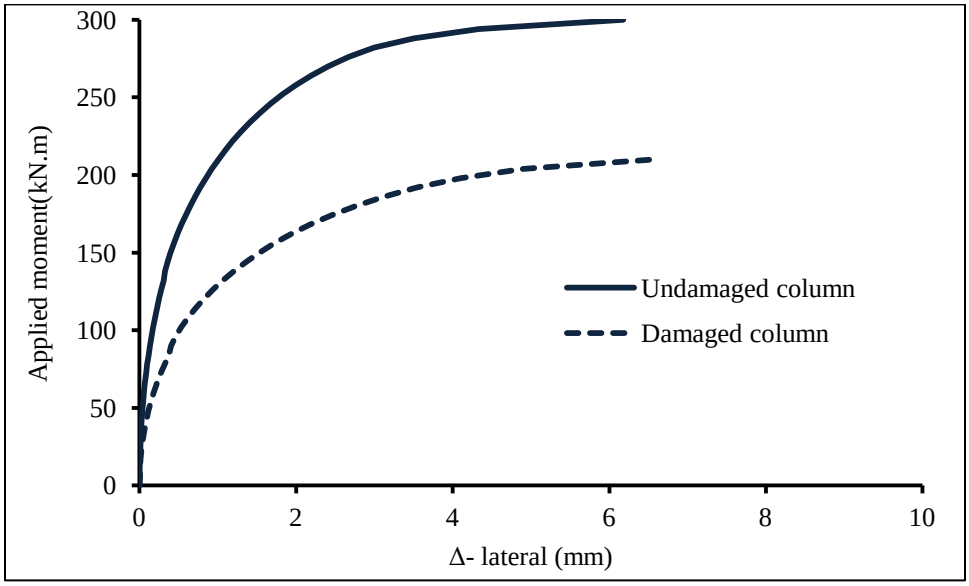

Figure 6.23: Applied moment vs. lateral displacement of the mid section of the bridge column right before static failure load; Bridge II.

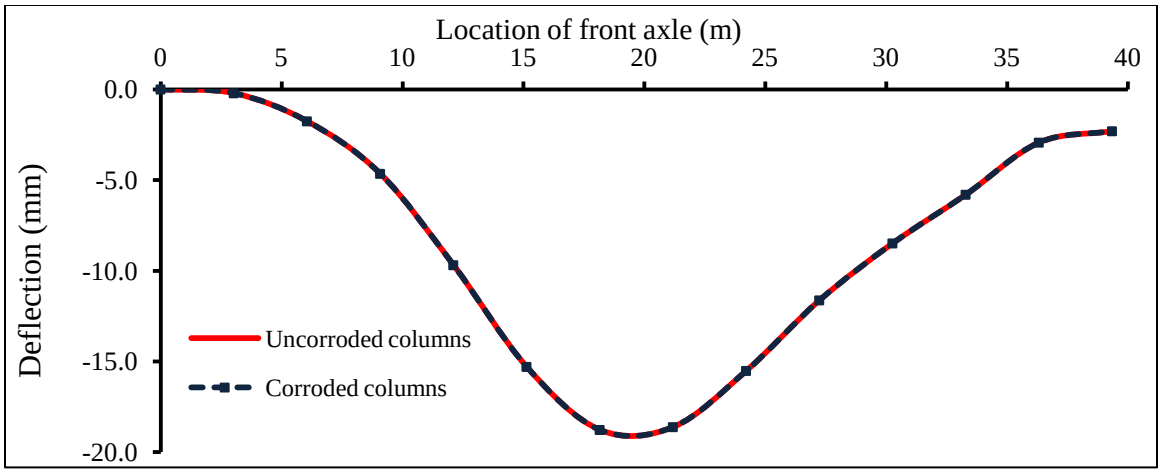

Figure 6.24: Comparison of dynamic deflections of superstructure under traffic load only and combined traffic and corrosion loads; Bridge II.

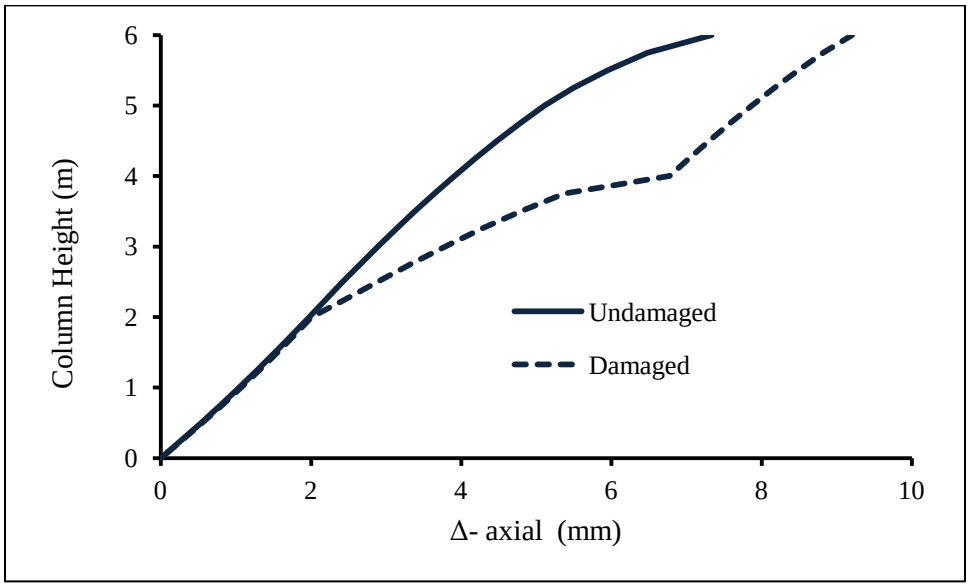

Figure 6.25: Column height vs. axial displacement of the bridge column at failure load; Bridge II.

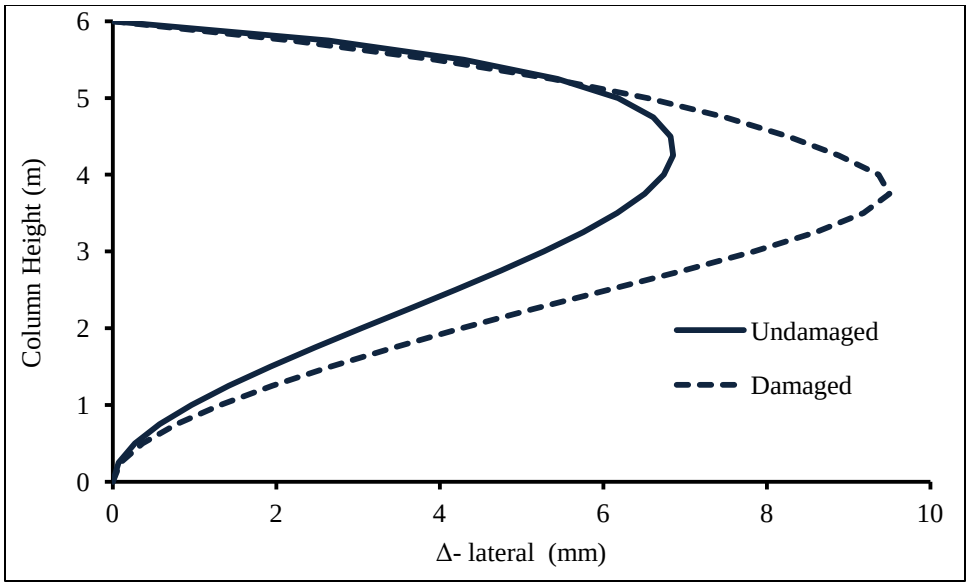

Figure 6.26: Column height vs. lateral displacement of the bridge column at failure load; Bridge II.

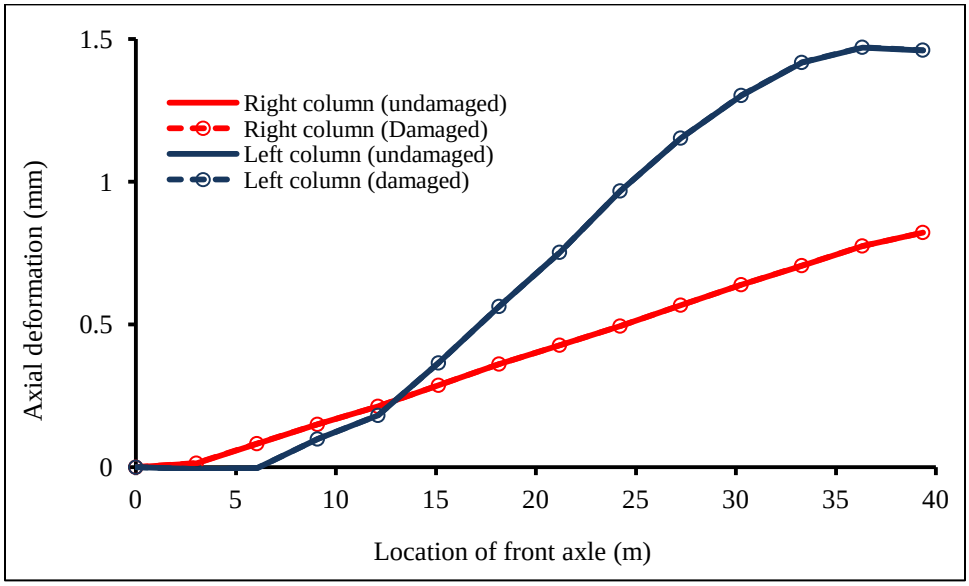

Figure 6.27: Truck position vs. maximum lateral deformation of the bridge columns; Bridge II.

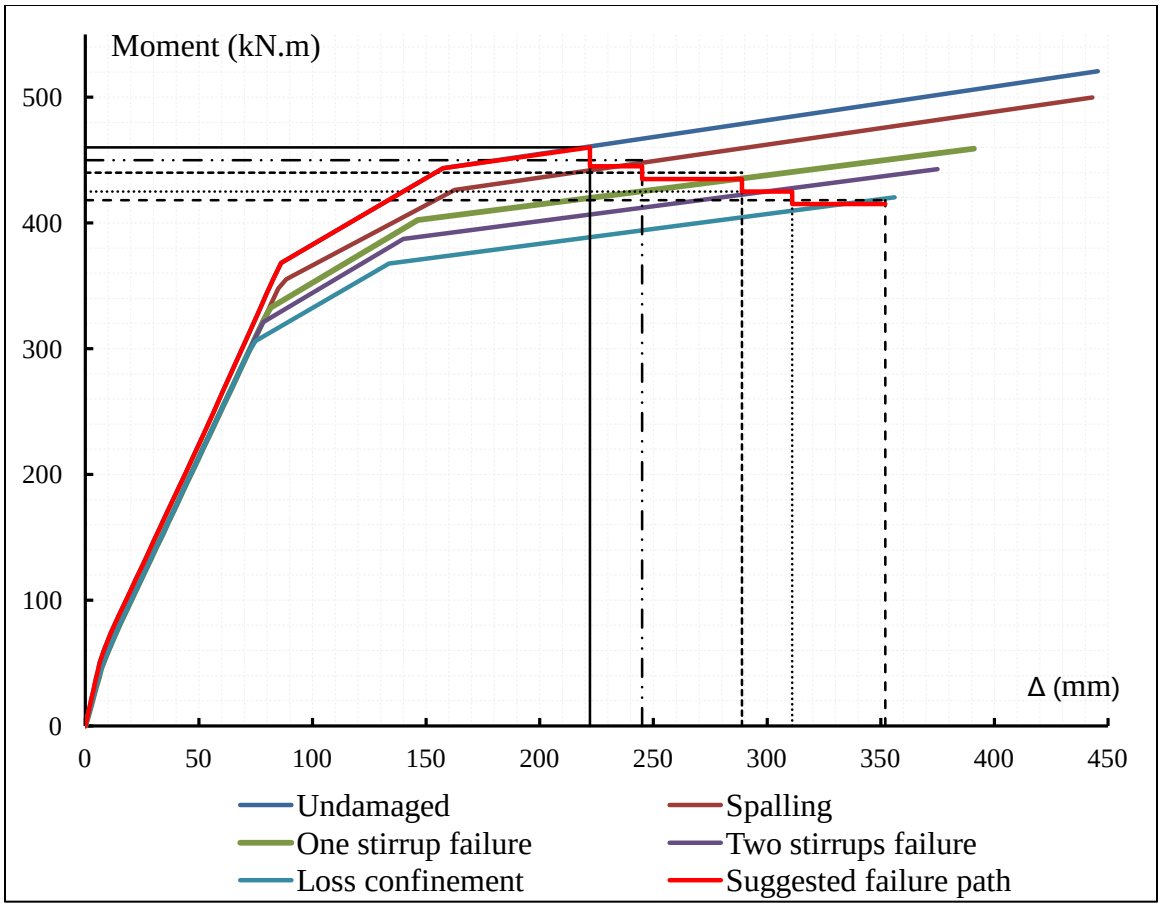

Figure 6.28: Envelope curve of load-displacement relationship of uncorroded column section; Bridge II.

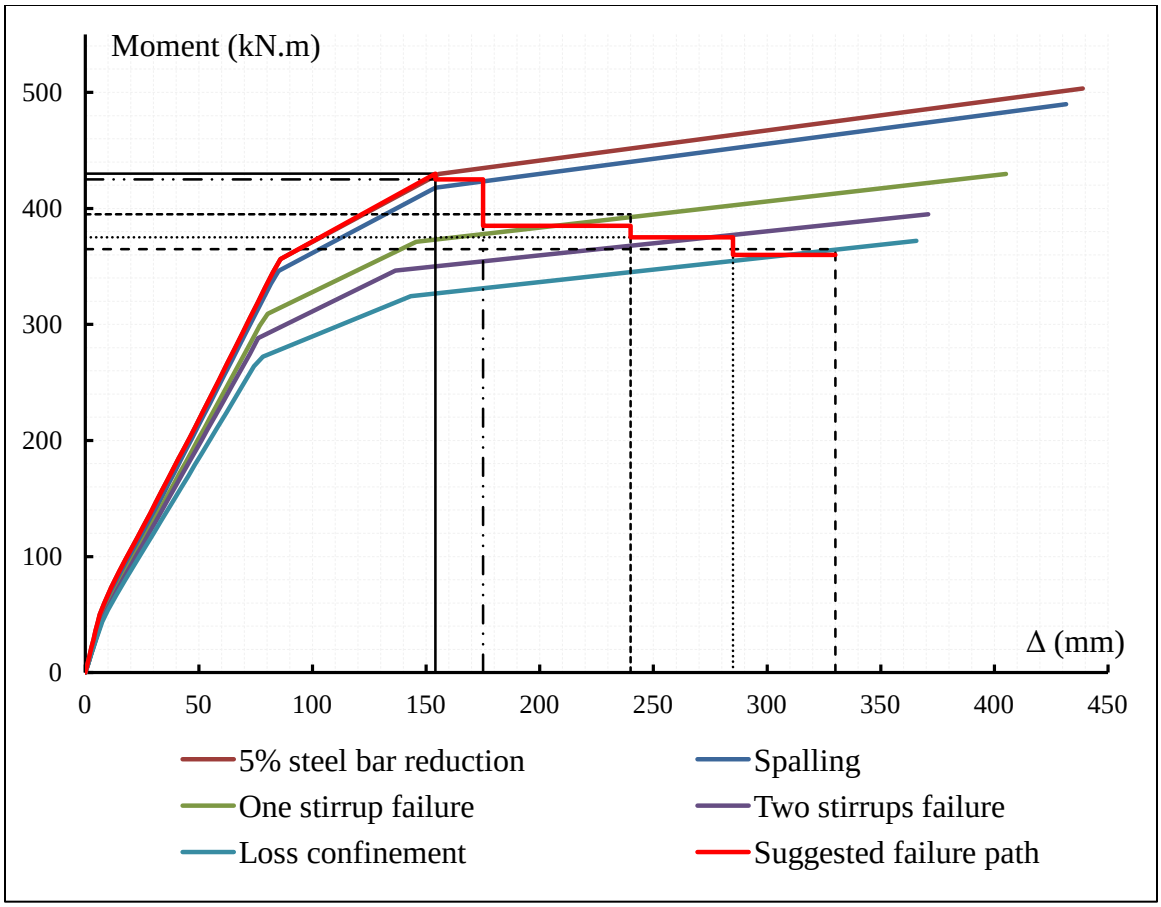

Figure 6.29: Envelope curve of load-displacement relationship of corroded column section; Bridge II.

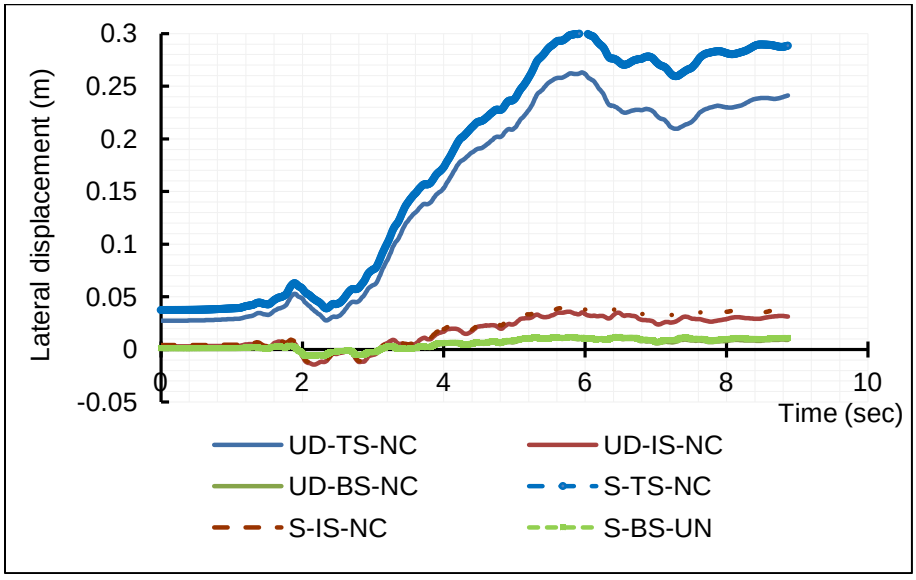

Figure 6.30: Lateral displacement for different sections of uncorroded column; Bridge II.

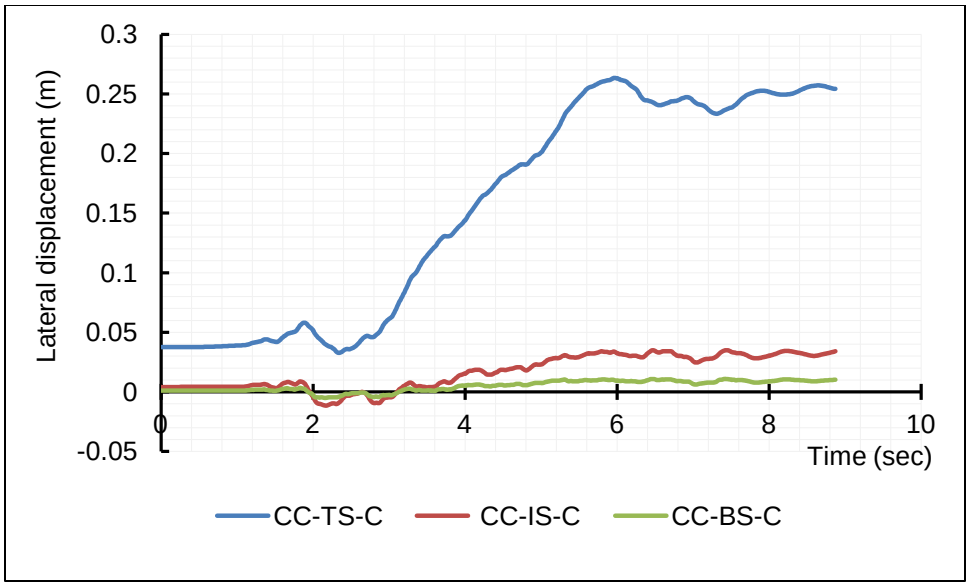

Figure 6.31: Lateral displacement for different sections of corroded column; Bridge II.

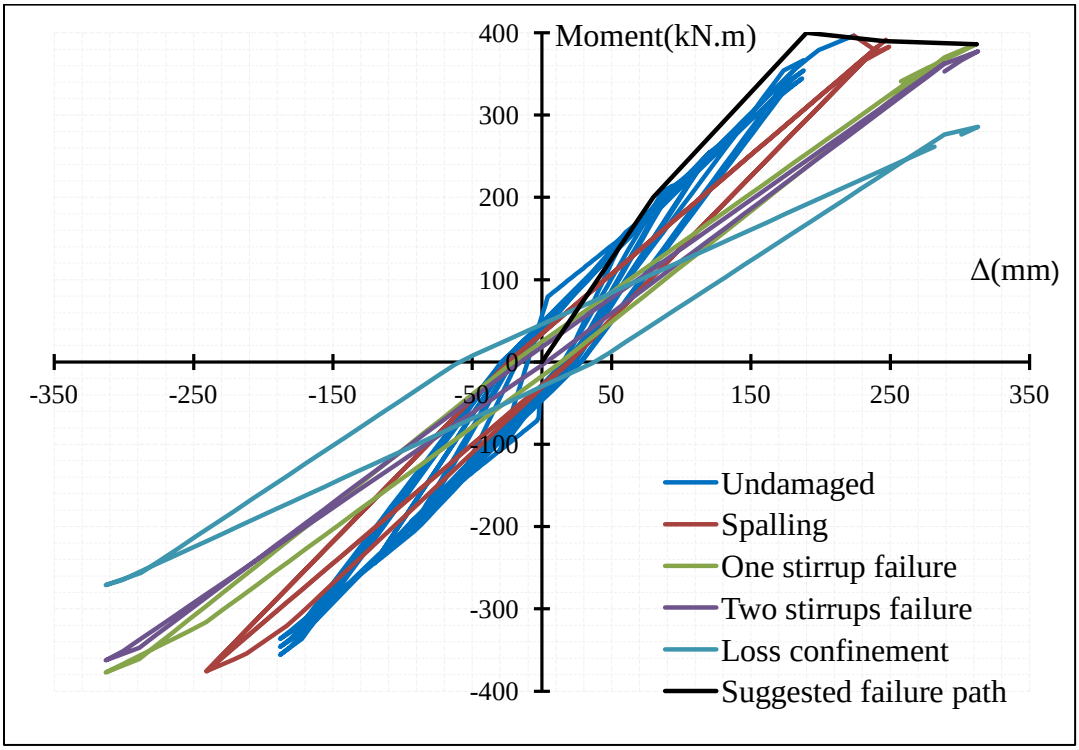

Figure 6.32: Load-displacement relationship of uncorroded column section; Bridge II.

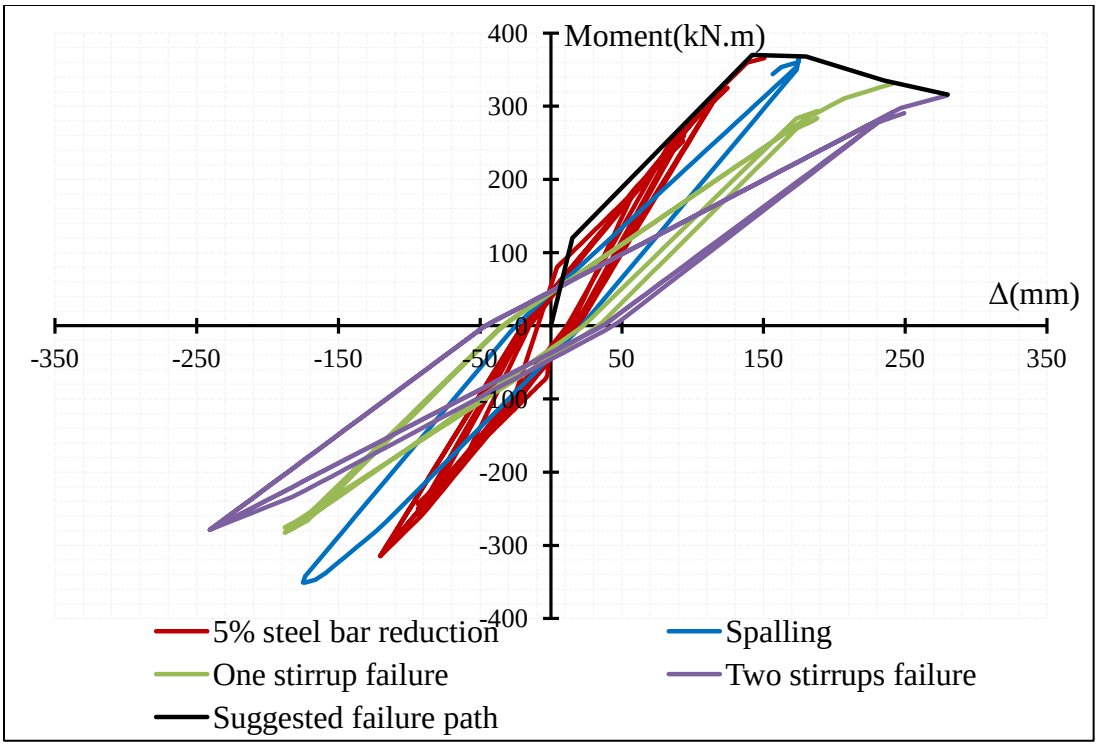

Figure 6.33: Load displacement relationship of relationship of corroded column section; Bridge II.

6.6 References

American Association of State Highway and Transportation Officials, AASHTO LRFD Bridge Design Specifications SI Units (4th Edition); 2007.

American Association of State Highway and Transportation Officials, Manual for condition evaluation of bridges, Washington, DC, 1994.

ASTM International, "Standard practice for preparing, cleaning, and evaluating corrosion test specimens." ASTM G1–03, West Conshohocken, PA; 2011

Branco, F. A., and Brito, J., Handbook of Concrete Bridge Management, ASCE Press, 2004.

Brown, G., Grave, S., Boorman, G., Bridge inspection standards - A review of international practice to benchmark bridge inspection standards for KiwiRail Network's bridges; Beca and KiwiRail; 2010.

Canadian Standards Association, Canadian Highway Bridge Design Code, S6-06, A; 2006.

Cairns, J., Plizzari, G. A., Du, Y., Law, D. W., Franzoni. Mechanical properties of corrosion reinforcement. ACI Materials Journal; 2005, 02(4): 256-264.

California Department of Transportation, Visual Catlog of Reinforced Concrete Bridge Damage. 2006.

Federal Highway Administration, Reliability of visual inspection for highway bridges, volume I: final report, FHWA-RD-01-020; June, 2001.

Hevener, W., Simplified live-load moment distribution factors for simple span slab on I-girder bridges. MSc. Thesis, Dept. Civil and Environmental Engineering, University of West Virginia, Morgantown,West Virginia,USA;2003, 151pages.

International Atomic Energy, Guidebook on non-destructive testing of concrete structures. Training course series No. 17. Vienna; 2002.

Lay, S. and Schiebl, P. Life cycle management of concrete infrastructures for improved sustainability. European Community Fifth Framework Program: GROWTH; 2003.

Lounis, Z., Vanier, D.J., Daigle, L., Sadiq, R., Almansour, H., Framework for Assessment of State, Performance and Management of Core Public Infrastructure, NRC Canada, Project 5332-Final Report; 2010.

Ministry of Transportation, Ontario, Ontario Structure Inspection Manual (OSIM), Policy, planning & Standards division engineering standards branch bridge office; April, 2008.

Mohammed, A., Almansour, H., Simplified non-linear FE model to predict staged capacity deterioration of RC columns subjected to combined ultimate or seismic and reinforcement corrosion loads. CSCE 3rd Specialty Conference on Material Engineering and Applied Mechanics, Montréal, Québec, Canada; 2013, May 29 to June1.

Mohammed, A., Almansour, H., Martín-Pérez, B., Nonlinear flexural analysis of reinforced concrete beam-column subjected to ultimate gravity loads combined with reinforcement corrosion, Part I: Sectional Analysis. Structure and Infrastructure Engineering, submitted, ID NSIE-2013-0261; 2013a.

Mohammed, A., Almansour, H., Martín-Pérez, B., Nonlinear flexural analysis of reinforced concrete beam-column subjected to ultimate gravity loads combined with reinforcement corrosion, Part II: finite element analysis. Structure and Infrastructure Engineering, submitted, ID NSIE-2013-0262; 2013b.

Mohammed, A., Almansour, H., Martín-Pérez, B., Evaluation of dynamic of slab-on-girder-bridge under moving trucks with corrosion-damaged columns", Engineering Structures, (6), 159-172;2014c.

Mohammed, A., Almansour, H., Martín-Pérez, B., Evaluation of seismic performance of slab-on-girder bridge columns subjected to reinforcement corrosion damages. Journal of Bridge Engineering (ASCE); to be submitted 2013d.

Mohammed, A., Almansour, H., Martín-Pérez, B., Semi-quantitative assessment framework for aging RC bridge columns. Engineering Failure Analysis; to be submitted 2013e.

Nutt, R. V., Schamber, R.A, and Zokaie, T., Distribution of wheel loads on highway bridges. Final report for national cooperative highway research program;1988.

Oyado, M., Saito, Y., Yasojima, A., and Kanakubo, T. Structural performance of corroded RC column under seismic Load. First International Workshop on Performance, Protection & Strengthening of Structures under Extreme Loading, Whistler, Canada; 2007.

Rashidi, M., Gibson, P., A methodology for bridge condition evaluation. Journal of Civil Engineering and Architecture; 2012, 6 (9), 1149-1157.

Chapter 7

Conclusions and Future Work

7.1 Introduction

This thesis is written in "paper format," wherein each chapter includes its own conclusions. However, for comprehensiveness, this chapter is added to combine all the conclusions and possible future work from all the chapters.

7.2 Summary of Conclusions

In this section, only the key conclusions are drawn from Chapters 2 through 6. The comprehensive conclusions of each chapter are presented at the end of each chapter. Following are the most significant conclusions:

- **The simplified nonlinear sectional analysis (NLSA) approach** presented in Chapter 2 is capable to simulate the mechanical behavior of reinforced concrete (RC) beam-columns at the sectional level for all possible loading situations including pure flexure, eccentric axial loading, or any loading state resulting from any combination of axial and flexural stresses. The approach is capable to integrate input data obtained from an enhanced inspection, including geometrical measurements of corrosion-damaged zones and any required material testing to identify the level of damage. The numerical integration of stresses over the section, which is divided into an arbitrary number of strips, improves the convergence and enables accelerated verification of the equilibrium. The number of strips in the numerical integration can be calibrated together with the load steps for the desired accuracy and high numerical efficiency. The proposed NLSA

shows high numerical stability and consistent convergence for all geometrical and material properties and loading cases. The NLSA presents a strong tool for practicing evaluation engineers to evaluate the structural capacity and behavior of beam-columns in critical sections.

- **The simplified nonlinear finite element analysis (NLFEA) approach** presented in Chapter 3 is capable of capturing the nonlinear structural behavior of corrosion-damaged aged beam-columns subjected to any possible loading. The results of the case studies lead to the general conclusion that critical sections identified in the design stage do not necessarily remain critical sections for the evaluation of an aged structure. The procedure proves to be numerically efficient and insensitive to values of the controlling parameters of the nonlinear analysis. It is also possible to integrate the proposed NLFEA into any nonlinear structural analysis program with minimum efforts for convergence.
- **The simplified hybrid linear/nonlinear dynamic finite element analysis (SHDFEA)** proposed in Chapter 4 proves to be numerically efficient and stable in all the studied cases. Although the nonlinear analysis presents the appropriate selection to evaluate the possible effects of the corrosion damage of the columns on the dynamic behaviour of the bridge, linear dynamic analysis is found to be a more economical alternative when the columns are overdesigned. It is also found that when the traffic load magnitude is well below the ultimate static capacity of the columns, even with severe local corrosion damage in the columns, their static behaviour remains mostly in the elastic range. This leads to a low sensitivity of

the dynamic parameters of the bridge structure to the corrosion damage of the columns, even though they could be in a state of critical safety and stability.

- **The simplified non-linear seismic analysis (SNLSA) approach** proposed in Chapter 5 is based on the nonlinear sectional analysis (NLSA) proposed in Chapter 2, the DRAIN-RC nonlinear time history analysis program, and Takeda hysteretic analysis. It proves to match experimental results with acceptable accuracy. It is found that the staged failure mechanism of the columns subjected to quasi-static load up to failure and to cyclic load up to failure can be simulated with very high accuracy using only the NLSA. It is also found that corrosion damage could result in a large drop of the column load and displacement capacities and large shrinkage in the hysteretic relationship, which indicates significant drops in the energy absorption capacities of the different columns. It is also concluded that for seismic critical zones, overdesign of the columns are recommended. Significant contraction of the column interaction capacity when subjected to severe corrosion damage for all load-over-capacity ratios is observed. This significant impact of reinforcement corrosion on the axial load-moment interaction relationship highlights the need for a conservative design of bridge columns in critical seismic zones when reinforcement corrosion is expected.
- **The semi-quantitative assessment framework (SQAF)** proposed in Chapter 6 evaluates slab-on-girder bridge columns subjected to reinforcement corrosion using the three evaluation limit states (ultimate, serviceability and earthquake limit states). The SQAF suggests the use of thresholds decided by the evaluation engineers based on the BMS requirements. The SQAF provides a systematic

assessment procedure that needs minimum numerical efforts, and it can be integrated into a bridge management system. It provides simplified analysis tools that enable practicing engineers to improve the accuracy and the cost effectiveness of the assessment of aging infrastructure. Although the framework is dependent on the accuracy of the input data, which is dependent on an enhanced inspection and any additional material testing, it presents a step towards the development of a fully quantitative assessment approach. The proposed assessment framework provides efficient analysis tools that help to quantify the important performance parameters of aged slab-on-girder bridge columns. The quantitative comparisons between the required and existing capacities or performance measures would give the bridge owners, practicing engineers and management team an accurate evaluation, leading to a reduction in the maintenance/rehabilitation cost and providing better safety. It also results in a reduction of the variation in the data collected using traditional inspection methods.

7.3 Future Work

1. Throughout the development and verification of the proposed nonlinear finite element analysis (NLFEA), there are several areas where future work can be envisioned, among which are:

i. Since NLFEA estimates the location of the neutral axis and the level of strains in every section over the length of the beam, then the depth of the flexural cracks can be estimated along the beam length. If the principal stresses can be interpolated in the shear critical zones, then the crack patterns in these zones can

also be estimated using the proposed analysis approach. Comparisons with available experimental results are important.

ii. It will be very interesting to develop an experimental program to examine the accuracy of the proposed NLFEA approach in estimating the effects of local bond failure on the stress redistribution, deformations, and failure mode of beam-column elements. It is also important to investigate the limitation of applicability of the proposed local bond loss model and the development of the arch action mechanism when an expansion of the bond failure zone occurs along the structural element (beam-column) length.

iii. Because of the inadequacy of the available experimental data, the verification case studies are limited to few sections and parameters. A comprehensive experimental program can improve the calibration of the NLFEA for optimum efficiency and accuracy.

2. Throughout the development and verification of the proposed simplified hybrid linear/nonlinear dynamic finite element analysis (SHDFEA), several areas where future work can be envisioned are:

i. To introduce corrosion damage on both the superstructure and the substructure of slab-on-girder bridges, continuous multi-span bridges, and frame bridges, and hence study the effects of traffic and corrosion-induced damage on the dynamic performance of these bridges.

ii. To investigate the effects of using recent standard multi-axle design truck on the dynamic performance of slab-on-girder bridges and frame bridges. A

comparison of the bridge dynamic performance under 2-axle and 5-axle moving trucks can be considered.

iii. Parametric study to identify and quantify a critical ratio of the superstructure stiffness to the substructure (column) stiffness, wherein the vibration is significant and cannot be ignored in evaluating the compound or coupling effects of traffic and corrosion on RC bridge columns behaviour.

iv. The nonlinear analysis of frame bridges with slender components (columns, and or beams) or slender rigid slab-abutment frame bridges, where new cost effective frame bridges are developed.

3. Throughout the development and verification of the simplified nonlinear seismic analysis (SNLSA) approach, several areas where future work can be explored are:

i. Experimental program investigating the structural behaviour of columns subjected to combined axial load and bending moment, localized reinforcement corrosion in different locations, and cyclic lateral loads. Such study should also focus on the bond loss to verify the proposed local bond loss model.

ii. Establish a comprehensive database incorporating all field observations, measurements and materials properties of corrosion-damaged bridge columns in high-risk seismic zones. This database together with the proposed SNLSA approach can improve bridge management and ensure infrastructure safety.

iii. Modeling the behaviour of RC frame bridges, RC continuous bridges, or RC multi-story frame parking garage elements subjected to reinforcement corrosion in high-risk seismic zones.

4. Throughout the development of the semi-quantitative assessment framework (SQAF) for aging reinforced concrete bridge columns, the following areas where future work can be conducted are identified as:

i. Develop a Windows-graphical interface for the framework and all its analysis approaches. The input and output can be graphical and a full assessment report can be printed according to user-controlled format.

ii. Develop a provincial or national database for deteriorated materials properties, damage locations and size, and history of inspection/assessment/rehabilitation. This database can be integrated with the SQAF to provide practical and simplified integration with a BMS.

iii. Integrate the time-dependent processes using higher level analytical approaches and hence moving forward to a fully quantitative assessment approach.

Appendix A

This paper is a reproduction of the conference paper that was published at the CSCE 3rd International Structural Specialty Conference, Edmonton, Alberta, Canada; 2012.

State-of-the-Art in Nonlinear Modeling of Concrete Frame Structures under the Combined Effect of Ultimate Loading and Reinforcement Corrosion

Abstract: Evaluating the structural safety and the ultimate capacity of frame structures is a major concern to infrastructure owners, engineers and researchers. Nonlinear modeling of reinforced concrete (RC) frames has become more important in the recent efforts to assess ultimate structural capacity of RC structures under the combined effect of mechanical and environmental loading. This paper presents a critical review of the state of the art in modeling the behaviour of RC structures when subjected to combined ultimate or service loads and corrosion of steel reinforcement. The paper addresses the need for development of a comprehensive nonlinear model that is conceptually simple yet numerically efficient, capable to capture all stages of damage and the structural behaviour and capacity with high accuracy and that can be integrated into a quantitative inspection process.

A1. Introduction

Typically, assessment of aging bridge structures is based on visual inspection where the level of deterioration/damage is rated qualitatively; however, integration of a simplified quantitative evaluation approach with the existing visual inspection could lead to a more accurate assessment and hence a cost-effective infrastructure management. This evaluation/ assessment requires the development of accurate, yet simplified, analysis tools that can estimate the ultimate capacity and mode of failure of deteriorated structures based on the state of damage due to reinforcement

corrosion. Nevertheless, limited efforts have been directed to the development of such analysis tools, where the combined effect of corrosion and ultimate load on non-linear elastoplastic mechanical behaviour is modeled.

With the advances in the understanding of failure mechanisms of reinforced concrete structures (RCS), nonlinear modeling of RC frames has become more important in recent efforts on exploring structural performance and ultimate capacity of aging RCS. In the past 40 years, various models have been developed to simulate the non-linear elasto-plastic structural behaviour of “newly constructed” RCS. Most of these models focus on the material nonlinearity of both the concrete and the reinforcing steel. Different nonlinear analytical, sectional, one- and two- dimensional finite element approaches have been introduced or adopted where the focus was on one or more of the following: (i) high numerical efficiency; (ii) high accuracy and best match with experimental results; (iii) simplicity of the model; or (iv) high level fracture mechanics techniques. On the other hand, many researchers have introduced simplified or advanced models to predict the effect of corrosion on concrete and reinforcement steel. However, limited studies have been conducted on the nonlinear behaviour of corrosion-induced damaged concrete structures.

On the other hand, the corrosion process of the steel reinforcement and the resulting changes in the mechanical properties of both the concrete and the steel can result in significant variation of the nonlinear behaviour of deteriorated concrete structures when the structure is subjected to an extreme (or ultimate) loading condition. Thus evaluating the structural safety and the ultimate capacity of frame structures compared to their original design capacities is of major concern to owners, engineers, and researchers.

The aim of this paper is to review the state of the art in nonlinear modeling of newly constructed or deteriorated reinforced concrete frame structures. It presents the requirements for a numerically efficient and accurate nonlinear model that enables the evaluation of ultimate capacity of reinforced concrete frames and modes of possible failures when subjected to simultaneous mechanical loading and reinforcement corrosion.

A2. Limit state design and nonlinear analysis of RC

The knowledge of the behaviour of structural concrete has increased with the advances in testing of reinforced concrete elements. It has been observed that reinforced concrete sections behave inelastically at high loads, and the elastic theory cannot give a reliable prediction of the ultimate strength of RC members, since inelastic strains, cracks, tension stiffening, etc, are not taken into account. Deficiencies in the elastic method have become evident, and the need for inelastic or elastoplastic analysis approaches that accurately predict reinforced concrete structures has been recognized. With the adoption of limit state design by most of the world design codes, it has been recognized that estimation of the ultimate strength and deformation capacities and the possible mode of failures is essential for structural design. On the other hand, the structural performance of structural elements and systems under service loads is related to a structural response that is in the elastic range. Both linear elastic and nonlinear elasto-plastic structural analysis approaches are used in the design/evaluation processes. In order to enable fast and accurate structural analysis, many computer algorithms have been developed; however, their numerical efficiency, sensitivity to convergence with the use of explicit or numerical integration procedures, etc, become of major interest to researchers.

A3. Development on non-linear modeling techniques

It is traditionally believed that Galileo Galilei made the first attempts at developing a theory of beams, but recent studies (Ballarini 2003) argue that Leonardo da Vinci was the first to make the crucial observations. Da Vinci lacked Hooke's law and calculus to complete the theory, whereas Galileo was held back by an incorrect assumption he made (Timoshenko 1953). Leonhard Euler and Daniel Bernoulli were the first to put together a useful theory circa 1750 (Han et al 1999). At the time, science and engineering were generally seen as very distinct fields, and there was considerable doubt that a mathematical product of academia could be trusted for practical safety applications. Bridges and buildings continued to be designed by precedent until the late 19th century, when the Eiffel Tower and Ferris wheel demonstrated the validity of the theory on large scales (William 2006).

Beam theory, and all further developments, was based on the assumption of elastic behaviour and small range of deformations. With the introduction of reinforced concrete in the early twentieth century, the concept of using a composite section built from two different materials was introduced, where the development of consistent behaviour and the evaluation of the force-deformation relationship throughout the loading-to-failure process were new challenges to the theory that had just been adopted in structural design. The focus in the following paragraphs is on recent developments in the area of non-linear elasto-plastic modeling of RC structures.

A3.1 Semi-analytical approaches

Several different semi-analytical models have been proposed in the past 40 years to represent nonlinear behaviour of RC structures. Lazaro and Richards (1973), Gunnin et al. (1977), and Carol and Murica (1989 a & b) proposed the use of special types of elements that were compatible with special geometric characteristics of RC frame structures. These elements were

rather linear elements with a stiffness mass formulation that was based on certain distribution of section rigidities. These elements were based on nonstandard frame element formulations and assumptions such as neglecting axial deformations, inserting internal degrees of freedom and using finite difference approximating schemes. They depended on simplified moment-curvature relationships and stiffness variations along the elements or on layered- section analysis algorithms. Resheidat et al. (1995) developed an analytical model to calculate the flexural rigidity of an RC column subjected to short-term axial load and biaxial bending. Material properties, steel ratio and axial load were taken into account for establishing a new equation that calculated the flexural rigidity of the column and its effects at yield curvature. This approach does not require considerable memory storage and processing time when implemented in a computer program for nonlinear analysis of large structures. Using such models results in considerable saving in computational cost and human effort; however, these models are usually made as ready-formulation packages, which become more sensitive leading to inaccurate results.

A3.2 Numerical models

Considerable efforts have been made to develop numerical models to represent the nonlinear behaviour of RC frames. One- and two-dimensional nonlinear finite element (FE) procedures have been introduced. The focus has been on high accuracy and calibration of the model to match the available experimental results, and sometimes on the numerical efficiency in terms of computing time and memory. Kreonke et al. (1973) and Pulmano et al. (1987) developed nonlinear analysis schemes of RC frames using one-dimensional FE in which computations were made incrementally to track the variations in section rigidity during load applications, and the inelastic material properties and stiffness of a beam-column element were characterized. Rasheed and Dinno (1994a) presented an incremental iterative analysis algorithm where nonlinear section

response was traced through the use of the explicit expressions of nonlinear section properties. In this model, a fourth-degree polynomial proposed by Kabaila (1964) and Basu (1967) was used to represent the concrete stress-strain relation in compression, while Gilbert and Warner (1978) model was used to represent a concrete stress-strain relation in the tensile zone, where tension softening was taken into account, noting that tension stiffening and local bond-slip effects were combined. A bilinear relation was adopted to simulate the stress-strain relation for reinforcing steel. The results of this model were compared to experimental results conducted by Espion and Halleux (1988). Although very good agreement was shown by the authors, the section response under high axial force, where the axial compression stress over the section is much higher than the tensile stresses resulting from flexure was not discussed. In Rasheed and Dinno (1994b), a closed-form expression of the elements of the stiffness matrix for two types of frame elements was derived. Both models, the sectional and the explicit closed-formed stiffness matrix, are very sensitive and the convergence in the iterative stages can only be reached using a properties-dependent increment.

Bentz (2000) proposed non-linear sectional analysis for different types of RC elements. The model is based on assuming (i) Euler- Bernoulli assumption that plane sections remain plane after deformation; (ii) there is no transverse clamping stress; and (iii) the biaxial behaviour can be modeled using the Modified Compression Field Theory. In this model, analysis of beams and columns subjected to arbitrary combinations of axial load, moment and shear were presented by one computer program (Resopnse-2000). Response-2000 proved to give very good match with experimental results. However, Response-2000 did not include the confinement effects on compression concrete members.

A3.3 Material models

The stress-strain relationship of the concrete is not only nonlinear, but also its trend is different from tension to compression. Reinforcing steel, on the other hand, has a similar stress-strain relationship in both tension and compression provided that no local buckling of the bars is expected. Modeling the stress-strain relationship of concrete in compression has been widely investigated; among many models presented in the literature, three models will be discussed in this paper. One of the widely accepted models is proposed by Hognestad in 1951. It consists of a second-order relationship (parabola) up to the ultimate stress and then a linearly dropping stress with the increase of strain up to failure. A fourth-degree polynomial was then proposed by Kabaila (1964) and Basu (1967) where the post ultimate behaviour was considered more precisely.

Transverse reinforcement, in form of closely spaced steel spirals or hoops, generally provides confinement of a concrete element's section. With low axial concrete stress levels, the concrete is unconfined. At stresses approaching the uniaxial concrete strength, the confinement becomes much effective, and the transverse strains become high because of the progressive internal cracking and the concrete bearing out against the transverse reinforcement. In fact, many researchers confirmed experimentally that the confinement can improve the stress-strain characteristics of the concrete as the lateral expansion of the concrete is restricted (Kent and Park 1970). Saatcioglu and Razvi (1992) modified the stress-strain relationship for confined and unconfined concrete taking into account the details of the reinforcement. The model can be applied to almost all popular cross-sectional shapes and different reinforcement arrangements. For unconfined cover concrete or the entire column section when the axial stress is low and the confinement of concrete core is negligible, the model assumes less strength and deformation capacity than those in Hognestad's model. As the lateral pressure is increased due to the

confinement, Saatcioglu and Razvi model shows that the concrete strength and ductility are enhanced significantly due to the increase of the lateral confinement pressure. The model always safely gives slight underestimation, and hence it is very useful in practice; however, it is not applicable if the applied axial load is less that 10% of the member axial capacity, and it gives underestimation when no ties/stirrups are distributed in some regions of the RC member.

Gilbert and Warner (1978) proposed a model to represent the tensile behaviour taking into account tension softening, tension stiffening and local bond-slip effects. The concrete in tension was assumed to behave linearly up to the first crack, where the initial tangent modulus in tension is set equal to the initial tangent modulus in compression, followed by a linear descending branch which represents strain softening. On the other hand, the stress-strain relationship for reinforcing bars has two general simplified representations, bilinear and trilinear relationships. In both models, the elasto-plastic behaviour is simulated with or without introducing strain hardening. Using such models has proved to give very good match with experimental results, and for more accurate representation the steel test data can be used; however, this would highly complicate the nonlinear model.

A4. Modeling of corrosion effects on reinforcing steel and concrete

In many parts of the world, corrosion of reinforcement is the main cause of the deterioration of concrete structures. The effects of reinforcement corrosion on the RC sections are: (i) reduction of the affected steel bars cross-sectional area and its ductility, (ii) reduction of concrete section as a result of longitudinal cracking and spalling, and (iii) losses of bond between rebars and concrete. These effects can cause reduction of the structural safety and capacity. Figure A.1

summarizes the main effects of reinforcement corrosion on the behaviour of concrete structures (Rodríguez et al. 1996).

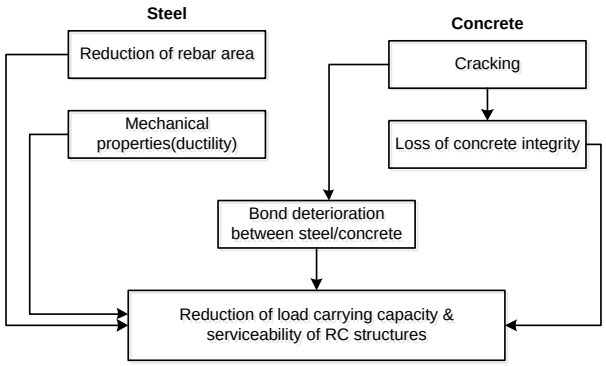

Figure A.1: Effects of reinforcement corrosion on RC structures (Rodríguez et al., 1996)

Change in structural performance of deteriorated RC elements depends on the location of the corrosion-affected zone and level of damage. For instance, it has been observed that stirrups/ties are more vulnerable to corrosion than longitudinal bars as they are closer to the RC concrete element external surface and they have greater perimeter/cross-sectional area ratio. They start corroding earlier than longitudinal reinforcement. It has been observed that localized concentrated corrosion with high rate leaded to larger rebar cross-section reduction. The reduction in structural performance/capacity due to stirrups corrosion could be serious specifically in RC columns as they provide the major component of the shear resistance, confinement of the concrete core and bracing of the longitudinal reinforcement. Significant effect of stirrups corrosion on axial and bending moment carrying capacity of deteriorated RC columns has been observed by Rodríguez et al. (1996) and Tapan and Aboutaha (2009).

Several experimental studies (Al-sulaimain el al. 1996; Mangat et al. 1999a; Cabrera 1996; Castel et al. 2000; Yubun et al. 2000; Li et al. 2005; Torres-Acosta et al. 2007) have been carried out to investigate the effect of corrosion on the serviceability and ultimate capacity of

deteriorated RC elements. Their major objectives were to evaluate the effect of reinforcement corrosion on RC element ductility, rebar-concrete bond behaviour and bond strength, change in failure modes of RC structures, and the effect of loading levels and corrosion rates on the concrete cracking, bond strength, deflection and residual loading capacity of flexural members. Rodríguez et al. (1996) conducted a comprehensive experimental study on RC columns subjected to reinforcement corrosion where they evaluated the effects of steel corrosion on the RC column behaviour. The authors observed that reinforcement corrosion reduced the column axial capacity and introduced a load eccentricity due to spalling of the concrete cover that led to buckling of the longitudinal reinforcement due to loss of one or more columns ties. The most important observations that can be made from the mentioned studies are that the reduction in ultimate flexural strength is attributed to the loss in the steel cross section and degradation in the bond between reinforcement and concrete and the steel ductility.

Recently, an analytical model to evaluate the load carrying capacity of deteriorated bridge columns was presented by Tapan and Aboutaha (2009 and 2011). They developed moment-axial load (M-P) interaction diagrams using modified analysis procedures and advanced deteriorated material models. The results of their model showed that the amount of strength loss depends on the location of the corrosion-affected zone and level of corrosion and related damage on the RC element cross-section. It is indicated that corrosion of tension reinforcement causes more strength reduction than corrosion of reinforcement in compression or “side” reinforcement (or reinforcement distributed in the sides parallel to the moment plane of action). The authors did not investigate the effect of stirrups/ties corrosion on shear capacity deterioration of the studied RC columns.

It was observed that the effects of pitting corrosion (or localized corrosion with high rate) is more significant on the RC element structural performance than general (or uniform) corrosion, and if occurring at critical links/stirrups it may result in premature buckling of the main bars (Rodríguez et al. 1996). Many empirical models for loss of cross-sectional area of reinforcement and loss of strength and ductility of reinforcement have been proposed. A recent study by Du et al. (2005a and 2005b) has introduced the following empirical equations to assess the cross-sectional area (A_s), yield strength (f), yield and ultimate strength (ε_y, ε_u) of corroded reinforcement;

$$A_s = A_{so} (1-0.01Q_{corr}) \quad (A.1)$$

$$f = (1-0.05Q_{corr}) f_y \quad (A.2)$$

$$\varepsilon_y = (1-0.05Q_{corr}) \varepsilon_{yo} \quad (A.3)$$

$$\varepsilon_u = (1-0.05Q_{corr}) \varepsilon_{uo} \quad (A.4)$$

where A_{so} is initial cross-sectional area, f_y is the yield strength, ε_{yo} is the yield strain, and ε_{uo} is the ultimate strain of uncorroded reinforcement, Q_{corr} is the amount of corrosion of reinforcement (Q_{corr} =0.046 (I_{corr}/d) t) ,I_{corr} is the corrosion rate of reinforcement in real structure ($\mu A/cm^2$), d is the diameter of the uncorroded reinforcement, and t is the time elapsed since the initiation of corrosion in years.

Rodríguez et al. 1996, Saito et al. 2007, and Oyado et al. 2007 carried out experimental work to study the behaviour of RC columns affected by reinforcement corrosion. They observed that some delamination of the concrete cover occurred on one or more sides of the corroded column. Saito et al. 2007, and Oyado et al. 2007 reported that corrosion-induced damage of the concrete

cover (due to cracking, delamination and/or spalling) significantly reduces the column load capacity under static loading conditions, accelerates the degradation of the capacity under cyclic/seismic loading conditions, and significantly reduces the energy absorption capacity of the columns. El Maaddawy et al. (2005) determined a relationship between the corrosion crack width and the degree of corrosion in terms of the percentage of the steel mass loss. Tapan and Aboutaha (2011) conducted analytical work to quantify the effect of reinforcement corrosion and loss of concrete cover on the structural behaviour of bridge columns. In their study, corrosion-induced cracking was simulated by considering the ratio of concrete cover to longitudinal reinforcement diameter, which plays an important role in the load carrying capacity of deteriorated RC columns. Numerical models, especially finite element models FEM, for predicting the time required for corrosion cracks to initiate and propagate have been widely presented. Numerous cracking models, such as smeared cracking, have been used to model corrosion-induced cracking of the concrete cover (Molina et al. 1993).

Many empirical and analytical models for the prediction of bond strength reduction due to reinforcement corrosion had been proposed. Kemp and Wilhelm (1979) proposed an empirical equation based on experimental work to determine the maximum bond stress of uncorroded RC beams, which consists of two components: the contribution of the concrete and the stirrups to the bond strength; later on, Saifullah and Clark (1994) proposed an empirical factor to predict the change in the bond strength due to reinforcement corrosion. This empirical factor was used to predict an initial increase in bond before concrete cracking and a reduction in bond as the percentage of steel mass loss due to corrosion increases. El Maaddawy et al. (2005) presented a numerical model to predict nonlinear flexural behaviour of corroded RC beams. In their study, the deflection of an RC beam was calculated using elongation of the steel reinforcement between

flexural cracks involving the effects of corrosion on the bond. Bhargava et al. (2007) proposed a more general empirical model in their study, where they presented an interesting comparison between many analytical and empirical models for prediction of bond strength when corrosion of reinforcement takes place. They suggested a general methodology to evaluate the flexural strength of RC beams that are corrosion damaged with significant loss of bond. Their model results were compared to test results and results from empirical formulae derived by other researchers.

Coronelli et al. (2002) and Deksoster et al. (2003) presented a general or simplified FEM to assess the global flexural behaviour of corroded reinforced concrete beams. The major concerns were to investigate the relationship between the degree of corrosion and the load capacity of RC elements, and to evaluate the maximum deflection and the related progressive reduction in element flexural stiffness. These models showed a good correlation with experimental results.

A more comprehensive finite element model based on a staged deterioration mechanism is to be proposed by Mohammed et al (to be submitted shortly for possible publication) taking into account the corrosion of both the longitudinal and lateral (stirrups/ties) reinforcement, possibly spalling, effects on level of confinement, the location of the corrosion-affected zone in relation to the critical zones for flexure and shear, reduction in bond and reinforcement ductility, and the progressive change in eccentricity.

A5. Combined versus coupled effects of loading and corrosion on RC structures

In general, literature related to structural performance of corroded RC structures is limited. Few experimental attempts have been conducted to understand structural performance of RC flexural elements under the combined/coupled effects of loading and corrosion. Yoon et al (2000)

conducted an experimental study to investigate the interaction between service level loading and corrosion on RC beams. They performed two series of experiments; one was to investigate the influence of pre-cracking or pre-loading on reinforcement corrosion, and the other was to study the influence of sustained loading on the corrosion process. The major observations were: (i) loading history and level have significant effects on both corrosion initiation and rate of propagation of corrosion; (ii) the failure mode of RC beams shifts from a shear failure to bond splitting as the degree of corrosion increased. Ballim et al. (2001) conducted experiment work to display the coupled effect of simultaneous loading and steel corrosion. In their set up, the reinforcement corrosion was accelerated while the load was applied. Their objective was to illustrate the significance of assessing the structural effects of reinforcement corrosion under simultaneous load. El Maaddawy et al. (2005 a & b) presented an analytical model and an experimental study to predict the nonlinear flexural behaviour of corroded RC beams. The analytical model was developed to investigate the combined effect of corrosion and sustained loads on the structural performance of RC beams. It accounted for the effects of the reduction in the steel area and the change in bond strength due to reinforcement corrosion. Experimental results showed that the time to corrosion cracking was significantly reduced, and the corrosion crack width was slightly increased by the presence of a sustained load. They also observed that there is no correlation between the reduction in the beam strength and presence of flexural cracks. Their results from the analytical model showed very good agreement with experimental results. Yingang et al. (2007) experimentally studied the combined effect of loading level and corrosion rate on the deflection and residual loading capacity of flexural members. They observed that beside the reduction in beam flexural strength (when the degree of corrosion

increased and the location of corrosion changed), its failure mode alters and its ductility behaviour affects.

Recent studies conducted by Saito et al. (2007) and Oyado et al. (2007) have aimed at providing better understanding of the behaviour of corroded RC columns under combined uniaxial compression, seismic, and corrosion loads, which may lead to quantify the safety and performance of aging RC members when subjected to service and earthquake loads. The studies presented the results of two sets of tests: (1) column specimens subjected to axial compression and corrosion load; and (2) column specimens that are exposed to axial, cyclic, and corrosion loads. In both test sets, the parameters were the length of corroded reinforcement, the simulation method of corrosion, and the corrosion level. They observed that corrosion of hoops causes reduction of deformation capacity, energy absorption and axial strength, and corrosion of the main reinforcement leads to the buckling of main bars, which further reduces the deformation and strength capacity. Berto et al. (2008) carried out a theoretical work to assess the corrosion effects on the seismic behaviour of RC structures, where the nonlinear analysis was performed using the general–purpose code MIDAS Gen. Choe et al. (2008) performed a numerical approach, using a commercial software (OpenSees), to develop probabilistic drift and shear force capacity models by integrating the effects of deterioration of corroded structural elements into a structural capacity model.

A6. Future outlook

The preceding sections outline recent development in experimental, analytical and numerical modeling of structural performance of RC structures subjected to combined mechanical and corrosion loads. This critical review shows that it is difficult to simulate the real behaviour of

damaged structures without deep and thorough understanding of all aspects of the deterioration mechanisms, damage stages and their effect on flexural and shear stiffness, ductility of materials and structural elements, progressive changes of internal forces and stress distributions due to spalling, mass losses, etc. On the other hand, integrating the mentioned aspects related to corrosion with nonlinear modeling of structural elements can provide insight on multiple possible failure mechanisms. A comprehensive model based on a staged deterioration mechanism to simulate the nonlinear behaviour of aged corrosion affected RC beams and columns subjected to possible ultimate loading is highly required to build an efficient quantitative structural assessment/evaluation tool. The model has to be numerically efficient and capable to simulate the mechanical behaviour at the section level and at the structural element level to predict all major structural parameters as well as possible modes of failure.

A7. Summary

This paper presents a critical review of the state of the art in modeling the behaviour of RC structures when subjected to combined ultimate and service loads and corrosion of steel reinforcement. The paper shows that the present methods of assessment of aging bridge structures is based on visual inspection where the level of deterioration/damage is rated qualitatively; however, integration of a simplified quantitative evaluation approach with the existing visual inspection could lead to more accurate assessment and hence a cost-effective infrastructure management. This evaluation/ assessment requires the development of accurate, yet simplified, analysis tools that can estimate the ultimate capacity and mode of failure of deteriorated structures based on the state of damage due to reinforcement corrosion. Nevertheless, limited efforts have been directed to the development of such analysis tools, where

the combined effects of corrosion and ultimate load on non-linear elastoplastic mechanical behaviour and damage stages are modeled.

A8. References

Al-Sulaimain, A., Al-Gahtani, S. M., Aziz R., Dakil, H., and Rasheeduzzafar.Effect of Reinforcement corrosion on Flexural Behaviour of concrete Slabs. Journal of Materials in Civil Engineering;1996, 8(2), 123-127.

Ballarini, Roberto. The Da Vinci-Euler-Bernoulli Beam Theory?. Mechanical Engineering Magazine Online (2003).

Ballim, Y., Reid, J., Kemp, A., Deflection of RC beams under simultaneous load and steel corrosion. ACI Magazine of Concrete Research;2001,53(3),171-181.

Basu. K., Computation of failure loads of composite column. Inst. Civ. Engrs;1967, London, 36: 557-578.

Bentz, E., Sectional analysis of reinforced concrete. PhD. Thesis, Dept. of Civil Engineering, University of Toronto, Toronto, Canada;2000, 318pp.

Berto, L., Vitaliani, R., Saetta, A., and Simion, P., Seismic assessment of existing structures affected by degradation phenomena. Structural Safety;2008, 31 (4),284-297.

Bhargava, K., Ghosh A. K., Mroi Y., and Ramanujam S. corrosion-induced bond strength degradation in reinforced concrete- analytical and empirical models. Nuclear Engineering and design;2007, 237,1140-1157

Cabrera, J. G., 1996.Deterioration of concrete due to reinforcement steel corrosion. Cement and Concrete Composites;1996, 18(1), 47-59.

Castel, A., François, R., and Arliguie, G., Mechanical behaviour of corroded reinforced concrete beams-Part 1: experimental study of corroded beams. Materials and Structures;2000, 33(9), 539-544.

Carol, I., and Murcia, J., Nonlinear time-dependent analysis of planar frames using an exact formulation –I. Theory. Computer and structures;1989. 33: 79-87.

Carol, I., and Murcia, J., Nonlinear time-dependent analysis of planar frames using an exact formulation –II. Structures and examples. Computer and structures;1989. 33: 89-102.

Choe, D.-F., Gardoni, P., Rosowsky, D., and Haukaas, T., Probabilistic capacity models and seismic fragility estimates for RC columns subject to corrosion. Reliability Engineering and System Safety;2008,93(3),383-393.

Coronelli, D. 2002 .Corrosion Cracking and Bond Strength Modeling for Corroded Bars in Reinforced Concrete. ACI Structural Journal;2002, 99(3), 267-276.

Du, Y., Clark, L., and Chan, A., Effect of corrosion on ductility of reinforcing bars. Mag. Concrete Res.;2005a,57(7):407-419.

Du, Y., Clark, L., and Chan, A., Residual capacity of corroded reinforcing bars. Mag. Concrete Res.;2005b, 57(3):135-147.

El Maaddawy, T., Soudki, K., and Topper, T., Analytical model to predict nonlinear flexural behavour of corroded reinforced concrete beams. ACI Structural Journal;2005a,102(56),550-559.

El Maaddawy, T., Soudki, K., and Topper, T., Long-term performance of corrosion-damaged reinforced concrete beams. ACI Structural Journal;2005b,102(66),649-656.

Espion, B., and Halleux, P.,1988. Moment curvature relationship of reinforced concrete sections under combined bending and normal force. Material and structures;1988, 21: 341- 351.

Han, S. M., Benaroya, H., and Wei, T. Dynamics of Transversely Vibrating Beams using four Engineering Theories, Academic Press.,(1999).

Gilbert, R. and Warner R.,Tension stiffening in reinforced concrete slabs. J. Strcut. Div. ASCE;1978.104(ST12),1885-1900.

Gunnin, B.,Rad,F., and Furlong, R.,A general nonlinear analysis of concrete structures and comparison with frame test. Computer and structures;1977,7:257-265.

Kabalia, A., Disc. of equation of the stress-strain curve of concrete. P. Desayi and S. Krishnana, J. Am. Concr. Inst.;1964,61,1227-1229.

Kemp, E. and Wilhelm, W., Investigation of the parameters influencing bond cracking. ACI Journal;1979, 76(1), 47-71.

Kent, D., and Park, R., 1971. Flexural members with confined concrete. Journal of the Structural Division;1971, ST(7): 19691990.

Kroenke, W., Gutzwiller, M., Lee, R., Finite element for reinforced concrete frame study. Journal of the Structural Division;1973, ST (7), 1371-1390.

Lazaro, A., and Richards, R., Full-range analysis of concrete frames. Journal of the Structural Division;1973, ST (8), 1761-1783.

Li, C., and Zheng, J., Propagation of reinforcement corrosion in concrete and its effect on structural deterioration. Magazine of Concrete Research;2005, 57(5), 261-271.

Mangat, P., and Elgarf, M., Flexural Strength of Concrete Beams with Corroded Reinforcement. ACI Structural journal;1999a, 96(1), 149-158.

McKenzie, William, 2006. Examples in Structural Analysis. Taylor & Francis.

Mohammed, A., Almansour, H., and Martín-Pérez, B., Nonlinear sectional analysis of RC section subjected to ultimate loads and reinforcement corrosion, (to be submitted shortly to Computer and Structures);2013.

Molina, F.J., Alonso, C., and Andrade, C., Cover cracking as a function of rebar corrosion: Part-2 –Numerical model, Materials and Structures;1993, 26(9)532-548.

Oyado, M., Saito, Y., Yasojima, A., and Kanakubo, T. Structural Performance of corroded RC column under seismic Load. *First International Workshop on Performance, Protection & Strengthening of Structures under Extreme Loading*, Whistler, Canada;2007.

Pulmano, V., Bakoss, S., and Shin, Y., 1987. A simplified non-linear analysis of concrete frames. Magaz. Conc. Res.;1987, 39: 29-34.

Rasheed, H., and Dinno, K., 1994a. An efficient nonlinear analysis of RS sections. *Computer and structures*. 53(3)613-623.

Rasheed, H., and Dinno, K., An improved nonlinear analysis of reinforced concrete frames. Computer and structures;1994b. 53(3)625-636.

Resheidat, M., Ghanma, M., Sutton, C., Chen, W., Flexural rigidity of biaxially loded reinforced concrete rectangular column sections. Computer and structures;1995,55(4)601-614.

Rodríguez, J., Ortega, L. M. and Casal, J., Load bearing capacity of concrete columns with corroded reinforcement. Corrosion of Reinforcement in Concrete Construction;1996, Royal Society of Chemistry: 220-230.

Saatcioglu, M., and Razvi, S., Strength and ductility of confined concrete. Journal of Structural Engineering;1992, 118(6): 1590-1607.
Saifullah, M., and Clark, L. 1994. Effect of corrosion rate on the bond strength of corroded reinforcement. Seventh International Conference on Corrosion and Corrosion Protection of Steel in Concrete;1994, R.N. Swamy, ed., Sheffield Academic Press. Sheffield,PP 591-602.

Saito, Y., Oyado, M., Kanakubo, T. and Yamamoto, Y., Structural performance of corroded RC column under uniaxial Compression Load. First International Workshop on Performance, Protection & Strengthening of Structures under Extreme Loading; 2007, Whistler, Canada.

Tapan, M., and Aboutaha, R., Load carrying capacity of deteriorated reinforced concrete columns. Computer and Concrete Construction;2009, 6(6):473-492

Tapan, M., and Aboutaha, R., Effect of steel corrosion and loss of concrete cover on strength of deteriorated RC columns. Construction and Building Materials;2011,25: 2596-2603.

Timoshenko, S., History of strength of materials. McGraw-Hill New York(1953)

Torres-Acosta, A., Navarro-Gutierrez, S., and Teran–Guillen, J., Residual flexure capacity of corroded reinforced concrete beams. Engineering Structures;2007, 29(6), 1145-1152.

Truesdell, C., The rational mechanics of flexible or elastic bodies, Venditioni Exponunt Orell Fussli Turici;1960, 1638-1788.

Yingang, D., Leslie, A., and Chan, A.,2007. Impact of reinforcement corrosion on ductile behaviour of reinforced concrete beams. *ACI Structural Journal*,104(28),285-293.

Yoon,S., Wng,K., Weiss,W., and Shah,S.,Interaction between loading ,corrosion, and serviceability of reinforced concrete. ACI Materials Journal;2000,97(6),637-644

Yubun, A., Balaguru, P., Chung, L.,Bond behaviour of corroded reinforcement bars. ACI Materials Journal; 2000, 97(28),214-220.

Appendix B

This paper is a reproduction of the conference paper that was published at the 8th International Conference on Short & Medium Span Bridges, Niagara Falls, Ontario, Canada, 2010.

Modeling RC Bridge Columns under the Combined Effects of Traffic and Reinforcement Corrosion.

Abstract

Significant increase in strength and stiffness of construction materials in the past five decades has led to a considerable reduction of bridge elements size and weight, resulting in more slender bridge structures that could have inadequate dynamic characteristics. For slab-on-girder bridges, the bridge superstructure traffic-induced vibration is reduced through dampers and discontinuity in the superstructure/substructure joints before affecting the bridge substructure. However, significant level of traffic vibration is observed in the substructure. On the other hand, reinforced concrete (RC) bridge columns in cold regions are affected by chloride-induced reinforcement corrosion from the application of de-icing salts in the winter, and their serviceability and strength capacity can be reduced over time. This paper presents a numerical model of individual and compound effects of traffic and corrosion-induced damage in RC bridge columns on the dynamic performance of the bridge superstructure. The procedure includes two time-dependent cycles presenting each process: an external cycle, which represents the corrosion process, and an internal cycle, which performs time-history analysis of the bridge under traffic load. The slab-on-girder bridge is modelled as a beam-on-two-

columns system (BOTC) using a two-dimensional finite element method and the truck is modelled as a two-degree of freedom dynamic system integrated with the bridge model. Corrosion-induced damage is introduced through the reduction of the reinforcing steel area and spalling of the concrete cover. It is found that the model is efficient in simulating the static and dynamic behaviour of slab-on-girder bridges. From the case study, it is found that although reinforcement corrosion of the bridge columns significantly reduces their capacity, it only causes a marginal increase in the bridge superstructure dynamic deflection under the dynamic movement of the truck.

B1. Introduction

Significant increase in strength and stiffness of construction materials in the past five decades has led to a considerable reduction of bridge elements size and weight, resulting in more slender bridge structures that have vulnerable dynamic characteristics. Furthermore, heavier and faster trucks are now standardized, and the average number of trucks passing bridges has dramatically increased. For the design and/or assessment of a bridge structure, it is imperative to evaluate its dynamic behaviour as well as the combined effect and/or interaction between traffic-induced vibration and environmental loads. In fact, the vibration response of a structure is increasingly being used as a means to detect and characterize damage in the structure. On the other hand, RC bridge columns in cold regions are affected by chloride-induced reinforcement corrosion, generated mainly from the application of de-icing salts in the winter, and their serviceability and strength capacity can be reduced over time.

Simply supported slab-on-girder bridges are the most popular type of bridges in North America. The redundancy of this bridge type depends on the number of girders and the stability of its substructure. Although the traffic-induced vibration is reduced through dampers and simply supports connections before affecting the bridge substructure, a significant level of traffic vibration is observed in the substructure. The dynamic response of a bridge subjected to moving loads is a very complex phenomenon and has been widely considered. For instance, many analytical models have been proposed to ensure better understanding of the dynamic effects of the bridge-vehicle interactions. The studies by Lin and Trethewey (1990), Law and Zhu (2004), Asnachinda et al. (2008), and Zambrano et al. (2008) have focused on developing analytical solutions for simply supported and continuous beams with uniform cross section subjected to a moving load. In order to obtain the dynamic response for both the moving dynamic system and the bridge, the governing equations for the interaction between the bridge system and the moving dynamic system were derived. However, the bridge system was represented by only the superstructure, while the substructure was omitted.

Field surveys have shown that RC bridge columns in cold climates are among the bridge elements with highest exposure to chlorides (Andersen 1997). Reinforcement corrosion is a continuous long-term process, leading to reduction in cross sectional area of the affected steel bars and loss of concrete section as a result of longitudinal cracking and spalling. Hence, reinforcement corrosion may cause significant changes in the bridge capacity and safety. A comprehensive study on RC columns subjected to reinforcement corrosion was performed by Rodríguez et al. (1996), in which the effects of steel corrosion on the RC column behaviour were evaluated experimentally. The authors

observed that reinforcement corrosion not only reduced the axial capacity of the columns, but it also introduced a load eccentricity due to spalling of the concrete cover and led to buckling of the longitudinal reinforcement due to premature loss of one or more columns ties.

The goal of this paper is to present a numerical model that combines the effects of traffic and corrosion of the columns of slab-on-girder bridges on the structural performance of the bridge superstructure. A simply supported slab-on-girder bridge is modelled as a two-dimensional frame consisting of a beam supported on two columns with a hinge beam-column joint in one of the beam sides and a roller on the other side. The truck load is modelled as a two-degree of freedom dynamic system. Corrosion-induced damage is introduced through the reduction of the reinforcement steel area and the column concrete section.

B2. Research significance

This paper presents a numerical model for slab-on-girder bridge columns under the combined effects of two processes, traffic load and reinforcement corrosion. The contribution of this study includes the development of a comprehensive tool to evaluate the structural performance of slab-on-girder bridge superstructure when the bridge columns are under the combined effect of the two processes. This enables the understanding of the many aspects of the progressive damage due to the combined effects of reinforcement corrosion and traffic loads. The model can also be used to study the effect of each load (traffic or corrosion) alone, and the combined effect of both loads, on the static and dynamic behaviour of the bridges under service loads. This paper presents

part of on-going research, where the non-linear elasto-plastic behaviour of the bridge under extreme loading conditions (ULS) is under development.

B3. Modelling the bridge structure, traffic and corrosion loads

Figure B-1 shows a flowchart of the proposed model. The model involves five major parts: (i) input data; (ii) formulation of structure and load matrices; (iii) static and dynamic analysis; (iv) corrosion process; and, (v) combined load results. The procedure includes two time-dependent cycles representing each process: (a) external cycle, which represents the corrosion process and is activated once the corrosion activation parameter is equal to 1 (or Corrosion = 1 in the input data); (b) internal cycle, which performs time-history analysis of the bridge under traffic load. The external or corrosion cycle starts running at time (T_{cor1}) and ends at time ($T_{cor\text{-}final}$) with time increment of (Δt_{cor}). During every corrosion time inclement, a time-history analysis of the bridge is performed.

The procedure commences with the input data of: (i) the structure, which includes its geometrical and material characteristics and boundary conditions; (ii) the traffic load; and (ii) the corrosion parameters. The results for the bridge performance are printed with reference to both processes time increments

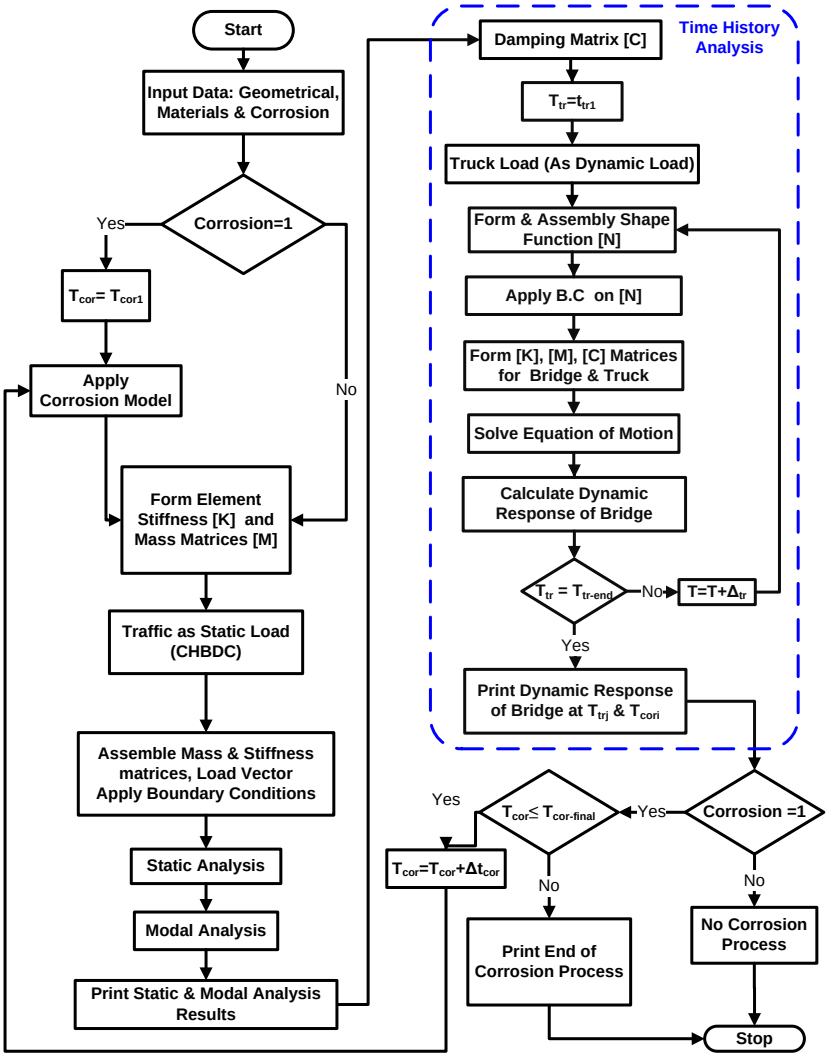

Figure B-1. Proposed model for combined effects of traffic and corrosion loads.

B3.1 Modelling the Bridge Structure and Traffic Load

A two-dimensional bridge system under a moving vehicle is modelled as a static and dynamic system using the direct stiffness method. Three types of analyses are carried out on the proposed model: (i) static analysis, wherein the traffic load is defined by a static truck load positioned to induce maximum static response; (ii) free vibration analysis; and (iii) forced vibration analysis, or time-history analysis. This enables evaluating the effects of the current deterioration of bridge concrete columns on the dynamic performance of

the bridge superstructure compared to its dynamic performance right after construction. Furthermore, studying the dynamic behaviour of the bridge could lead to identify a critical ratio of the superstructure stiffness to the substructure (columns) stiffness, wherein the vibration is significant and cannot be ignored in evaluating the combined effects of traffic and corrosion loads.

B3.1.1 Bridge Model

A typical slab-on-girder bridge is simply supported on columns or abutments. Since the focus of this study is on the behaviour of bridge columns, hence it is essential to model both the superstructure and substructure as one structural system. The model is required to effectively simulate the connection between the two parts. Since the load distribution, and hence the stress distribution, in the lateral direction (orthogonal to the traffic direction) is lightly affecting the bridge column behaviour, the bridge is modelled as a two-dimensional frame. The frame in this model is basically formed from a beam, representing the superstructure, and two columns. The connections between the beam and the columns are represented by an internal hinge on one side and a roller on the other side. The model also accounts for possible eccentricity in both connections. The base of the two columns is assumed fully fixed.

For the purpose of calculating the beam properties such as structural rigidity, which are equivalent to the properties of the slab-on-girder superstructure, the slab is assumed to be compositely connected to the girders. In the present model, the lateral slab flexural action and the girders tensional rigidities are ignored. The columns are considered as a composite section for the essential step of including the effect of reinforcement steel loss

when the corrosion model is applied. Both the composite beam and the columns are introduced as a 2D finite frame element with three degrees of freedom for each node. Self weight of the bridge elements is evaluated as a uniform load. The damping matrix is derived assuming a linear relation between damping of the bridge elements and their mass and stiffness.

The internal beam-column joints (connections) are to be considered as follows:

1. Hinge: (i) continuity in the vertical displacement *V*, i.e. beam and column have the same *V*; (ii) continuity in the horizontal displacement; (iii) discontinuity in the rotations, i.e. beam and column have independent rotations, or $\theta_{beam} \neq \theta_{column}$. .

2. Roller: (i) continuity in the vertical displacement; (ii) discontinuity in the horizontal displacement, or $U_{beam} \neq U_{column}$; (iii) discontinuity in the rotations, or $\theta_{beam} \neq \theta_{column}$.

B3.1.2 Vehicle Model

The vehicle is modelled as a two degree of freedom: vertical displacement (y) and rotation (θ) as shown in Figure B-2. It is assumed that the two axles of the vehicle remain in contact with the surface of the bridge superstructure. Only vertical vibration is considered. The force load of the vehicle-bridge system is considered as a point load moving along the bridge. The governing equations of the moving dynamic system and the bridge are presented in Lin and Trethewey (1990).

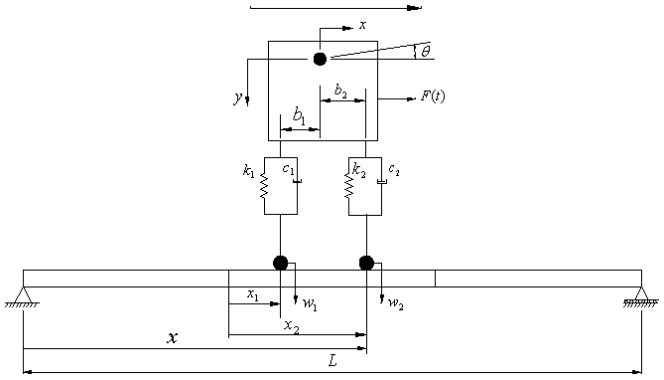

Figure B-2. Vehicle model (adopted from Lin and Trethewey, 1990).

B3.1.3 Dynamic Bridge System

The overall vehicle-bridge system is introduced as follows (Lin and Trethewey 1990):

$$\begin{bmatrix} [M] & \sum_{i=1}^{2}[N_i]^T f_{yi} & \sum_{i=1}^{2}[N_i]^T f_{\theta i} \\ [0] & m_1 & 0 \\ [0] & 0 & I_\theta \end{bmatrix} \begin{Bmatrix} \{\ddot{d}\} \\ \{\ddot{y}\} \\ \{\ddot{\theta}\} \end{Bmatrix} + \begin{bmatrix} [C] & \{0\} & \{0\} \\ \sum_{i=1}^{2} -c_i[N_i] & \sum_{i=1}^{2} c_i & \sum_{i=1}^{n}(-1)^{i+1}c_i b_i \\ \sum(-1)^i b_i c_i[N_i] & \sum(-1)^{i+1}c_i b_i & \sum_{i=1}^{2} c_i b_i^2 \end{bmatrix} \begin{Bmatrix} \{\dot{d}\} \\ \{\dot{y}\} \\ \{\dot{\theta}\} \end{Bmatrix} + \begin{bmatrix} [K] & \{0\} & \{0\} \\ \sum_{i=1}^{2}(-c_i \dot{x}[N_i]_x - k_i[N_i]) & \sum_{i=1}^{2} k_i & \sum_{i=1}^{n}(-1)^{i+1}k_i b_i \\ \sum(-1)^i(b_i c_i \dot{x}[N_i]_x + b_i k_i[N_i]) & \sum(-1)^{i+1}k_i b_i & \sum_{i=1}^{2} k_i b_i^2 \end{bmatrix} \begin{Bmatrix} \{d\} \\ \{y\} \\ \{\theta\} \end{Bmatrix} = \begin{Bmatrix} \sum_{i=1}^{2}[N]^T f_i \\ 0 \\ d_1 F(t) \end{Bmatrix} \tag{B.1}$$

where [*M*], [*K*], [*C*] are the structural mass, stiffness, and damping matrices of the bridge, $\ddot{d}$, $\dot{d}$, d are the nodal acceleration, velocity and displacement vectors, respectively, f_i is the magnitude of a concentrated force, [*N*] is the shape function, m_1, k_i, c_i are the spring mass, stiffness ,and damping of an axle of the moving system, $\ddot{y}$, $\dot{y}$, y are the vertical displacement, velocity and acceleration of the spring mass, and b_i is the vehicle axle position from its center of gravity.

In order to check the performance of the proposed model, the vehicle model is first integrated with the bridge superstructure (as originally proposed by Lin and Trethewey, 1990), and then it is integrated with the proposed beam-and-columns system. The combined equations of the vehicle–bridge system as given by Eq. (B.1) is solved by the step-by-step integration method, and the dynamic response of the bridge under the moving vehicle is expressed as a function of the transverse displacement of the structure $w(x,t)$, i.e., $w = [N]\{d\}$.

B3.2 Modeling the Corrosion Load

The effect of reinforcement corrosion is modelled here by reducing the rebar cross-sectional area over time. The change in the RC elements sectional properties (area and moment of inertia) leads to a variation of their stiffness matrices. The loss of reinforcing steel due to corrosion is evaluated by applying Faraday's law, from which the thickness reduction $x(t)$ of the reinforcing bar after time t can be calculated according to Eq. (B.2):

$$x(t) = \frac{M}{zF\rho_s} \cdot i_{corr} \cdot t \qquad \text{(B.2)}$$

where M is the metal molar mass (55.85 g/mol for iron), z is the valence of the ion formed as a result of iron oxidation (i.e., $z = 2$ for $Fe \rightarrow Fe^{2+} + 2e^-$), F is Faraday's constant (F = 96,485 C/mol), ρ_s is the density of iron (ρ_s = 7.85 g/cm^3), i_{corr} is the corrosion current density, and t is the time elapsed since corrosion started. By substituting the values of M, z, F and ρ_s into Eq. (B.2), the rate of thickness reduction results in $x(t) = 0.0116 \cdot i_{corr} \cdot t$, where $x(t)$ is given in mm, i_{corr} is given in μA/cm^2, and t is given in years. The depth of the corrosive penetration attack $p(t)$ is calculated from:

$$p(t) = R \cdot x(t) = R \cdot 0.0116 \cdot i_{corr} \cdot t \quad \text{(B.3)}$$

where R is the ratio between the maximum penetration of a pit $p_{\max}$ and average penetration p_{av} corresponding to uniform corrosion. Parameter R is also known as the pitting ratio. Val (2007) has reported that the maximum penetration of pitting on the surface of a rebar is about 4-8 times the average penetration corresponding to uniform corrosion. Assuming that the pit can be idealized as a hemisphere, as illustrated in Figure B-3, the cross-sectional area A_s of a group of n reinforcing bars after t years of corrosion can be estimated as:

$$A_s(t) = n\frac{\pi D_o^{\,2}}{4} - \sum_{i=1}^{n} A_{p,i}(t) \geq 0.0 \quad \text{(B.4)}$$

where D_o is the initial reinforcing bar diameter and $A_{p,i}(t)$ is the cross-sectional area of a pit after time t, which is a function of $p(t)$ and calculated according to Val (2007).

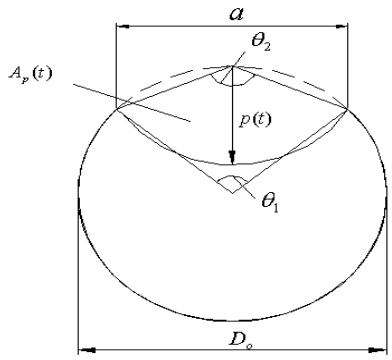

Figure B-3. Pit configuration (adapted from Val, 2007).

B4. Case study

The proposed model as illustrated in Figure B-1 is validated through a case study of a slab-on-steel and a slab-on-prestressed concrete girder bridges with center to center span

of 20 m. Both bridges are simply-supported on RC piers formed from five rectangular 600×350 mm^2 columns, connected from the top to a beam where the bridge superstructure girders rest on. The 6-m height columns are assumed to have full fixity at the foundation level. The bridges superstructure consists of a concrete slab compositely casted on steel or prestressed concrete girders as shown in Table B-1. The two bridges are assumed to have been built in the early sixties, and the concrete compressive strength f'_c for all the concrete components of both bridges is assumed 30 MPa. Details of the slab thickness, girder geometrical properties, girder spacing, bridge width and number of girders are given in Table B-1. The present case study involves performing different static and dynamic loading cases using a two-axle truck of a total mass of 34.4×10^3 kg, where the body mass is 30,189 kg, the front axle mass is 2,806 kg, and the rear axle mass is 1,403 kg. The truck mass moment of inertia is 263,052 kg·m^2, the stiffness of each axle is 5,363,163 N/m and the axle spacing is 6.19 m (Ali 1999). Since the proposed model is a two-dimensional model and the variation through the bridge width perpendicular to the traffic direction is ignored, the reported results, stiffness, mass, and damping are average values per traffic lane.

B4.1 Convergence study

To verify the validity of the proposed model under static and traffic loads, it is necessary to ensure the correct implementation of the internal hinge and roller at the beam-column joints. Depending on the column stiffness, the deformations of the columns add more deformations to the top beam (or the superstructure) in the BOTC frame compared to the case of a simply-supported beam. The static analysis is performed using a two-axle truck load by considering two cases: (i) a simply-supported beam (SSB); and (ii) the proposed

beam on a two-column system (BOTC). Figure B-4 shows that BOTC gives slightly higher deflection than SSB as expected.

Table B-1: General properties of two bridges, slab-on-steel girder and slab-on-prestressed girder bridges.

Type of girder	Year Built	Skew Angel ^{o}	Span Length m	Girder Spacing m	Girder Properties A m^2	I m^4	H m	Transverse width m	Slab Thick m	No. of Girder
Steel	1965	0.0	20.0	2.69	.0303	.00405	.915	17.69	.2159	7
Prestressed	1963	0.0	20.0	2.08	.333	.0571	1.4213	14.03	.165	7

The dynamic analysis part of the proposed model is examined by two convergence studies. For both convergence studies, the truck speed is equal to 100 km/h. In the first convergence study, the number of element is assumed fixed (NE = 40), and the number of integration points, NI, varies from 5 to 100. Figure B-5 shows the dynamic deflection under the front axle of the truck along the bridge span for different NI. It is found that after NI = 24, the change in the deflection becomes negligible. In the second convergence study, the number of integration points is constant (NI = 50) and the number of elements is varied from 4 to 40. It is found that after NE = 16 the results becomes stable and the change in the dynamic deflection due to the increase in the number of elements is negligible (see Figure B-6).

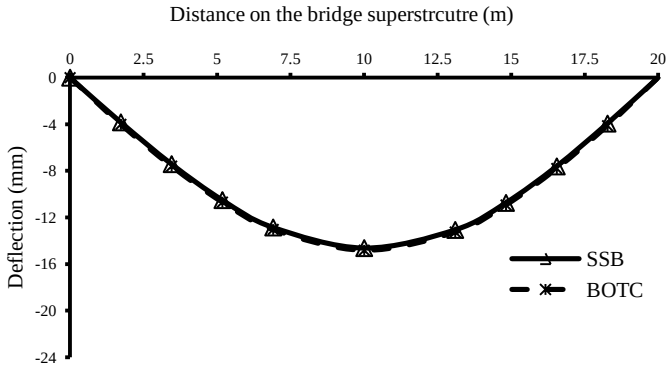

Figure B-4. Mid-span deflection of BOTC compared to SSB under truck load.

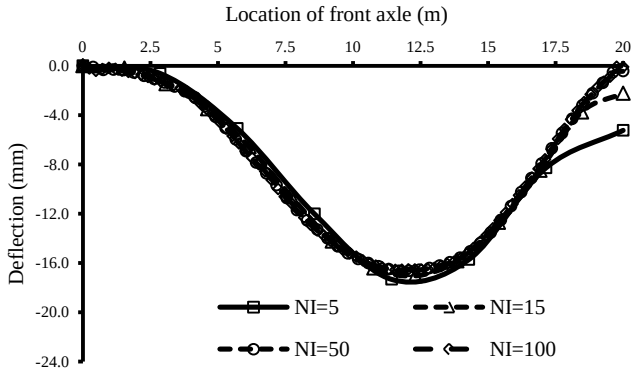

Figure B-5. Convergence study 1: number of elements NE = 40 and truck speed = 100 km/h for different number of integration points (NI).

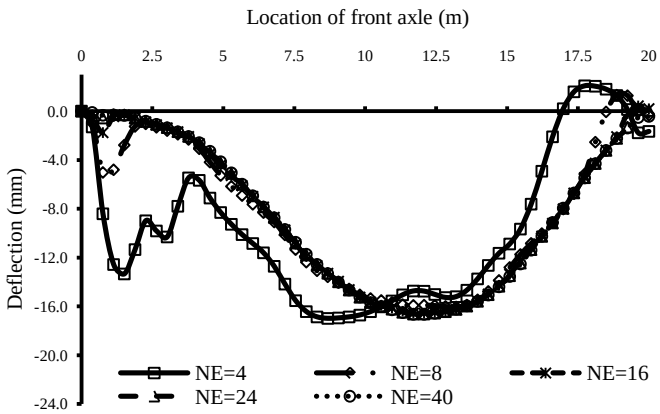

Figure B-6. Convergence study 2: number of integration points NI = 50 and truck speed = 100 km/h for different number of elements (NE).

B4.2 Dynamic deformations for different truck speeds

Figure B-7 shows the dynamic deflections of the bridge superstructure under the truck axles when the truck crosses the bridge (slab-on-steel girders) at the typical design speed of 100km/h. The proposed model accurately shows the entry and the exit of each of the truck axles and the range where the maximum deflection is expected. Figure B-8 shows the dynamic deflection of the slab-on-steel girders bridge superstructure under the front axle for different truck speeds compared to the static deflection. In this comparison, the static deflection is calculated under the front axle, and the truck location is changed successively while the deflection is calculated for every position on the bridge superstructure from the static equilibrium. The dynamic deflection curve is very close to the static deflection when the truck speed is low, and the dynamic deflection increases as the truck speed increases. The impact factors are calculated from the ratio of the maximum dynamic deflection to the maximum static deflection, which range between 1.07 to 1.23 as shown in Table 4B-2.

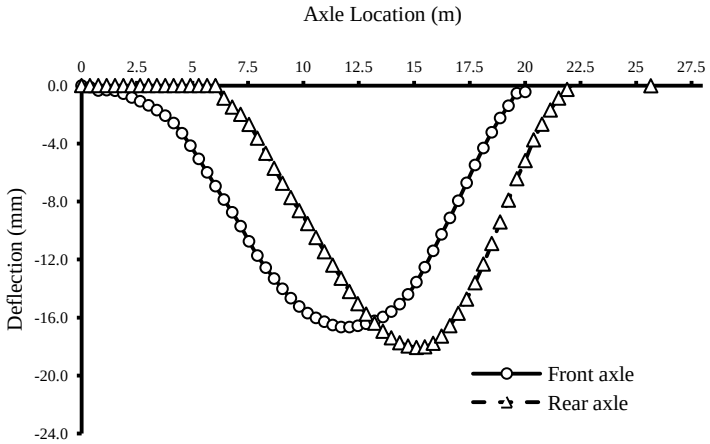

Figure B-7. Dynamic deflection of BOTC under front and rear axles for a truck speed =100 km/h.

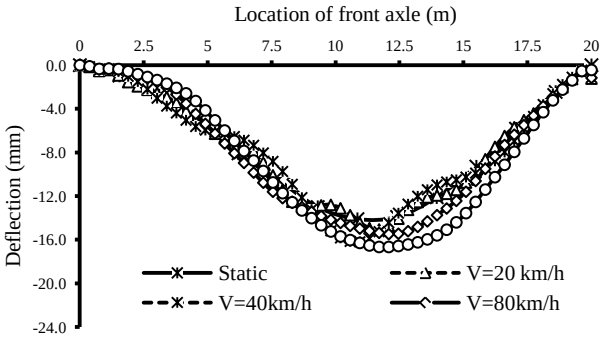

Figure B-8. Dynamic deflection of BOTC under front axle for different truck speeds.

Table B-2: Impact factors under two-axles moving truck.

Velocity (km/h)	Impact Factor
20	1.067
40	1.147
80	1.097
100	1.18
120	1.229

B4.3 Bridge structure under combined traffic and corrosion loads

The behaviour of the bridge structure under combined traffic and corrosion loads is studied here. Corrosion-induced damage is simulated by assuming a steel mass loss of 30%, which is equivalent to 10 years of corrosion with a corrosion current density of 1μA/cm², and by assuming that the concrete cover of the columns has spalled out. For the two-axle truck moving over the bridge at a speed of 40 km/h, Figure B-9 shows a very small increase in the dynamic deflection due to the reduction in steel area and spalling of the concrete cover from two sides of the RC bridge columns.

For a longer period of the corrosion process, say for 40 years, the reduction in reinforcing steel area could reach significant levels (assuming no maintenance is taken place). This would result in a large reduction of the column capacity. Figure 5B-10 shows the interaction diagram of one column of the bridge pier, where 40 years of corrosion results in significant reduction of the capacity. If the column capacity is compared to the un-factored loads on the column, which is 536 kN for the slab on prestressed concrete girders and 382 kN for the slab on steel girders, it is clear that the safety margin is significantly decreased.

If all these effects are combined, then the influence of the corrosion process on the column ultimate axial capacity is significant. However, in the elastic range of the column load-deformation relationships, the only parameters affecting the deformation are the load level, the cross sectional properties (area and moment of inertia) and the modulus of elasticity. Since the ratio of the steel area to the column cross-sectional area and ratio of the concrete cover to the column cross-sectional area are small, then their losses are

marginally affecting the deformations in the elastic range. In the present case study, it is clear that the change in the dynamic deflection of the bridge superstructure due to the corrosion of the column reinforcement is not enough to be an indication of the significant reduction of the pier capacity.

B4.4 Effect of girder material on dynamic deflection of bridge superstructure

For the investigated bridge span of 20 m, Figure B-11 shows that a significant difference in the superstructure dynamic deflections is observed when the steel girders are replaced by pre-stressed concrete girders. In this case study, the slab-on-steel girder bridge has less stiffness and mass per lane for the same span length. The corrosion of the longitudinal reinforcement and the concrete cover losses of the bridge columns have marginal effect on the dynamic deflections of the bridge superstructure. Further investigation is needed to evaluate the effect of different values of the superstructure and the column stiffness on the dynamic deflection of the bridge superstructure under the combined traffic and corrosion loads. This can be achieved by using high strength materials, longer bridge span, and larger girder spacing.

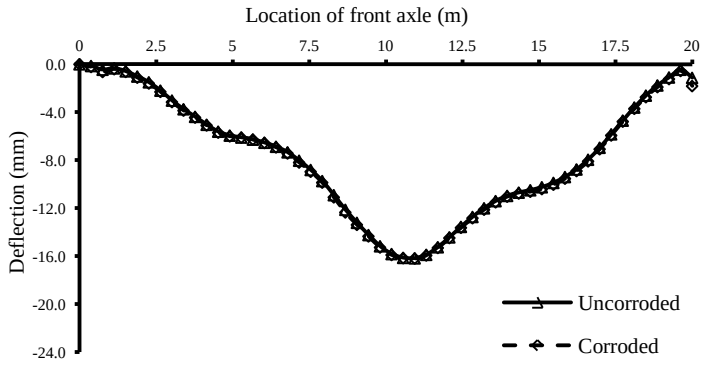

Figure B-9. Comparison of dynamic deflections of superstructure under traffic load only and combined traffic and corrosion loads (steel girders).

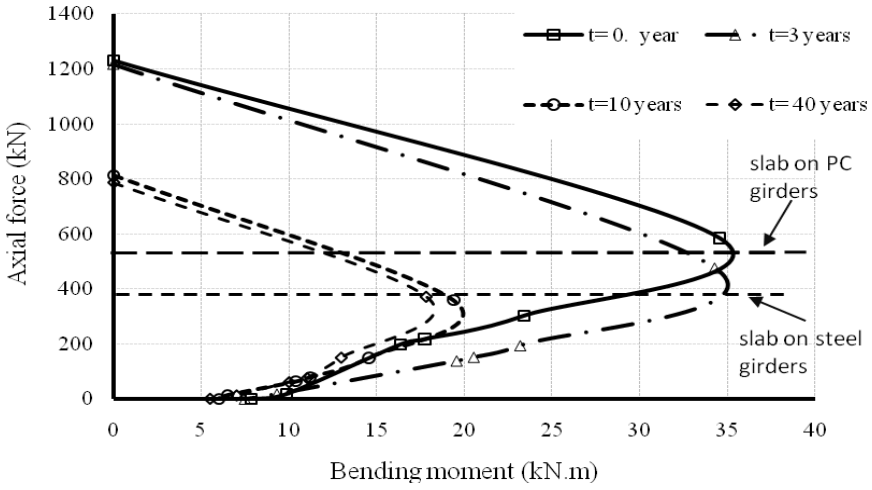

Figure B-10. Interaction diagram for RC bridge column at different corrosion stages.

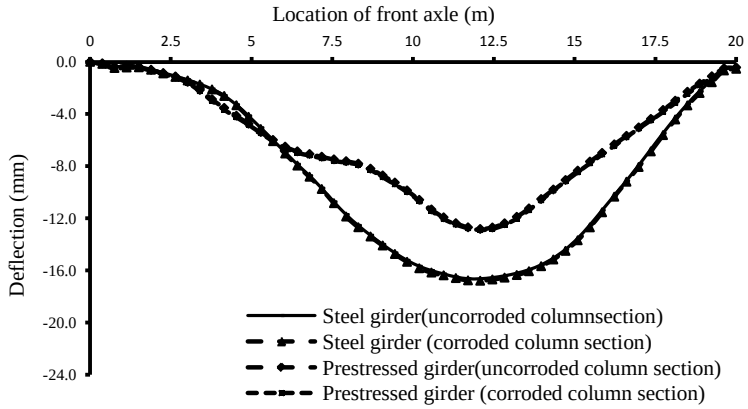

Figure B-11. Comparison of dynamic deflections of superstructure under traffic load only and under combined traffic and corrosion loads for slab on steel and prestressed concrete girders.

B5. Summary and conclusions

In this paper a numerical model of individual and compound effects of traffic and corrosion-induced damage of RC bridge columns on the performance of the bridge

superstructure is introduced. The procedure includes two time-dependent cycles representing the two time-dependent processes: (i) external cycle, which represents the corrosion process; and (b) internal cycle, which performs time history analysis of the bridge under traffic load. The slab-on-girder bridge type is modelled as a beam on a two-column system using two dimensional finite element method, and the truck is modelled as a two degree of freedom dynamic system integrated with the bridge model. Corrosion-induced damage is introduced through the reduction of the reinforcing steel area and spalling of the concrete cover. The model is implemented into a computer program and the validation and a case study is performed.

The individual and compound effects of traffic and corrosion loads have been investigated on a 20-m slab-on-steel and concrete girder bridge on concrete piers (columns) through: (i) static load of the two axle truck; (ii) different truck speeds and girder materials; and, (iii) different levels of corrosion.

It is found that the model is efficient in simulating the static and dynamic behaviour of slab-on-girder bridges. It is capable of capturing all the combined effects of the traffic load and the reinforcement corrosion on the bridge dynamic deformations. From the case study, it is found that the corrosion of the bridge columns results in marginal increase in the bridge superstructure dynamic deflection under truck dynamic movement, even though it results in significant reduction in the column capacity. The results highlight that the assessment of the dynamic behaviour of the bridge superstructure due to corrosion-induced damage in the RC columns is not indicative of the reduction in the columns capacity.

B6. Future work

Thorough investigations are to be performed to evaluate the effects of the superstructure stiffness, span length of bridge superstructure, column dimensions, and different levels of corrosion intensity on the static and dynamic performance of the bridge column. This would lead to identify and quantify a critical ratio of the superstructure stiffness to the substructure (column) stiffness, wherein the vibration is significant and cannot be ignored in evaluating the compound or coupling effects of traffic and corrosion on RC bridge columns behaviour.

B7. Acknowledgments

The financial support provided by The Libyan General Public Committee of Higher Education is gratefully appreciated.

B8. References

Ali, A. 1999. Dynamic Analysis of Bridges Using the Finite Element Strips Method. Ph.D. Thesis, Dept. of Civil Engineering, University of Ottawa, Ottawa, 213 pages.

Andersen, A. 1997. HETEK, Investigation of Chloride Penetration into Bridge Columns Exposed to De-Icing Salt. Copenhagen, Denmark.

Asnachinda P., Pinkaew T. and Laman J.A. 2008. Multiple Vehicle Axle Load Identification From Continuous Bridge Bending Moment Response. Engineering Structures, 30(10): 2800-2817.

Law, S. and Zhu, X. 2004. Dynamic Behaviour of Damaged Concrete Bridge Structures Under Moving Vehicular Loads. Engineering Structures, 26(9): 1279-1293.

Lin, Y.H. and Trethewey, M.W. 1990. Finite Element Analysis of Elastic Beams Subjected to Moving Dynamic Loads. Journal of Sound and Vibration, 136(2): 323-342.

Rodríguez, J., Ortega, L. M. and Casal, J. (1996). Load Bearing Capacity of Concrete Columns with Corroded Reinforcement. Corrosion of Reinforcement in Concrete Construction, Royal Society of Chemistry: 220-230.

Val, D.V. 2007. Deterioration of Strength of RC Beams Due to Corrosion and its Influence on Beam Reliability. Journal of Structural Engineering, 133(9): 1297-1306.

Zambrano, A., Rauci, M. and Malngone, P. (2008). Vehicle-Structure Interaction to Analyse the Primary Dynamic Aspects of Railway Bridges. Structure and Infrastructure Engineering, 4(2): 107-121.

Appendix C

In this appendix, two extreme loading and design alternatives are investigated to show the capabilities of the proposed SHDFEA to model any possible loading condition and any possible column design. In the first case study, the effects of very large load eccentricity are studied on the same columns of Bridge A in the chapter. The second case study is on an extreme possible design of Bridge A column, where the column is redesigned for a very high load over capacity ratio using the performance-based design concept.

C1. Effects of high columns eccentricity on the dynamic deformations of a slab-on-girder bridge

As shown in the chapter, the hinge and rollers joints connecting the slab-on-girder bridge superstructure to the columns decrease the oscillation of the dynamic load transferred to the columns when the superstructure is subjected to a moving truck. On the other hand, the damage in the columns slightly affects the dynamic response of the bridge superstructure as shown as well. Sometimes the columns are affected by high lateral loads or external moments. It is of high interest to investigate if such high moments can increase the change of the bridge superstructure dynamic displacement when the columns have severe corrosion damage. Hence the comparisons in this section include the case of a typical load eccentricity and the case of high eccentricity of the load transferred from the superstructure to the columns.

Figure C-1.a shows the applied axial load versus the axial displacement relationship up to ultimate static load, while Figure C-1.b shows the applied moment versus the lateral displacement relationship up to ultimate static load. Both figures show the large changes

in the column structural capacity and deformability range at ultimate loading when the eccentricity is increased. Figures C-1.c and C-1.d show respectively the truck position versus the maximum lateral deformation of the right and left columns for different eccentricities of the load. Both figures illustrate the high change in the dynamic lateral displacement when the column axial load has high eccentricity. Figures C-1.e and C-1.f show respectively the lateral displacement versus the column height of the right and left columns for different eccentricities. The figures show that there is no change of the mode of vibration in both columns (right and left) when the load eccentricity is increased. It is evident that only the first mode of vibration is excited for both columns; however, the amplitude of the dynamic lateral displacement is higher for the left column (with a hinge joint). This can be explained by the transfer of the horizontal dynamic displacement of the bridge superstructure in the direction of the traffic to the left column through the hinge. On the other hand, the horizontal dynamic displacement of the bridge superstructure is released through the movement of the roller in the right column, resulting in lower lateral displacement amplitude. Figure C-1.g, which plots the dynamic deflection of the superstructure for different eccentricities of the column load, proves that the high eccentricity of the axial load on the columns does not affect the dynamic deflection of the superstructure.

C2. Effects of high load over capacity ratio in an optimized bridge column design

With the high progress in the strength of new materials and the successive development of performance-based design approaches, investigating the level of sensitivity of the dynamic displacements of bridges with columns designed for high loads over capacity ratios is of major interest. In addition, if these columns are affected by reinforcement

corrosion damage, then evaluating the changes in their static and dynamic response becomes a critical concern for bridge engineers. In the present investigation, the column of Bridge A in the chapter is redesigned based on the applied load and the nonlinear behaviour and ultimate resistance of the column. The result is a column with a smaller section and with lower reinforcement ratio, as shown in Figure C-2.a.

Figures C-2.b and C-2.c show the applied axial load versus the axial displacement relationship up to ultimate static load for the case of zero eccentricity and 0.15H eccentricity, respectively. Figure C-2.d shows the applied moment versus the lateral displacement relationship up to ultimate static load (with 0.15H eccentricity). The load or moment versus displacement relationships for the traditionally-designed column (TA) and performance-based designed column (PB) are obtained for two cases: (i) undamaged columns (or U), and (ii) corrosion-damaged columns (D). The level of corrosion damage here is the same as explained in the case study (Bridge A) of the chapter. Figures C-2.e and C-2.f show larger axial and lateral displacements for the case of the column designed for a high load-over-capacity ratio compared to the traditionally-designed column. The figures show that the mode of vibration is not changed with the change in the load-over-capacity ratio, but the displacement amplitude is increased. The effect of the corrosion damage on the location of the maximum lateral displacement zone is also observed in a similar manner in both design cases.

Figure C-2.g shows that for both design approaches, the effect of corrosion damage on the deflections of the superstructure under the front axle of the truck is negligible. However, the axial and lateral displacements of the columns when the truck passes over the bridge are slightly increased in the case of undamaged columns designed according to

a performance-based approach compared to damaged ones (see Figures C-2.h, C-2.i, and C-2.j). This can be explained by the slight changes in the mode of vibrations and the resulting changes in displacements distributions.

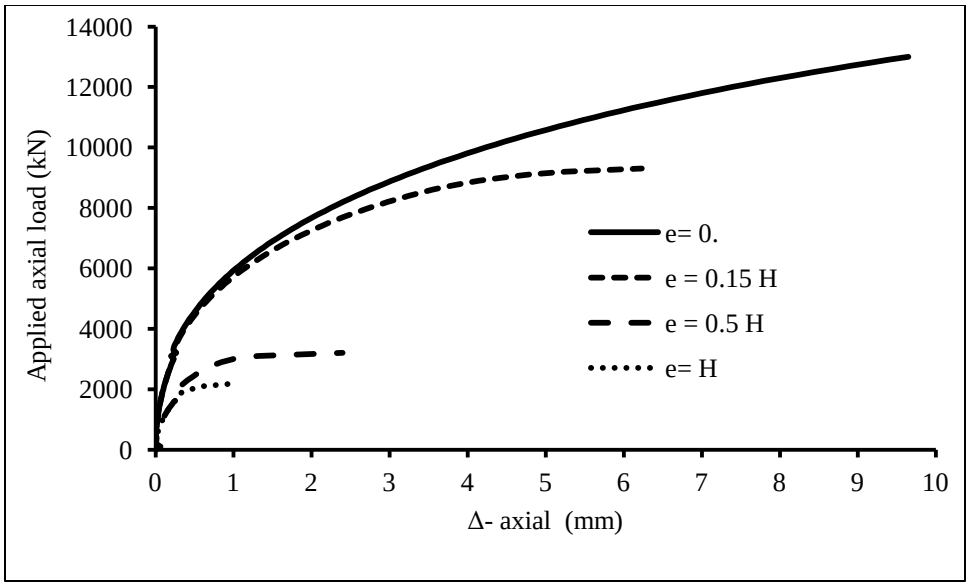

Figure C-1.a: Applied axial load versus axial displacement of the top section of the bridge column.

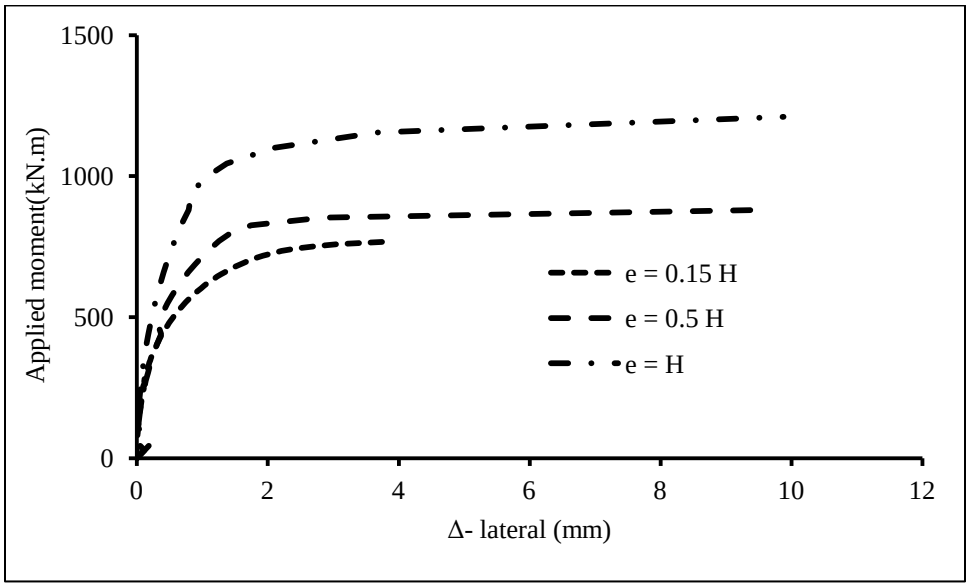

Figure C-1.b: Applied moment versus lateral displacement of the top section of the bridge column (with roller internal boundary).

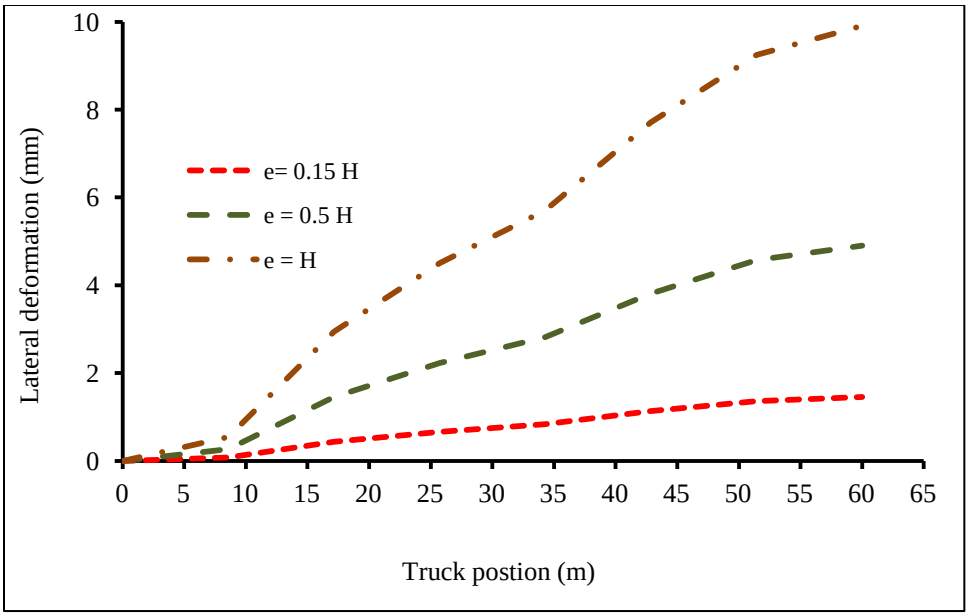

Figure C-1.c: Truck position versus maximum lateral deformation of the right column for different eccentricities.

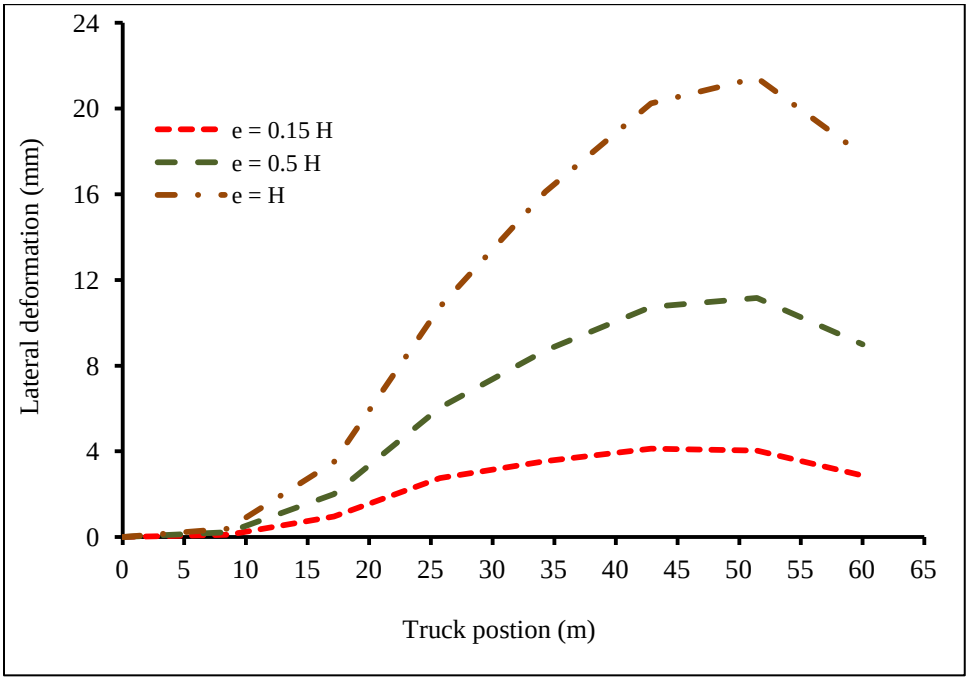

Figure C-1.d: Truck position versus maximum lateral deformation of the left column for different eccentricities.

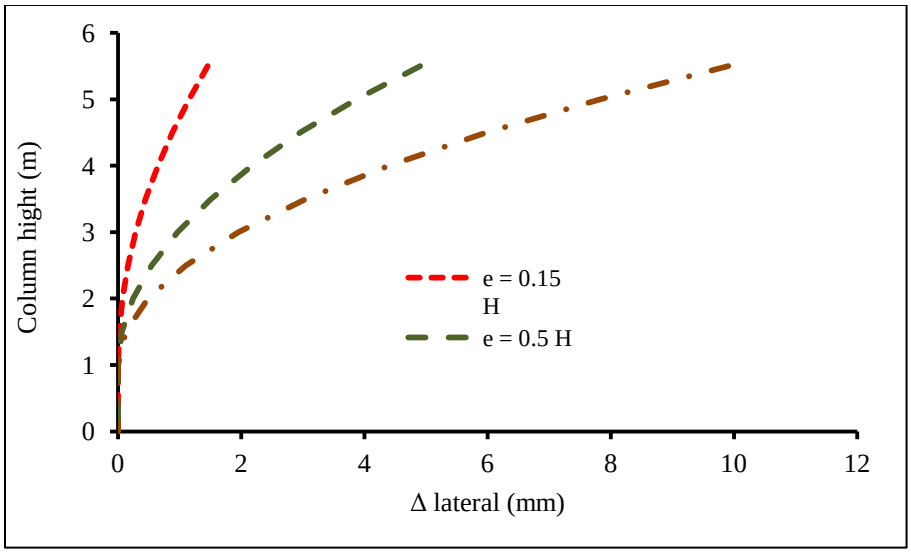

Figure C-1.e: Column height versus lateral displacement of the right column for different eccentricities.

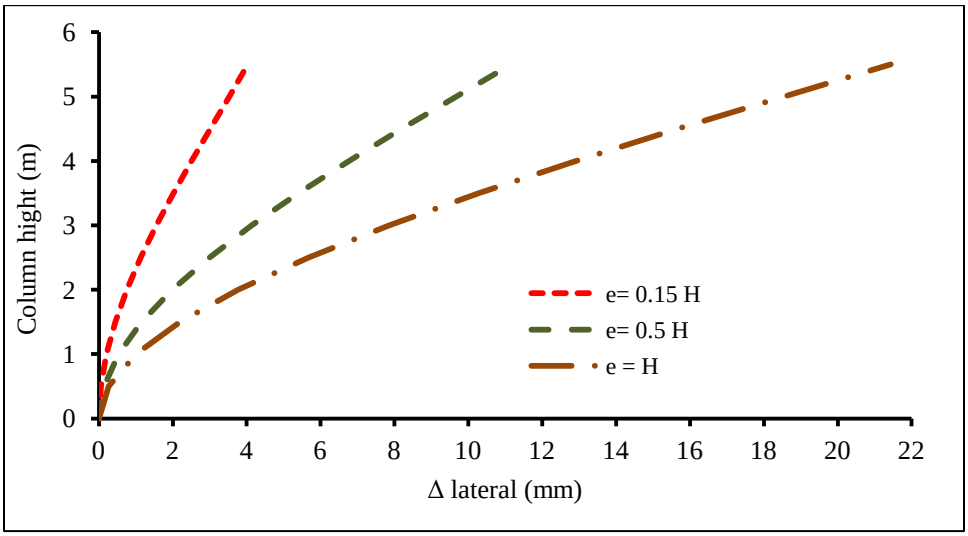

Figure C-1.f: Column height versus lateral displacement of the left column for different eccentricities.

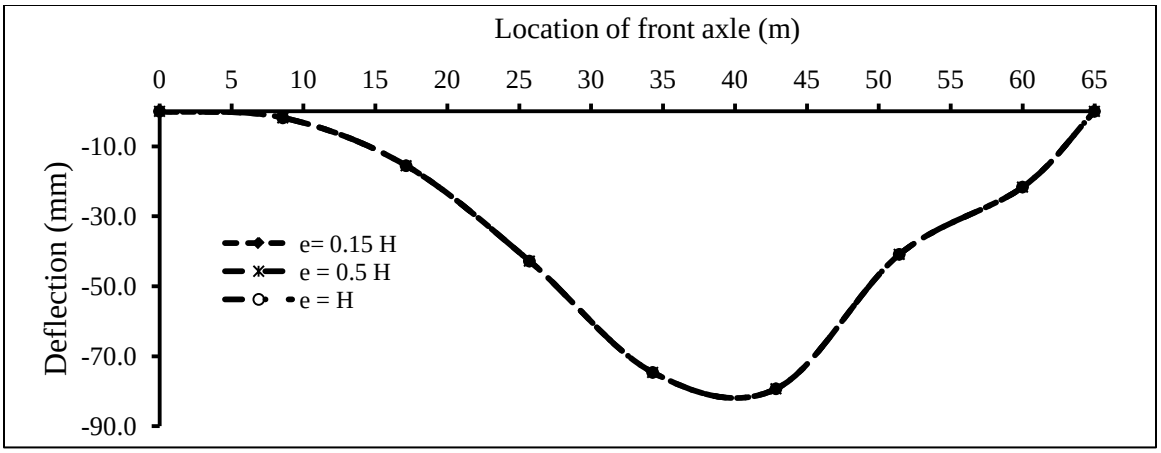

Figure C-1.g: Comparison of dynamic deflections of superstructure under traffic load only for different column load eccentricities.

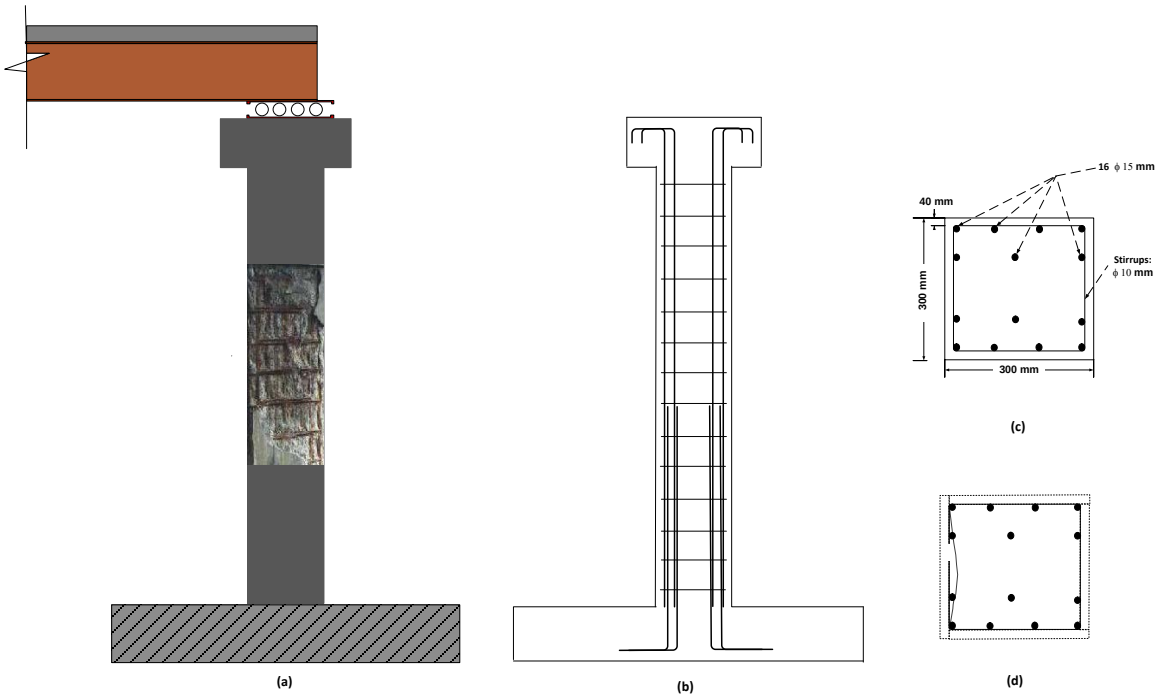

Figure C-2-a: Column design based on performance-based design approach and optimum load over capacity, reinforcement details and damage due to corrosion in critical corrosion zone.

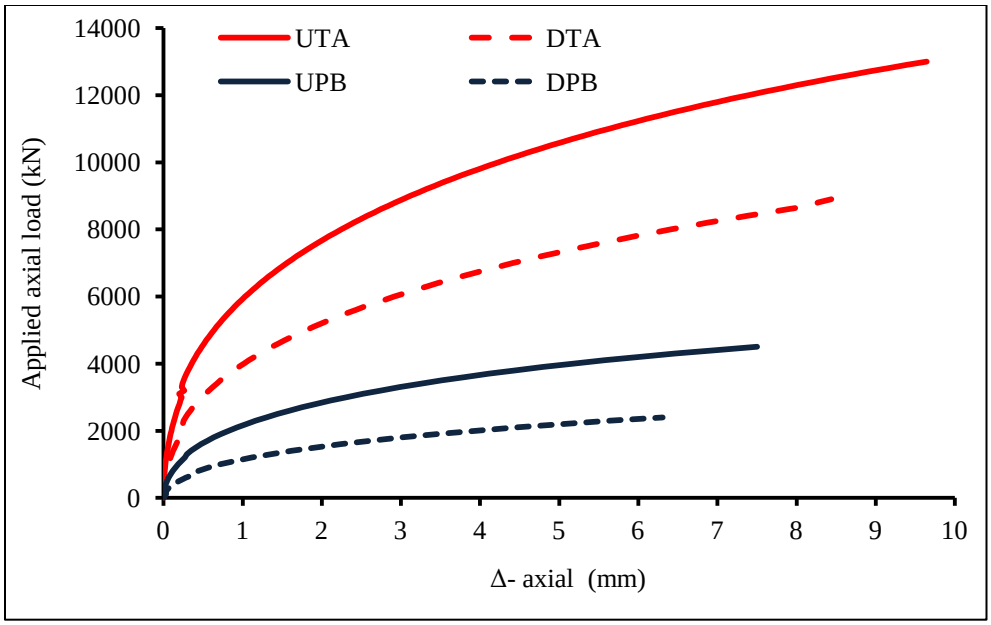

Figure C-2.b: Applied axial load versus axial displacement of the top section of the bridge column with zero eccentricity. UTA: undamaged column - traditional design approach; DTA: damaged column - traditional approach; UPB: undamaged column - performance-based design; DPB: damaged column - performance-based design.

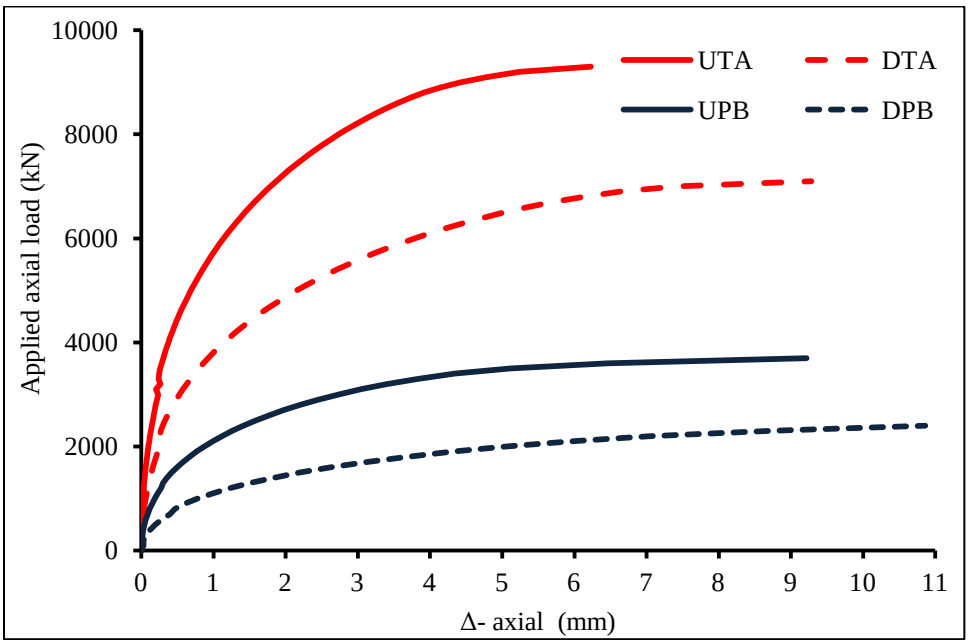

Figure C-2.c: Applied axial load versus axial displacement of the top section of the bridge column with 0.15H eccentricity for traditional and performance-based column designs.

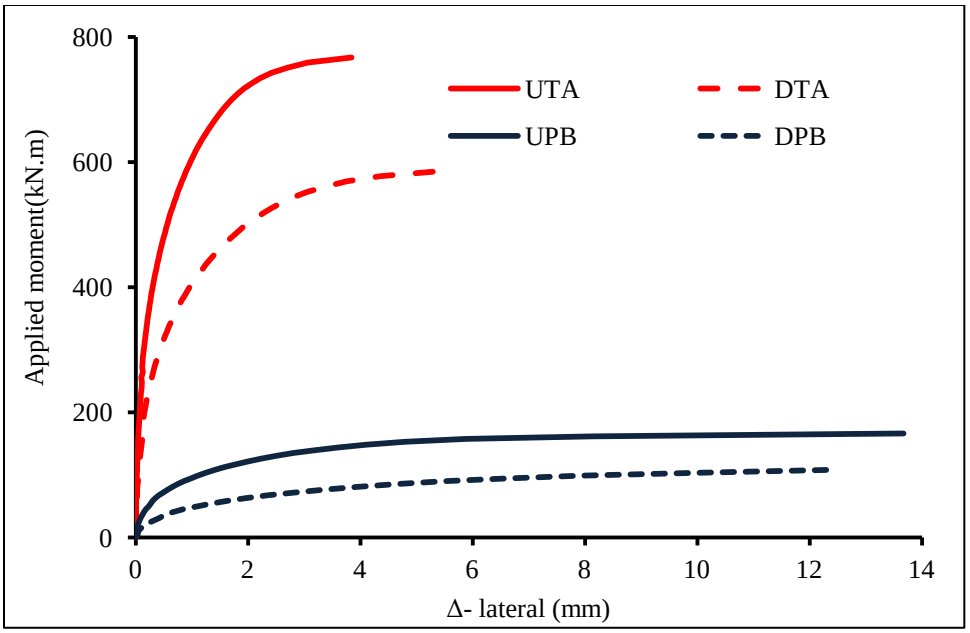

Figure C-2.d: Applied moment versus lateral displacement of the top section of the bridge column for traditional and performance-based column designs.

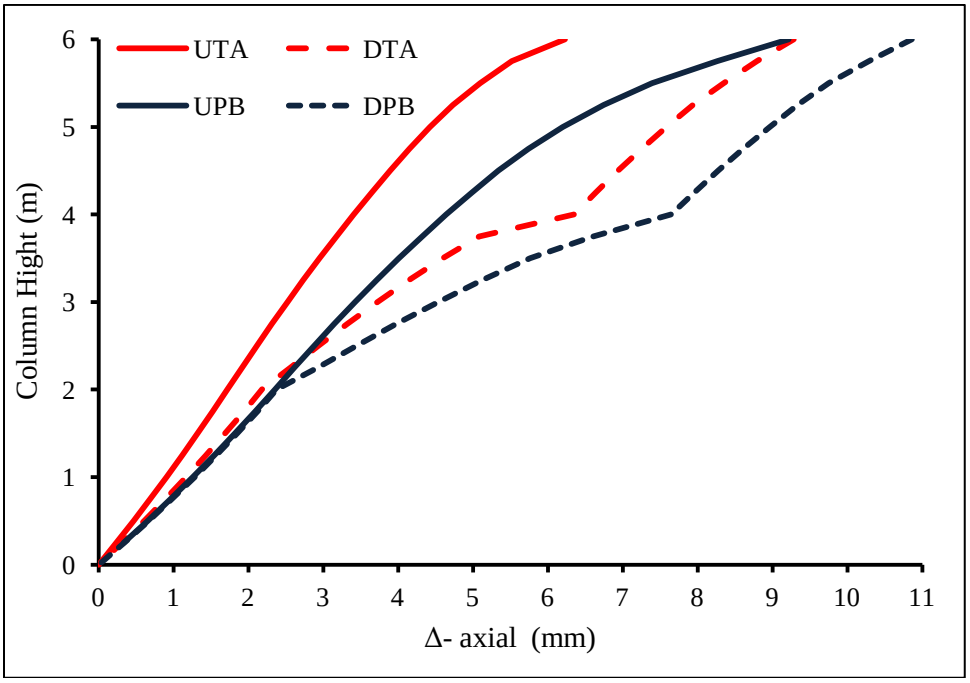

Figure C-2.e: Column height versus axial displacement of the bridge column at ultimate load for traditional and performance-based column designs.

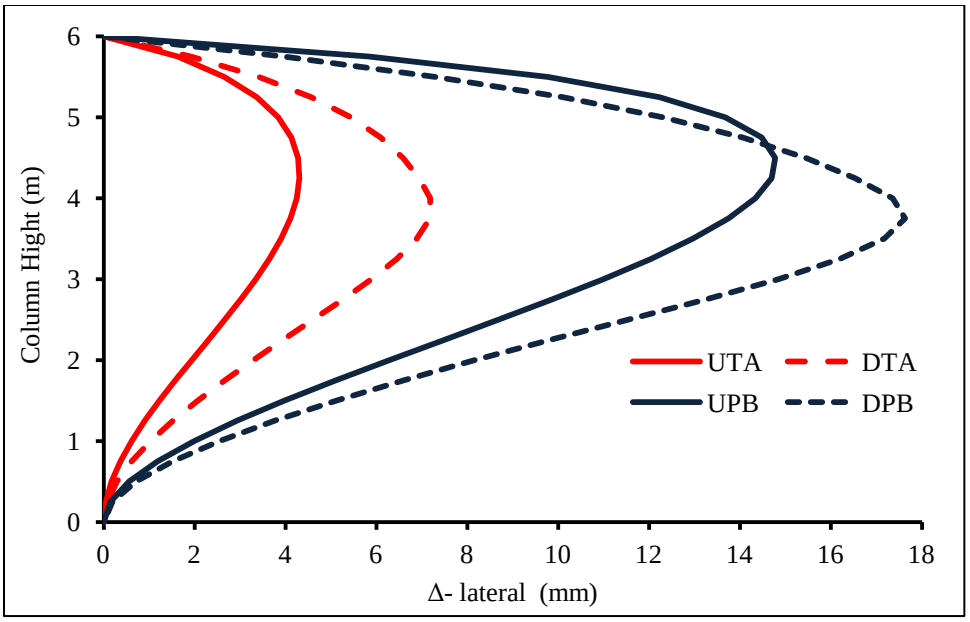

Figure C-2.f: Column height versus lateral displacement of the bridge column at ultimate load for traditional and performance-based column designs.

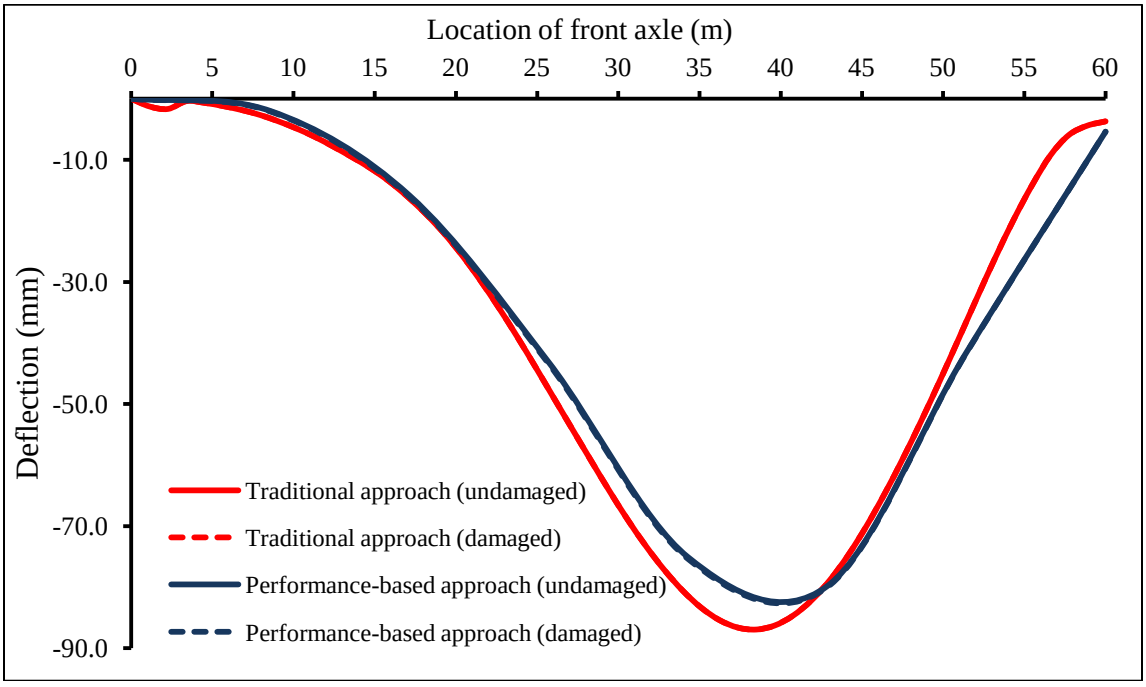

Figure C-2.g: Comparison of dynamic deflections of the bridge superstructure under only moving truck, and combined moving truck and corrosion loads for traditional and performance-based column designs.

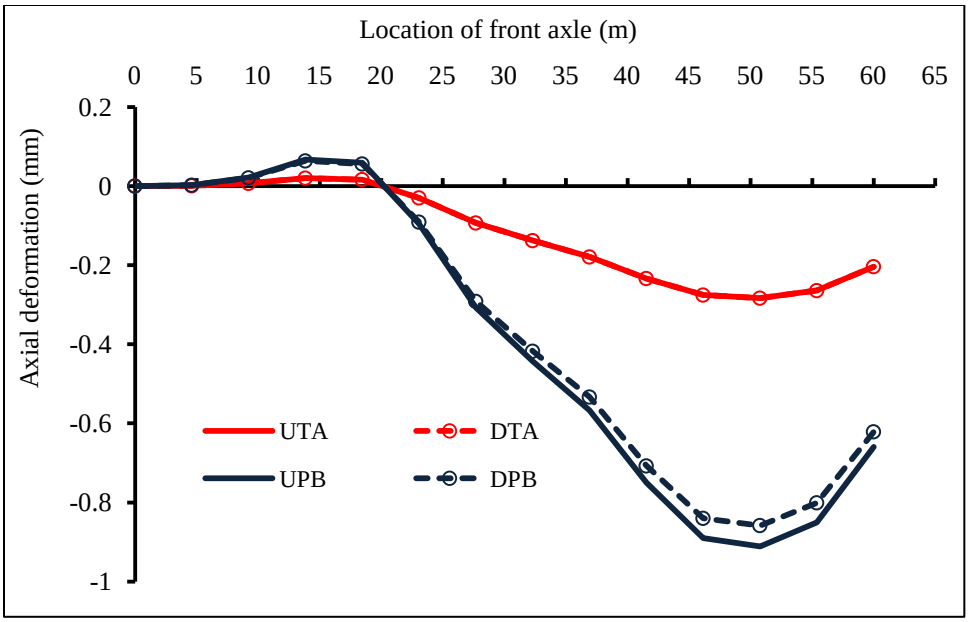

Figure C-2.h: Truck position versus maximum axial deformation of the right column for traditional and performance-based designs.

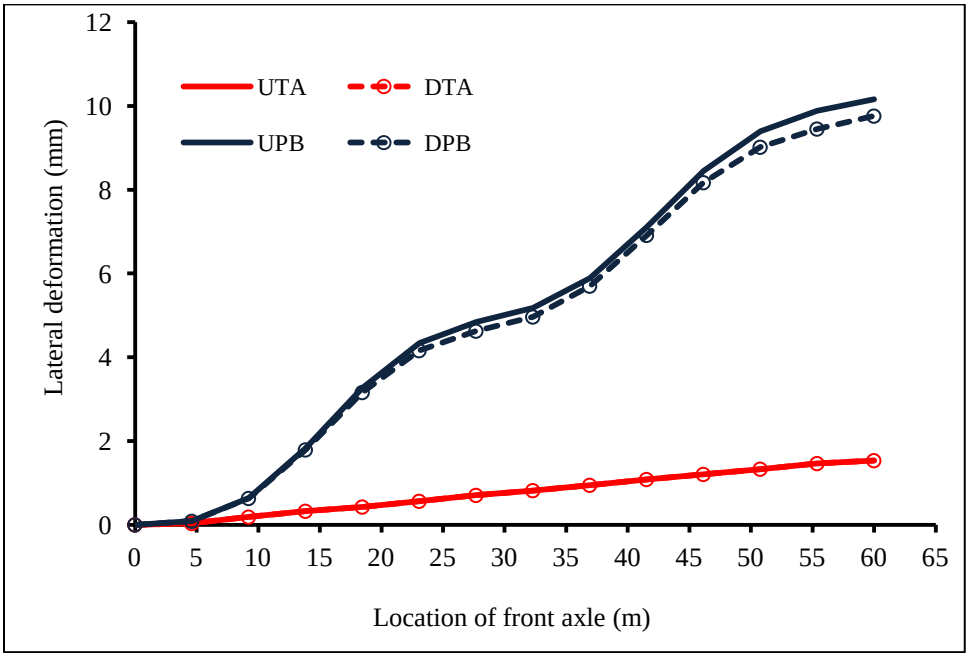

Figure C-2.i: Truck position versus maximum lateral deformation of the right column for traditional and performance-based designs.

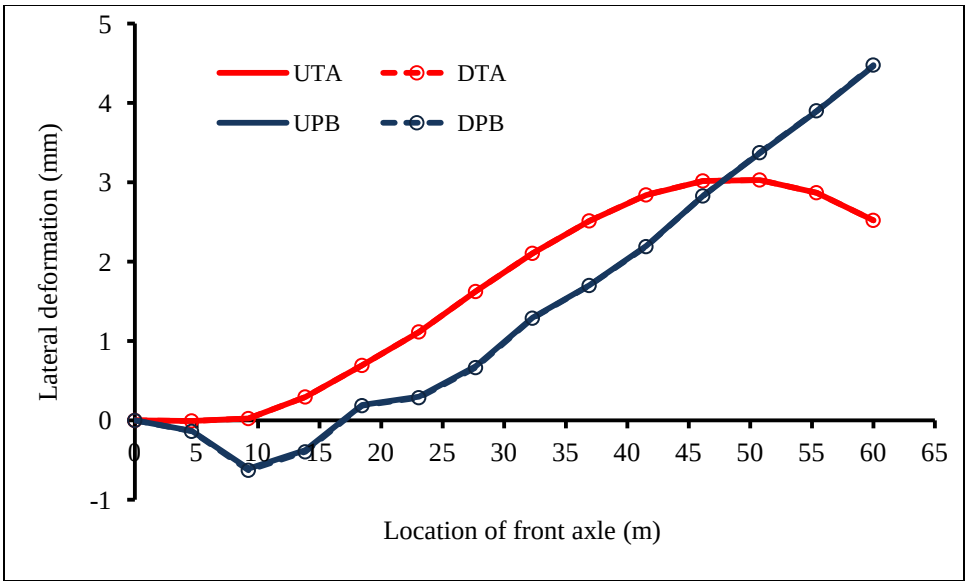

Figure C-2.j: Truck position versus maximum lateral deformation of the left column for traditional and performance-based approaches.

Appendix D

This paper is a reproduction of the conference paper that was published at the CSCE 3rd Specialty Conference on Material Engineering and Applied Mechanics, Montréal, Québec, 2013.

Simplified Non-linear FE Model to Predict Staged Capacity Deterioration of RC Columns Subjected to Combined Ultimate or Seismic and Reinforcement Corrosion Loads.

Abstract: The quasi-static and the low frequency cyclic loading-to-failure tests have shown that the stiffness degradation and strength of RC columns are reduced in a staged pattern. Although several studies have demonstrated this strength and stiffness degradation using complicated high-level 2D and 3D modeling approaches, a simplified numerical approach is required. Simplified non-linear finite element model developed by the authors is used in this paper to capture the staged damage and collapse of RC columns subjected to extreme loads. The model performs inelastic sectional and element analysis phases considering the instantaneous and successive changes of the sectional and element properties throughout the progress of the loading steps and the critical stages of corrosion-induced damages. The model considers all possible state of strain distributions on a concrete beam-column, and the nonlinear instantaneous sectional properties and the internal forces are calculated ensuring the equilibrium of all the internal and external forces in the section level. It is found that the proposed simplified nonlinear finite element model is numerically stable in all cases of strain distributions, both in static and dynamic analysis. The model shows that the load displacement curve of the columns

subjected to quasi-static loading or the envelop of the load-displacement hysteretic relationship can be found using quasi-static analysis. The model can predict the nonlinear behavior of non-corroded and corroded specimens with high accuracy. Further research is required to accurately define the critical stages of damages incorporating field and experimental data of damaged RC columns and higher level non-linear finite element techniques.

D1. Introduction

Thorough understanding of the deterioration mechanisms and identification of damage stages are essential base for any model simulating the behaviour of damaged structures. The effects of such damage stages on flexural and shear stiffness, ductility of materials and structural elements, progressive changes of internal forces and stress distributions due to spalling, mass losses, etc, could lead to identify threshold structural capacities for an efficient quantitative infrastructure management approach. Visual inspection is the most widely used method for the assessment of the physical condition of bridges; however, it is a subjective approach provides only qualitative condition assessment of bridge structures. The main objective of the development of a quantitative assessment approach is to minimize the risk of missing the detection of a critical and unsafe condition of a bridge element/system, or avoiding an over-conservative assessment that may result in unnecessary and costly repairs and/or replacement. The limits between different assessment rating categories based on visual inspection are not yet well separated. The wide transition zones between these assessment rating categories could lead to a contradictory in an inspector identification of critical distress symptoms of an important bridge in the transportation network. Yet, a fully time dependent quantitative

assessment approach is far from realistically being available in the short term seen, but an integration of the visual inspection and a simplified quantitative assessment approach is proposed here as an effective transition step.

Consequently, establishing force-deformation characteristics of reinforced concrete columns subjected to extreme loads (axial, flexure and or seismic loads) combined with reinforcement corrosion are of major importance. Over the past four decades, the quasi-static and the low frequency cyclic loading-to-failure tests have been well-developed to evaluate the strength and stiffness degradation (together with the energy dissipation, in the case of cyclic loading) of non-corroded reinforced concrete columns. The results of these tests show that the stiffness and strength are reduced in a staged pattern. Experimental observations showed that typical sequence of damage stages of both quasi-static and cycle loading testes are starting with concrete cracking followed by longitudinal reinforcement yielding, spalling of the concrete cover, lateral reinforcement failure and local or global loose of confinement, and possible longitudinal reinforcement buckling and fracture.

Several analytical and numerical models have been proposed to capture one of these limit-cases of damage. Consequently, many researchers proposed advanced two-dimensional (2D) and three-dimensional (3D) models that capture such staged capacity deterioration of RC elements. Assimilating such models in a cost effective and numerically stable assessment approach is very challenging and could not be practical for field engineers. Furthermore, there is no simplified approach that accurately predicts stiffness, strength and hence residual load capacity of the structural element in these critical damage stages. Such a simplified approach may provide practical engineers with

efficient quantifying evaluation management tool for better decisions on the operation status of RC bridges.

In this paper, a simplified yet efficient non-linear finite element model that simulates the staged failure and estimates the load capacity of the deteriorated RC elements in each critical stage is presented. The model is aimed at a capability to imitate the mechanical behaviour at the section level taking into account the boundary conditions and member geometry in the structural level. The corrosion-induced damage is established at the sectional level through the reduction of the reinforcing steel area, spalling of the concrete cover, loose of concrete confinement and possible buckling of deteriorated steel rebars.

D2. Modeling Approach and Assumptions

The procedure to establish the load-deformation characteristics requires three basic steps: definition of constitutive material properties; performing inelastic sectional analysis; and performing a structural analysis. Of course, the effect of sectional geometry, steel reinforcement and confinement of core concrete, are considered in the sectional level while the effect of the boundary conditions and loading pattern are considered in the structure level modeling.

Several different approaches have been proposed to model the stress-strain relationship of concrete and reinforcing steel in compression and in tension. Kabaila 1964 and Basu1967 proposed a fourth-degree polynomial compressive stress-strain relationship followed by multi-linear post ultimate relationships with definite post-failure residual stress. This approach is apparently based on Hognestad second-order compressive stress-strain relationship of concrete up to ultimate stress followed by a linear stress drop up to failure, Figure D-1. On the other hand, many researchers experimentally confirmed that the

confinement can improve the stress-strain characteristics of the concrete as the lateral expansion of the concrete is restricted (Kent and Park 1970). In 1992, Saatcioglu and Razvi modified the stress-strain relationship of confined and unconfined concrete taking into account the reinforcement details. Their model assumed less strength and deformation capacity than those in Hognestad's model for unconfined cover concrete or the entire column section when the axial stress is low and the confinement of concrete core is negligible. In this paper, both models (a fourth-degree polynomial and Saatcioglu and Razvi models) are used according to the state of axial stress recognising to major element behaviours; flexural dominant or compression dominant behaviour. To represent the concrete stress-strain relationship in tension, Gilbert and Warner 1978 model has been used where tension softening, tension stiffening and local bond-slip effects are all taken into account. On the other hand, tri-linear stress-strain relationships is assumed for the reinforcing steel both in tension and in compression assuming no local rebar buckling is expected. More details of material models are provided by Mohammed et al. 2013a.

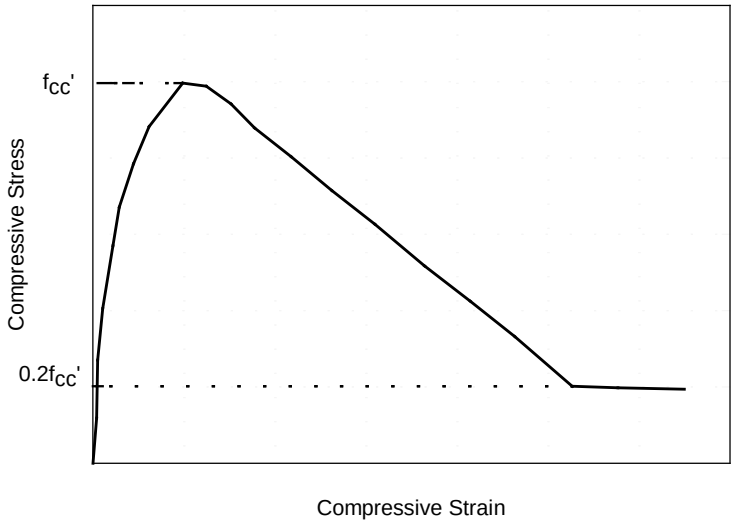

Figure D-1: Stress-strain relation for compressive concrete.

Sectional analysis is an essential step to consider the elasto-plastic development of concrete stresses and the variation of sectional characteristics throughout the crack propagation and the changes in the stress distributions in the section level. The concrete and the steel are assumed in a full composite action and the effects of shear deformations are neglected. Based on the strain distribution over the section, an iterative nonlinear process is conducted to satisfy the equilibrium of the forces on the section in every step of the load increment (axial, moment or both). If the section is subjected to only flexural stresses, the strain distribution is variable from extreme tensile strain at one end to extreme compressive strain on the other end (see Figure D-2.b). As the cracks initiated and propagated, the neutral axis migrates toward the extreme compression fiber with further increase of the strain level. If the section is subjected to axial stresses only, the strain distribution is constant compression (see Figure D-2.c). On the other hand, if a combination of axial stress and flexural stress is applied on the section, then the strain will be one of two cases: (i) pure compression (see Figure D-2.d); (ii) variable high compressive strain to low tensile strain (see Figure D-2.e). The most popular state of strain distribution for beam columns is case (ii), while case c is for typical beams, and case d is for typical columns with low eccentricity. The nonlinear stress distribution is shown in Figure D-2.f. In the FEM model (Mohammed, et al, 2013a) and to integrate the nonlinear stresses over the concrete and the steel, the section is divided into number of strips, where the stresses at the center of these strips are determined from the material nonlinear stress-strain relationships. It is found that this approach is numerically stable in all cases of strain distributions shown in Figure D-2. The nonlinear instantaneous

sectional properties (EA_i and EI_i) and the internal forces are then calculated ensuring the equilibrium of all the internal and external forces in the section level.

Depending on the assumption of the number of sections per element and the instantaneous nonlinear sectional properties, the stiffness, mass and dumping matrices are derived for each element and assembled over the structure for each load step. In the structure level of nonlinear modelling, it is assumed that: (i) all deformations (displacements, rotations, etc.) are continues functions over the structural element throughout all the load increment steps; and (ii) the equilibrium has to be satisfied in the section and structure levels. More details of inelastic sectional and member analysis can be found in Mohammed et al. 2013a &b.

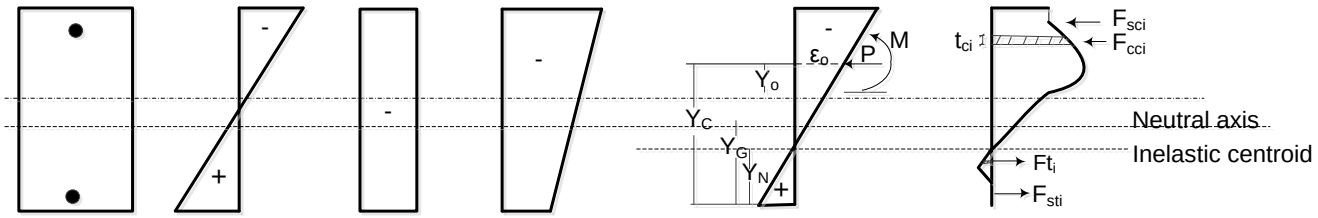

(a) (b) (c) (d) (e) (f)

Figure D-2: Stress-strain distribution; (a) cross section; (b) strain distribution due to flexural; (c) strain distribution due to axial load; (d) strain distribution due to flexural & axial load; (e) depths distribution; (f) concrete & steel stresses.

D3. Modeling Effects of Corrosion

As the change in RC section properties (area and moment of inertia) leads to a reduction in elements stiffness, the effect of reinforcement corrosion is modelled here by reducing the rebar cross-sectional area and its ductility. Removing concrete cover may also result in increased eccentricity of the applied axial load (Rodríguez et al, 1996). It has been observed that losing stirrups/ties can be more vulnerable to corrosion than longitudinal

bars as they are usually closer to the external surface of the structure, and they have greater perimeter/cross-sectional area ratio. Partial loss of bond at the steel-to-concrete interface is one of the important effects of corrosion. Depending on the affected length of the bars, loose of bond could lead to increase the deformations of RC element (El Maaddawy et al, 2005). Bond failure could occur in severely large corrosion affected RC members of when the joints of framed structures are severely damaged. In addition, the degradation of bond-slip relationships as consequence of corrosion effects causes increases in the global drift ratio of RC structures due to increases in lateral displacement, (Yalciner et al, 2012). In this study, concrete is assumed to be compositely connected to steel at the section level prior to corrosion and when the corrosion takes place, the bond is assumed to be fully lost in the affected zones. Based on field observations, it is assumed, in this study, that localized corrosion damages occur in critical zones of the bridge where the salty water splashed on the column surface or the bridge top where the salty water leaks from the expansion/ construction joints of the superstructure (Mohammed et al, 2013a &b). This will only result in local loose of bond. The damaged material models are integrated in the sectional level modeling for different deterioration stages and/or corrosion amounts.

Also, it was observed that corrosion pressure has limited effect on softening of concrete through the concrete core as the corrosion level increases. After formulation of longitudinal crack along the height of corroded reinforcing bar, the bar deflects by corrosion pressure towards the weakest part and concrete cover spall off (Rodríguez et al. 1996 and Oyado et al. 2007).

Since bridge columns usually subjected to a high axial load and low eccentricity; therefore, the main concern of simulating corrosion effects on the RC bridge columns are loss stirrups, confinement and buckle the reinforcement bars. In some cases and with severe localized corrosion, the behavior bridge columns could switch from compression to flexural depending on the level of applied load and the level and location of corrosion.

D4. Estimation of Staged Deterioration of Ultimate and Seismic Capacity

In order to simulate the failure mechanism of RC elements when subjected to ultimate or seismic load, it is essential to capture all stages of damage and the structural behaviour and capacity with high accuracy. The characteristics and capabilities of the proposed simplified nonlinear FEM model such as its accuracy, applicability, versatility, and its efficiency are demonstrated in the following sections in comparison with available experimental results. The main focus in this paper is on the effectiveness of the model to simulate the force-deformation relationship of different RC element subjected to extreme loads (ultimate or seismic loads). More details of numerical validations and comparisons can be found in Mohammed et al.2013a & b.

D4.1 Validation of the Proposed Model

The proposed model is validated though its two modeling levels; sectional level and element (structure) level. The convergence of the model depends on the optimum selection of three major parameters: (i) the load step; (ii) element size ;(iii) number of section per element. The convergence should be achieved in each load step where slow convergence or divergence categorized as numerical instability.

The preliminary validity of the proposed model is performed by investigating a simply supported beam subjected to uniform distributed load. The experimental load-deflection

curve of this beam is originally presented by De Cossio-Siess 1960. A numerical simulation based on closed form derivation of the beam nonlinear stiffness from the flexibility matrix is proposed by Rasheed and Dinno 1994. The load deflection relationship estimated by the proposed model compared to experimental results and Rasheed and Dinno model result are shown in Figure D-3. The results of both models, the proposed and Rasheed and Dinno, are almost identical and underestimate the experimental results.

This example shows that the model is capable to safely simulate the section mechanical behaviour with high numerical stability. Conversely, the use of the other model requires intensive time and large number of trials to reach a numerical stability, and tuning the convergence is a case by case problem. Rasheed and Dinno model requires satisfying a normalized convergence criterion for the moment of the axial rigidity about the inelastic centroid, which is very sensitive criterion and can be satisfied only for very limited cases.

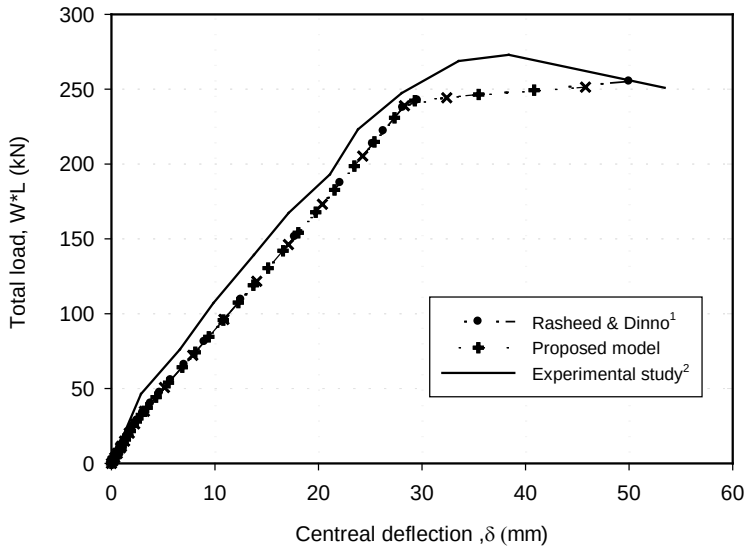

Figure D-3: Load-central deflection response of simply supported beam subjected to uniform distributed load; [1] Rasheed and Dinno 1994 ; [2] De Cossio-Siess1960.

D4.2 Case Study I: RC Column under Compression Loads

Saatcioglu and Razvi 1992 investigated the behaviour and design of normal-strength and high-strength concrete columns subjected to earthquake loads. One of their study specimens is selected for the comparison with the proposed model results. The specimen is a square column of 250 mm X 250 mm cross section, and 1500 mm height; a clear concrete cover of 10 mm is provided; the concrete compressive strengths was established by standard cylinder tests with concrete compressive strength $f_c' = 60\ \text{MPa}$; the longitudinal bars were 16mm in diameter (No15), and had yield strength of 450 MPa; the volumetric rations (ρ_s) of the lateral reinforcement is 1.4 %; the spacing of transverse reinforcement is 85 mm; the specimen was tested under monotonically increasing. Figure D-4 shows axial load-axial strain relationships established from the experimental test of the column compared to the stress-strain relationship from the proposed model. The model results match the experimental results in the elastic range and underestimate the stress after the yield where the predicted collapse strain is also less than that in the test.

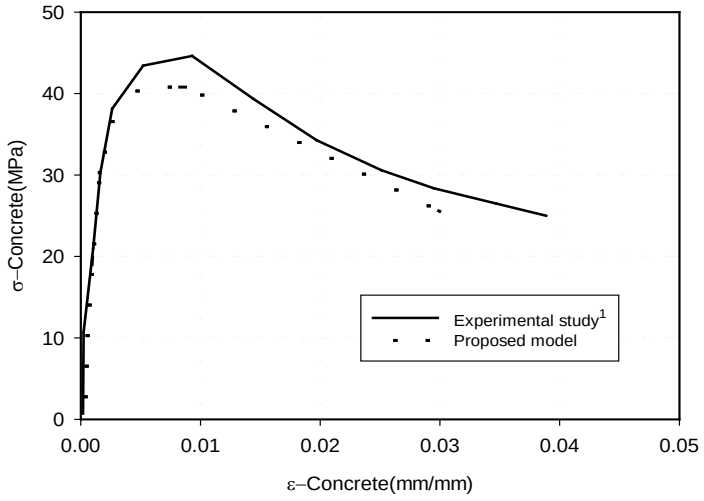

Figure D-4: Stress-strain of extreme fiber of confined zone of the selected specimen; [1] Saatcioglu & Razvi 1992.

D4.3 Case Study II: RC Column under Cyclic Loading

In this case study, an RC column tested by Saatcioglu and Ozcebe 1989 is investigated. The column represents part of a first-story column in-between the foundation and the inflection point the column is designed as an earthquake-resistant. The test results show the effects of axial load, transverse reinforcement, and bidirectional loading on column ductility. The column is square with 350 mm X 350 mm cross-section and 900 mm height. The concrete compressive strength is 37.3 MPa; the longitudinal rebars diameter is 25 mm with yield strength of 425 MPa and the longitudinal reinforcement ratio is 3.27%; and the spacing of ϕ 10 transverse reinforcement was 65 mm center to center. The proposed model is used to predict the load-deformation curve of the column and its load-displacement hysteretic relationship. The model use Takeda's approach to establish the load-displacement hysteretic relationship.

Figure D-5.a shows a good match of the model results and the experimental results in the elastic range and again the model underestimates the stresses after the yield point. Figure D-5.b shows the predicted envelop of the hysteretic relationship plotted on the experimental results, which shows very good match.

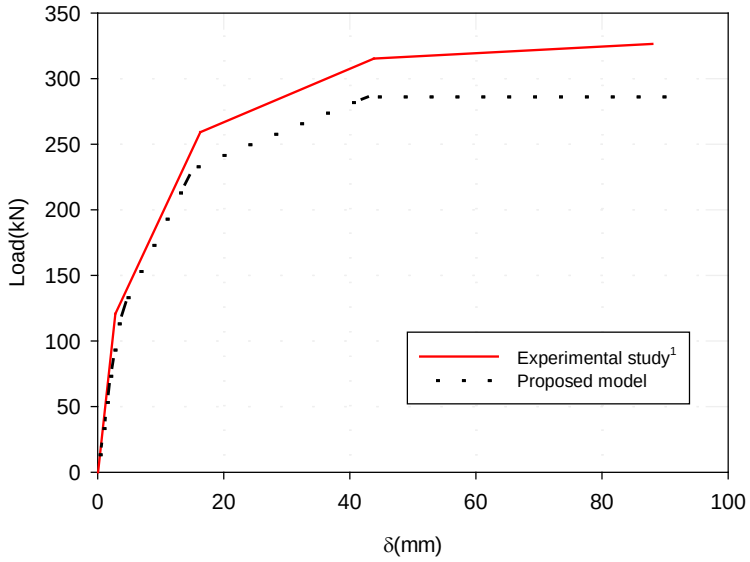

Figure D-5.a: Lateral load-top deflection of the selected specimen;[1]Saatcioglu & Ozcebe 1989.

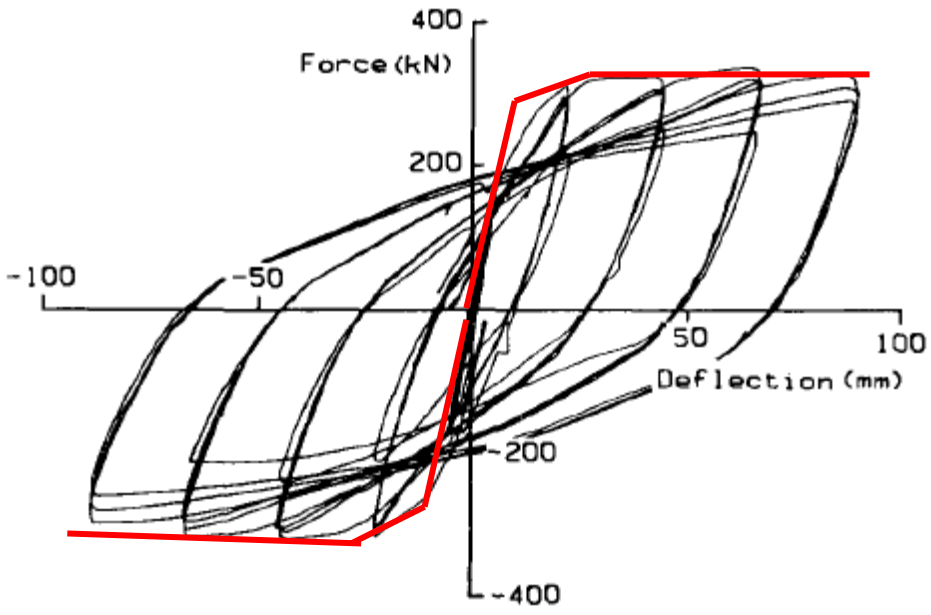

Figure D-5.b: Lateral load-top deflection hysteretic relationships, after Saatcioglu & Ozcebe 1989.

D4.4 Case Study III: RC Column Subjected to Cyclic Load and Reinforcement Corrosion

In this case study, two RC columns subjected to combined cyclic load and reinforcement corrosion are investigated. The columns investigated in this paper are Column No1 and Column No 4 out of the eleven cantilever column specimens tested by Oyado et al, 2007.The columns were exposed to different levels of corrosion then subjected to the cyclic load. The columns are 1650 mm long and square cross sectional dimensions of a 450 X 450 mm. The mechanical properties of the concrete of both columns are: (i) compressive strength: 30.5 MPa; (ii) tensile strength: 2.64 MPa (from tensile splitting test); and (iii) modulus of elasticity: 25.5 GPa. Column No1 is the control specimen while Column No4 is made with the scraped bars at the loading side. It is observed that throughout the application of the cyclic load, the concrete cover close to the column support damaged and split in parts gradually the case of the control specimen, Column No1. Conversely, in the case of testing Column No4 under cyclic loading, the concrete cover at the zones affected by the reinforcement corrosion splits in one piece. Figures D-6.a and 6.b show the envelop of hysteretic response of the control and the corroded specimen, as collected from the tests and as predicted by the proposed model. It is observed that the decline of the maximum lateral resistance force of the corroded specimen is only 10% compared to the control specimen; however, significant reduction of the displacement at maximum lateral load capacity reaches 50 % in the corroded specimen. The lateral load capacity of the last loading cycle of the corroded specimen is also decline to half of the related capacity of the control specimen, while the maximum displacement at the last loading cycle decline by 40 %.

The load-displacement envelops curves for non-corroded and corroded specimens are simulated with reasonable accuracy where most of the critical characteristics are captured. The model identify all critical damage stages where the load resistance capacity decreased, namely: cover spalling; one stirrup failure; two stirrups failure; and complete loss of confinement of the core concrete as shown in Figures D6-a and 6-b. It is important to mention that the model can estimate accurately the envelop curves of both columns either by conducting the hysteretic load-displacement analysis or by conducting static non-linear analysis for each of the damage stages, then the final load displacement envelop curve is plotted through defining the displacement at each damage stage.

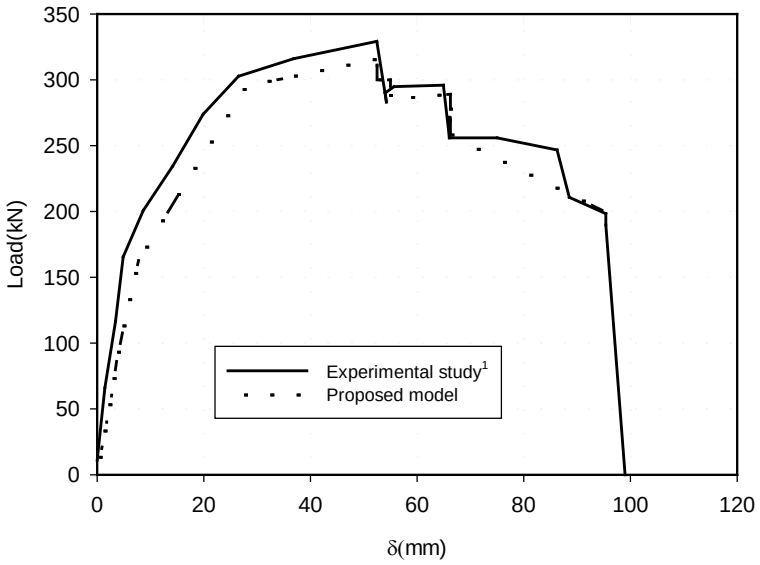

Figure D-6.a: Envelope curve of load-displacement relationship of control specimen, Column No 1 ([1]Oyado et al.2007).

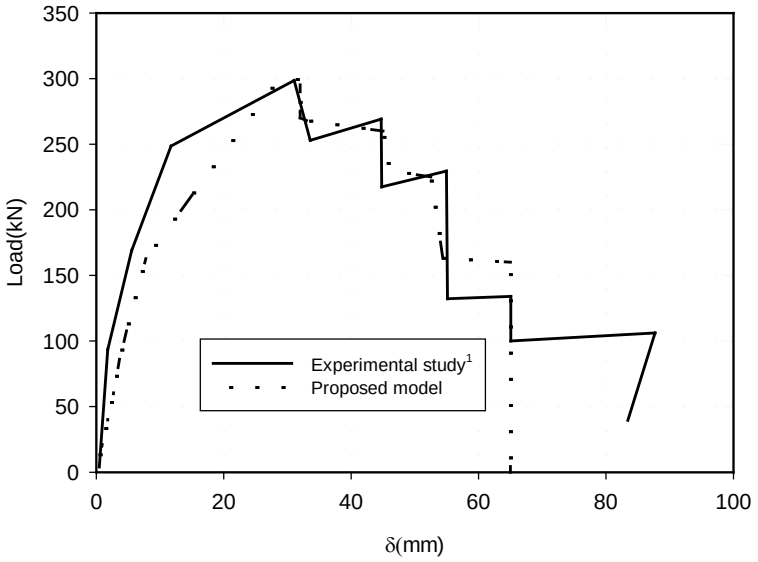

Figure D-6.b: Envelope curve of load-displacement relationship of the specimen subjected to reinforcement corrosion, Column No 4 ([1]Oyado et al.2007).

D5. Summary and Conclusion

Several studies have demonstrated the strength and stiffness degradation of RC columns using quasi-static and the low frequency cyclic loading-to-failure tests or using complicated 2D and 3D modeling approaches. However, a simplified numerical approach is required to predict stiffness and strength deterioration of RC columns subjected to extreme loads (ultimate or seismic). Simplified nonlinear finite element model of RC elements subjected to any combination of axial, flexure, and lateral static or cyclic loads is developed by the authors (see Mohammed et al 2013a & b). The capabilities to capture the staged collapse of such RC element are investigated in this paper. The model employs nonlinear constitutive material properties, performs inelastic sectional analysis considering the instantaneous and successive changes of the sectional and element properties throughout the progress of the loading steps and the critical stages of corrosion-induced damages. The model considers all possible state of strain distributions

on a reinforced concrete beam-column element and the nonlinear instantaneous sectional properties and internal forces are calculated ensuring the equilibrium of all the internal and external forces in the section level. Depending on the assumption of the number of sections per element and instantaneous nonlinear sectional properties, the stiffness, mass and dumping matrices are derived for each element and assembled over the structure for each load step.

It is found that the proposed simplified nonlinear finite element model is numerically stable in all cases of strain distributions, both in dynamic and static analysis. The model shows that the load displacement curve of the columns subjected to quasi-static loading or the envelop of the load-displacement hysteretic relationship can be found using quasi-static analysis. The model can predict the nonlinear behavior of non-corroded and corroded specimens with high accuracy.

D6. Future Work

The simplified nonlinear finite element model developed by the authors together with the capability to model staged deterioration of structural capacity open the research in three major areas:

(i) Assessment of bridge elements current capacity where the accurate identification of the critical stages of damages is required. Incorporating field and experimental data on the damaged RC bridge elements could result in practical approach for engineers.

(ii) Modeling the behaviour of RC frame bridge, RC continuous bridge, or RC multi-story frame elements subjected to combined ultimate loads or seismic load and reinforcement corrosion;

(iii) Development of non-linear finite element model based on two-dimensional finite elements (plane stress/plane strain, or shell elements) would be important to capture the shear, shear-flexural, and time dependent bond lose effects on the staged damage mechanism.

D7. References

Basu. K., 1967. Computation of failure loads of composite column. Inst. Civ. Engrs, London, 36: 557-578.

De. Cossio R. D. and Siess C. R., 1960. Behaviour and strength in shear of beams and frames without web reinforcement. Journal-American Concrete Institute,(56):695-735.

El Maaddawy, T., Soudki, K., and Topper, T.,2005a. Long-term performance of corrosion-damaged reinforced concrete beams. ACI Structural Journal,102(66),649-656.

Gilbert, R. and Warner R.,1978. Tension stiffening in reinforced concrete slabs. J. Strcut. Div. ASCE .104(ST12),1885-1900.

Kabalia, A., 1964. Disc. of equation of the stress-strain curve of concrete. P. Desayi and S. Krishnana, J. Am. Concr. Inst. 61,1227-1229.

Mohammed, A., Almansour, H., and Martín-Pérez, B., 2013a.Nonlinear sectional analysis of RC section subjected to ultimate loads and reinforcement corrosion, (to be submitted shortly to Computer and Structures).

Mohammed, A., Almansour, H., and Martín-Pérez, B., 2013b. Nonlinear flexural analysis of RC beam-column subjected to ultimate loads and reinforcement corrosion, (to be submitted shortly to Computer and Structures).

Oyado, M., Saito, Y., Yasojima, A., and Kanakubo, T. 2007.Structural Performance of corroded RC column under seismic Load. First International Workshop on Performance, Protection & Strengthening of Structures under Extreme Loading, Whistler, Canada.

Rasheed, H., and Dinno, K., 1994. An improved nonlinear analysis of reinforced concrete frames. Computer and structures. 53(3)625-636.

Rodríguez, J., Ortega, L. M. and Casal, J.,1996. Load bearing capacity of concrete columns with corroded reinforcement. Corrosion of Reinforcement in Concrete Construction, Royal Society of Chemistry: 220-230.

Saatcioglu, M., and Ozcebe, G., 1989. Response of reinforced concrete columns to simulated seismic loading. ACI Structural Journal, 86-(1): 3-12.

Saatcioglu, M., and Razvi, S., 1992. Strength and ductility of confined concrete. Journal of Structural Engineering, 118(6): 1590-1607.

Yalciner H., Sensoys., and Eren O., 2012. Time-dependent seismic performance assessment of a single-degree-of-freedom frame subject to corrosion. Engineering Failure Analysis,(19):109-122.

Appendix E

This paper is a reproduction of the conference paper that was published at the CSCE 2rd International Engineering Mechanical and Materials Specialty Conference, Ottawa, Ontario, 2011.

Combined Effect of Reinforcement Corrosion and Seismic Loads on RC Bridge Columns: Modelling

Abstract: Columns are often the most vulnerable elements in reinforced concrete (RC) bridges as their failure could lead to bridge collapse. Characteristically, columns are subjected to combined static and dynamic eccentric and lateral forces due to traffic, self-weight, and earthquake loads. For the assessment of bridge columns in seismic areas, it is essential to evaluate their state of damage, strength and deformation capacity over their service life. In this paper, a nonlinear elasto-plastic numerical model to simulate bridge columns under the combined effects of reinforcement corrosion and seismic excitation is presented. The study includes the development of a comprehensive and yet simple tool to evaluate the seismic performance, and the residual strength and deformation capacity of aging RC bridge columns suffering from reinforcement corrosion. The model enables evaluating aging and deteriorated RC bridge columns safety, the decline in their energy dissipation capability, and the level of earthquake excitation that they may survive. Hence, the model can represent a useful tool for bridge engineers to optimize the use of available resources and define the critical capacity of bridge columns against earthquake events. It is found that the model is efficient in simulating the behaviour of the column under corrosion and seismic loads. From the case study, it is found that the load carrying

capacity of the corroded column is much lower than that of non-corroded columns. The results show significant reduction in the column displacement capacity and energy dissipation capability due to rebar corrosion. The corrosion-induced damage could result in accelerated degradation of the bridge columns and reduce its ultimate strength.

E1. Introduction

Columns are often the most vulnerable elements in reinforced concrete (RC) bridges as their failure could lead to bridge collapse. Characteristically, columns are subjected to combined static and dynamic eccentric and lateral forces due to traffic, self-weight and earthquake loads. For the assessment of bridge columns in seismic areas, it is essential to evaluate their state of damage, strength and deformation capacity over their service life. In bridge design codes the major concern is the bridge serviceability and safety under applied loads, including seismic loads, without an explicit attempt to account for deterioration. However, RC bridge columns in cold regions are affected by chloride-induced reinforcement corrosion, generated mainly from the application of de-icing salts in the winter. Hence, in the evaluation of RC columns of aging bridges, where reinforcing steel corrosion is a potential or on-going problem, the main goal is to determine the capacity of the deteriorated RC columns, their safety margin related to the load demand, and whether or not this capacity will further decline over time.

Reinforcing steel corrosion is a long-term process with accumulated influence, while seismic loads are accidental by nature. The interaction and combination of both loads could be a result of two possible scenarios: (i) corrosion is in progress or in an advanced stage and an earthquake occurs; or (ii) the structure survived a medium size earthquake with some minor damage in the form of cracks, which could accelerate the initiation or

the progress of the corrosion process. Whereas the first case is important in evaluating the safety and capacity of the structure under seismic load, the second case is important in elevating the alert to accelerate the bridge inspection-evaluation cycle.

Saito et al. (2007) presented the fundamental properties of strength and deformation capacity of corroded RC columns subjected to seismic load. The study had two set of specimens: (i) columns subjected to axial compression load only; and (ii) columns that were exposed to axial compression and cyclic lateral load. In both tests, the studied parameters were the length of corroded reinforcing bar, the corrosion simulation method, and the corrosion level. They observed that the corrosion of longitudinal bars and hoops causes reduction in the column deformation capacity. They proposed a stress-strain model and corresponding deformation capacity by considering the reduction of cross section of corroded reinforcing bars. Attributed to the lack of the theoretical data and relevant information, this study did not give attention to the deteriorated concrete elements performance under dynamic load. Choe et al. (2008) developed probabilistic drift and shear force capacity models by integrating the effects of deterioration of corroded structural elements into a structural capacity model. In their study, a numerical approach was performed using the OpenSees software to obtain the fragility estimate for a given column, which was modeled by fiber-discretized cross sections, where each fibre contains a uniaxial inelastic material model. Also, the probabilistic model for reinforcement corrosion (corrosion initiation, corrosion rate, and loss of cross-section area) was carried out to characterize the prediction of service life of existing and new structures and their life-cycle cost analysis. The numerical study calculated that at the beginning of the corrosion propagation phase, the sensitivity with respect to the structural

capacity parameter model increased only in the first year of the corrosion propagation, decreased around the time of transition from the diffusion phase and the corrosion phase, and thereafter it increased gradually. Berto et al. (2009) conducted a theoretical investigation to assess the corrosion effects on the seismic behaviour of RC structures. The assessment processes were carried out under a moderate corrosive attack taking into account two parameters: reinforcing bars section reduction and concrete cover degradation. A nonlinear static analysis was performed using MIDAS Gen software, by considering gravitational and seismic loads and representing the structure by the lumped plasticity approach. The work of Choe et al. (2008) and Berto et al. (2009) are more focused on the consideration of loss of the reinforcement cross-sectional area in order to evaluate the structural capacity model. It is attributed to the lack of experimental tests and to the difficulty of developing simple numerical models to simulate the real behaviour of corroded structures.

The goal of this paper is to present a numerical model to evaluate the combined effects of corrosion-induced damage and seismic load on the performance of RC bridge columns. The emphasis is on the time frames diversity between the two processes and the instantaneous seismic capacity of an aging column. The procedure includes an external cycle to represent the corrosion process, which is introduced through the reduction of the reinforcing steel area and ductility and concrete cover. Step-by-step integration for the time-history analysis and the hysteretic behaviour of the RC column is then performed using an efficient algorithm.

E2. Research Significance

This paper presents a nonlinear elasto-plastic numerical model to simulate bridge columns under the combined effects of reinforcement corrosion and seismic excitation. The contribution of this study includes the development of a comprehensive and yet simple tool to evaluate the seismic performance and the residual strength and deformation capacity of aging RC bridge columns affected by reinforcement corrosion. This numerical tool enables the evaluation of aging and deteriorated RC bridge columns safety, the decline in their energy dissipation mechanism, and the level of earthquake excitation that they may survive. Hence, the model can represent a useful tool for bridge engineers to optimize the use of available resources and define the critical capacity of bridge columns against earthquake events.

E3. Proposed Model

Figure E-1 shows a flowchart of the proposed model. The model involves six major parts: (i) input data; (ii) formulation of the structure and load matrices; (iii) static and dynamic analyses, wherein the traffic loads are included; (iv) corrosion process; (v) time-history analysis under earthquake load; and, (vi) results. The procedure includes an external cycle to represent the corrosion process, which is activated once the corrosion activation parameter is equal to 1. The corrosion cycle starts at time T_{cor1} and ends at time $T_{cor\text{-}final}$ with time increment of Δt_{cor}. During every corrosion time-increment, a time-history analysis of the column is performed if desired (by activating the seismic parameter, or seismic=1 in the input data).

The procedure starts with the input data of: (i) the structure, which includes geometrical and material characteristics and boundary conditions; and (ii) control parameters. The

results for the column performance are printed with reference to each selected time increment or selected ones.

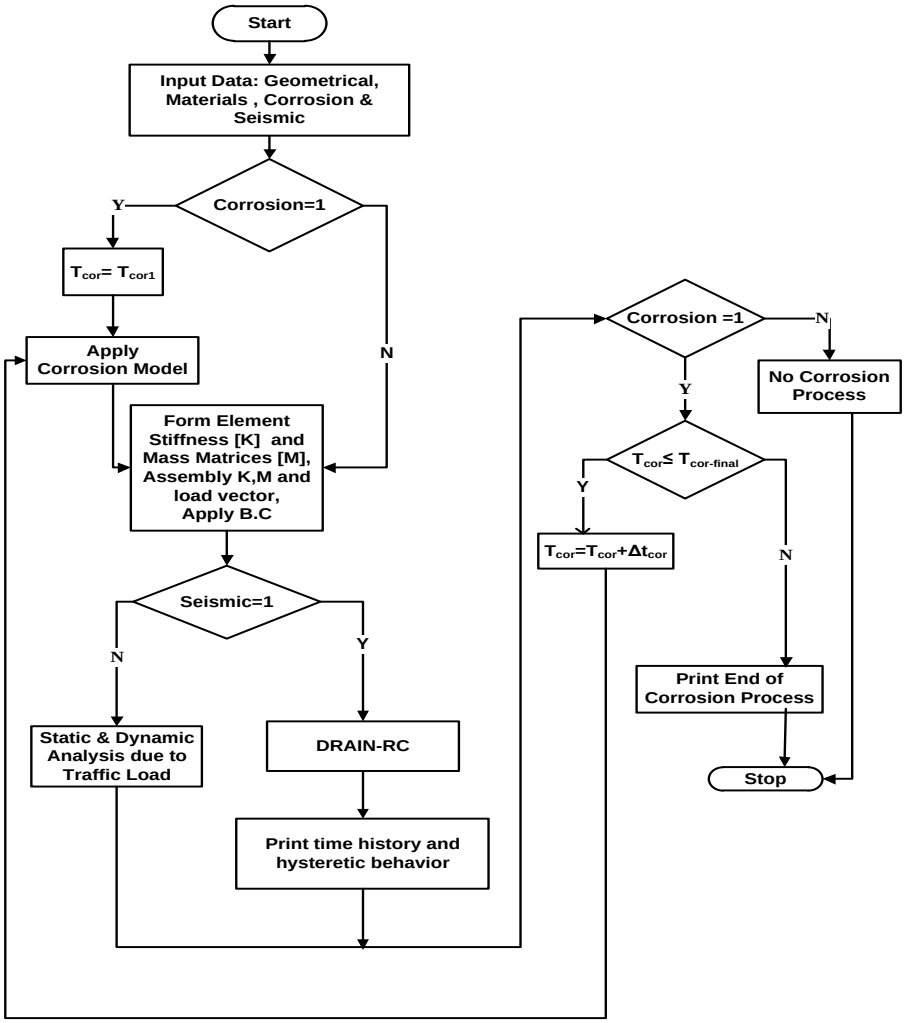

Figure E-1: Proposed model for combined effects of corrosion and seismic loads.

E3.1 Bridge Structure

Since the focus of this study is on the behaviour of bridge columns, the considered structure is a slab-on-girder bridge (which is usually simply supported on piers or abutment), Figure E-2.a. Also, it is essential to model both the superstructure and

substructure as one structural system. The model is required to effectively simulate the integration of the two parts. In slab-on-girder bridges and assuming practical girder spacing, the traffic load distribution in the lateral direction (orthogonal to the traffic direction) can be assumed uniform, and, hence, the bridge is modelled as a two-dimensional frame (Figure E-2.b). The frame in this model is basically formed from a beam, representing the superstructure, and two piers. The connections between the beam and the piers are represented by an internal hinge on one side and a roller on the other side. The model also accounts for possible eccentricity in both connections. The base of the two piers is assumed fully fixed. For the purpose of calculating the beam properties, the slab is assumed to be compositely connected to the girders. In the present model, the lateral slab flexural action and the girders tensional rigidities are ignored. Each pier consists of a cap beam, where the bridge superstructure girders rest on, and supporting columns forming a frame. In order to include the effect of reinforcement loss when corrosion is applied, the column is considered as a composite section. The beam and the columns are modeled using a beam-column element with three degrees of freedom per node. The damping matrix is derived assuming a linear proportion between damping of the elements and their mass and stiffness.

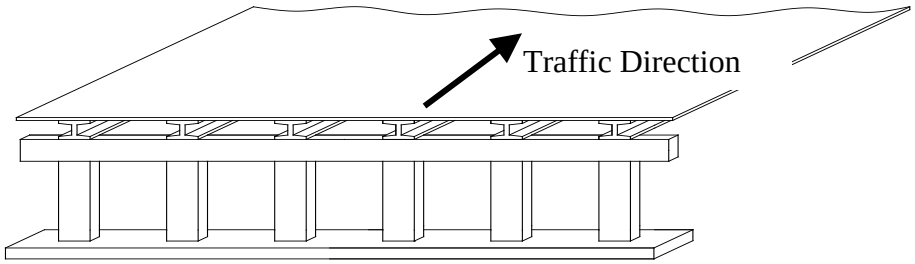

Figure E-2.a: 3-D bridge system.

Figure E-2.b: 2-D bridge system.

E3.2 Nonlinear Modelling and Time-History Analysis

The computer program developed in this study is integrated with the computer program DRAIN-RC, which is used to perform inelastic dynamic history analysis as shown in Figure E-1. The original version of the program (DRAIN-2D) was developed by Kanaan and Powell (1973) to conduct dynamic analysis of inelastic plane structures. The program was modified by Alsiwat (1993) and Shoostari (1998) by adding new hysteretic models for shear and anchorage slip and including new features such as inelastic static analysis (push-over) and P-Δ effects. In DRAIN, the structure is discretized into a number of

elements with degrees of freedom at the nodes. Each node can have up to three degrees of freedom, two translations and one rotation, and provisions are made for restraining either degree of freedom. The global stiffness of the structure is assembled from individual element stiffness using the direct stiffness method, whereas the mass of the structure is assumed lumped at the joints resulting in a diagonal mass matrix. Damping can be specified as either mass dependent or stiffness dependent Raleigh damping. Ground motion is entered as accelerations specified at constant time intervals and can differ for horizontal and vertical directions. The dynamic response is determined using a step-by-step integration technique, with the assumption of constant average acceleration during each time step. In assembling the stiffness matrix, the tangent stiffness at the beginning of each step is assumed to remain constant during the step. The stiffness of each element is updated at the beginning of each step, and if the nonlinear analysis option is selected, errors due to possible overshooting are corrected by applying a corrective load at the beginning of the next step.

E3.3 Corrosion Load

The effect of reinforcement corrosion is modelled here by reducing the rebar cross-sectional area over time. The change in the RC elements sectional properties (area and moment of inertia) leads to a reduction in their stiffness. The loss of reinforcing steel due to corrosion is evaluated by applying Faraday's law, from which the thickness reduction $x(t)$ of the reinforcing bar after time t can be calculated according to Eq. E.1:

$$x(t) = \frac{M}{zF\rho_s} \cdot i_{corr} \cdot t \qquad \text{(E.1)}$$

where M is the metal molar mass (55.85 g/mol for iron), z is the valence of the ion formed as a result of iron oxidation (i.e., z = 2 for $Fe \rightarrow Fe^{2+} + 2e^{-}$), F is Faraday's constant (F = 96,485 C/mol), ρ_s is the density of iron (ρ_s = 7.85 g/cm^3), i_{corr} is the corrosion current density, and t is the time elapsed since corrosion started. By substituting the values of M, z, F and ρ_s into Eq. E-1, the rate of thickness reduction results in $x(t) = 0.0116.i_{corr}.t$, where $x(t)$ is given in mm, i_{corr} is given in $\mu A/cm^2$, and t is given in years. Although Faraday's law assumes that all electrical current is used up by the corrosion process, it gives a conservative estimate of the steel loss due to corrosion. The depth of the corrosive penetration attack $p(t)$ is calculated from:

$$p(t) = R \cdot x(t) = R \cdot 0.0116 \cdot i_{corr} \cdot t \qquad \text{(E.2)}$$

where R is the ratio between the maximum penetration of a pit (p(t)) and average penetration (x(t)) corresponding to uniform corrosion. Parameter R is also known as the pitting ratio. Val (2007) has reported that the maximum penetration of pitting on the surface of a rebar is about 4-8 times the average penetration corresponding to uniform corrosion. Assuming that the pit can be idealized as a hemisphere, as illustrated in Figure E-3.a, and 3.b the cross-sectional area A_s of a group of n reinforcing bars after t years of corrosion can be estimated as:

$$A_s(t) = n\frac{\pi D_o^{\,2}}{4} - \sum_{i=1}^{n} A_{p,i}(t) \geq 0.0 \qquad \text{(E.3)}$$

where D_o is the initial reinforcing bar diameter and $A_{p,i}(t)$ is the cross-sectional area of a pit after time t, which is a function of $p(t)$ and calculated according to Val (2007).

Corrosion-induced damage is also simulated by assuming that the concrete cover of the columns has spalled out (Figure E-3.c).

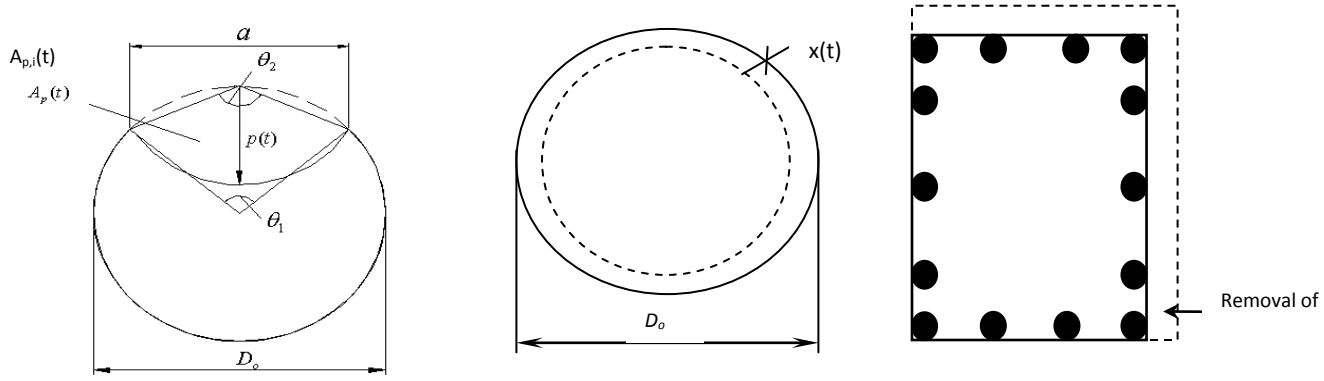

(a) Pit configuration (adapted from Val, 2007) (b) Uniform corrosion (c) Spalling of the concrete cover

Figure E-3: Corrosion model

The ductility of reinforcing bars has also been observed to be affected by corrosion. Many empirical models for loss of ductility have been proposed. Lay and Schiebl (2003) and Cairns et al. (2005) have established the following empirical equations to assess indirectly the residual ductility of reinforcement due to corrosion:

$$f_y(t) = (1.0 - \alpha_y . A_s(t)) f_y \quad \text{(E.4)}$$

$$f_u(t) = (1.0 - \alpha_u . A_s(t)) f_u \quad \text{(E.5)}$$

where $f_y(t)$ is the yield strength at time t, $f_u(t)$ is the ultimate tensile strength at time t, f_y and f_u are the yield and ultimate tensile strengths of a non-corroded bar, respectively, $A_s(t)$ is the cross section loss as a function of time t, and α_y, α_u are regression coefficients (Lay and Schiebl 2003).

It is worth noting that bond degradation due to reinforcing steel corrosion might become a concern for RC bridge columns located in seismic areas. The model presented here ignores these effects for the sake of simplicity. The regions that are more likely to be affected by corrosion along the column height are assumed to be far from the foundation-column joint. Hence the effect of bond-degradation due to corrosion on the seismic performance is not considered in this paper and will be included in next phase of this research.

E4. Load Combination and Interaction

The focus of the current study is on the combined effect of reinforcement corrosion and seismic load on highway bridge columns. However, the possible combination of other loads, such as self load and traffic loads has to be also taken into account. From the modeling point of view, three scenarios of bridge loading combination during an earthquake are possible: (i) earthquake and permanent loads (earthquake occurs when there is no traffic on the bridge); (ii) earthquake and full traffic loads (earthquake occurs during rush hour); (iii) earthquake and one truck (or more) is moving on the bridge. In the second scenario, the traffic load can be considered as static load (or multi lane loading). In the last scenario and for short span bridges, the duration of an earthquake is much longer than the time required for a truck to pass the bridge with a design velocity of 100 km/h. However, the frequency and the amplitude of the bridge vibration due to earthquake excitation is very high compared to the bridge vibration due to single or multiple trucks passing the bridge at the same time. The dynamic interaction between the resulting vibrations due to both excitations is relatively complicated and out of the scope of the present study. Therefore, when combining the earthquake and corrosion loads, the

traffic load is simplified as an equivalent static load (taking into account the dynamic impact factor) or taken as a dynamic excitation of two-degrees of freedom system (see Mohammed et al 2010), ignoring the dynamic interaction between the traffic and the earthquake.

The proposed model, as illustrated in Figure E-1, analyzes the combined effects of different loads; the two main subroutines (corrosion and DRAIN-RC) are to be called through the main program. Individual and/or combined analysis can be selected. DRAIN-RC imports the input data file already created by the main program. The main program controls the DRAIN-RC solver and runs each analysis step and extracts DRAIN-RC results. The extracted analysis results are then processed by the main program, providing the predicted corrosion-induced damage and the seismic performance of the column related to the instantaneous stage of corrosion (if requested in the input data).

E5. Case Study

The proposed model is examined through a case study of a slab-on-steel girder bridge with center to center span of 49.1 m. The bridge is simply supported on RC piers formed from eight rectangular 600×400 mm columns, connected from the top to a beam where the bridge superstructure girders rest on. The 6.0 m high columns are assumed to have full fixity at the foundation level. Detailed properties of the bridge superstructure are given in Table E-1. The concrete compressive strength f'_c for all the concrete components of the bridge is assumed equal to 30 MPa.

A one-dimensional bridge substructure system is analyzed under a load combination consistent with CHBDC 2006 (CAN/CSA-S6-00), wherein the traffic load has to be taken as 50% of the equivalent static service level (for single truck and lane loading). The

seismic load is also taken into account. The one-dimensional static analysis is conducted using preliminary column dimensions to determine values of bending moment and axial forces at each column. These values are used to design the columns. Multiple cycles of analysis and design are necessary to reach an optimum size of the pier and the columns.

Table E-1: General properties of slab-on-steel girder bridge.

Type of girder	Year Built	Skew Angle ^{o}	Span Length m	Girder Spacing m	Girder Properties A m^2	I m^4	H m	Transverse width m	Slab Thick m	No. of Girders
Steel	1977	0.0	49.11	2.64	0.0496	0.0187	2.898	20.487	0.2159	8

E6. Results and Discussions

Field surveys have shown that the most critical sections of bridge columns, which are suffering from corrosion, are the top and bottom sections (Andersen 1997). For this study, it is assumed that the bottom section at the traffic level under the bridge is at 2.0 m above the column base, and the top section is at 6.0 m above the bridge base. Figure E-4 illustrates the cross section of the RC column. Corrosion-induced damage is simulated by assuming a steel mass loss of 30%, which is equivalent to 10 years of corrosion with a corrosion current density of 1 $\mu A/cm^2$. The reduction of the concrete cross section due to spalling of the concrete cover and the reduction in the ductility of reinforcing bars are also considered.

The specified ground motion record used plays an important role in attaining realistic results. It is possible that two different earthquakes with the same intensity excite a given structure differently. Therefore, the correlation between the response spectrum of a given

earthquake record and the fundamental period of the structure is very important in selecting an earthquake record that is used in the analysis and results in comprehensive structural performance. In the present study, condensed data of a short Ottawa earthquake record is used as shown in Figure E-5. Detailed investigation to evaluate the sensitivity of the proposed model to different earthquake records is currently on-going.

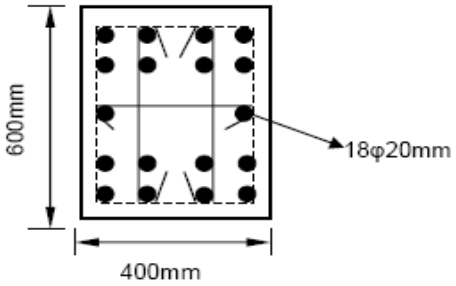

Figure E-4: Column section.

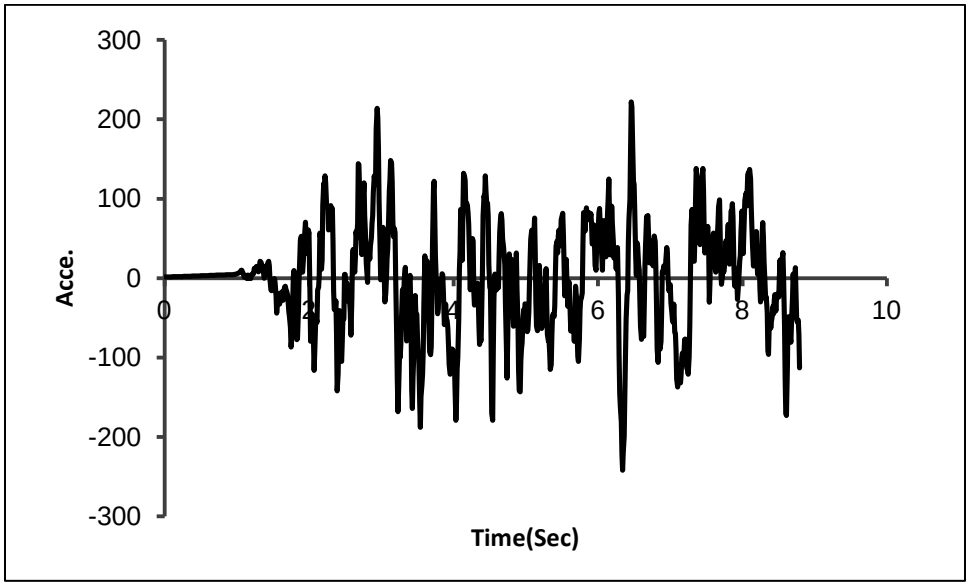

Figure E-5: Earthquake record used.

The loss of the cross section of the column due to concrete spalling as well as the reduction in the area and ductility of the reinforcing steel lead to a reduction in the load carrying capacity of the column. As shown in Figure E-6, the load-deformation relationship of the corroded section is much lower than that of the uncorroded section. The yield moment is reduced from 380 kN.m to 274 kN.m, and the displacement ductility is also reduced from 3.8 to 3.2. Figure E-7 shows the interaction diagram of the considered column at the cross section where corrosion results in a significant decrease of the column capacity. The ultimate limit state is not satisfied in this case, as the column capacity is less than the applied factored axial load and moment, which are 2,900 kN and 244 kN·m, respectively.

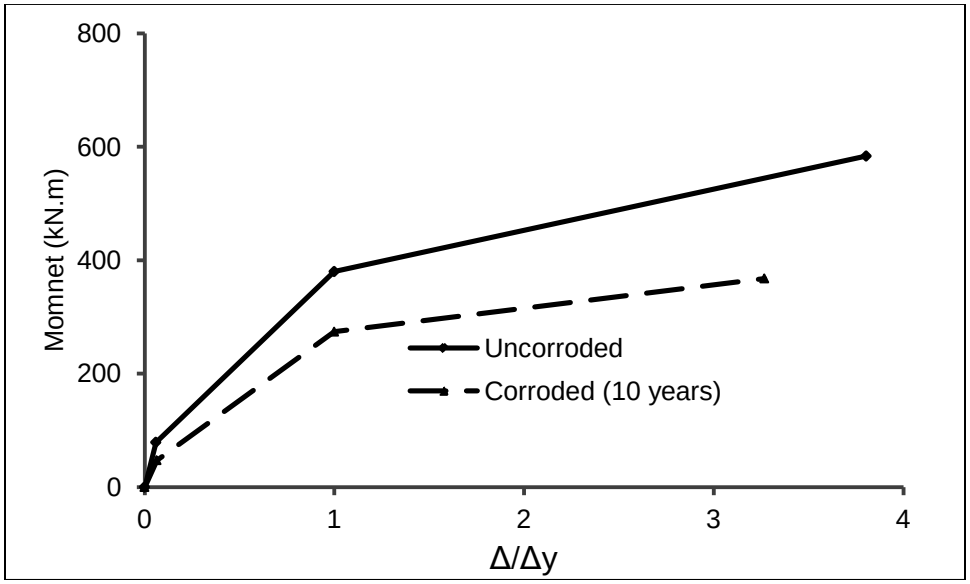

Figure E-6: Moment-deflection curve of the bridge column section.

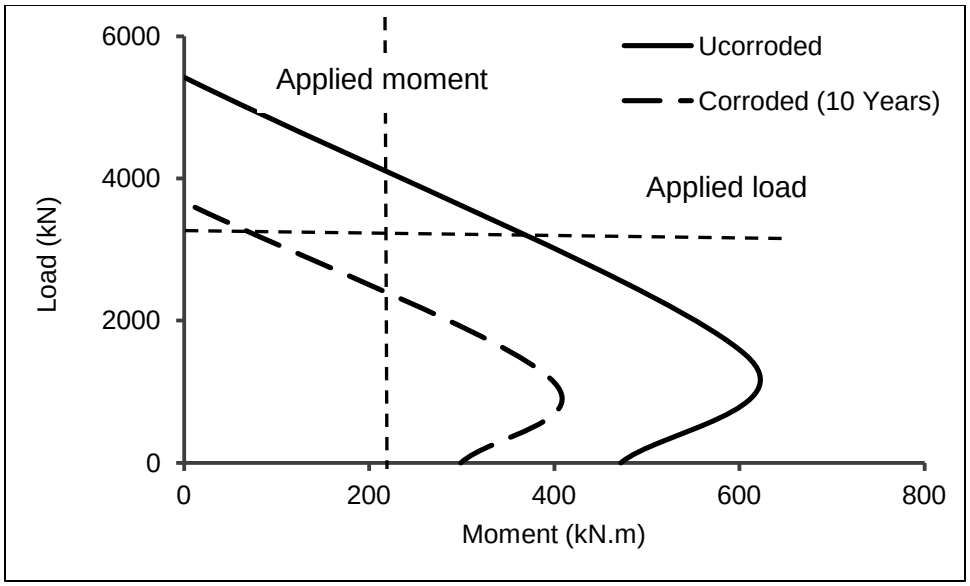

Figure E-7: Interaction diagram of the bridge column section.

Since both the steel area and concrete cover of the column at the critical cross section are reduced, their losses have a significant effect on the column stiffness. Depending on the inelastic behaviour of the column, the corroded section of the column will have less deformation capacity than the non-corroded section. With the reduction in the column flexural stiffness and the reduction in the reinforcing steel ductility, the lateral displacement history of the corroded section is increased when the bridge is subjected to seismic load. Figures E-8 and E-9 respectively show the significant successive increases in the lateral displacement through the time history of the corroded bottom and top column sections compared to the original non-corroded sections.

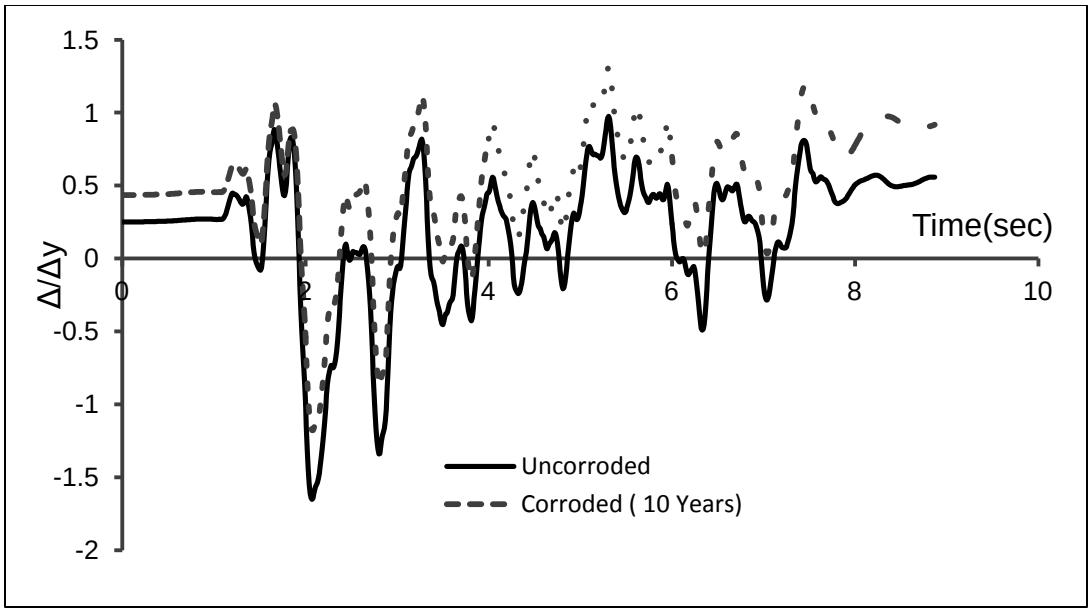

Figure E-8: Lateral displacement of the bottom section of the bridge column.

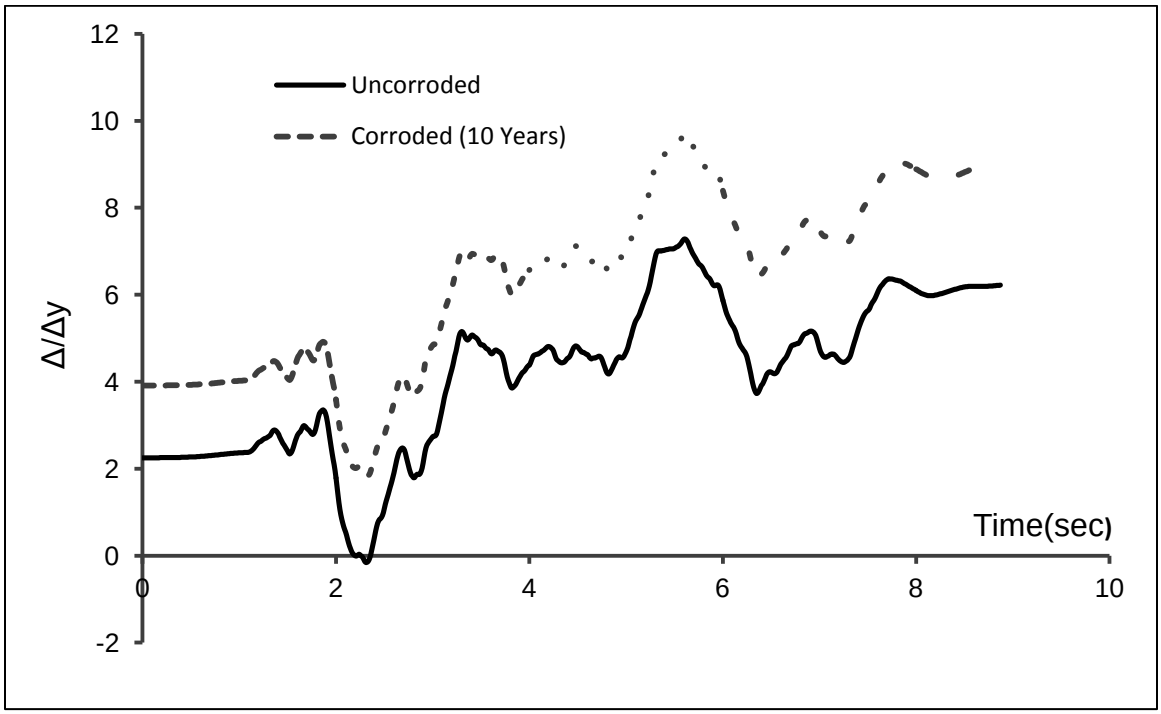

Figure E-9: Lateral displacement of the top section of the bridge column.

Figure E-10 shows the moment-displacement history of the corroded and uncorroded bottom section of the column. The area inside the hysteretic loop is considered as an indirect measure of the energy dissipated by the plastic hinge. It is obvious that the

corrosion of the longitudinal reinforcement results in significant degradation in the ultimate flexural capacity of the column and its capability to dissipate energy.

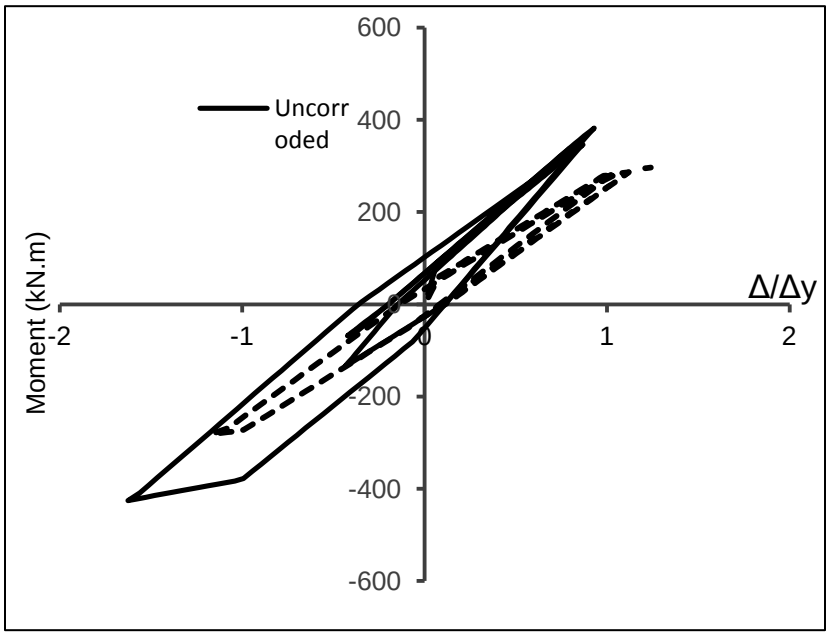

Figure E-10: Moment-displacement of the bottom section of the column.

The ductility index of the column, which represents the ability of the column to withstand the ground motion with sufficient deformation capacity, can be computed in the DRAIN-RC subroutine of the proposed model. The results show that the corroded section possesses a lower ductility (2.9) compared to that of a non-corroded section (4.1).

The experimental investigation carried by Rodríguez et al. (1996) showed that the reduction in the concrete cover results in an added eccentricity of the applied axial load. There is also an eccentricity due to discontinuity in the superstructure/substructure joints. If the effects of these two eccentricities are combined with those of an earthquake, then the influence of the corrosion of the longitudinal reinforcement on the column ultimate capacity is further magnified.

E7. Summary and Conclusions

In this paper, a nonlinear elasto-plastic numerical model to simulate bridge columns under combined effects of reinforcement corrosion and seismic excitation is presented. The study includes the development of a comprehensive and simple tool to evaluate the seismic performance and the residual strength and deformation capacity of aging RC bridge columns with corroding reinforcement. This approach enables evaluating aging and deteriorated RC bridge columns safety, the decline in their energy dissipation capability, and the level of earthquake excitation that they may survive. Hence, the model can represent a strong tool for bridge engineers to optimize the use of available resources and define the critical capacity of bridge columns against earthquake events.

The proposed procedure includes an external cycle to represent the corrosion process, which is introduced through the reduction of the cross sectional area and the ductility of the reinforcing steel and the decrease in concrete cover. Step-by-step integration is then used for the time-history analysis and the hysteretic behaviour of the RC column.

The individual and combined effects of seismic and corrosion loads have been investigated on a 49.0 m slab-on-steel girder bridge on concrete piers. It is found that the model is efficient in simulating the behaviour of the column under corrosion and seismic loads. From the case study, it is found that the load carrying capacity of the corroded column is much lower than that of the uncorroded column. The results show significant reduction in the column displacement capacity and energy dissipation capability. The corrosion-induced damage could result in accelerated degradation of the bridge columns and reduce its ultimate strength.

E8. Future Work

Thorough investigation is to be performed to evaluate the effects of different values of various geometric, loading and corrosion parameters on the structural behaviour and capacity of RC bridge columns. This can be achieved by using different superstructure materials and stiffness, column design, and different levels of corrosion intensity. This analysis leads to the assessment of the safety, ductility and failure mode of aging RC bridge columns that are suffering from corrosion-induced damage. On the other hand, the predictions of this model need to be validated by comparison to experimental results obtained from scaled models of bridges tested under experimental combined axial and flexural loads of static and dynamic analyses. The interaction between the bond degradation due to corrosion and seismic performance of the columns is to be evaluated in next phase of this study.

E9. References

Alsiwati, J. 1993. Effect of anchorage slip and inelastic shear on seismic response of reinforced concrete frames. Ph.D. Thesis, Dept. of Civil Engineering, University of Ottawa, Ottawa, 367 pp.

Andersen, A. 1997. HETEK, Investigation of Chloride Penetration into Bridge Columns Exposed to De-Icing Salt. Copenhagen, Denmark.

Berto, L., Vitaliani, R., Saetta, A., and Simion, P. 2009. Seismic Assessment of Existing Structures Affected by Degradation Phenomena. Structural Safety, 31(4): 284-297.

Cairns, J., Plizzari, G. A., Du, Y., Law, D. W., Franzoni. 2005. Mechanical properties of corrosion reinforcement. ACI Materials Journal, 102(4): 256-264.

CAN/CSA S6-06. 2006. Canadian Highway Bridge Design Code, Canadian Standards Association, Mississauga, ON, 800 pp.

Choe, D.-F., Gardoni, P., Rosowsky, D., Haukaas, T. 2008. Probabilistic capacity models and seismic fragility estimates for RC columns subject to corrosion. Reliability Engineering and System Safety, 93(3): 383-393.

Kanaan, A., E., and Powell, G. H. 1973. Drain-2D User's Manual, Earthquake Engineering Research Center, Report No. EERC 73-22, University of California, Berkeley.

Lay, S. and Schiebl, P. 2003. Life cycle Management of concrete Infrastructures for improved Sustainability. European Community Fifth Framework Program: GROWTH.

Mohammed, A., Almansour, H, and Martín-Pérez, B. 2010. Modelling RC bridge columns under the combined effects of traffic and reinforcement corrosion. 8th International Conference on Short & Medium Span Bridges, Niagara Falls, Ontario, Canada, Paper 168, 10 pp.

Rodríguez, J., Ortega, L. M. and Casal, J. 1996. Load Bearing Capacity of Concrete Columns with Corroded Reinforcement. Corrosion of Reinforcement in Concrete Construction, Royal Society of Chemistry: 220-230.

Saito, Y., Oyado, M., Kanakubo, T. and Yamamoto, Y. 2007. Structural performance of corroded RC column under uniaxial compression load. First International Workshop on Performance, Protection & Strengthening of Structures under Extreme Loading, Whistler, Canada.

Shooshtari, A. 1998. Seismic drift demands of reinforced concrete building. Ph.D. Thesis, Dept. of Civil Engineering, University of Ottawa, Ottawa, 385 pp.

Val, D.V. 2007. Deterioration of Strength of RC Beam Due to Corrosion and its Influence on Beam Reliability. Journal of Structural Engineering, 133(9): 1297-1306.

Appendix F

This appendix shows additional figures that provide more details, only briefly presented in Chapter 5: (i) the development of the path of the "staged failure mechanism" for different bridge columns designed for different load over capacity ratios (LOCR); (ii) the detailed results of time history analysis that is summarized in Chapter 5; and, (iii) detailed interaction diagrams for each LOCR and for each stage of damage.

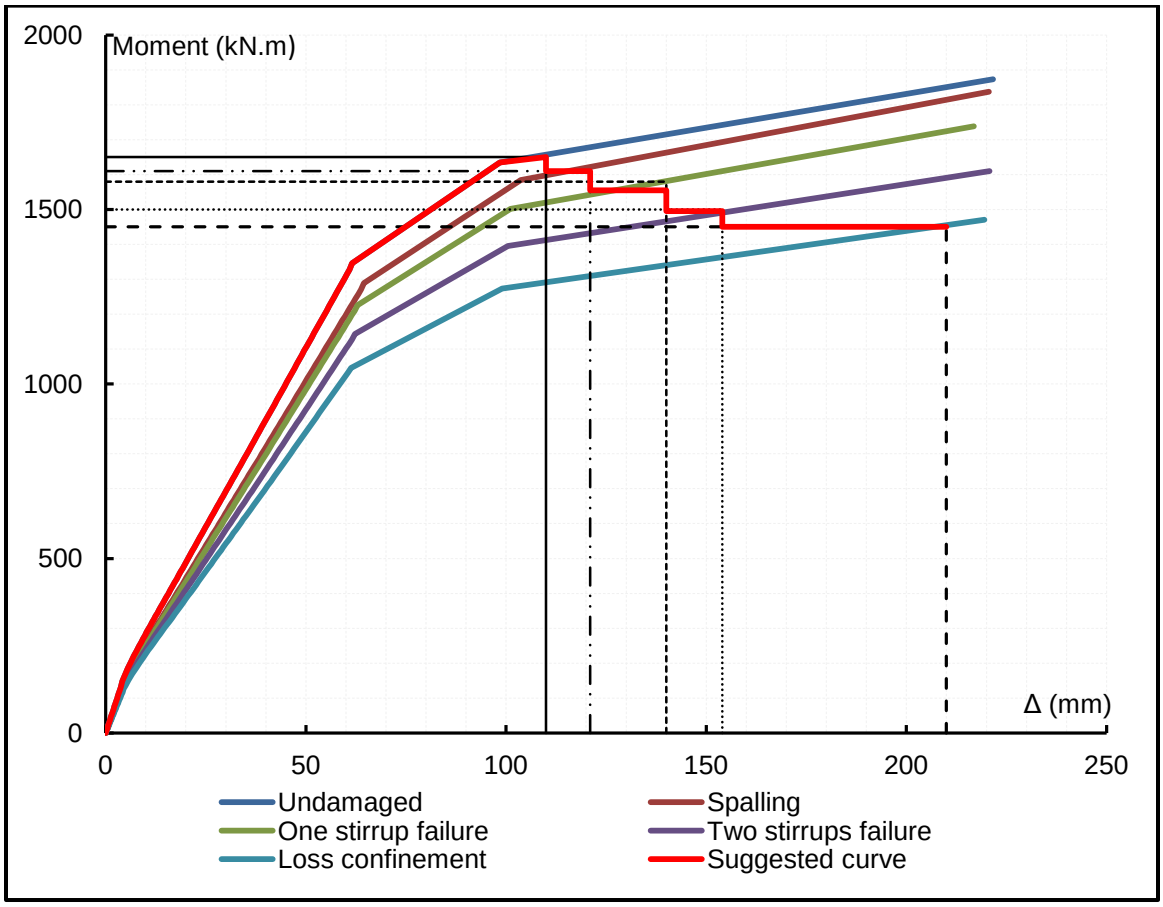

Figure F-1: Envelope curve of load-displacement relationship of uncorroded column with LOCR = 25%.

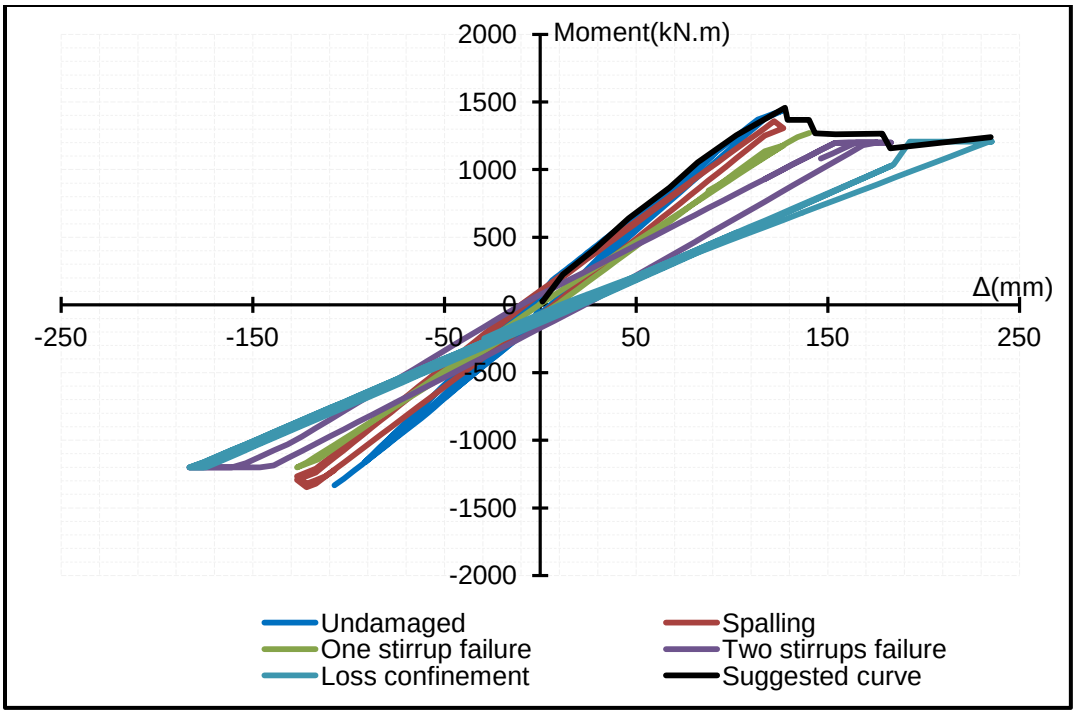

Figure F-2: Load displacement relationship of uncorroded column with LOCR = 25%.

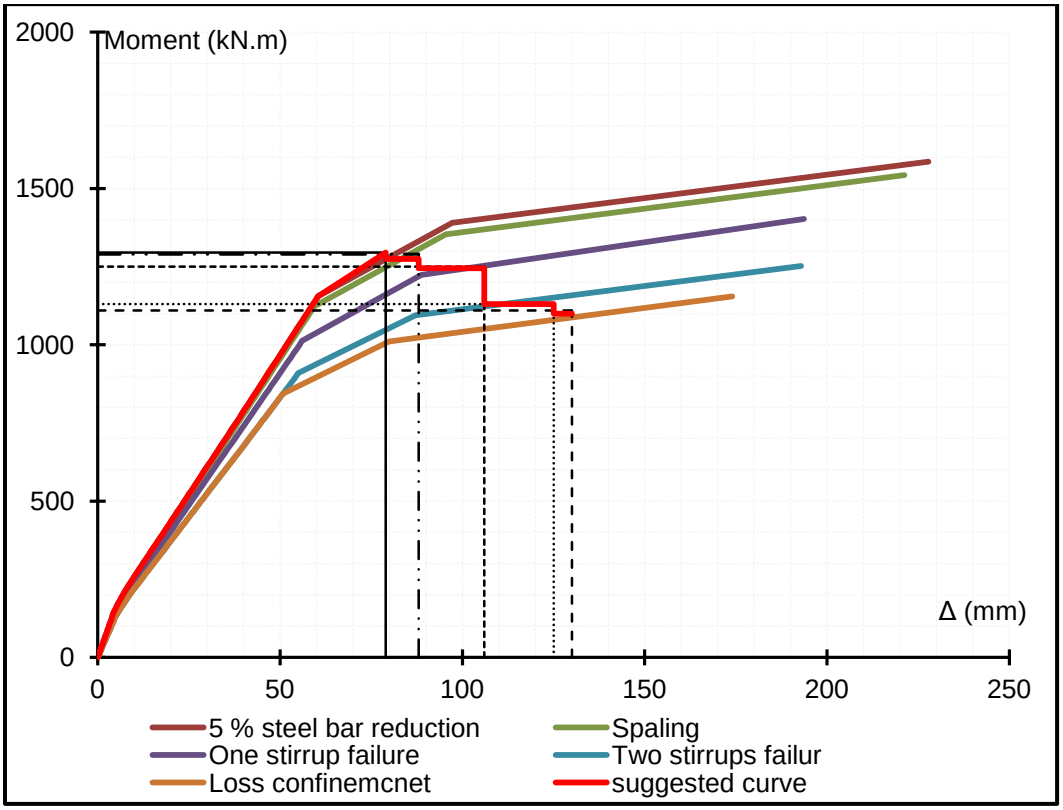

Figure F-3: Envelope curve of load-displacement relationship of corroded column with LOCR = 25%.

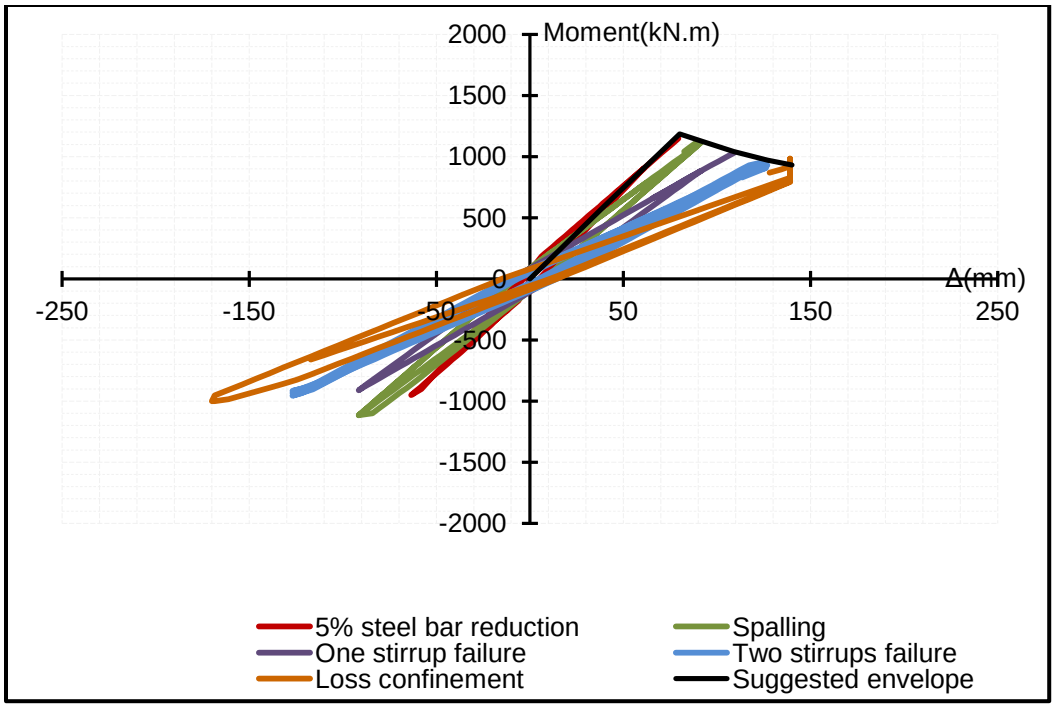

Figure F-4: Load displacement relationship of corroded column with LOCR = 25%.

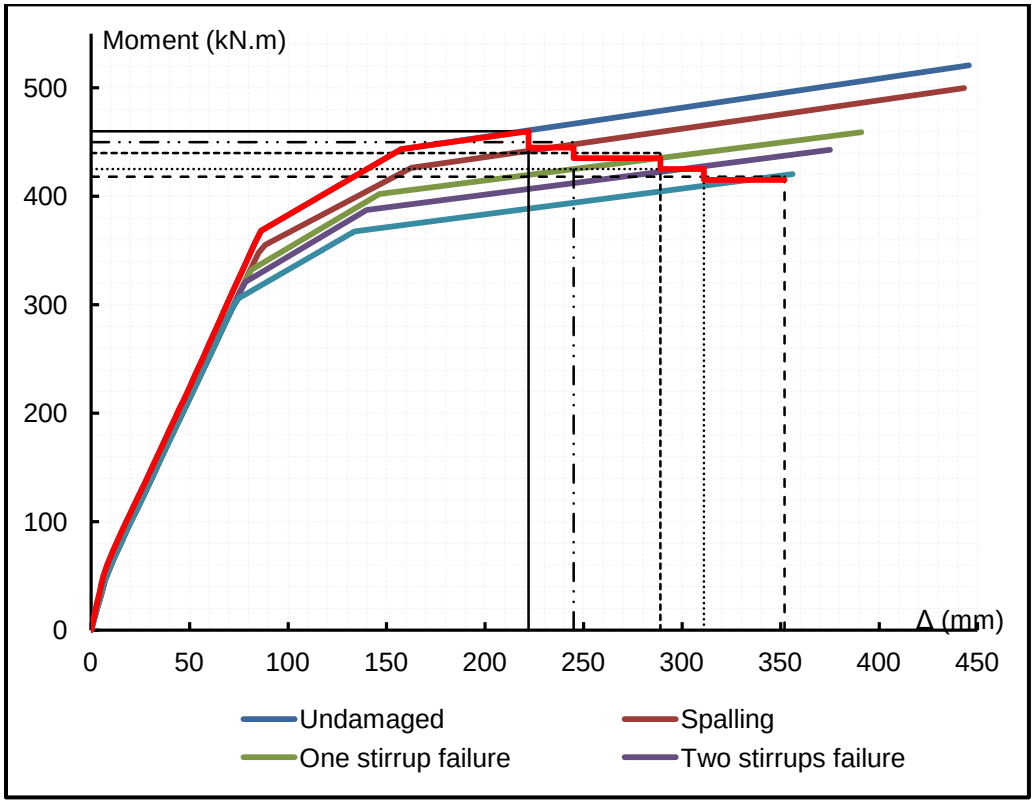

Figure F-5: Envelope curve of load-displacement relationship of uncorroded column with LOCR = 60%.

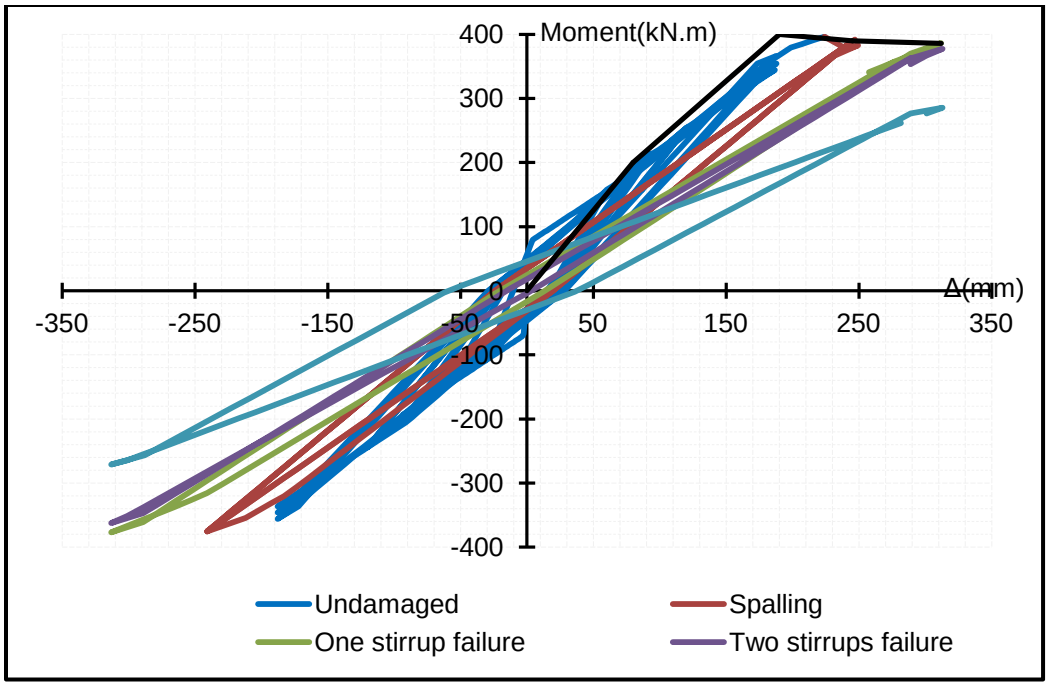

Figure F-6: Load displacement relationship of uncorroded column with LOCR = 60%.

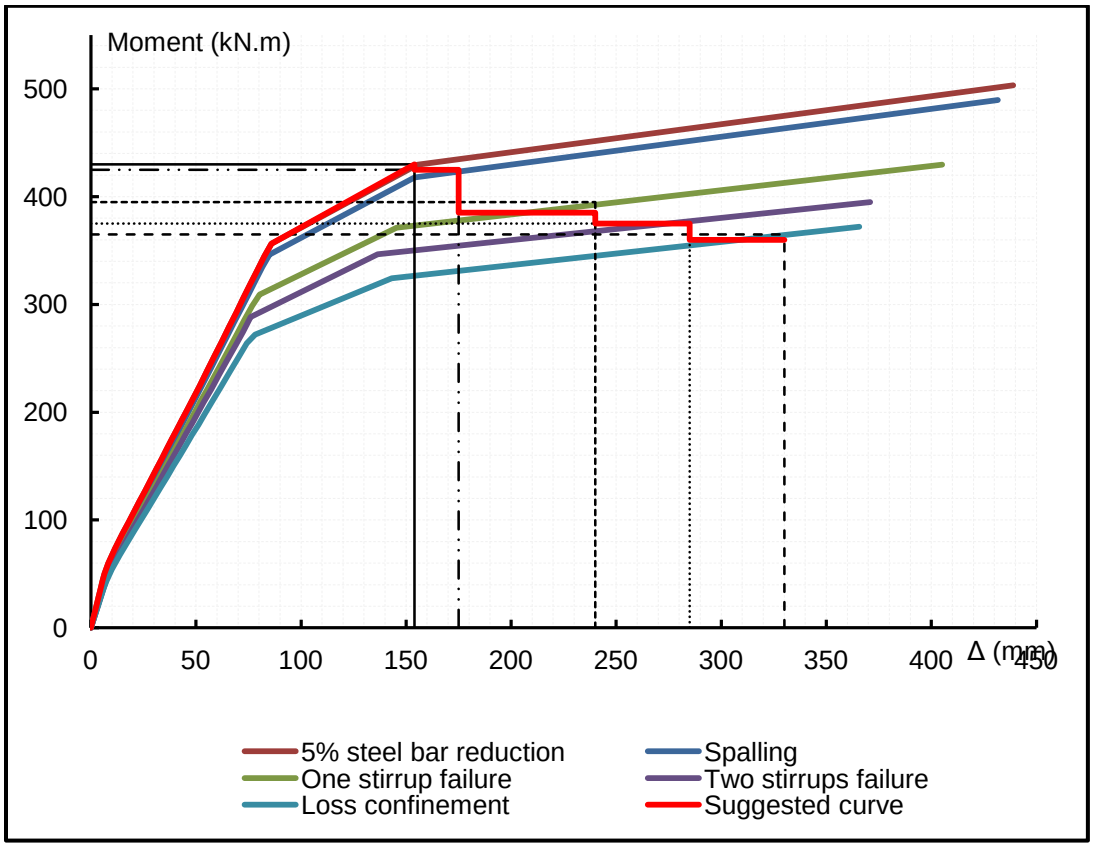

Figure F-7: Envelope curve of load-displacement relationship of corroded column with LOCR = 60%.

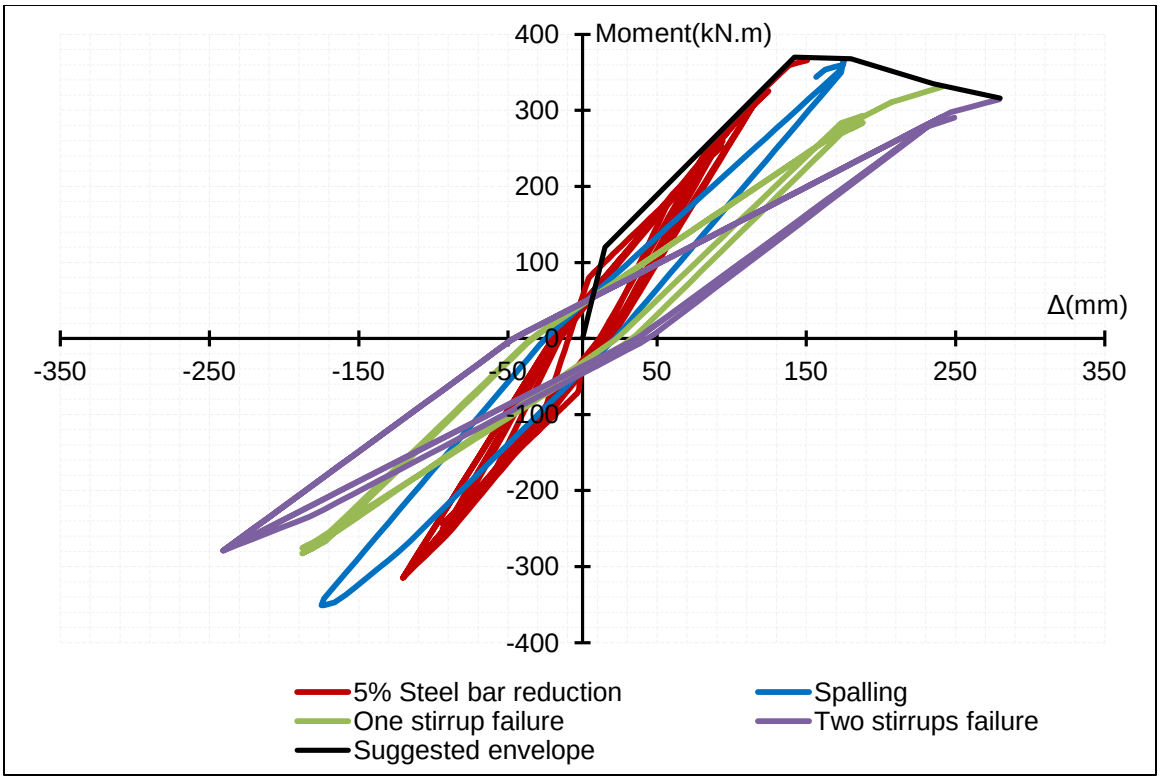

Figure F-8: Load displacement relationship of corroded column with LOCR = 60%.

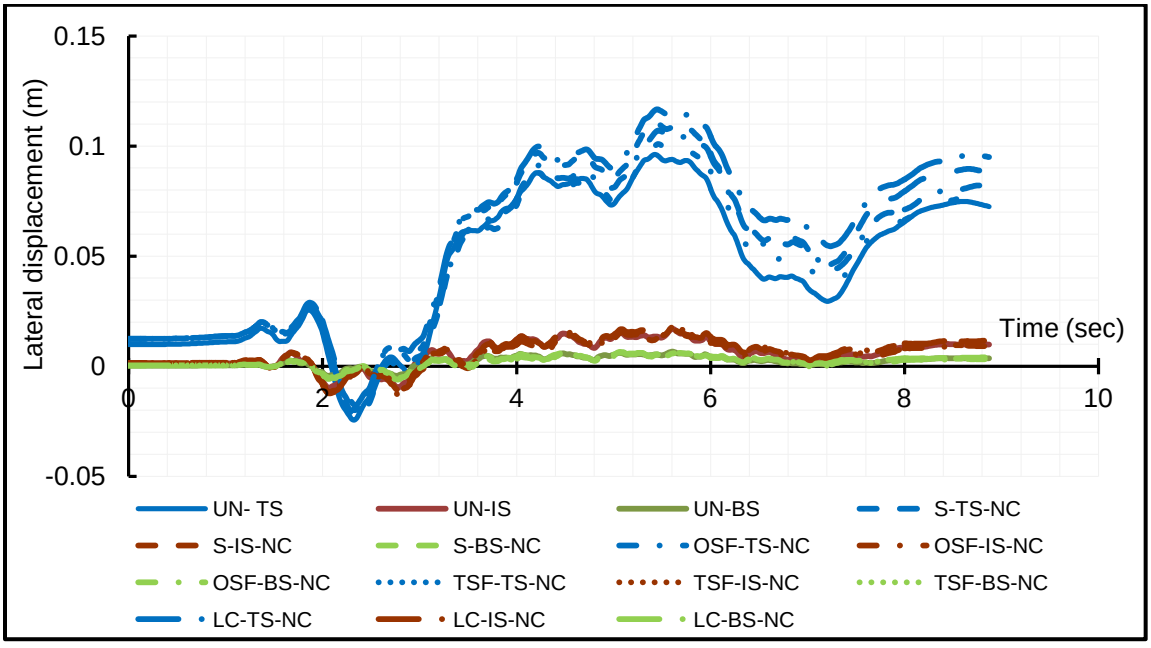

Figure F-9: Time history of lateral displacement for different sections of an un-corroded column with LOCR = 25%.

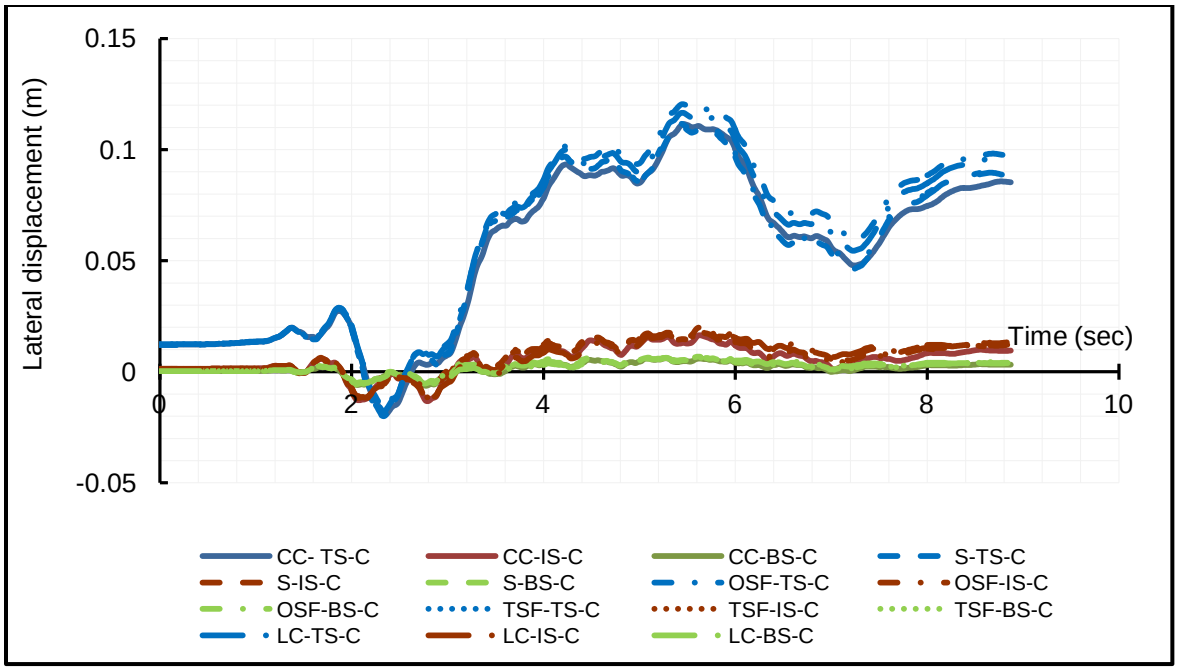

Figure F-10: Time history of lateral displacement for different sections of a corroded column with LOCR = 25%.

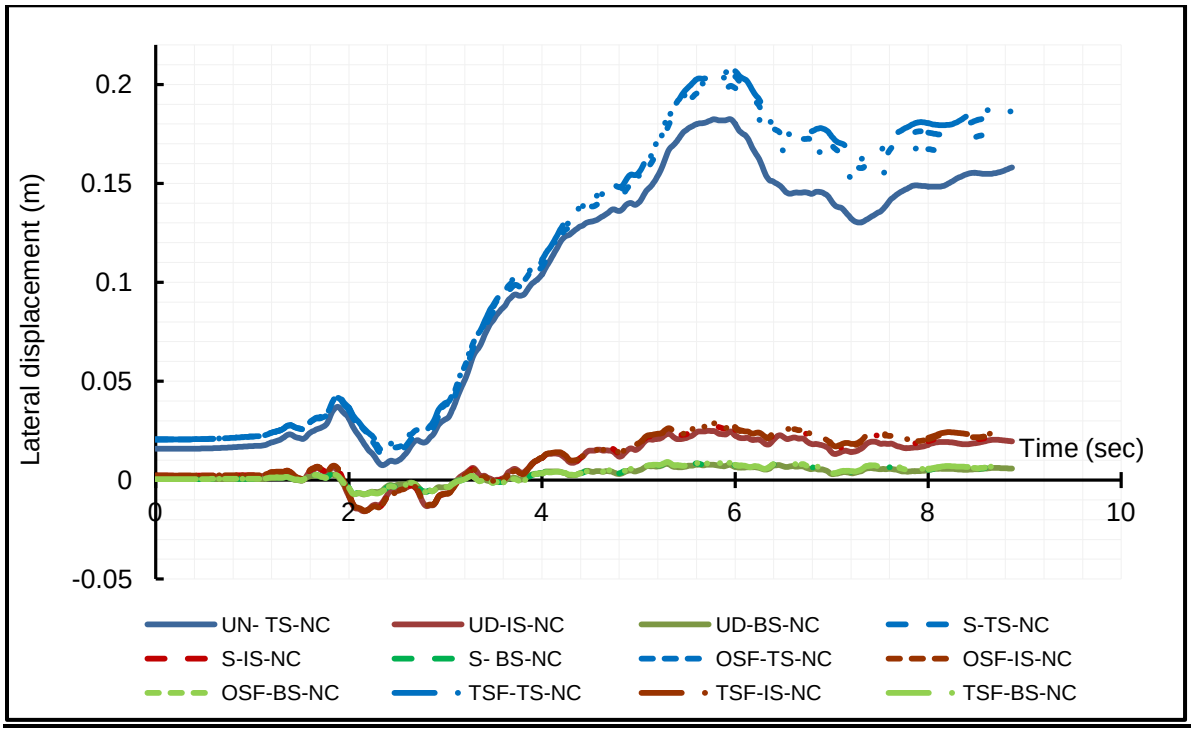

Figure F-11: Time history of lateral displacement for different sections of a un-corroded column with LOCR = 60%.

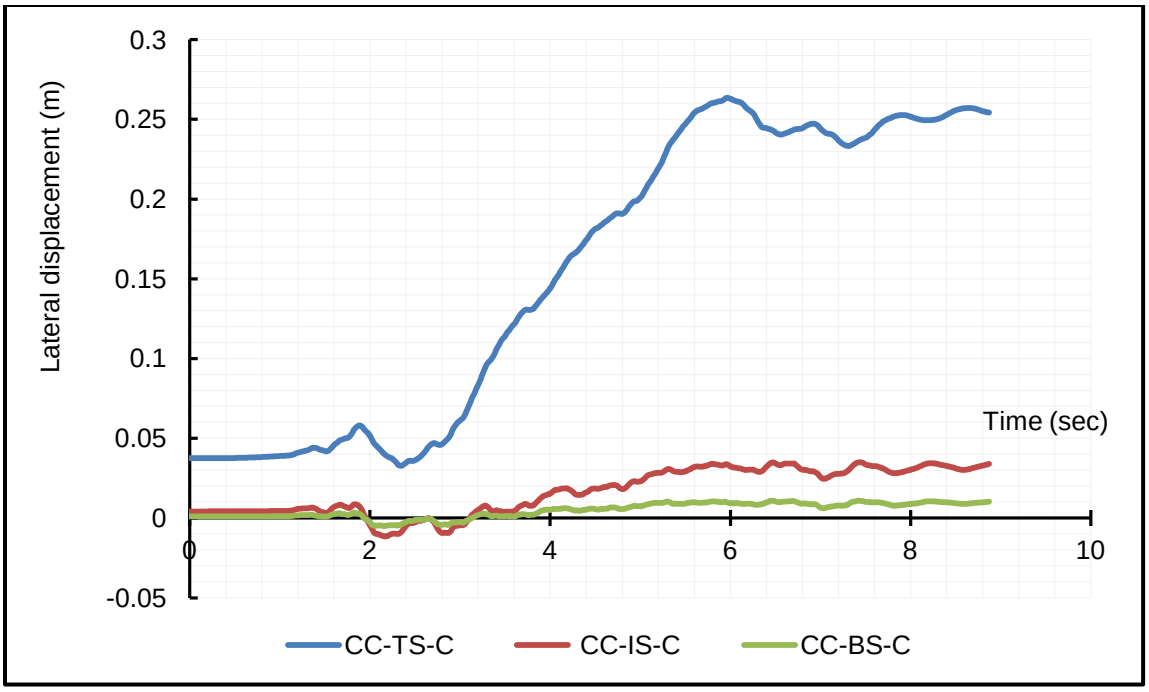

Figure F-12: Time history of lateral displacement for different sections of a corroded column with LOCR = 60%.

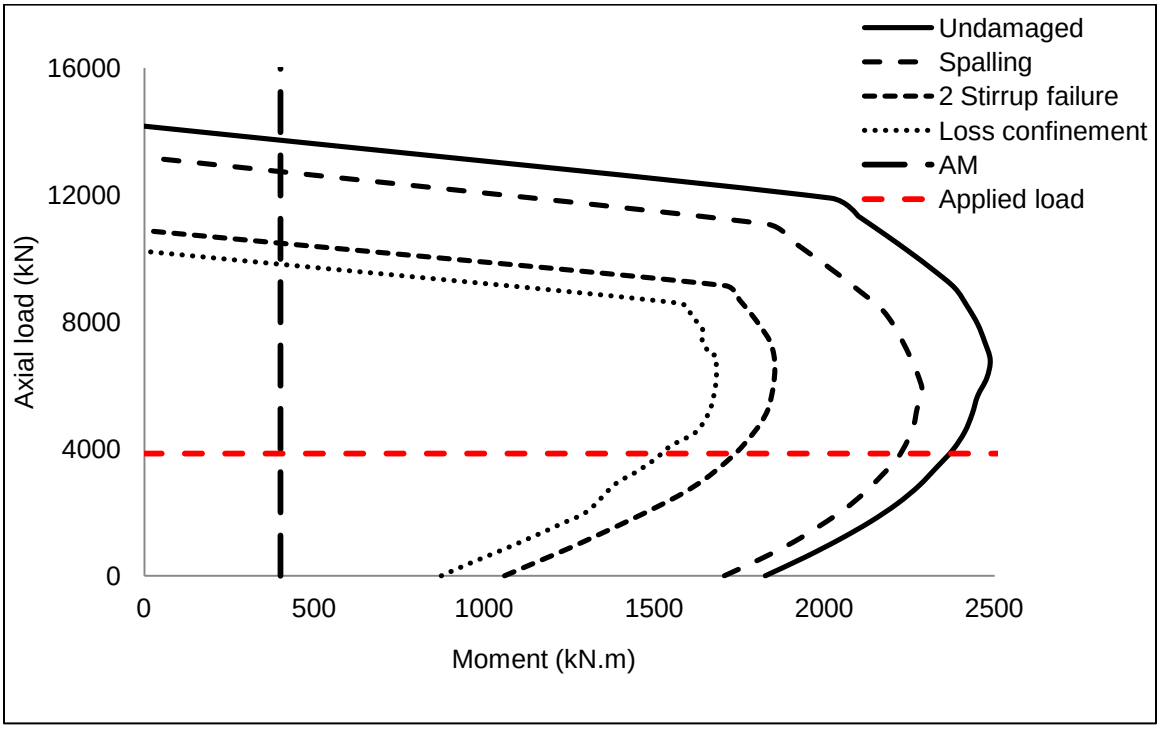

Figure F-13: Interaction diagram of LOCR 25% column section for different corrosion scenarios.

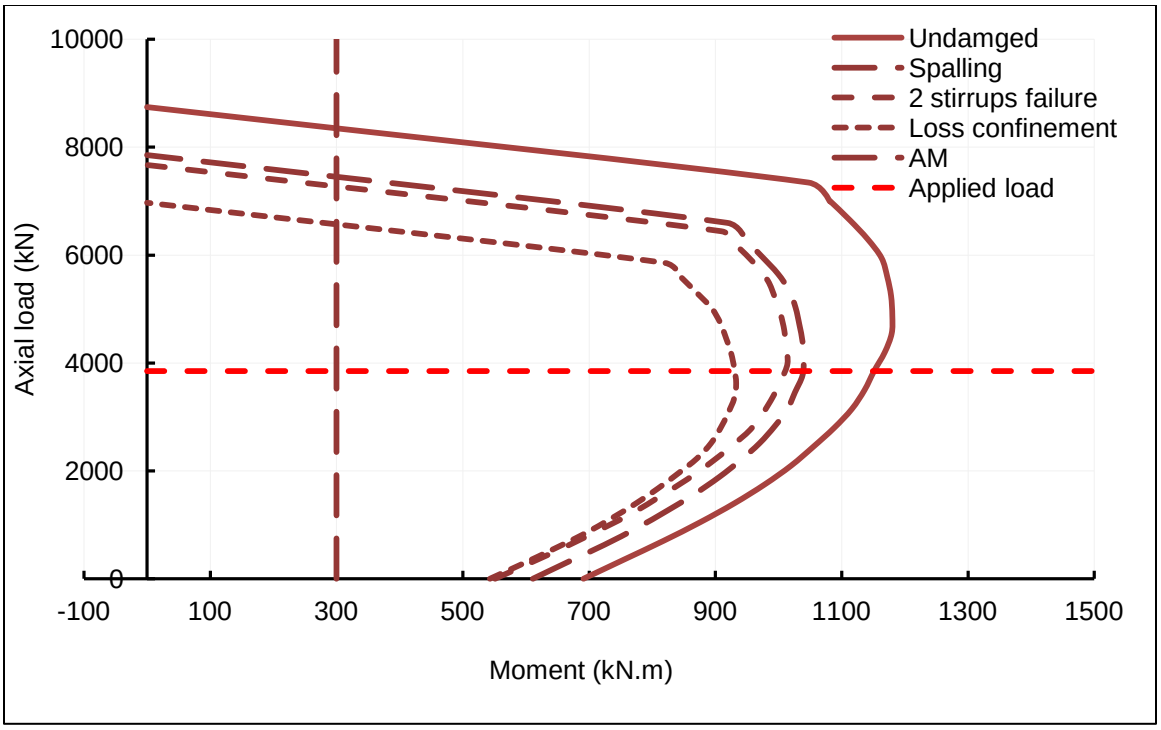

Figure F-14: Interaction diagram of LOCR 40% column section for different corrosion scenarios.

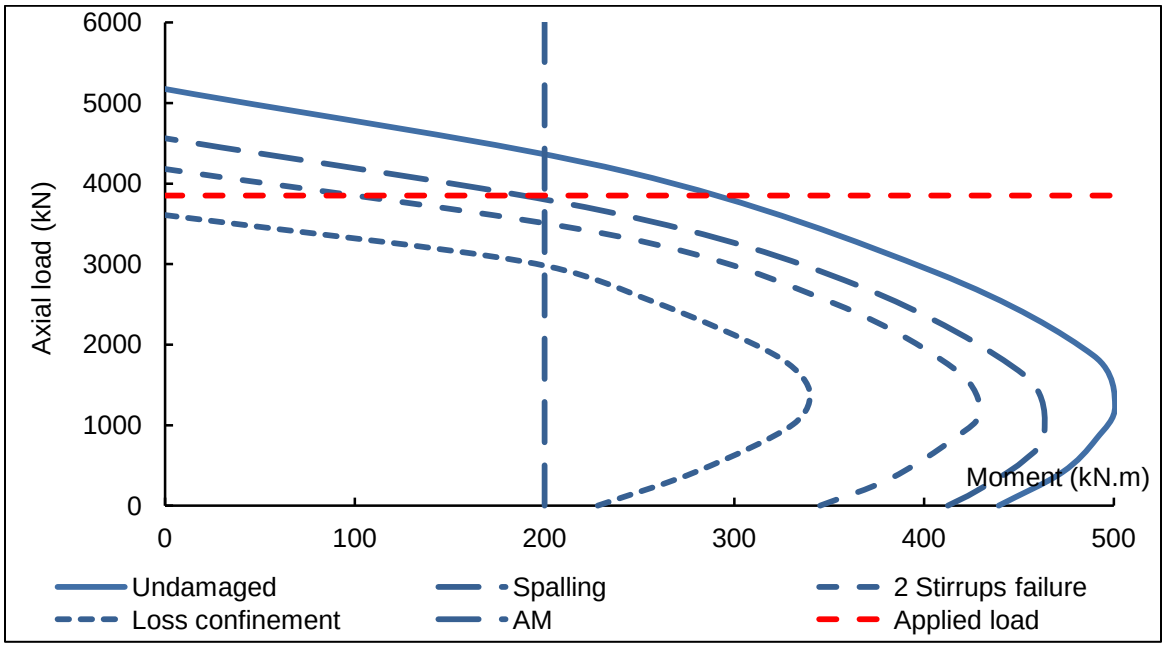

Figure F-15: Interaction diagram of LOCR 60% column section for different corrosion scenarios.